Mathematical modelling of heterogeneity in tumour-immune cell interactions

Heidi Jessica Dritschel

St Anne's College

University of Oxford

A thesis submitted for a degree of

Doctor of Philosophy

Hilary 2018

Firstly I would like to express my gratitude to my supervisors Helen and Sarah for their endless guidance, insight and support. I feel privileged having learnt so much from them throughout this process. I would also like to thank my industrial supervisor and mentor Andreas for his guidance and insight throughout.

I am also grateful to my parents for their constant support, encouragement and guidance throughout. In particular, I would like to say a special thank you to my father for inspiring me to study mathematics in the first place, and his help, guidance and conversation throughout — thank you for opening my eyes to the beauty and art of mathematics.

I would also like to acknowledge both of my sisters, Monica and Andrea, and my brothers, Cameron and Gregory for their love and support.

Finally I would like to thank all of my friends for their support and for keeping me grounded. In particular I would like to mention Julia, Sarah, Alba, Johanna and Fergus. I would also like to thank my dance teacher Ellie for inspiring me to think creatively in a different way.

Abstract

Tumours are highly heterogeneous entities. To understand cancer development from its initiation to metastases, research is needed to reveal the impact of heterogeneous populations of immune cells and tumour cells on outcomes. The presence of T cells of the adaptive immune response are correlated with favourable outcomes across a broad range of cancers. In this thesis we focus specifically on the T cell population and the impact of heterogeneity in both immune and tumour cells on model outcomes. To reveal the role played by the various aspects of heterogeneity in tumour-immune cell interactions, we develop a suite of mathematical models that explores in turn heterogeneity in: subpopulations of T cells; in different states of functionality of the same T cell (or states of exhaustion); and different subpopulations of tumour cells.

The models are formulated as ordinary differential equations. Each model is examined through a combination of numerical and analytical techniques. All three models exhibit three generic responses to immune cells: tumour elimination, equilibrium and escape (the three Es of immunoediting) [52]. The first model focuses on the behaviour of a tumour interacting with two subpopulations of T cells: helper and cytotoxic T cells. The likelihood of tumour elimination, equilibrium and escape is found to vary with both the rates of infiltration of cytotoxic and helper T cells. The results indicate that combined immunotherapies, where both rates of infiltration are increased comparably, may elicit the most favourable response outcomes.

The second model focuses on heterogeneity in the level of functionality of the cytotoxic T cells (exhaustion state). Tumour elimination, equilibrium and escape are found to depend on the rates of exhaustion of individual T cell functions, together with the ratio of the baseline T cell population (in the absence of a tumour) to the T cell population required to arrest tumour growth. The model suggests that the appropriate treatment is to block the ability of the tumour to dampen T cell proliferation.

The final model focuses on heterogeneity in both tumour and T cell populations. The tumour population is divided into an immune-resistant and an immune-sensitive subpopulation, and the T cell population is divided into a cytotoxic and an exhausted subpopulation. The likelihood of tumour elimination, equilibrium and escape are found to vary with the rate of infiltration of cytotoxic T cells, together with the growth rate of the tumour, the rate at which immune-sensitive tumour cells produce immune-resistant tumour cells, the rate of conversion of cytotoxic T cells to exhausted T cells and the exhausted T cell kill rate. The results suggest that boosting the infiltration of cytotoxic T cells would be most effective and that the necessary increase depends on the growth rate of the tumour.

This thesis uses a series of ODE models to comprehensively study how aspects of tumour-immune system heterogeneity impact tumour progression. All three models show a close link between moderate immunosuppression and the presence of a dormant tumour state. The results suggest a number of potentially promising therapies depending on the degree of immunosuppression, tumour growth rate, and immune cell composition.

Contents

List of Figures

Chapter 1

Introduction

'. . . there is no doubt that immunotherapy will from here on be a key part of treatment for a growing number of cancers. Perhaps the most telling measure of its success is that some oncologists have started to complain, quietly, of a shortage of specialist doctors. Patients keep coming back instead of dying.'

The Economist, September 16th 2017

The work in this thesis was supported in part by Hoffmann La Roche. The results bear upon finding new therapies for a broad range of cancers, exploiting a better understanding of T cell function in tumour-immune dynamics. The research carried out in this thesis addresses the role of different aspects of heterogeneity in immune and tumour populations. The findings may help in the design of new patient specific treatment protocols.

1.1 The immune system

The human immune system has evolved into a three-armed system of defence that is able to recognise and eliminate functionally and physically diverse pathogens while at the same time distinguishing between self and non-self tissue. Outer physical barriers blocking the entry of pathogens into the host are the first line of defence. If breached, the second arm of defence is innate and non-specific. If this line of defence is unable to rid the host of the invader then the last arm of defence, the adaptive and specific arm, is recruited. The innate immune system has existed since the first single cell organism evolved approximately 3.5 billion years ago [106]. The adaptive immune system was formed, in evolutionary terms, much later to defend complex multi-cellular organisms, specifically vertebrates, against increasingly complex pathogens [11].

Insights into how the immune system works to protect the host against invading pathogens first arose from separate investigations conducted by Metchnikoff and Erlich in the late 19th century. Metchnikoff's work, published in 1884 [133], focused on the innate (non-specific) arm of the immune system. Through his studies of marine non-vertebrates he observed that cells could engulf and consequently eliminate pathogenic microbes. He termed this process 'phagocytosis'. From the results of his studies he concluded that phagocytosis was the primary mechanism by which the innate immune system eliminated pathogens. Erlich, on the other hand, observed how the adaptive (specific) arm of the immune system could recognise and eliminate a pathogen. In 1897 he developed the 'side-chain theory' [58] to describe this function of the adaptive immune system. His theory was based upon experimental models using mice in which he observed cells with receptors that bound only with specific antigens. Once bound, these cells were activated producing antibodies specific to the antigen [59]. His insights into the immune cells production of antibodies specific for a particular pathogen contributed to the development of modern vaccinations [148].

A key consequence of Metchnikoff and Erlich's findings was the realisation that the innate and adaptive arms were independent and, as a result, there was considerable debate about their relative importance. In 1903 Wright *et al.* [204] challenged the idea that the two arms were independent by observing that the innate and adaptive arms of the immune system can work together to eliminate a pathogen. Although Wright's work highlighted a link between the two arms of defence, details of how cells of the innate and adaptive arms interact remained poorly understood until the work of Hoffmann, Beutler, and Steinman [149, 182, 181, 173], a century later. Their research provided experimental insight into how the innate and adaptive arms of the immune system communicate and cooperate; they were awarded the Nobel Prize in Physiology or Medicine in 2011 for this research. In the next section, we focus in more detail on the innate and adaptive arms of the immune system and how they communicate and cooperate to rid the host of a pathogen.

1.1.1 Innate and adaptive arms of the immune system

To enter the host, pathogens must first penetrate physical barriers such as the skin, epithelial cilia and mucus membranes which line the digestive, respiratory and reproductive tracts. The innate arm is the first line of defence in vertebrates and the only line of defence in non-vertebrates [94]. Once these physical barriers have been breached, cells of the innate immune response respond. A distinguishing feature of these cells is their lack of specificity for a particular pathogen. Instead cells of the

innate arm recognise these cells through their expression of signature molecules (e.g. pathogen associated molecular patterns [109]). Large numbers of non-specific cells are distributed throughout the body, stationed where physical barriers may be breached. The non-specificity of the innate response and the large numbers of cells involved enable the host rapidly to mount an attack against a pathogen.

Increasingly sophisticated pathogens, found in multi-cellular organisms, place a greater demand on the innate arm. As a result, a diverse array of non-specific receptors can recognise these pathogens (e.g. transmembrane pattern recognition receptors, Toll-like receptors, C-type lectin receptors, leucine-rich repeat-containing receptors and retinoic acid-inducible gene I-like receptors [93]). In addition to pathogen clearance, cells of the innate immune system are needed to activate and maintain an effective adaptive immune response.

If the innate arm of the immune system is unable to eliminate a pathogen, the adaptive arm is engaged to mount a specific attack against the encountered foreign antigen [95]. Across the large population of cells of the adaptive immune system, a small number of cells have receptors that are specific for a particular foreign antigen. This level of receptor diversity is achieved through the recombination of receptor molecule genes by the proteins RAG 1 and RAG 2 [89, 95]. When a foreign antigen is first encountered the limited pool of these cells with the matching antigen receptor are sought out by antigen presenting cells for activation. Upon encountering the foreign antigen, the specific adaptive immune cells proliferate, differentiating into memory (long-lived) and effector (short-lived) cells. This proliferation continues until a substantial population of antigen specific cells have amassed to mount an effective immune response. This typically takes a couple of days from when the foreign antigen was first recognised by the adaptive immune response [95]. A key advantage of the adaptive arm is the production of memory cells. These memory cells are long-lived, existing in a non-functional state until the foreign antigen is re-encountered. The presence of an increased population of antigen specific adaptive immune cells enables the immune system to rapidly recognise and eliminate the pathogen when it is re-encountered.

Until recently it was believed that the innate and adaptive arms of the immune system were independent and that the process of pathogen elimination was unidirectional (from the innate to the adaptive arm). We now know, to mount an effective immune response in vertebrates, there must be bi-directional cooperation between cells of the innate and adaptive arms [73].

1.1.2 Cells of the immune system

Once physical barriers have been breached in vertebrates, there are two arms of defence: the non-specific innate arm and the specific adaptive arm. Both the innate and adaptive arms of the immune system are composed of white blood cells (leukocytes) which arise when pluripotent hematopoietic stem cells, located in the bone marrow, differentiate. The two main cell types that arise from the differentiation of lymphoid and myeloid progenitors are lymphoblasts and myeloblasts (see Figure 1.1). In this thesis we focus specifically on the T cells that differentiate from lymphoid progenitors and therefore our discussion is primarily focused on the lymphoid progenitors. Next we briefly discuss monocytes which differentiate from myeloid progenitor cells. These are relevant to the research presented in this thesis as monocytes present antigen which can be recognised by both T and B cells of the specific response and are necessary for the activation of these cells.

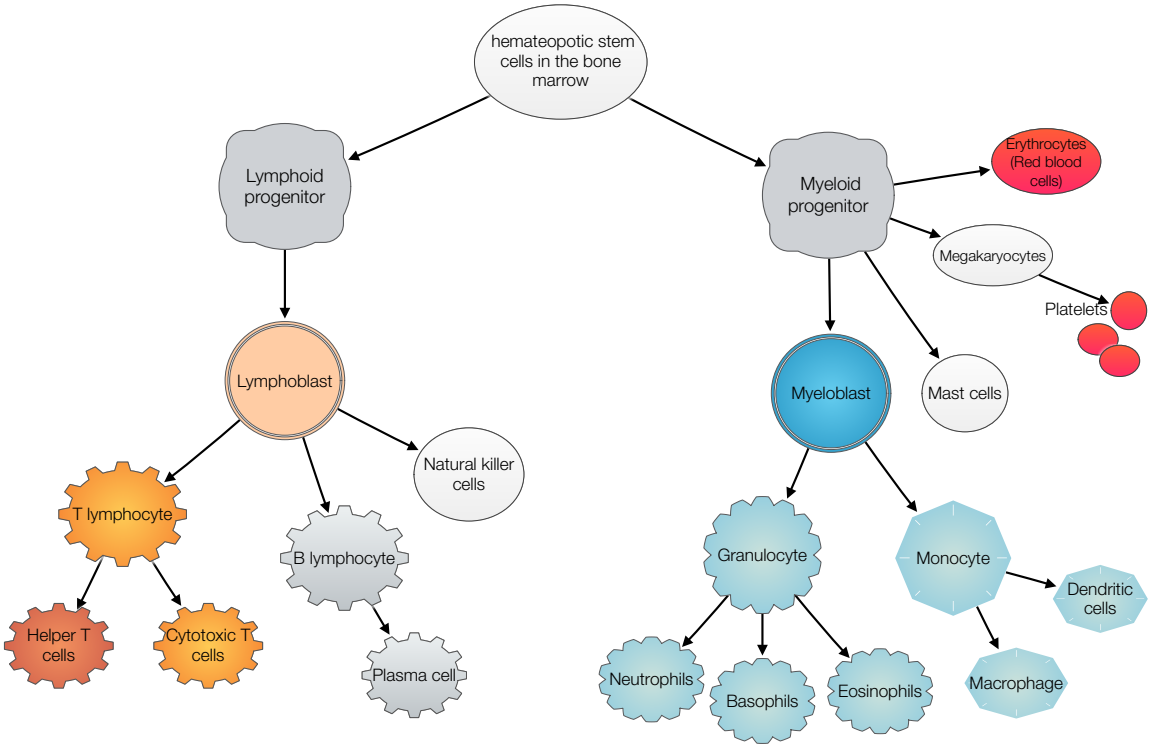

Figure 1.1: Schematic diagram showing how differentiation of pluripotent stem cells in the bone marrow which gives rise to the cells of the innate and adaptive immune systems.

1.1.2.1 Myeloid progenitors

Myeloid progenitors generate both white and red blood cells. Specifically, these precursor cells differentiate into specialised types: erythrocytes (red blood cells), megakaryocytes (which produce platelets) and myeloblasts (white blood cell precursors). Myeloblasts differentiate further into two groups of white blood cells: granulocytes and monocytes. Here we focus our discussion on monocytes.

On entry to an infected tissue, monocytes mature into macrophages or dendritic cells. Like granulocytes, they recognise and engulf pathogens by phagocytosis. In this way the monocytes display fragments of the pathogen, known formally as antigen, on their surface. Due to this display of antigen, macrophages and dendritic cells are called antigen presenting cells (APCs). These cells communicate with the cells of the adaptive arm by displaying antigen on their surface to naive cells of the adaptive immune system. This process of activation occurs in the peripheral lymphoid vessels. Here APCs present the antigen displayed on a major histocompatibility complex (MHC) molecule to the cells of the adaptive arm with the matching receptor [138]. The MHC molecule, a self-molecule, is necessary to display the antigen so that the adaptive cells know that the APC is not a pathogen. Although dendritic cells share many similarities with macrophages, they differ in the class of MHC molecules that they express. Specifically they express high levels of MHC II class molecules (instead of MHC I class molecules) which are required for the activation of helper T cells.

1.1.2.2 Lymphoid progenitors

Lymphoid progenitors first differentiate into lymphoblasts and then further differentiate into either natural killer cells (NK cells), T lymphocytes (T cells) or B lymphocytes (B cells). NK cells are important for killing intracellular pathogens. They are a non-specific type of lymphocyte containing cytotoxic granules. One of the most important properties of NK cells is their ability to distinguish between self and infected/transformed self tissues. They recognise infected self-cells via their down regulation of MHC class I molecule expression and play a key role in fighting tumour cells (transformed self-cells) [118]. They also regulate the immune response through their production of specific cytokines such as IFN-γ [194].

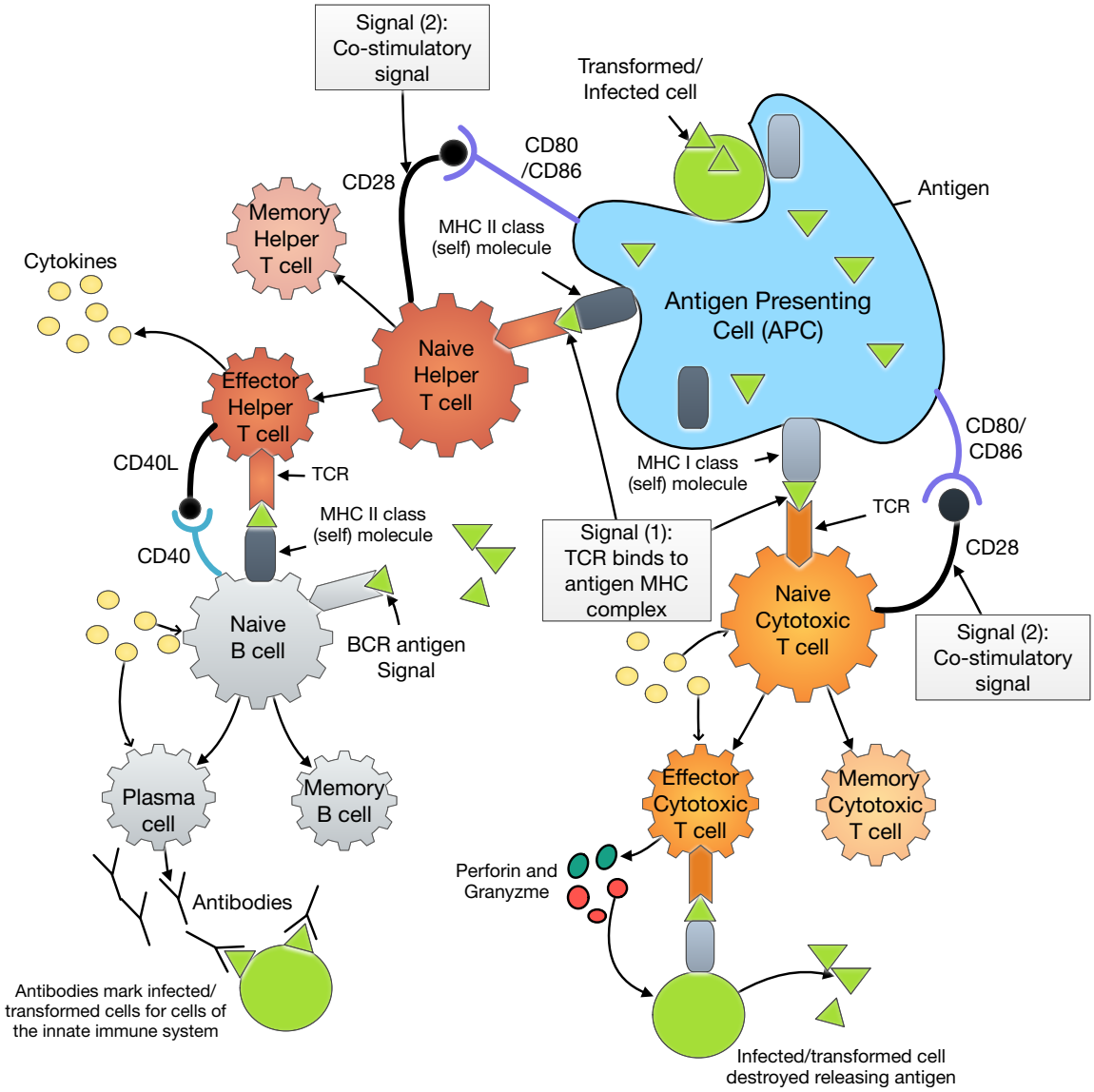

Figure 1.2: Schematic diagram illustrating how B and T cells of the adaptive immune response are activated.

The T and B cells constitute the adaptive immune system. T cells are responsible for the cell mediated response while B cells govern the humoral response. Both populations originate from pluripotent haematopoietic stem cells in the bone marrow; B cells mature in the bone marrow while lymphocyte precursors populate the thymus where they undergo a series of developmental steps including undergoing positive and negative selection and maturation into naive T cells that exit the thymus and migrate to lymphoid tissues. Naive T cells continually migrate both within lymph nodes scanning for antigen presented by dendritic cells and undergo a process of recirculation leaving individual lymph nodes every 12 -24hrs, and entering circulation

before re-entering lymphoid tissues. This process of continual migration and entry into different lymphoid tissues maximises the probability any one individual naive T cell will interact with its cognate antigen. T and B cell populations are highly diverse with unique receptors, known as T and B cell receptors respectively (TCRs and BCRs). The highly diverse repertoire of TCRs can respond to a diverse set of antigens restricted by the pre-cursor frequency, the effect of negative selection process on developing B and T cells to remove autoreactive clones and the restriction set of peptides that can be presented by self MHC. B cells recognize the 3D shape and charge of antigens which can include proteins, carbohydrates, lipids and small chemical molecules. In comparison conventional T cells only recognize short peptides bound to the self-MHC molecules. When antigenic stimulation occurs, B and T cells differentiate into effector (short lived) cells. B cell activation occurs as a result of soluble antigenic stimulation together with activation via (effector) helper T cells as illustrated in Figure 1.2. Upon BCR stimulation, B cells can be stimulated to undergo rounds of affinity maturation leading to higher affinity responses and secretion of antibodies. Some of the B cells will mature into memory cells, others will undergo a process of maturation into terminally differentiated plasma cells that are specialized secretory cells that produce large amounts of antibody. These antibodies attach to the infected/transformed cell alerting the cells of the innate immune system, consequently promoting their phagocytosis. Effector cytotoxic lymphocytes (CTLs) are activated by antigenic peptide MHC class I complexes on target cells (e.g. virally infected or tumour cells) leading to cell killing through the directed release of granzymes and perforin that are directly cytolytic to the target cell. The process of lymphocyte activation, proliferation and antigen, tumour or pathogen removal through either directly cytolytic or humoral process is maintained, until either the source of antigens is eliminated or the immune system becomes refractory to antigenic stimulation [95]. Upon activation a small proportion of T and B lymphocytes differentiate into long lived memory cells instead of differentiating into fully functional effector cells. Upon re-encounter with specific antigen, memory T and B cells are rapidly induced to generate an amplified immune response due to a combination of a higher frequency of antigen specific lymphocytes and more potent responses on a per cell basis.

There are two subpopulations of T cells, cytotoxic and helper, which recognise MHC class I and II molecules, respectively. MHC class I molecules are expressed by all nucleated cells in the body while MHC class II molecule expression is limited primarily to APCs. Naive T cells require two independent signals for their activation [139]. The first signal is the binding of the cognate antigen displayed on an MHC molecule by

an APC to the TCR. The T cell receptor α and β chains are part of a larger complex of proteins consisting of 4 chains of the CD3 complex of proteins (ε, δ, γ, ζ) that form a high order protein complex with the TCR and transmits intracellular signals resulting in gene transcription after stabilised high affinity binding to specific antigen-MHC complexes. The second signal is the engagement of a co-receptor on the surface of the T cell with a stimulatory molecule. (Note, co-receptors can be stimulatory or inhibitory.) In order to activate the T cell a stimulatory molecule on the surface of the T cell must bind to the appropriate ligand on the APC (e.g. CD28 present on surface of the T cell and CD80 or CD86 presented on the surface of the APC). T cell inactivation can occur as a result of inhibitory molecule signalling The best known inhibitory receptors being Cytotoxic T Lymphocyte Antigen 4 (CTLA-4), an inhibitory receptor that is transiently up-regulated in response to TCR stimulation which competes for the co-receptor CD28 for binding to CD80 and CD86, and Programmed cell Death 1 protein PD-1 which is up-regulated upon chronic TCR stimulation and binds to PD-L1.

Effector helper T cells influence all aspects of an immune response. For example, they activate B cells and signal them to switch production from one antibody to another (class switch recombination), promote proliferation of effector cytotoxic T cells at the site of infection, and recruit help from appropriate cells of the innate immune response to fight off invaders. This latter function allows them to control inflammation levels at the site of infection [92]. These T cells orchestrate an effective immune response by their production of specific patterns of cytokines. After the naive helper T cells are activated they produce the cytokine IL-2, promoting their own survival and proliferation. As these cells proliferate they differentiate into functionally distinct sub-populations defined by their unique cytokine signatures (Th1, Th2, Th17 and iTreg, for example) [137, 169]. The dominant population will depend on the make up of the microenvironment (i.e. the background cytokine milieu).

Effector CTLs enter into peripheral tissues dynamically scanning for cells expressing antigen (either virally infected cells or transformed healthy cells in cancer). Upon recognition, they bind to and induce potent killing of the target cells. T cells induce killing both indirectly and directly. They produce cytokines such as IFN-γ and TNF-α that triggers apoptosis of the target cell. The main way in which effector cytotoxic T cells kill is by direct cell contact. This can be done in two ways. Either cytotoxic T cell expression of the Fas-L ligand binds to Fas receptors on the target cell triggering apoptosis, or upon binding with the target cell the T cells release perforins and granzymes which penetrate and kill the target cell. The models presented in this

thesis all include cytotoxic T cells due to their direct killing capacity and their specificity to a specific tumour antigen. This thesis primarily focuses on cytotoxic T cells but also examines the coordination of helper and cytotoxic T cells in an anti-tumour immune response.

1.2 Cancer

Cancer is the second leading cause of death worldwide following heart disease. The International Agency for Research on Cancer (IARC) estimated that in 2012 there were approximately 14.1 million incidences of cancer, resulting in 8.2 million deaths worldwide [193]. The majority of cancer cases arise from somatic mutations caused by environmental factors. With age, the likelihood of these mutations increases and therefore with increasing life expectancies and population growth, these figures are expected to rise significantly.

Cancer denotes a range of diseases all resulting from the accumulation of genetic mutations in a healthy cell [82]. Cancer can occur within any cell in the body. As a result there are more than 200 known cancer types [156]. Mutations in the genome arise due to age, as well as environmental and genetic factors. Examples of environmental factors that are known to cause mutations include: tobacco, obesity, low rates of physical activity, UV radiation, pollution, stress, diet, and alcohol [156]. Genetic transmission is also a factor through the inheritance of an abnormal gene from a parent. For example inherited mutations in the BRCA 1 and BRCA 2 genes give rise to inherited breast and ovarian cancers.

Tumours comprise a diverse array of different cell types including cancer cells, endothelial cells, fibroblasts, epithelial cells and cells of the immune system. Cancer cells are malignant cells arising from the accumulation of mutations in the genes controlling cell regulation [158]. Both intrinsic (genetic) factors and extrinsic factors (such as chronic inflammation, viral infection, smoking and age) facilitate the induction of an incipient tumour. Two main classes of genes are associated with increased cancer incidence rate: oncogenes and tumour suppressor genes [198]. Oncogenes denote genes that act to prevent apoptosis of malfunctioning cells, allowing these cells to continue to proliferate. The up-regulation of these genes through genetic mutations facilitates tumour development. Tumour suppressor genes (also referred to as anti-oncogenes) are necessary to prevent cancer development by regulating normal cell growth and inducing apoptosis. Mutations in these genes down-regulate or cause

the complete loss of cell regulation. Tumorigenesis is a multi-step process that alters pathways controlling normal tissue homoeostasis, cell proliferation and death. Through alterations in genes, growth factors, signalling pathways and various other mechanisms the tumour is able to continue to grow, avoiding apoptosis and ageing of the cells.

The key properties of cancer have been outlined by Hanahan and Weinberg (2011) [86]. They describe eight 'hallmarks' unique to cancer cells which drive the progression of a pre-malignant neoplasm to a malignant tumour. These hallmarks are 'sustained proliferation', 'evading growth suppressors', 'activating invasion and metastasis', 'enabling replicative immortality', 'inducing angiogenesis', 'resisting cell death', 'reprogramming energy metabolism' and 'evading immune destruction'. The first six hallmarks listed above were outlined in Hanahan and Weinberg's initial work [85]. These hallmarks are mainly associated with the intracellular signalling network that is deregulated and manipulated by the malignant cells to promote their own uncontrolled proliferation and dominance. Hanahan and Weinberg (2011) [86] updated their list to include two new hallmarks, which focus on the micro-environment of the tumour rather than genetic properties. In this thesis, the immune system and its relationship with cancer is of particular interest, featured as one of these new hallmarks. We elaborate on this relationship next.

1.3 Cancer and the immune system

A paradox exists in immune responses to tumours. Although most of the time the immune system productively responds to tumour cells leading to their elimination, a number of processes can lead to inflammatory immune microenvironments that actively inhibits the adaptive T cell response and, can help drive tumour growth and metastasis through modulation of extracellular matrix, production of growth factors and the induction of vascular remodeling.

The ability of the immune system to recognise and eliminate different carcinomas was first proposed by Ehrlich in 1908 [57]. Ehrlich's ideas were developed and formalised as the theory of 'immune surveillance' by Burnet and Thomas (1970) [27]. They stated that cells of the immune system search for and can detect transformed self-cells. Since this theory only describes the initial interactions of immune cells with cancer cells, it can not explain other phenomena such as tumour dormancy where the tumour ceases to grow for long periods of time co-existing with cells of the immune

system, and escape, where tumour cells acquire mechanisms by which to evade the immune system to resume uncontrolled growth.

In 2004, Dunn *et al.* [52] developed a more complete theory to capture these behaviours. His theory of 'immunediting' describes the dynamic interplay between cancer and the immune system which results in either elimination, equilibrium or escape of the tumour. These generic behaviours are exhibited by all of the models presented in this thesis, by design. The immune system can detect and eliminate cancer malignancies in the early stages of development via immune surveillance [27, 176]. However pruning of the malignant cells by the immune cells, leaves behind those cancer cells which are poorly antigenic and poorly immunogenic allowing them to rapidly expand [53]. The malignant cells also shape the local microenvironment by producing immunosuppressive cytokines (e.g. IL-10 and TGF-β). These processes leave behind a suppressive microenvironment which allows the tumour mass to redirect the immune system, creating an ideal environment for tumorigenesis. The three Es of Immunoediting play a central role in this thesis. We summarise each of these phases in Table 1.1 below.

Three Es of Immunoediting	**Description**
Elimination (immunosurveillance)	Identification and partial destruction of the tumour by cells of the innate immune response. This releases tumour antigen which in turn is picked up by activated mature dendritic cells. The dendritic cells then recruit T cells of the adaptive immune response specific to the tumour. These T cells proliferate and move to the tumour site where they eliminate the tumour.
Equilibrium	When elimination is not completely successful the tumour cells remaining enter into an equilibrium with cells of the immune response. This state can last for long periods of time (tens of years).
Escape	Tumour cells mutate at a high rate giving some a selective advantage over the immune response. Specifically a tumour cell that is poorly immunogenic and antigenic will escape detection by the immune response leading to its rapid, uncontrolled proliferation.

Table 1.1: Summary of the three Es of Immunoediting as outlined by Dunn *et al.* (2004) [52].

A number of cyclic steps are required to elicit an effective anti-tumour immune response by the T cell arm of the adaptive immune response. These steps were outlined and summarised as the 'Cancer-Immunity Cycle' in a recent review article by Chen and Mellman (2013) [35]. They include: (1) the release of cancer antigen

upon cancer cell death, (2) presentation of cancer antigen via APCs, (3) the activation of T cells in the lymph nodes (presentation of cognate antigen to the specific T cell), (4) the trafficking of activated T cells through the blood vessels to the tumour tissue, (5) infiltration of the T cells into the tumour, (6) T cell recognition of cancer cells and (7) T cell killing of the cancer cells. This final step leads to the release of tumour antigen (step (1)) and the cycle repeats.

In theory this cycle continues until the tumour has been eliminated. Unfortunately there are many cases where the cycle breaks down, ultimately resulting in tumour escape. Chen and Mellman (2013) [35] summarise at each step how the tumour can break the Cancer-Immunity Cycle. For example, at the priming and activation stages which take place in the lymph nodes, T cells may fail to recognise tumour cells which are poorly immunogenic or poorly antigenic and may not be properly activated due to lack of co-stimulatory signals. Breakdown can also occur at the tumour. First infiltration of the T cells into the tumour may be hindered. Lymphocytes that do manage to infiltrate into the parenchyma of the tumour are often anergised through a lack of appropriate signalling and the presence of a highly regulatory environment. This can drive the formation of an immunosuppressive microenvironment leading to accumulation of regulatory T cells, generating a cycle of anergy and immune suppression in the tumour inhibiting effector T cell responses. The production of cytokines by tumour cells and regulatory cells (e.g. Tregs) signals to the effector T cells to up-regulate their expression of inhibitory receptors (IRs), ultimately damping the T cell's response. High expression of these IRs are found in the tumour microenvironment and are associated with an increasingly dysfunctional state of the T cells [196, 201]. Tumour cells, tumour fibroblasts and antigen presenting cells can be induced to express ligands for immunoregulatory receptors checkpoint inhibitors including programmed death ligand-1 (PD-L1) which binds to and inhibits PD-1 expressing T and NK cells. When the IRs on the T cell are bound with their matching ligands, the inhibitor pathways are activated. As a result, immunoregulatory signalling occurs within the T cell. In turn, normal proliferation is damped, cytokine production is reduced and the T cell killing capacity is diminished. The up-regulation of IRs is a result of signals in the TME as well chronic exposure to high levels of tumour antigen. It is termed 'T cell exhaustion' and was first observed in chronic human and mouse viral infections including lymphocytic choriomengitis virus (LCMV), human immunodeficiency virus (HIV) and hepatitis C virus (HCV) [199]. Regulatory T cells are characterized by the high expression of CTLA-4 and PD-1, the high expression of CTLA-4 may be important in modulating the effector T cell response. The role of T cell exhaustion

in an anti-tumour immune response is the primary focus of the research presented in this thesis.

Besides T cell exhaustion, the tumour also manipulates cells of the innate response to facilitate its own growth. For example, it can halt the normal differentiation of macrophages, dendritic cells and neutrophils, resulting in the development of immature myeloid cells known as myeloid derived suppressor cells (MDSCs). MDSCs are detrimental for an immune response. They promote the differentiation of naive helper T cells into Treg cells. These cells then suppress the activation and proliferation of NK cells and helper and cytotoxic T cells both indirectly, through the production of suppressive cytokines such as TGF-β, and directly, by the secretion of granyzme-B which kills these cells [78].

Other immune cells can differentiate into multiple subtypes whose functions are dictated by their microenvironment. For example, macrophages polarize into either immune promoting (M1 macrophages) or immune suppressing (M2 macrophages) [128]. Macrophages differentiate into an M1 population in the presence of IL-2, TNF-α and IFN-γ cytokines. This promotes helper T cell, cytotoxic T cell and NK cell proliferation. In contrast, in the presence of TGF-β and IL-10 cytokines, M2 macrophages are formed promoting the proliferation of the Treg cell population and other suppressive cell populations promoting tumorigenesis.

Both innate and adaptive arms of the immune system work together to prevent pre-malignant neoplasms developing into malignant tumours. Despite this, the tumour often evades elimination by targeting one or more steps of the Cancer-Immunity Cycle, manipulating the immune system to facilitate its own growth. In the next section, we discuss the current understanding of how T cell exhaustion occurs in cancer, one of the focal points of this thesis.

1.3.1 T cell exhaustion in cancer

T cell exhaustion was first observed in mice with lymphocytic choriomeningitis virus (LCMV) infection [206]. T cell exhaustion was later observed in other chronic infections such as human immunodeficiency virus (HIV), hepatitis C virus (HCV), hepatitis B virus (HBV) and cancer, in both mice and humans [80, 199, 175, 154, 112]. T cell exhaustion is a result of chronic exposure to high levels of antigen.

A distinguishing feature of exhausted T cells is their high and sustained expression of inhibitory receptors such as programmed death 1 (PD-1), cytotoxic T lymphocyte associated protein 4 (CTLA-4), Lymphocyte activation gene-3 (Lag-3), T cell immunoglobulin-3 (Tim-3), T cell immunoglobulin and ITIM domain (TIGIT),

as well as B and T lymphocyte attenuators (BTLA) [199, 7, 14]. Although many parallels can be drawn between T cell exhaustion in chronic viral infections and cancer, the patterns of inhibitory receptor (IR) expression are distinct. This suggests that there may be alternative mechanisms driving T cell exhaustion in the tumour microenvironment [63, 200].

During an immune response against an acute infection, IRs are transiently up-regulated by T cells. Engagement of IRs are vital for preventing auto-immunity (attack of healthy cells) [209]. In cancer and chronic infections such as HIV and HPV, IR expression is sustained [146]. These IRs bind with ligands produced by tumour cells and APCs in the tumour microenvironment sending immunoregulatory signals to the nucleus which then dampens the T cell's function. Of the large number of IRs, the two that have received the most attention are CTLA-4, which acts during the activation phase, and PD-1, which acts during later stages and is expressed primarily by effector T cells to prevent tissue damage [191].

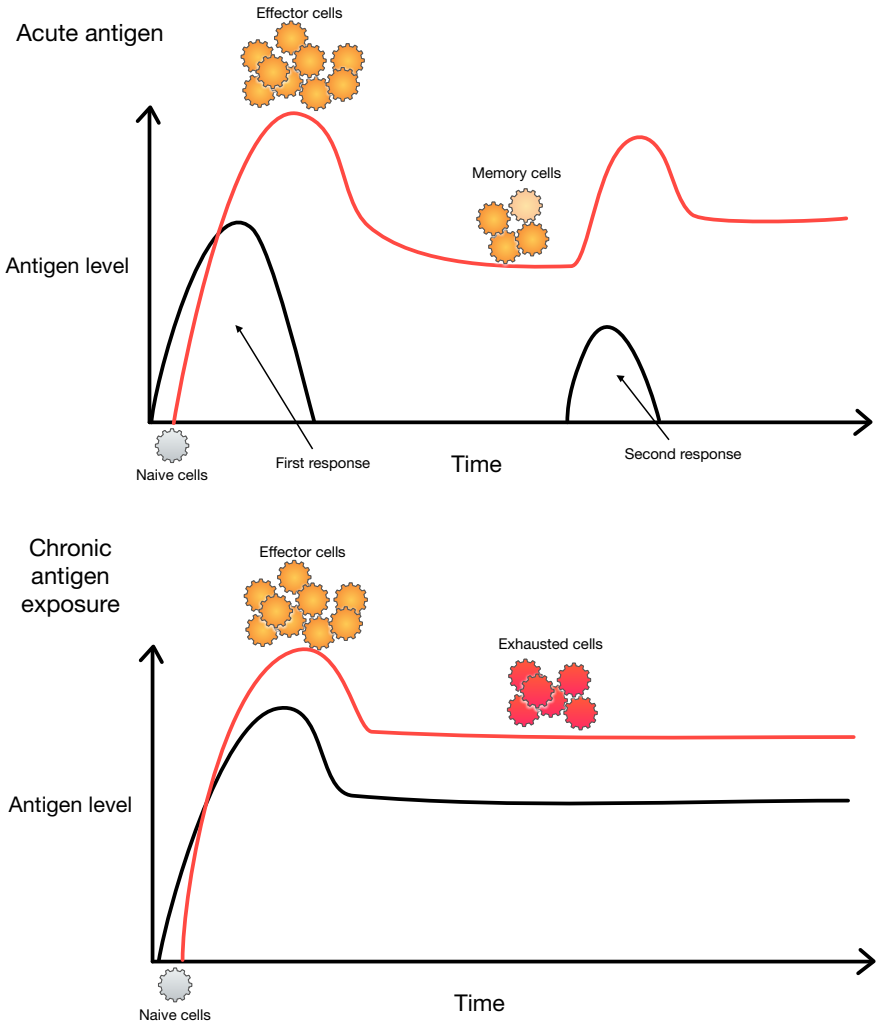

Figure 1.3: Schematic illustrating the long time effects of chronic versus acute antigen exposure on the adaptive immune response.

In addition to the engagement of IRs, other factors contribute to the state of exhaustion of the T cell. Tregs and MDSCs, both present in high levels in the tumour microenvironment, also impact the functional state of the T cells. Like tumour cells, they manipulate the T cell through their production of immunosuppressive molecules such as IL-10, TGF-β, IFN-α and Indoleamine 2, 3-dioxygenase. Additionally, the lack of glucose in the TME affects a metabolic change in the environment which inhibits normal T cell function [18].

Therapies known as checkpoint blockades have recently been employed to block the engagement of IR pathways [125, 146]. Durable outcomes have been observed in a proportion of patients with certain types of aggressive cancer including metastatic melanoma, head and neck cancer, Lynch syndrome tumours and some small lung cell

carcinomas [29, 84]. Response rates are highly variable and highest in melanoma and non-existent in other tumour types. Additionally, dual blockades have yielded stronger responses than the blockade of a single pathway [34, 203]. Such promising outcomes are stimulating a wave of new research focused on harnessing the immune system against cancer. In the next section we discuss several immunotherapies that have been designed to target various stages of the Cancer-Immunity Cycle [35].

1.3.2 Immunotherapies

Although high success rates are often observed in early stage tumours using existing therapies (e.g. chemotherapy, radiotherapy, surgical removal), their potential is limited in more aggressive tumours, often leading to only short term tumour shrinkage and often provide no changes to life expectancy. Cytotoxic treatments (which are non-specific) elicit high toxicity side effects as they do not discriminate between healthy and malignant cells.

The identification of tumour specific antigens has permitted development of therapeutics to stimulate anti-tumour immune responses. These include tumour vaccines, engineered T cell receptor based therapies, bi-specific stimulatory antibodies and chimeric antigen receptors. An advantage of immunotherapies is their potential to prevent relapse through the production of memory cells; an army of adaptive immune cells primed specifically for a particular tumour antigen. Upon re-encounter with the specific tumour antigen, a rapid immune response is mounted due to a population of primed tumour antigen specific immune cells.

Several therapies have been designed to target specific aspects of the anti-tumour immune response. Some of these have shown great promise in pre-clinical studies [135]. Nonetheless the degree of success has yet to be translated into the clinic. Several factors are believed to contribute to the failure in the clinic. These factors include the timing, dosage and administration of the drug, and the limited understanding of the immunosuppressive mechanisms used by the tumour to avoid escape. In this thesis we focus on different approaches to model aspects of immunosuppression and their effect on an anti-tumour immune response. We examine how the timing, dosage and administration of the drug impact recovery.

The recent success and consequent approval of immunotherapies designed to target checkpoint blockades (monoclonal antibodies) have revived research into new immunotherapy designs [132, 145, 150]. These antibodies are designed to block inhibitory receptor pathways which when engaged with their matching ligand (e.g. PD-L1 or PD-L2) dampen the T cell response (e.g. inducing apoptosis of activated T cells,

enhancing the Treg population, and hindering proliferation and cytokine production). A number of antibodies have been designed and approved by the FDA for advanced cancers. For example ipilimumab, an antibody designed to block the CTLA-4 receptor on the T cell, was approved by the FDA for the treatment of patients with advanced melanoma. Approximately 15% and 20% of those treated showed durable responses (extending longer than 2.5 years). Another set of antibodies have been designed and FDA approved to block the PD-1 receptor on the T cell [178]. Two of the most well known include pembroluzimab and nivolumab as treatments for advanced melanoma.

In addition to checkpoint blockades, several novel immunotherapies have been designed to either enhance/boost the immune response or reverse/block the immunosuppressive effects of the tumour. We summarise below examples of each type of immunotherapy (for further details, see the review article of Farkona *et al.* (2016) [61]).

Bi-specific antibodies. T Cell Bispecific (TCB) antibodies have been designed to bind together T cells and tumour cells to stimulate polyclonal activation of the T cells and potent killing of the tumour cells. A TCB bi-specific antibody has two separate functional binding sites, one that binds to CD3ϵ, an invariant component of the T cell receptor complex, and the other binding site being specific for a specific tumour antigen. This type of therapeutic approach bypasses normal check-points that inhibit anti-tumour immune responses, but still depend on successful entry of T cells into tumours and can result in significant off-target toxicological side effects as the normal checks and balances of the immune system are over ridden. These include non-specific activation of the T cell without the need for co-stimulatory signals. Normally T cells must encounter the specific tumour antigen that matches their TCR and also be stimulated with co-stimulatory signals to become fully activated effector T cells. This process can take a significant amount of time during which the tumour can expand in the absence of the immune response. An advantage of this type of therapy is that co-stimulatory signals are not required to activate the T cells and poor TCR affinity will not prevent proper activation of the T cells. In patients with healthy (non-exhausted T cells) such treatment results in enhanced T cell activation, cytokine production and killing capacity [171, 16].

Adoptive T cell transfer. Here, effector T cells are given a boost by expanding the tumour antigen specific population ex-vivo. First circulating or tumour infiltrating T

cells are extracted from the host and those that are specific to the targeted tumour antigen are selected. This pool of cells are then stimulated to proliferate without the constraints of an immunosuppressive environment. Once a substantial population of tumour antigen specific T cells have been generated, they are re-infused into the host. One of the key disadvantages of this therapy is choosing an appropriate tumour antigen to target to avoid creating an army of cells that can kill off healthy self tissue [131]. Nonetheless this therapy has the potential to elicit a potent anti-tumour immune response if the suppressive nature of the microenvironment created by the tumour could be better managed. Although adaptive T cell therapy was developed over 30 years ago its clinical efficacy has been limited by the technical hurdles and the culturing of large numbers of T cells ex-vivo without altering their capacity to home to specific tumours and have cytolytic activity post transfer.

Oncolytic viruses. These viruses select, infect and kill cancerous tissue but do not effect healthy tissue [166]. Although this therapy has the potential for success, the immune system rapidly detects and eliminates the viruses before they can reach the cancer cells. Success depends on suppressing the immune system sufficiently so that the virus reaches the tumour site and expands [167].

Dendritic cell vaccination. Here, circulating dendritic cells are extracted and then expanded, matured and loaded with tumour antigen ex-vivo. These loaded cells are then re-infused into the host as fully functional dendritic cells primed to activate the adaptive arm of the immune system. The maturation of this population, ensured by activating these cells ex-vivo, is a key component of this form of treatment as immature dendritic cells exert immunosuppressive functions. An example of an FDA approved form of this therapy, also used for the treatment of prostrate cancer and melanoma, is sipuleucel-T [97]. Despite the potential for DC based vaccines and FDA approval for sipuleucel there is no clinical evidence that they can lead to long term durable responses, in contrast to check-point inhibitors.

Immunostimulatory cytokines. Here, immunostimulatory cytokines are infused into the host. These signalling molecules can activate a broad immune response, involving both the innate and adaptive arms of the immune response, by creating an environment which supports an anti-tumour immune response. However, these therapies need to be carefully administrated because they can result in an uncontrolled

immune response that can cause organ failure and eventual death of the host.

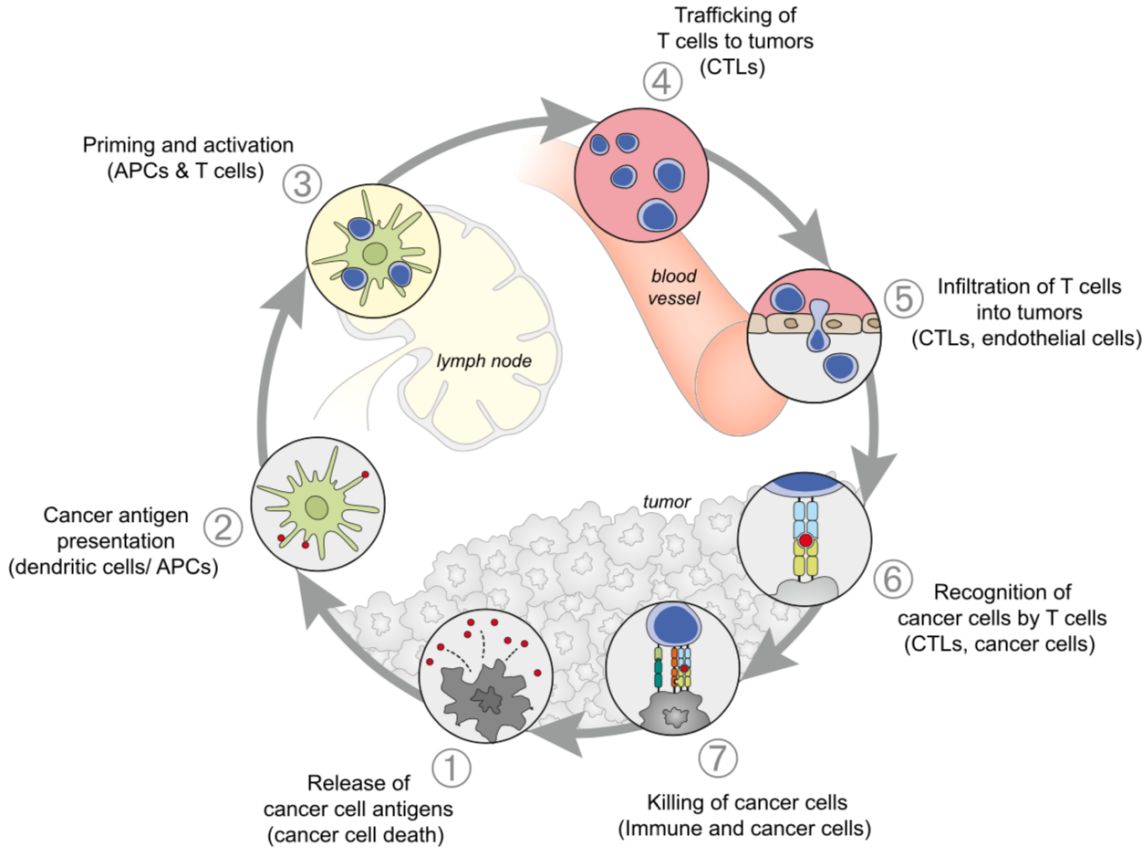

Figure 1.4: Figure illustrating the stages of the Cancer-Immunity Cycle from Chen and Mellman (2013) [35].

To elicit an effective immune response against cancer, each stage of an anti-tumour immune response must be targeted. The key stages of this cycle were outlinded by Chen and Mellman (2013) [35] (see Figure 1.4). Therapies that target the various stages of an effective anti-tumour immune response have been developed (e.g. dendritic cell priming, T cell activation, inhibition of the activation of checkpoint receptors and changing the immunosuppressive microenvironment into a immunostimulatory environment through the addition of particular cytokines) with varying degrees of success. However, these therapies are short lived and are generally unable to eradicate the disease from the host. To elicit long term tumour regression and eventual elimination, combinations of different therapies (both immunotherapies and other therapies such as chemotherapies and radiotherapies for example) are needed. Recent studies have focussed on the efficacy of different treatment combinations. For

example, when Lerret *et al.* (2013) [115] combined radiotherapy with adoptive T cell transfer of the cytotoxic T cell population, they found that advanced breast cancer was in some cases completely eradicated from the host. Further studies are needed to explore other therapy combinations.

1.4 Mathematical models of cancer

Tumourigenesis is a multi-step process initiated by genetic mutations. These mutations induce changes in the signalling circuitry of the cell, affecting behaviour at the cellular and tissue levels. Due to the complexity of the disease, mathematical models may be used to enhance our mechanistic understanding of tumour initiation, progression, invasion and metastases. Theoretical tools are also useful for hypothesis testing and generation as well as in the experimental design (e.g. testing of different drug combinations and patient stratification based on response outcomes).

Tumours are highly heterogeneous entities composed of both progenitor and more mature cancer cells. The heterogeneity observed within a tumour is generated by epigenetic, genetic and environmental factors. To attempt to understand the complexity of tumour growth, a variety of modelling approaches are used to study cancer dynamics. Such approaches are either deterministic or stochastic in time, and are either continuous, discrete or homogeneous in space. All variations are possible. The choice of modelling approach is typically tailored to the question being addressed. For example, continuum approaches may be used to capture population level dynamics (considering cell densities at a tissue level and modelling vascular growth, diffusion of chemicals and growth factors present in the environment), as well as subcellular dynamics. On the other hand, discrete models tend to focus on cell-cell interactions as well as interactions between cells and their microenvironment. Furthermore there are hybrid models that combine both approaches and can be either deterministic or stochastic in time. Stochastic time dependence has been used to model dynamics arising from molecular changes (e.g. genetic mutations) and mutations associated with age and external factors such as smoking and exposure to ultra-violet radiation [24] (see Durrett (2015) [54] for a recent review).

In studies of interactions of the tumour and its microenvironment, continuum approaches have often been adopted. Such models account for growth factors and chemical nutrients at the tissue level. Cytokines, chemokines and/or nutrients may induce chemotaxis, cell proliferation and movement. A number of models to date assume spatial homogeneity for simplicity and model cell populations and chemical

concentrations in an ordinary differential equation (ODE) framework. These ODE models have been used to address fundamental questions in cancer dynamics. For example ODE models have been used to study angiogenesis [168] as well as interactions between tumour and immune cells [56]. Partial differential equation (PDE) models allow variation in space and time as well as other dependent variables such as age and size. These PDE models have been commonly used to study various stages of tumour development from the early avascular stage [32, 162] to the later vascular [26, 28] and invasive stages [75]. PDE models typically focus on one or two spatial dimensions. They may exhibit travelling wave solutions and other spatial patterns depending on model parameters [142].

Finally hybrid models, combining discrete and continuum (with or without stochastic effects) approaches, can capture dynamics arising from interactions occurring across multiple scales i.e. from the molecular to tissue level [44, 8, 120]. For example Anderson *et al.* (2006) [10] proposed a model of tumour invasion that accounts for both clonal evolution of cancer cells and interactions with the microenvironment. Hybrid models are computationally expensive and do not facilitate mathematical analysis. Other hallmarks of cancer [85, 86] such as the induction of angiogenesis have been studied through mathematical models [33]. The literature now is too large to review all models. Instead, we focus on mathematical models developed to study aspects of the anti-tumour immune response.

1.4.1 Models of tumour-immune cell interactions

Most existing models consist of two coupled time-dependent ODEs based on predator-prey systems, with the tumour cells as the 'prey' and the immune cells as the 'predators' [110, 119, 65, 147, 202]. With just two dependent variables it is possible to characterise both the local and global stability of steady states via a phase-plane analysis, as well as the bifurcation structure as model parameters vary.

As our understanding of the intricate network that constitutes the immune system has increased, other modelling approaches have been used to study immune-tumour dynamics [1]. These include

- delay differential equations, in which time delays account for the apparent time between initial encounter of a naive T cell with its matching antigen and the effector response [46, 159];
- PDE models which account for spatial heterogeneity [130, 129];

- agent based models (or cellular automata) which account for the phenotypic plasticity of tumour and immune cells and their interactions [15];
- kinetic theory models which account for heterogeneous cell populations that interact stochastically [20];
- multiscale models which account for interactions between subcellular, cellular and tissue scale processes [126, 144, 183] .

Note most of these models focus on the early avascular stage of tumour development. This is the approach adopted in this thesis.

1.4.1.1 Continuum models

Continuum models are used to study interactions involving large numbers of cells, allowing the dynamics to be examined more efficiently than is possible for analogous discrete models. Such models can be either deterministic or stochastic in nature. Deterministic models include ODEs, where the tumour environment is assumed to be well-mixed (spatially homogeneous), and PDEs, where spatial effects are accounted for. In both cases, populations of tumour cells and cytotoxic T cells are not normally subdivided into distinct states. This thesis introduces new models which account for heterogeneity in tumour and cytotoxic T cells, modelled by ODEs.

Ordinary Differential Equations (ODEs)

ODEs have been widely used to study the interactions between the immune system and cancer cells (see Eftimie *et al.* (2011) [56] for a comprehensive review). One of the pioneering ODE models, which has since been adopted and modified by a number of authors [130, 108, 42, 180, 161], was proposed by Kuzentsov et al. (1994) [110] to understand tumour dormancy and to explain how the tumour escapes from this state. The model focuses on the interactions between cytotoxic immune cells (cytotoxic T cells or natural killer cells) and tumour cells and includes estimates of some model parameters from a study of B cell lymphoma (BCL) in mice. For specific choices of model parameters and for typical numbers of effector cytotoxic T cells, the model predicted that the immune cells can control the growth of the tumour if the number of tumour cells is below a critical value; otherwise, the tumour escapes. They observed that the rate of T cell inactivation determines the transition from a dormant to an escape state. This model was recently modified by Roesch *et al.* (2014) [161] to study the role of the immune system in the response to treatment with chemotherapy and to explain why intensive chemotherapy treatments can have adverse effects on

tumour control. They modified Kuznetsov's model so that the immune cells only interacted with the outer surface of the tumour. Their model explains the variations observed in patient outcomes as a function of the initial tumour size, immunogenicity, tumour growth rate and the sensitivity of the tumour to chemotherapy. Variations in these parameters can explain all of the behaviours observed in five different treatment regimes.

To explore the role of additional components of the immune system in tumour-immune dynamics, further variables must be considered. De Pillis *et al.* (2005) [41] included natural killer cells, the innate analogue of the cytotoxic T cell population (in addition to cytotoxic T cells and tumour cells), and validated their results against experimental data from murine and human studies. They concluded that natural killer cells require the additional help of the cytotoxic T cells to drive the system to tumour elimination. In their model immunosuppressive effects used by the tumour to subvert the immune response were neglected.

Advances in quantitative approaches including single cell RNAseq, multi-dimensional imaging and cytometry provide tools to develop parameterized models, providing a basis for developing the next generation of immunological models. In the models discussed above, parameters were estimated from fitting the results to experimental and clinical data, where available. Due to limitations in data and the difficulty in obtaining them, other models have taken a more theoretical approach by looking at simple systems of equations to determine how specific steady states depend on key parameters [22]. Confronted with the same problem, in this thesis we adopt a similar approach to Besse *et al.* (2017), identifying regions of parameter space which give rise to expected behaviours (see Table 1.1).

The role of immunosuppression on tumour escape has been the focus of several models [160, 114, 100]. Robertson-Tessi *et al.* (2012) [160] proposed a detailed mathematical framework (twelve ODEs) describing interactions between multiple cell types and cytokines involved in an immune response to cancer, capturing the three Es of immunoediting [52]. Here helper T cells were subdivided into three distinct subpopulations based on their maturity (pre-activated state, effector and memory states). Their aim was to determine which aspect of the immune response is dominant at different stages of tumour development, and which immunosuppressive effects facilitate tumour escape. Their analysis was limited to numerical simulations rather than analytical identification of the steady states and their linear stability. A simpler version of this model is developed in this thesis enabling a comprehensive study of immunosuppression. This model encapsulates many regulatory components of the immune

response through a model of T cell exhaustion, while still capturing the three Es of immunoediting.

Not only do mathematical models have the capacity to identify key factors driving tumour escape but they can also be used to classify patients and predict response outcomes with or without treatment. Such models have the potential to identify the best therapeutic regime for an individual, for example the combination of therapies to be given and how they should be delivered [107]. Kirschner and Panetta (1998) [102] were among the first researchers to examine the effects of immunotherapy using an ODE model of tumour cells, cytotoxic T cells and the cytokine IL-2. Two different immunotherapies, both designed to boost the immune system, were examined. They concluded that IL-2 therapy alone could not drive the system to a tumour-free state but, interestingly, adoptive T cell transfer alone or in combination with IL-2 therapy could.

Since then, a number of models of tumour-immune interactions have included the effects of various immunotherapies to understand when (if at all) these therapies drive a patient destined for tumour-escape to either a tumour-free or tumour equilibrium state without prompting an overzealous immune response [65, 103, 48]. Nani *et al.* (2000) [140] proposed a system of four ordinary differential equations to model healthy cells, tumour cells, cytotoxic T cells and a cytokine, exploring the effects of adoptive T cell therapy on the dynamics by considering the steady states and their linear stability. In separate work, Kronik *et al.* (2010) [108] focused on a vaccination therapy targeting the dendritic cells of the innate immune response for patients with prostrate cancer, validating their model against patient data. In addition to models that describe immunotherapy and the effect of boosting the immune system, other models have explored the synergistic effect of different therapies. For example De Pillis *et al.* (2006) [40] investigated the combined effects of chemotherapy and immunotherapy and identified situations in which the individual therapies were unable to eliminate the tumour, but their combination, could eliminate it. Likewise in this thesis, we examine the effects of single and combined therapies on tumour escape, novelly including an exhausted T cell population.

Partial Differential Equations (PDEs)

PDE models of tumour-immune interactions have been developed to account for cell movement driven by chemotaxis and random motility. These reaction-diffusion models are typically limited to Cartesian or radially symmetric geometries [3, 129, 130, 142]. Such models have been developed to study various aspects of the immune

response, such as interactions between macrophages and a growing tumour mass [142, 143]. Many spatial models have their foundations in the pioneering work of Kuznetsov *et al.* [110] (see for example [130, 3, 129]). Matzavinos *et al.* [130] extended the work of Kuznetsov *et al.* by including diffusive and chemotaxis terms to describe cell movement. They found quasi-stationary heterogeneous spatial patterns, which reduce to limit cycle solutions in the corresponding spatially homogeneous system. They identified critical parameters in which a small number of cancer cells exist for an extended period of time before the tumour begins to rapidly grow.

PDE models have also been used to study the effects of immunotherapies on the dynamics of an anti-tumour immune response. Joshi *et al.* (2009) [96] formulated a model to study solid tumour growth in the context of an immune response when treated with adoptive T cell therapy and a cancer vaccine. This enabled them to determine effective treatment protocols. Their model extended the model of Matzavinos *et al.* [130] by including a generic APC of the innate immune response. They found that adoptive T cell therapy promoted tumour cell growth, confirming behaviour observed experimentally. Moreover they found that cancer vaccines targeting the APCs reduced the tumour's growth rate and prevented re-emergence from a tumour dormant state. Due to complexity of human immune responses this has not yet translated into clinical success.

1.4.1.2 Discrete models

Continuum approaches are useful for understanding the behaviour of large populations of cells. However, such approaches do not resolve detail at the cell level and thus fail to describe behaviours that arise from interactions between small numbers of cells (where random fluctuations can influence outcomes). In such cases discrete models are useful. In discrete models each element (e.g. a cell) typically requires a number of rules (which may or may not be probability based) to decide both individual cell behaviour and local interactions, often nearest neighbour. These models can be computationally expensive when many rules are included and/or many elements are considered.

Discrete models can be either on-lattice, where cells are confined to move on a grid of finite size, or off-lattice, where cells move freely through space and time. We describe below the two main approaches that have been used to model tumour-immune interactions: agent based models and kinetic theory models.

Agent Based models

Kim *et al.* (2012) [101] developed an on-lattice, agent-based model to describe interactions between tumour and cytotoxic T cells and coupled these to a system of delay differential equations to describe T cell activation in the lymph nodes. The model was used to investigate whether memory T cells, primed against a specific tumour antigen, could prevent the outgrowth of a tumour and, if so, how many primed cells would be needed to prevent tumour development. They found that the effectiveness of the T cells in eliminating the pre-malignant tumour mass depends on the time taken to detect the malignant cells, and the time taken to eliminate the neoplasm. Baar *et al.* (2016) [15] used an off-lattice approach to study the effect of immunotherapy on melanoma. They considered stochastic interactions of cytotoxic T cells, cytokines and tumour cells, accounting for phenotypic switches and genetic mutations of the tumour cells. Two different timescales were identified in their model: fast genotypic switches and rare genotypic switches. They concluded that large stochastic fluctuations may hinder the success of therapy. More recently, Macfarlane *et al.* (2018) [121] developed an on-lattice agent-based model distinguishing the type of random motion exhibited by inactive and active T cells (Lévy versus brownian). Their model included dendritic cells, cytotoxic T cells and tumour cells. They find their model is able to reproduce, qualitatively, observed spatial patterns in experimental data. They conclude that increasing the dendritic cell population can hinder effective tumour removal due to space limitations reducing the number of cytotoxic T cells that may be present in the tumour microenvironment. Their results suggest that therapies designed to target the activation stage may not have a significant effect on the anti-tumour immune response.

Kinetic theory

Kinetic theory with its origins in molecular dynamics has been used as a way to account mathematically for the stochastic nature of interactions between individual cells, for example genetic changes and cell to cell interactions [13, 21, 19]. The approach is similar to that of modelling gas particles. Here an evolution equation is proposed which describes the statistical (probability density) distribution of the internal state of individuals, which governs how the individuals interact with others around them. This approach allows one to model interacting heterogeneous cell populations and examine emerging collective behaviour. Bellomo *et al.* (1994) [20] were the first to propose a generalised kinetic theory framework to model the interactions between different populations of tumour and immune cells, introducing heterogeneity through their activation state. Since then, similar models have been developed to

study for example the competition between cells of the immune system in tumour progression. A summary of such models is given in [19].

1.4.1.3 Hybrid and multi-scale models

Hybrid and multi-scale approaches, combining discrete and continuum methods, capture interactions occurring at different scales (e.g. from the molecular to the tissue level) between tumour and immune cells. Here information at both the microscopic and the macroscopic scales are accounted for. These approaches have been widely used to study various aspects of cancer growth [155].

Mallet *et al.* (2006) [126] developed a hybrid model of tumour-immune dynamics. In addition to tumour cells and host cells, the model includes two populations of immune cells — natural killer cells (innate immune response) and cytotoxic T cells (adaptive immune response). The behaviours of each cell type are described by a cellular automata (CA) model enabling them to study the early formation of a neoplasm, where there are small numbers of tumour cells, followed by the later stages of tumour development. At the macroscopic scale, the nutrients needed for the proliferation and survival of all four cell populations were modelled by two reaction-diffusion equations. For simplicity they considered a two-dimensional domain. They demonstrated that, in the absence of an immune response, the growth of the tumour mirrors what was observed experimentally. In the presence of an immune response, the model exhibits oscillitory behaviour similar to that seen in ODE models of tumour-immune interactions (see e.g. [110]). Their model captures the three Es of immunoediting depending on the rates of T cell infiltration and death.

Alemani *et al.* [4] proposed an alternative approach to the classic CA-PDE model to capture behaviours occurring at the microscopic and macroscopic scales. They argued that information is lost when trying to bridge probabilistic and deterministic approaches. They used the Lattice Boltzmann (LB) method to capture effects occurring at the macroscopic scale, instead of a deterministic PDE approach. As in [126] they used a hybrid approach to model interactions between tumour cells, natural killer cells and cytotoxic T cells, in the presence of a nutrient source modelled by the LB method. They also included a population of necrotic cells and thereby captured the three layers of an avascular tumour: a necrotic layer, a quiescent layer (containing necrotic and live cancer cells) and a proliferative layer (containing live cancer cells). They concluded that their model is able to capture patterns observed clinically such as tumour border irregularity and tumour patterns in the shape of fingers. They find that these shapes depend on the rate of uptake of nutrients by the tumour cells

and the probability of necrosis, respectively. They further find that the immune cells accumulate around the edge of the tumour close to the source of nutrients.

1.4.2 Summary

Mathematical models are important tools which have been widely used in cancer research to test hypotheses and make predictions. The predictions made from mathematical models may in turn generate new hypotheses thereby providing a two way feedback. For example DePillis *et al.* (2005) [41] developed a model around available experimental data suggesting that the kill function of natural killer cells and cytotoxic T cells differ significantly. They concluded that further experimental work is required to determine if this is behaviour is robust.

Although the amount and quality of experimental and clinical data have increased significantly over the last decade, a broader range of variables at a higher sampling frequency needs to be acquired to improve model fitting. To bridge this gap, more interdisciplinary collaborations between clinicians, engineers, physicists and mathematicians are essential. This has been recently highlighted by Anderson *et al.* (2013) [9] in a Royal Society Interface focus article titled 'Mathematics of the Integrative Cancer Biology Program'. They argue that mathematical models are vital for understanding experimental data, providing a detailed picture of both spatial and temporal processes that is out of reach experimentally. In this way, they argue that mathematical models can drive experiments as well as interpret experimental findings.

The proliferation of models and model types summarised in this introduction illustrates that there is no consensus in the mathematical biology community on the most useful approaches to model cancer-immune dynamics. This may only be resolved by substantially more and higher quality clinical data coupled with closer collaboration between theoretical and clinical researchers.

1.5 Thesis overview

The main thrust of the research presented in this thesis is to develop and analyse simple mathematical models describing the interactions between tumour and immune cells, with a focus on the T cell arm of the adaptive immune response. All three models developed in this thesis address the heterogeneous character of the tumour and immune cell populations. Heterogeneity manifests itself in several ways. We specifically explore heterogeneity in (1) T cell subpopulations (helper and cytotoxic T cells), (2) states of T cell exhaustion (affecting T cell killing, infiltration and proliferation),

and (3) subpopulations of tumour cells and cytotoxic T cells. The models developed generate new insight into key mechanisms of immunosuppression for a broad range of patient specific traits, such as the rates of T cell infiltration, tumour growth, and tumour counter-attack. The models also identify potentially effective immunotherapy treatments.

One of the greatest problems faced in cancer research today is our limited understanding of various aspects of heterogeneity in the tumour mass. In this thesis we pose three questions which are addressed through the development of three distinct ordinary differential equation (ODE) models. These questions are:

1. Given disagreement in the field about the importance of helper T cells in either facilitating or suppressing tumour growth, what is the relative effectiveness of cytotoxic versus helper T cells in controlling tumour growth?

2. How do the rates of exhaustion of individual T cell functions, specifically their killing, infiltration and proliferation rates, suppress or facilitate tumour escape?

3. Given that infiltrating T cell populations exist in various functional states, how do the ratios of exhausted to functional T cells and immune-resistant to non-resistant tumour cells affect tumour escape?

In this thesis we address these questions by adopting a theoretical approach, using ordinary differential equation (ODE) models. This is arguably a necessary first step in understanding the exceedingly complex factors at play in tumour-immune dynamics. This approach enables one to readily identify regions of parameter space associated with distinct dynamical behaviour. The models also may be valuable for designing future immunotherapies, and in particular explain why certain approaches may fail for certain patient groups. The models also suggest that certain combined therapies may be promising. To be confident in the hypotheses made regarding the key mechanisms of immunosuppression, time-series data from patients with immune systems in various states of health for varying cancers (more or less aggressive) are necessary. Such data would enable us to fit the model parameters, confirming or disproving our conclusions.

This thesis builds a series of models which attempt to balance mathematical tractability and biological realism. As such, they allow a comprehensive exploration of immunosuppression in tumour-immune dynamics. The ODE models developed are designed to have the fewest parameters possible to make it practical to fully explore the model dynamics. This stands in contrast to a number of other models studying immunosuppresion. For example, the model of Robertson-Tessi *et al.* (2012) [160],

which consists of 12 ODEs and 41 parameters, can only be studied numerically and for limited parameter variations. The novelty of the approach taken in this thesis is to reduce such complex models to their essential features, encapsulating a wide range of immunosuppressive features. While this approach, will by design never be fully accurate, it allows one to go further in identifying key aspects of tumour-immune dynamics.

Chapter 2 addresses question (1) above by extending the predator-prey model of tumour and cytotoxic T cells originally developed by Kuznetsov *et al.* [110] to include a helper T cell population, implicitly accounting for the increasing immunosuppressive pressure of the tumour as it increases in size. We study the model by first examining its qualitative behaviour, identifying where in parameter space the model exhibits the three Es of immunoediting. We then determine the model attractors by identifying the steady states and their linear stability. We further identify a stable limit cycle emerging from a Hopf bifurcation along a steady state branch of solutions. This limit cycle is described analytically by a weakly nonlinear analysis near its point of emergence.

In Chapter 3, to address question (2) above, a constellation of immunosuppressive pressures are modelled by mimicking their effects on T cell exhaustion. T cell exhaustion is accounted for through diminishing rates of T cell infiltration, killing and proliferation, in proportion to the size of the tumour. This allows us to distinguish the role of these T cell functions in tumour escape. As in the previous chapter, we first explore the qualitative behaviour, identifying regions of parameter space exhibiting the three Es of immunoediting. This is done largely numerically due to the complexity of the model equations. A reduced model is therefore analysed in which the T cell functions are combined into a single variable. This permits substantial analytical progress, including a detailed map of the existence of steady states as a function of parameters. It also enables us to identify and describe a stable limit cycle solution from its point of emergence to its point of disappearance.

In Chapter 4, to address question (3) above, salient aspects of the heterogeneity explored in the previous two chapters are combined to study heterogeneous populations of both tumour and immune cells. This model includes subpopulations of immune-resistant and immune-sensitive tumour cells, as well as subpopulations of cytotoxic and exhausted T cells (cytotoxic T cells in two different functional states). Following the approach adopted in the previous chapters, we first explore the qualitative behaviour to identify the regions of parameter space exhibiting the three Es of immunoediting. We go on to identify steady states and their linear stability. Notably,

limit cycle solutions are not observed. Through a recasting of the steady state equations, in which the fractions of immune-resistant to total tumour cells and exhausted to total T cells at steady state are taken as parameters, a comprehensive map of the model behaviour is obtained. This approach provides two patient specific parameters associated with a tumour equilibrium state (dormant or malignant). The long term fate of a perturbed tumour equilibrium state is explored showing how the cell population fractions and associated patient specific parameters dictate whether a tumour is eliminated, settles to a dormant state, or escapes. We conclude this chapter by mimicking the effects of two immunotherapies, a TCB antibody and an IL-2 therapy, both singularly and in combination.

The overall conclusions are presented in Chapter 5. We consider the balance between mathematical tractability and realism, as well as the effects of heterogeneity and immunosuppression. The latter is distinguished by tumour type and patient groups. We consider also the implications of the present results for the advancement of novel cancer treatments using the immune system, and how, with appropriate data these results could be confirmed and used to test various treatment protocols. We end with a discussion of possible model extensions. These include for example an examination of spatial variations of T cells and tumour cells which are known to play an important role at macroscopic scales.

Chapter 2

A model of cytotoxic and helper T cell interactions in a tumour environment

The research in this chapter has been published in the special issue of Letters in Biomathematics: *Modeling Tumor-Immune Dynamics, Disease Progression, and Treatment* (2018) [50].

2.1 Introduction

To provide mechanistic insight into the 'Hallmark' properties driving tumour progression outlined by Hanahan and Weinberg (2011) [86], a wide range of mathematical models have been developed. These models have been used to examine all stages of tumour development, from the early stages of tumour initiation and progression, to later stages of development where the tumour micro-environment becomes important [6]. The focus in this thesis is to provide insights into the ways a tumour may bypass immunosurveillance and ultimately escape. For this purpose, we develop mechanistic models of the tumour micro-environment and the interaction between tumour cells and cells of the immune system, specifically T cells of the adaptive arm.

T cells are one of the most important components of the immune system in the fight against cancer. There are two populations of T cells, helper and cytotoxic, which are distinguished by their expression of CD4 and CD8 proteins, respectively. Naive helper T cells are activated by antigen presented with a major histocompatibility complex (MHC) class II molecule by an antigen presenting cell (APC). Naive cytotoxic T cells are activated by antigen presented with an MHC class I molecule. Once activated the helper and cytotoxic T cells perform complementary functions to

eliminate the tumour. Helper T cells further differentiate into subpopulations classified by the specific cytokines that they produce. In this way, they regulate multiple aspects of an immune response. For example, they promote the proliferation of cytotoxic T cells, they recruit and promote the proliferation of cells of the innate immune response and, consequently they control levels of inflammation at the tumour site [92, 124]. (In this work, we do not distinguish these subpopulations.) Cytotoxic T cells scan peripheral tissues for virally infected and transformed cells, upon antigen specific stimulation through peptide - MHC - TCR stimulation, the target cell can be killed.

Most experimental and clinical studies have focused on the role played by cytotoxic T cells in tumour elimination [66] and neglected the role of helper T cells [91, 153]. Recently, several authors have argued that helper T cells form a vital component of an anti-tumour immune response [17, 124, 190]. In this chapter, we focus on the complementary roles played by effector helper and cytotoxic T cells as cytokine producers and tumour cell killers respectively. For simplicity, unlike Robertson-Tessi *et al.* (2012) [160] we do not consider naive and memory helper and cytotoxic T cell populations. Our focus is to identify which T cell population should be targeted to boost the anti-tumour actions of helper and cytotoxic T cell populations in the tumour micro-environment.

A number of novel immunotherapies have been designed to either enhance/boost the immune response or reverse/block the immunosuppressive effects of the tumour. In this work we focus on adoptive T cell transfer therapy. This therapy overrides inhibitory signals releasing the repertoire of tumour antigen specific T cells to undergo effector function [163, 165]. Most therapies target the cytotoxic T cells which are able to recognize and directly kill tumour cells. Work needs to be done to explore the potential of targeting the helper T cell population instead of, or in addition to, the cytotoxic T cell population [207], and is the focus of this chapter.

Many existing ODE models view tumour-immune interactions as a predator-prey system, where the tumour cells are the prey and the immune cells are the predators [110, 119, 65, 147, 202]. The helper T cell population has been included implicitly and explicitly in past theoretical studies. Kirschner *et al.* [102] proposed a system of three ODEs for the cytokine IL-2 produced by the helper T cells, cytotoxic T cells and tumour cells. The inclusion of the cytokine IL-2 can be thought of as implicitly accounting for the helper T cell population. They found that the tumour antigenicity is a critical parameter determining whether tumour escape, equilibrium or elimination occurs. They also identified stable periodic solutions, mirroring clinical observations

of tumour suppression and regrowth. Robertson-Tessi *et al.* (2012) [160] proposed a detailed mathematical framework (twelve ODEs) describing interactions between multiple cell types and cytokines involved in an immune response to cancer, capturing the three Es of Immunoediting [52]. Here helper T cells were explicitly included and further subdivided into three distinct subpopulations based on their maturity status (e.g., naive, effector, memory). Their aim was to determine which aspect of the immune response is dominant at different stages of tumour development, and which immunosuppressive effects facilitate tumour escape. However due to its complexity, investigation of the model was limited to numerical simulations rather than analytical identification of the steady states and their linear stability.

In this chapter, a simplified ODE model accounting for the interactions of tumour cells with helper and cytotoxic T cells is developed. Specifically the model presented in this chapter is designed to address the following question:

- Given disagreement in the field about the importance of helper T cells in either facilitating or suppressing tumour growth, what is the relative effectiveness of cytotoxic versus helper T cells in controlling tumour growth?

The model proposed in this chapter extends the pioneering study of Kuznetsov *et al.* (1994) [110] by including helper T cells and accounting implicitly for immunosuppressive effects. Kuznetsov *et al.* considered just two components: a tumour population and a cytotoxic immune population. The simplicity of their model enabled them to fit parameters against experimental data for mice. The model was used to identify the conditions that would lead to tumour escape from a dormant tumour state. Our proposed model also draws on key components of the more complex model developed by Robertson-Tessi *et al.* [160] that included both helper and cytotoxic T cells in an anti-tumour immune response, and examined the impact of different effects of immunosuppression at various stages of tumour development. The simpler model proposed here has the advantage of being analytically tractable while retaining both a helper T cell population in addition to a cytotoxic T cell population and implicit forms of immunosuppression. This permits the identification and characterization of the stability of steady states as a function of model parameters, as well as the derivation of an amplitude equation to describe time-dependent oscillatory solutions observed from numerical integration of the model equations. As clinical trials have shown that the level of tumour infiltrating T cells correlates with patient outcomes [113, 98, 91], we focus on understanding how changes in the rates of infiltration of cytotoxic and helper T cells affect the model dynamics. This model reveals that the

three Es of immunoediting depend highly on the infiltration rates of the helper and cytotoxic T cells. The results identifying where in parameter space tumour elimination, equilibrium and escape occur are used to identify conditions under which cytotoxic and/or helper T cells should be targeted by adoptive T cell therapy. We find that the parameters associated with immunosuppression play a decisive role in tumour-elimination.

The remainder of this chapter is organised as follows. We formulate our mathematical model in Section 2.2, while in Section 2.3 we present simulation results that show how our model captures the three Es of immunoediting; the model can exhibit oscillatory solutions which we view as equilibrium solutions since the tumour cell number remains bounded at all times. In Section 2.4 we identify the steady state solutions, and indicate those regions of parameter space in which multiple steady state solutions exist. In Section 2.5 we describe both the local linear stability and the global nonlinear stability of the steady state solutions. In Section 2.6 we examine system bifurcations as the rate of infiltration of the cytotoxic T cells is varied. Here we identify a Hopf bifurcation from a branch of oscillatory solutions which emerges from a small tumour steady state solution branch. In Section 2.7, we confirm the existence and stability of the associated limit cycle and determine its amplitude by performing a weakly nonlinear analysis in the neighbourhood of the Hopf bifurcation. In Section 2.8 we perform a parameter sensitivity analysis, focusing on how the tumour's growth dynamics change as parameters controlling the immunosuppressive effects of the tumour are varied. The chapter concludes in Section 2.9 where we summarise the key results, discuss their therapeutic implications, and outline directions that merit further investigation.

2.2 The Mathematical Model

2.2.1 Model development

We propose a system of three, time-dependent, ordinary differential equations (ODEs) to model the interactions between cytotoxic and helper T cells and tumour cells in a well-mixed (*i.e.* spatially uniform) tumour microenvironment (TME), see Figure 2.1. With t denoting time, the dependent variables $N(t)$, $T_H(t)$, and $T_C(t)$, represent numbers of tumour cells, and helper and cytotoxic T cells respectively.

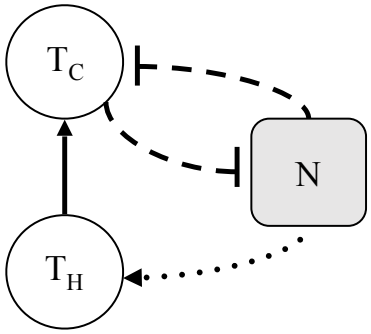

Figure 2.1: Schematic of the tumour-immune cell interactions included in equations (2.11)–(2.13). The circles indicate the helper and cytotoxic T cells, $T_H(t)$ and $T_C(t)$. The square symbol represents the tumour population $N(t)$. Interactions that directly increase a population are indicated by continuous lines while suppressive interactions are illustrated by dashed lines. The dotted line indicates an interaction that is immune promoting in the presence of a small tumour burden becoming immunosuppressive in the presence of a large tumour burden.

We assume that the evolution of the tumour cell population is dominated by cell proliferation and cell death (due to interactions with cytotoxic T cells). Guided by previous studies which have shown that tumour growth can be described by simple, phenomenological growth laws (e.g. exponential, Gompertzian, power law, logistic [76, 170]), we here assume that, in the absence of an immune response, the tumour grows logistically, with carrying capacity κ (units: number of cells) and growth rate γ (units: day^{-1}). This growth law places an upper bound on the tumour size (assuming $0 \leq N(0) < \kappa$ where $N(0)$ is the size of the tumour at time $t = 0$). Consequently, we interpret the system settling to a large number of tumour cells ($N \approx \kappa$) close to its carrying capacity as tumour escape. The simpler model of exponential growth appears to be problematic. The problem surfaces when considering steady states for which the cytotoxic T cell population is independent of the tumour population. By contrast in the logistic growth model the T cell population decreases to zero as the tumour population increases towards its carrying capacity, as expected.

We assume further that once an immune response has been stimulated, the tumour cells come into contact with cytotoxic T cells at a rate which is proportional to the product of their cell numbers, with constant of proportionality k (units: number of cells^{-1} day^{-1}), and that such contacts lead to tumour cell death, with probability p, or inactivation of the cytotoxic T cell, with probability $(1 - p)$. Combining these processes, we propose the following ODE for the time evolution of the tumour cells:

$$\frac{dN}{dt} = \underbrace{\gamma(1 - N/\kappa)N}_{\text{logisitic growth}} - \underbrace{pkT_C N}_{\text{immune induced death}} . \tag{2.1}$$

We assume that the evolution of the helper and cytotoxic T cells is dominated by infiltration from the lymph nodes, proliferation in response to the tumour population and natural cell death. Note that T cell proliferation actually occurs in the tissue draining lymph nodes, however for simplicity we assume here that T cell proliferation occurs in the tumour. We assume that the two T cell populations infiltrate the tumour tissue from the lymph nodes at constant rates σ_H and σ_C (units: number of cells day^{-1}), and die at rates δ_H and δ_C (units: day^{-1}). Naive T cells are regularly produced by hematopoietic stem cells and therefore a constant population of these naive T cells are present in the circulating blood stream. We can assume that the flow of blood is constant and therefore, in addition to direct stimulation of T cells in the presence of tumour antigen, there is a constant influx of primed T cells from the circulating blood. Furthermore, this assumption enables us to implicitly account for the presence of a constant pool of memory T cells present in the absence of antigen stimulation [60]. This approach has been widely adopted in similar models to account for a background level of circulating T cells [110, 41, 56]. We suppose that immunosuppressive processes induced by the tumour affect the proliferation of the helper T cells and, consequently, the activation of the cytotoxic T cells. Specifically we assume that the helper T cells proliferate at a rate which has biphasic dependence on the number of tumour cells, $N(t)$, with constant of proportionality α (units: day^{-1}). The parameter $\tilde{N}$ (units: number of cells) is the number of tumour cells at which helper T cell proliferation is half-maximal. The proliferation rate (per T_H cell) attains a maximum value of $\alpha/2$ when $N = \tilde{N}$ and decays to zero as $N \to \infty$. A similar biphasic term has been adopted in a related study [174]. Additionally, through their production of cytokines (e.g. IL-2, IFN-γ), helper T cells play an important role in instigating and sustaining the proliferation of cytotoxic T cells [153, 2]. We account for these effects by assuming that cytotoxic T cells proliferate at a rate proportional to the product of the helper and cytotoxic T cells, with constant of proportionality β (units: number of cells^{-1}day^{-1}). Combining these additional processes, we propose the following ODEs to describe the time evolution of the helper and cytotoxic T cells:

$$\frac{dT_H}{dt} = \underbrace{\sigma_H}_{\text{infiltration}} + \underbrace{\frac{\alpha \tilde{N} N T_H}{\tilde{N}^2 + N^2}}_{\text{proliferation}} - \underbrace{\delta_H T_H}_{\text{natural death}}, \tag{2.2}$$

$$\frac{dT_C}{dt} = \underbrace{\sigma_C}_{\text{infiltration}} + \underbrace{\beta T_C T_H}_{\text{production}} - \underbrace{(1-p) k T_C N}_{\text{de-activation}} - \underbrace{\delta_C T_C}_{\text{natural death}}. \tag{2.3}$$

As discussed in Chapter 1, a number of different immune cells play an important role in an anti-tumour immune response, but not all have been included here for simplicity (or are only included implicitly). For example, regulatory T cells are an important T cell population, but they would make the model unnecessarily complicated for a first approach to the problem.

We close equations (2.1)–(2.3) by prescribing the following initial conditions:

$$N(0) = N_0, \quad T_H(0) = T_{H0}, \quad T_C(0) = T_{C0}\,, \tag{2.4}$$

wherein the positive constants N_0, T_{H0} and T_{C0} denote the initial concentrations of the tumour cells, helper T cells and cytotoxic T cells respectively.

2.2.2 Parameter values

In the absence of suitable experimental data, we base our estimates of the values of the parameters that appear in equations (2.1)–(2.3) on those available in the modelling literature (see Table 2.1). Specifically, we choose dimensional parameter values that lie within the ranges specified in Table 2.1 for which the model exhibits qualitative behaviour consistent with the three Es of Immunoediting [52] (see Sections 2.5 and 2.8).

When investigating how the behaviour of the model depends upon parameters, the infiltration rates of the helper and cytotoxic T cells, σ_H and σ_C respectively, are of particular interest. Our focus on σ_H and σ_C is motivated by experiments in which high levels of infiltrating helper and cytotoxic T cells were found to improve prognosis for tumour patients [153, 152, 91].

Parameter	Description	Value (units)	References
γ	tumour growth rate	$0.01 - 0.5$ (day^{-1})	[110, 161, 119, 202, 184]
κ	carrying capacity of tumour cells	$10^9 - 2 \times 10^9$ (number of cells)	[41, 110, 12]
p	probability a cytotoxic T cell will kill a tumour cell	0–1 (dimensionless)	
k	rate at which cytotoxic T cells kill tumour cells	3.4×10^{-10}–1.0×10^{-3} (number of cells^{-1} day^{-1})	[110] [117, 108, 202]
σ_H	infiltration rate of helper T cells	0 – 0.063 (cell day^{-1})	no available literature
α	increase in helper T cell proliferation rate due to tumour cells	1.9 (day^{-1})	[160]
$\tilde{N}$	tumour size at which immune suppression becomes important	2×10^7 – 9.8×10^8 (number of cells)	[110] [41, 202, 12, 117, 119]
δ_H	death rate of helper T cells	0.1 (day^{-1})	[205]
σ_C	infiltration rate of cytotoxic T cells	1.3×10^4 (cell day^{-1})	[110]
β	increase in cytotoxic T cell proliferation rate due to helper T cells	16 (number of cells^{-1}day^{-1})	[160]
δ_C	death rate of cytotoxic T cells	$2.0 \times 10^{-3} - 1$ (day^{-1})	[41, 161, 110, 119, 12, 108, 117]

Table 2.1: Estimates from the modelling literature of the values of the dimensional parameters that appear in equations (2.1)–(2.3).

2.2.3 Nondimensionalised equations

We nondimensionalise equations (2.1)–(2.4) by rescaling time with ${\delta_C}^{-1}$, the half-life of the cytotoxic T cells, the tumour and cytotoxic T cell populations with κ, the carrying capacity of the tumour cells, and the helper T cells with δ_C/β. Thus, using hats to denote dimensionless variables, we substitute into equations (2.1)–(2.4)

$$\hat{N} = \frac{N}{\kappa}, \quad \hat{T}_C = \frac{T_C}{\kappa}, \quad \hat{T}_H = \frac{T_H \beta}{\delta_C}, \quad \hat{t} = t\delta_C \,, \tag{2.5}$$

and obtain

$$\frac{d\hat{N}}{d\hat{t}} = \hat{\gamma}(1-\hat{N})\hat{N} - p\hat{k}\hat{T}_C\hat{N} \,, \tag{2.6}$$

$$\frac{d\hat{T}_H}{d\hat{t}} = \hat{\sigma}_H + \frac{\hat{\alpha}\hat{N}\hat{T}_H}{\hat{\tilde{N}}^2 + \hat{N}^2} - \hat{\delta}_H\hat{T}_H \,, \tag{2.7}$$

$$\frac{d\hat{T}_C}{d\hat{t}} = \hat{\sigma}_C + \hat{T}_C\hat{T}_H - (1-p)\hat{k}\hat{T}_C\hat{N} - \hat{T}_C \,, \tag{2.8}$$

with initial conditions

$$\hat{N}(0) = \hat{N}_0, \quad \hat{T}_H(0) = \hat{T}_{H0}, \quad \hat{T}_C(0) = \hat{T}_{C0} \,, \tag{2.9}$$

where

$$\hat{\gamma} = \frac{\gamma}{\delta_C}, \quad \hat{k} = \frac{k\kappa}{\delta_C}, \quad \hat{\tilde{N}} = \tilde{N}/\kappa,$$
$$\hat{\sigma}_C = \frac{\sigma_C}{\kappa\delta_C}, \quad \hat{\sigma}_H = \frac{\sigma_H\beta}{{\delta_C}^2}, \quad \hat{\alpha} = \frac{\alpha\tilde{N}}{\delta_C\kappa}, \quad \hat{\delta}_H = \frac{\delta_H}{\delta_C}, \tag{2.10}$$
$$\hat{N}_0 = \frac{N_0}{\kappa}, \quad \hat{T}_{H0} = \frac{T_{H0}\beta}{\delta_C} \quad \text{and} \quad \hat{T}_{C0} = \frac{T_{C0}}{\kappa}\,.$$

For ease of presentation, we henceforth drop hats in equations (2.6)–(2.9). Table 2.2 lists the default set of dimensionless parameters used when solving these equations. We note that there may be considerable variation in these values due to uncertainty in their dimensional values.

Dimensionless parameter	**Description**	**Value**
γ	tumour growth rate	10
p	probability a cytotoxic T cell will kill a tumour cell	0.5
k	rate at which cytotoxic T cells kill tumour cells	4.15
σ_H	infiltration rate of helper T cells	0.5
α	increase in helper T cell proliferation rate due to tumour cells	0.19
$\tilde{N}$	tumour size at which suppressive effects come into play	0.04
δ_H	death rate of helper T cells	1
σ_C	infiltration rate of cytotoxic T cells	2.0

Table 2.2: Summary of the default parameter values used in the dimensionless equations (2.6)–(2.8) together with the dimensionless maximum cell populations (see Section 2.2.2). The dimensional parameters used to obtain these dimensionless values are $\gamma = 4.1$ day^{-1}, $k = 8.5 \times 10^{-10}$ number of cells^{-1} day^{-1}, $\alpha = 1.9$ day^{-1}, $\kappa = 2.0 \times 10^9$ number of cells, $\delta_C = 0.41$ day^{-1}, $\delta_H = 0.41$ day^{-1} and $\tilde{N} = 8.1 \times 10^7$ number of cells.

2.3 Qualitative behaviour

We solve equations (2.6)–(2.9) numerically using the Dormand-Prince explicit adaptive time-stepping method in Python (dopri5), which is based on a combination of fourth and fifth order Runge-Kutta schemes [49]. This numerical method can accommodate stiff equations such as in the present case where parameter values span several orders of magnitude.

In Figure 2.2 simulations for three values of σ_C, the infiltration rate of cytotoxic T cells into the tumour, reveal that the model reproduces the three Es of immunoediting

[52]. For moderate values of σ_C (see Figure 2.2 (a,b,c)), we observe bistability between a stable limit cycle (as resolved numerically and confirmed later in Section 2.7.4) which oscillates with small amplitude about a small tumour burden (representing an equilibrium state as the tumour cell number remains bounded at all times) and a steady state with a large tumour burden (corresponding to tumour escape). In the oscillatory equilibrium state, the tumour, cytotoxic and helper T cell populations oscillate out of phase: the growth of the tumour stimulates the proliferation of the helper T cells, which in turn promotes the proliferation of the cytotoxic T cells, driving down the tumour population. In tumour escape, the cytotoxic and helper T cell populations settle to constant values below their baseline values occurring in the absence of a tumour. Note that we nondimensionalised the tumour population by its carrying capacity, κ, and therefore a large tumour population has a dimensionless value close to one.

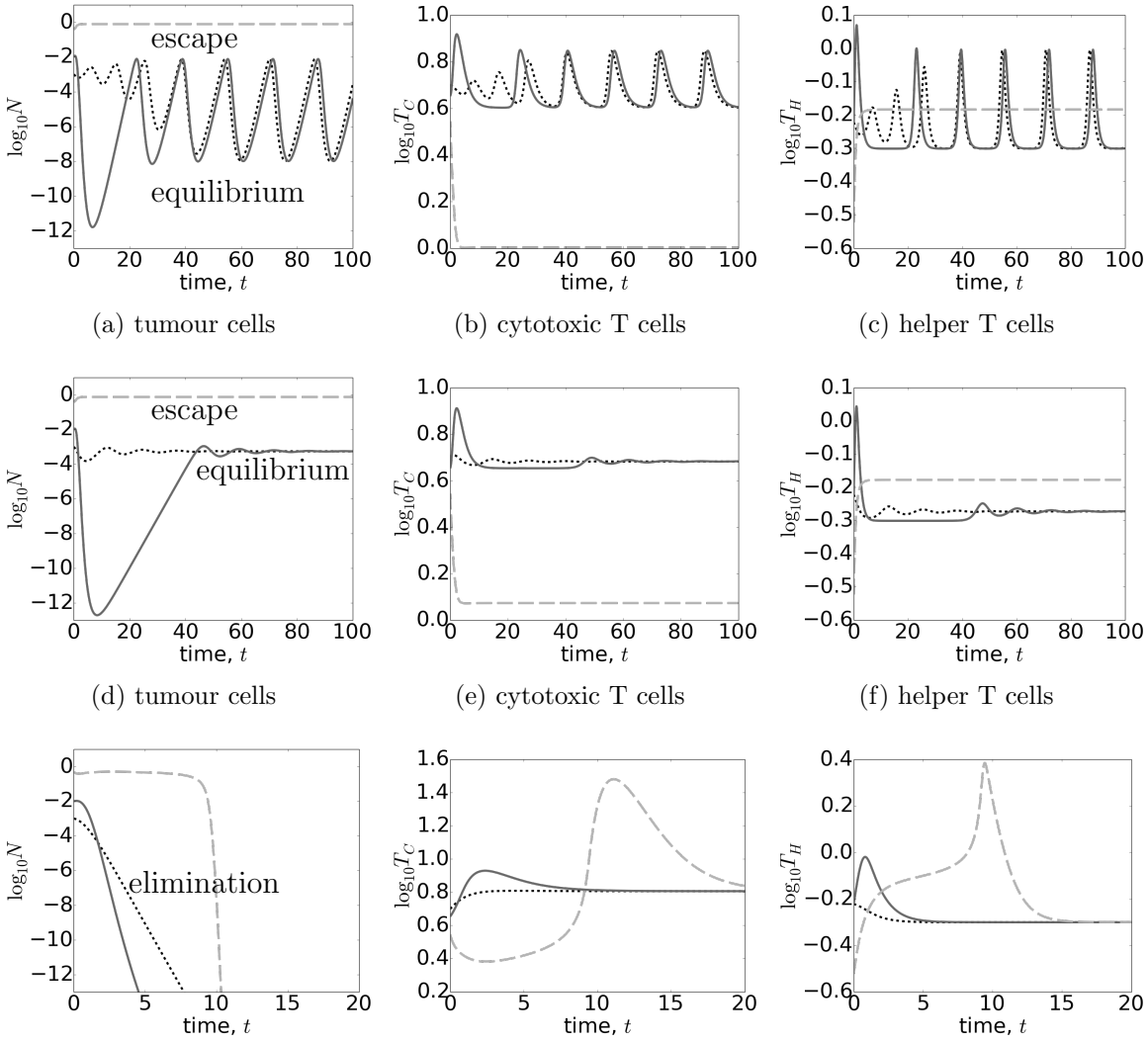

(a) tumour cells (b) cytotoxic T cells (c) helper T cells

(d) tumour cells (e) cytotoxic T cells (f) helper T cells

(g) tumour cells (h) cytotoxic T cells (i) helper T cells

Figure 2.2: Series of plots showing the dynamics of the tumour cells, $N(t)$, the helper T cells, $T_H(t)$, and the cytotoxic T cells, $T_C(t)$, as defined by equations (2.6)–(2.8) for three values of the basal infiltration rate of the cytotoxic T cells, $\sigma_C = 2.0,\ 2.25$ and 3.2 (top, middle and bottom rows respectively) with all remaining parameters fixed at their default values. In each plot three initial conditions are considered and distinguished by linestyle: $(N_0, T_{C0}, T_{H0}) = (0.001, 5.0, 0.6)$ shown by the dotted black curve, $(N_0, T_{C0}, T_{H0}) = (0.01, 4.5, 0.6)$ shown by the solid grey curve; $(N_0, T_{C0}, T_{H0}) = (0.5, 3.5, 0.3)$ shown by the dashed light grey curve.

For a small increase in the value of σ_C from 2 to 2.25 (see Figure 2.2 (d,e,f)), we retain bistability between a tumour equilibrium and tumour escape. However, in this case we observe that the tumour equilibrium solution is no longer oscillitory but settles to a stable steady state with a small tumour burden.

For a larger value of σ_C (see Figure 2.2 (g,h,i)), we observe monostability of a

tumour-free state corresponding to tumour elimination. Here the immune system is strong enough to eliminate the tumour. We conclude that our model may exhibit multi-stability, and that the nature and multiplicity of stable solutions change as the infiltration rate of the cytotoxic T cells varies.

2.4 Steady state analysis

The qualitative behaviours presented in Section 2.3 reveal that equations (2.6)–(2.9) possess several distinct attractors: stable steady state solutions and a stable limit cycle solution. As a first step to understanding the solution structure of the model, we next identify and characterise its steady state solutions.

Setting the time-derivatives to zero in equations (2.6)–(2.8) yields three algebraic equations that define the steady state solutions $(N, T_H, T_C) = (N^*, T_H^*, T_C^*)$:

$$0 = N^* \left(\gamma(1 - N^*) - pkT_C^*\right) , \tag{2.11}$$

$$0 = \sigma_H + T_H^* \left(\frac{\alpha N^*}{\tilde{N}^2 + N^{*2}} - \delta_H \right) , \tag{2.12}$$

$$0 = \sigma_C + T_C^* \left(T_H^* - (1-p)kN^* - 1\right) . \tag{2.13}$$

We note, from equation (2.11), that for physically realistic solutions $N^* \in [0, 1)$. The solutions depend on five parameter groupings,

$$\tilde{k} = (1-p)k, \quad \tilde{\gamma} = \frac{\gamma}{pk}, \quad \tilde{\sigma}_C = \frac{\sigma_C}{\tilde{\gamma}}, \quad \bar{\sigma}_H = \frac{\sigma_H}{\delta_H} \quad \text{and} \quad \bar{\alpha} = \frac{\alpha}{\delta_H} . \tag{2.14}$$

First of all, equations (2.11)–(2.13) admit a tumour-free solution,

$$N^* = 0, \quad T_H^* = \bar{\sigma}_H, \quad T_C^* = \frac{\tilde{\gamma}\tilde{\sigma}_C}{1 - \bar{\sigma}_H} , \tag{2.15}$$

This solution is physically realistic provided $0 \leq \bar{\sigma}_H < 1$. All other steady state solutions have $0 < N^* < 1$ and $T_C^* = \tilde{\gamma}(1 - N^*)$. Further, by eliminating T_C^* from equations (2.12)–(2.13), it is straightforward to show that these steady state solutions lie at the intersection of the following two curves:

$$T_H^* = H_a(N^*) \equiv \frac{\bar{\sigma}_H(\tilde{N}^2 + N^{*2})}{\tilde{N}^2 + N^{*2} - \bar{\alpha}N^*} , \tag{2.16}$$

$$T_H^* = H_b(N^*) \equiv 1 + \tilde{k}N^* - \frac{\tilde{\sigma}_C}{1 - N^*} . \tag{2.17}$$

In Figure 2.3 we use equations (2.16)–(2.17) to show how the qualitative behaviour of the curves of $T_H^* = H_a(N^*)$ and $T_H^* = H_b(N^*)$ change as the system parameters vary. For $T_H^* = H_a(N^*)$ three cases may arise:

1. $\bar{\alpha} < 2\tilde{N}$: $H_a(N^*) > 0$ for $N^* \in (0,1)$ and attains a finite maximum in the feasible range;

2. $2\tilde{N} \leq \bar{\alpha} < 1 + \tilde{N}^2$: $H_a(N^*)$ has two asymptotes $N^*_{\pm}$ in the range $N^* \in (0,1)$; between the asymptotes, $H_a(N^*) < 0$ and otherwise it is positive;

3. $\bar{\alpha} \geq 1 + \tilde{N}^2$: $H_a(N^*) > 0$ to the left of the asymptote at $N^*_- \in (0,1)$ and $H_a(N^*)$ is negative otherwise.

Inspection of equation (2.17) reveals that three cases may arise as the parameters are varied:

- $H_b(N^*) < 0$ for all $N^* \in (0,1)$;
- $H_b(N^*)$ decreases monotonically for $N^* \in (0,1)$, with $H_b(0) > 0 > H_b(1)$;
- $H_b(N^*)$ attains a positive maximum at some point $N^* \in (0,1)$.

Since the dependence of $H_b(N^*)$ on the model parameters is more involved than for $H_a(N^*)$, further details are left to Appendix A. Notably $H_b(N^*)$ always becomes negative for N^* sufficiently close to 1. The full range of behaviours can only be realised by varying both $\tilde{k}$ and $\tilde{\sigma}_C$. It is not enough to fix $\tilde{k}$ to a single value and vary $\tilde{\sigma}_C$.

Recall that the physically realistic steady state solutions for which $N^* > 0$ lie at those intersections of equations (2.16)–(2.17) for which $T^*_H = H_a(N^*) = H_b(N^*) > 0$. Guided by the results presented in Figure 2.3, in Figure 2.4 we show how the number and nature of these steady state solutions change as we vary $\bar{\alpha}$ and $\tilde{\sigma}_C$ for a fixed value of $\tilde{k} = 2$ close to the default value (see Table 2.2).

For completeness, also indicated on these figures is the tumour-free steady state solution defined by equation (2.15). In practice, up to 4 such steady states may arise (see Appendix A for details), although this occurs only in a tiny portion of parameter space.

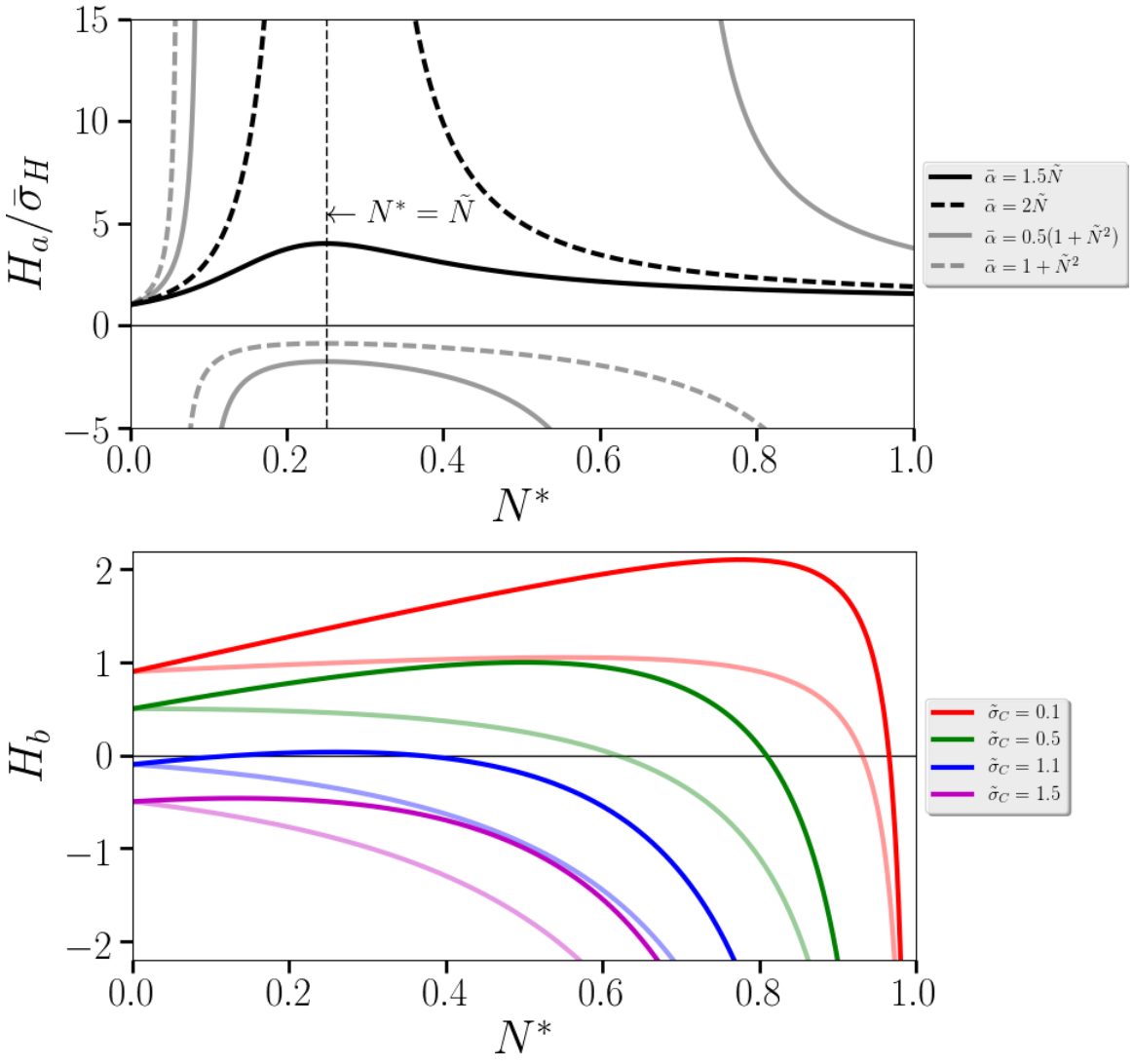

Figure 2.3: Form of the functions $H_a(N^*)$ and $H_b(N^*)$ from equations (2.16) and (2.17) for selected choices of $\bar{\alpha}$ fixing $\tilde{N} = 0.25$ and $\bar{\sigma}_H$ in H_a, and for selected choices of $\tilde{k}$ and $\tilde{\sigma}_C$ in H_b. In the plot of H_a, the curves for different $\bar{\alpha}$ are distinguished by linestyle as indicated. In the plot of H_b, the different choices of $\tilde{\sigma}_C$ are distinguished by colour as indicated. The lighter shade corresponds to $\tilde{k} = 0.5$, while the darker shade corresponds to $\tilde{k} = 2$.

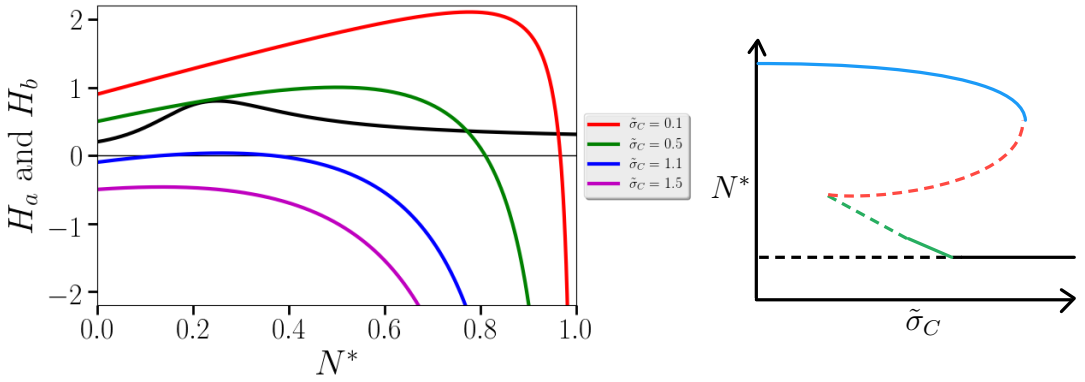

(a) $\bar{\alpha} < 2\tilde{N}$

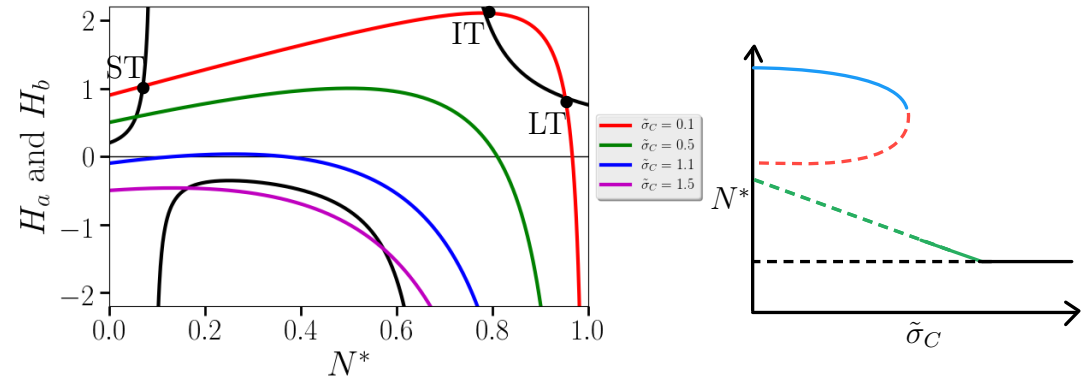

(b) $2\tilde{N} \leq \bar{\alpha} \leq 1 + \tilde{N}^2$

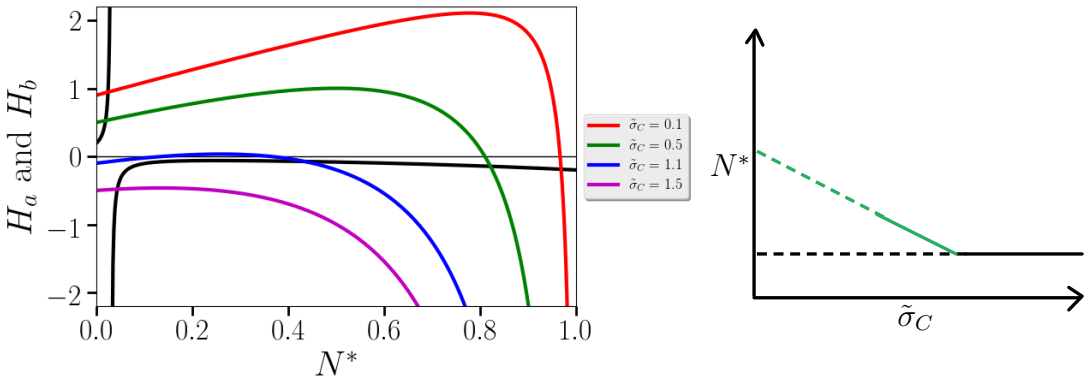

(c) $\bar{\alpha} > 1 + \tilde{N}^2$

Figure 2.4: Series of diagrams showing how the physically realistic steady state solutions of equations (2.11) and (2.13) change as $\bar{\alpha}$ and $\tilde{\sigma}_C$ vary, or, equivalently, the intersections of equations (2.16) and (2.17) for which $T_H^* = H_a(N^*) = H_b(N^*) > 0$ and $N^* \in (0, 1)$. The qualitative behaviours of $T_H^* = H_a(N^*)$ as $\bar{\alpha}$ varies are indicated by the black curves on the left hand plots of panels (a), (b) and (c). For each case, we plot $T_H^* = H_b(N^*)$ for discrete values of $\tilde{\sigma}_C$ (=0.1, 0.5, 1.0 and 1.5) with $\tilde{k} = 2$ and $\bar{\sigma}_H = 1$ to illustrate the range of behaviours that can arise. The bifurcation diagrams on the right side of panels (a), (b) and (c) indicate how the number and nature of the steady state solutions change as $\tilde{\sigma}_C$ is varied continuously. Dashed lines indicate regions of linear instability (see Section 2.5).

It is straightforward to show that if $2\tilde{N} < \bar{\alpha} < 1 + \tilde{N}^2$ (see Figure 2.4(b)) then equation (2.16) has two asymptotes at $N^* = N^*_{\pm}$, where

$$N^*_{\pm} = \tfrac{1}{2}\bar{\alpha} \pm \sqrt{\tfrac{1}{4}\bar{\alpha}^2 - \tilde{N}^2}\,. \tag{2.18}$$

Further, if $0 < \tilde{\sigma}_C < 1 - \bar{\sigma}_H$ then $H_b(0) > H_a(0)$ and there is a physically realistic steady state solution with $0 < N^* < N^*_-$. For small values of $\tilde{\sigma}_C$ (i.e., low rates of infiltration of the cytotoxic T cells) such that $0 < \tilde{\sigma}_C < 1 - \bar{\sigma}_H$, there are three physically realistic steady state solutions with $N^* > 0$ while for large values of $\tilde{\sigma}_C$ the immune response is so strong that the tumour is eliminated and only the tumour-free steady state solution persists. As $\tilde{\sigma}_C$ increases between these extremes, first the steady state with small N^* is lost (at a transcritical bifurcation; see Section 2.5) and then the other two steady state solutions with $N^* > 0$ collide at a fold bifurcation.

For $\bar{\alpha} \geq 1 + \tilde{N}^2$ (see Figure 2.4(c)), the asymptote $N^*_+ \geq 1$, and therefore there can be no further intersections beyond $N^* = N^*_-$. Only one steady state solution is possible in this case. The case $\bar{\alpha} < 2\tilde{N}$ illustrated in Figure 2.4(a), where $H_a(N^*)$ attains a finite maximum, is more complicated and detailed in Appendix A.

For the default parameters used in this study, we have $2\tilde{N} \leq \bar{\alpha} \leq 1 + \tilde{N}^2$ (see Figure 2.5 which is similar in form to Figure 2.4 (b)). In this case, for sufficiently small $\tilde{\sigma}_C$, three intersections occur: one at small N^* and two at moderate N^*. As $\tilde{\sigma}_C$ increases the two solutions at moderate N^* are lost followed by, for larger $\tilde{\sigma}_C$, the solution at small N^*. As $\tilde{N}^2/\bar{\alpha} \ll 1$, the intersection at small N^* is $\mathcal{O}(\tilde{N}^2/\bar{\alpha})$, enabling accurate approximations for many features of the model.

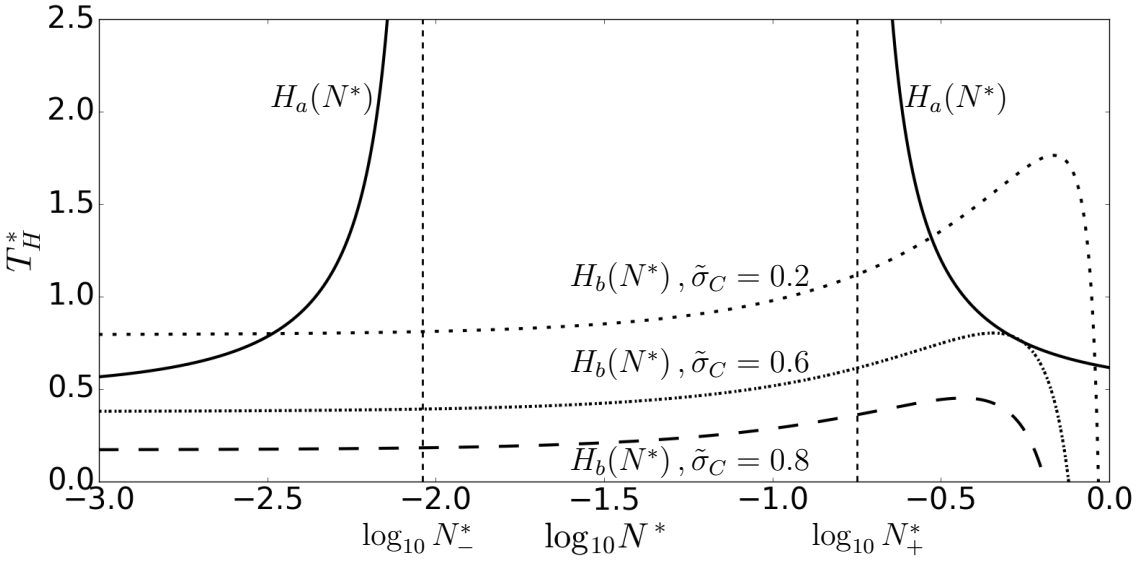

Figure 2.5: Dependence of the nature and number of tumour equilibrium steady state solutions ($N^* > 0$) on $\tilde{\sigma}_C$. Intersections of equations (2.16) and (2.17) (solid and dashed curves respectively) are shown for three values of $\tilde{\sigma}_C$ ($\tilde{\sigma}_C = 0.2, 0.6$ and 0.8), with all other parameters fixed at their default values. The two vertical dashed lines indicate the asymptotes $N_\pm^*$ of equation (2.16).

2.5 Local and global stability

In this section we begin by discussing the local, linear stability of the tumour steady states. This is subsequently used to understand the global, nonlinear stability of the system in a few representative cases.

2.5.1 Linear stability

To understand the local stability of the tumour equilibria, we start by linearising about the steady state solutions (N^*, T_H^*, T_C^*), seeking solutions of the form

$$N = N^* + \epsilon \check{N} e^{\lambda t} + O(\epsilon^2), \tag{2.19a}$$

$$T_H = T_H^* + \epsilon \check{T}_H e^{\lambda t} + O(\epsilon^2), \tag{2.19b}$$

$$T_C = T_C^* + \epsilon \check{T}_C e^{\lambda t} + O(\epsilon^2), \tag{2.19c}$$

where $\check{N}$, $\check{T}_H$, $\check{T}_C$ and λ are constants, and $0 < \epsilon \ll 1$ is a small parameter. Substituting (2.19) into equations (2.6)–(2.8) and equating to zero terms of $O(\epsilon)$ we deduce that the eigenvalues $\lambda = \lambda_n$ $(n = 1, 2, 3)$ satisfy $|\mathcal{J} - \lambda \mathcal{I}| = 0$ where the Jacobian

$\mathcal{J}(N^*, T_H^*, T_C^*)$ is given by

$$\mathcal{J} = \begin{pmatrix} \gamma(1-2N^*) - pkT_C^* & 0 & -pkN^* \\ \dfrac{\alpha T_H^*(\tilde{N}^2 - N^{*2})}{(\tilde{N}^2 + N^{*2})^2} & \dfrac{\alpha N^*}{(\tilde{N}^2 + N^{*2})^2} - \delta_H & 0 \\ -(1-p)kT_C^* & T_C^* & T_H^* - (1-p)kN^* - 1 \end{pmatrix}. \quad (2.20)$$

Instability of a steady state solution corresponds to $\max_{n=1,2,3} \Re(\lambda_n) > 0$. Conversely the steady state is linearly stable if $\Re(\lambda_n) < 0$ for $n = 1, 2, 3$. Note that in general the eigenvalues depend not only on the parameter groupings presented in (2.14), but also on the parameters γ, p, k, α and δ_H. For ease of presentation, it is convenient to use both sets of parameters in subsequent analyses.

It is straightforward to show that the eigenvalues associated with the tumour-free steady state $(N^*, T_H^*, T_C^*) = (0, \bar{\sigma}_H, \tilde{\gamma}\tilde{\sigma}_C/(1-\bar{\sigma}_H))$ are

$$\lambda_1 = \gamma\left(1 - \frac{\tilde{\sigma}_C}{1-\bar{\sigma}_H}\right), \quad \lambda_2 = -\delta_H \quad \text{and} \quad \lambda_3 = -(1-\bar{\sigma}_H). \quad (2.21)$$

We deduce that where it exists (i.e. where $0 < \bar{\sigma}_H < 1$) the tumour-free steady state is linearly stable if

$$\max(0, 1-\tilde{\sigma}_C) < \bar{\sigma}_H < 1. \quad (2.22)$$

We remark that the region of parameter space in which the small tumour steady state exists corresponds to the region in which the tumour-free steady state is linearly unstable.

To provide a more complete picture of the (N, T_H, T_C) phase space, we next examine the eigenvalues associated with each of the steady states as $\tilde{\sigma}_C$ varies, and furthermore consider the nonlinear dynamics starting in the neighbourhood of the unstable steady states. This bridges the gap between the steady state analysis, linear stability analysis and the observed qualitative behaviour presented in Section 2.3.

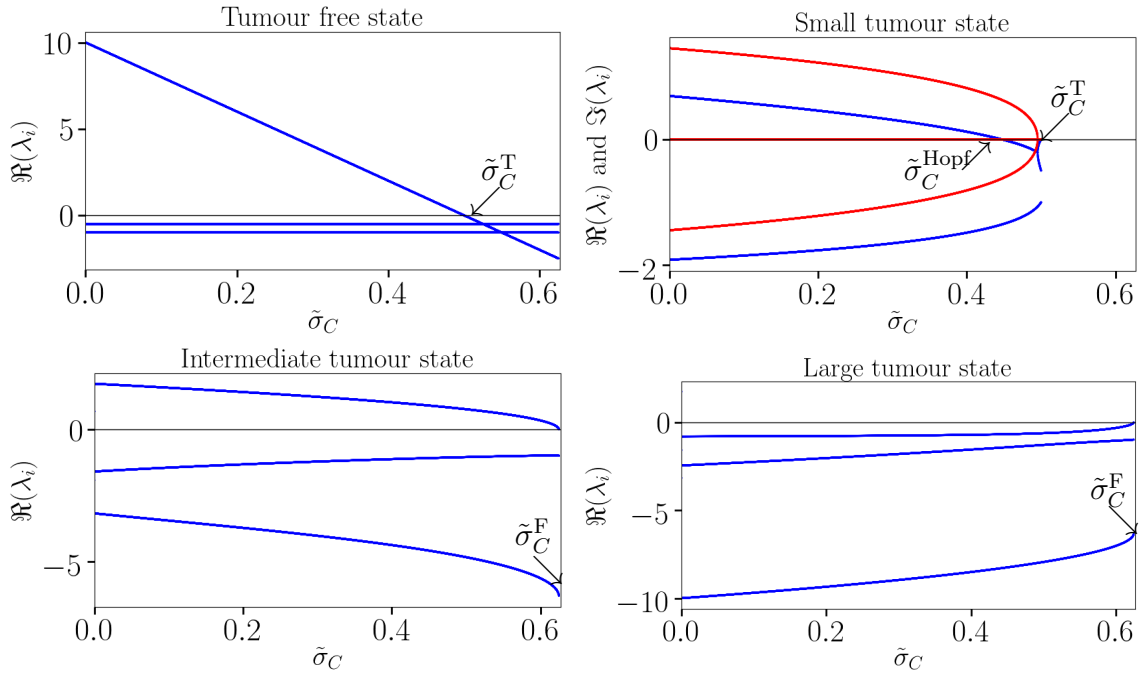

Figure 2.6: Variations in the real (red) and imaginary (blue) parts of the eigenvalues λ_i $(i = 1, 2, 3)$ associated with each of the steady states as $\tilde{\sigma}_C$ is varied, with all remaining parameters fixed at their default values. Key: $\tilde{\sigma}_C^{\mathrm{T}}$ marks a transcritical bifurcation point; $\tilde{\sigma}_C^{\mathrm{F}}$ marks a fold bifurcation point; $\tilde{\sigma}_C^{\mathrm{Hopf}}$ marks a Hopf bifurcation point, described in detail in Section 2.7. Note, for the tumour-free, intermediate tumour and large tumour steady states the eigenvalues are purely real. For the small tumour steady state, with decreasing $\tilde{\sigma}_C$ the upper pair of real eigenvalues to the right of $\tilde{\sigma}_C^{\mathrm{T}}$ collide at the transcritical bifurcation and give rise to a pair of complex conjugate eigenvalues for $\tilde{\sigma}_C < \tilde{\sigma}_C^{\mathrm{T}}$. The real part of these eigenvalues lies along the upper blue branch connected to $\tilde{\sigma}_C^{\mathrm{T}}$. The lower stable blue branch is separate and is purely real.

Figure 2.6 shows how the real and imaginary parts of the eigenvalues of all steady states vary with $\tilde{\sigma}_C$. For the tumour-free state only one of the eigenvalues varies with $\tilde{\sigma}_C$ (see equation (2.21)). For $\tilde{\sigma}_C < \tilde{\sigma}_C^{\mathrm{T}}$, there are two stable eigenvalues and one unstable eigenvalue whose growth rate increases linearly with decreasing $\tilde{\sigma}_C$. All of the eigenvalues associated with the tumour-free state are real. This critical point is called a hyperbolic point since there are no complex eigenvalues for $\tilde{\sigma}_C < \tilde{\sigma}_C^{\mathrm{T}}$. For $\tilde{\sigma}_C > \tilde{\sigma}_C^{\mathrm{T}}$, all eigenvalues are real and negative corresponding to the tumour-free steady state being an attractor (i.e. any linear perturbation to the tumour-free steady state decays). The intermediate tumour state, like the tumour-free state, is also hyperbolic. Where the intermediate tumour state exists, it is unstable. Two of the eigenvalues are negative and one is positive just as for the tumour-free state for $\tilde{\sigma}_C < \tilde{\sigma}_C^{\mathrm{T}}$. The large tumour state is stable where it exists ($\tilde{\sigma}_C < \tilde{\sigma}_C^{\mathrm{F}}$). The large tumour state is therefore

an attractor. The small tumour state is distinct from the other steady states. For $\tilde{\sigma}_C > \tilde{\sigma}_C^{\mathrm{T}}$ this state is non-physical ($N^* < 0$) and is therefore disregarded. The small tumour steady state arises at the transcritical bifurcation $\tilde{\sigma}_C = \tilde{\sigma}_C^{\mathrm{T}}$ where the tumour-free steady state changes stability. This gives rise to a complex conjugate pair of eigenvalues and a third stable eigenvalue with zero imaginary part and therefore this point represents a spiral point. For $\tilde{\sigma}_C^{\mathrm{Hopf}} \leq \tilde{\sigma}_C \leq \tilde{\sigma}_C^{\mathrm{T}}$ there is one complex conjugate pair of eigenvalues with negative real part, plus a real eigenvalue that is negative. For $\tilde{\sigma}_C < \tilde{\sigma}_C^{\mathrm{Hopf}}$ the complex conjugate eigenvalue changes to have a positive real part. This analysis reveals how small perturbations in the neighbourhood of unstable steady steady states are attracted towards stable steady states.

2.5.2 Global stability

Global, nonlinear stability is examined by locating the stable and unstable manifolds connecting the steady states in the (N, T_H, T_C) phase space. The manifolds are computed by numerically integrating equations (2.6)–(2.8), initialised in the unstable directions near each unstable steady state. This is done by perturbing each steady state by 10^{-3} times the normalised eigenvector $\mathbf{v}_m$ of the specific eigenvalue λ_m for which $\mathcal{J}\mathbf{v}_m = \lambda_m \mathbf{v}_m$. As $-\mathbf{v}_m$ is also a normalised eigenvector, we can perturb each steady state in two directions. One direction corresponds to increasing N while the other direction corresponds to decreasing N. For the tumour-free state only the perturbation increasing N is possible. When $N(0) > N^*$ we say we are 'above' the steady state, while when $N(0) < N^*$ we say we are 'below' the steady state.

In Figure 2.7 we take a value of $\tilde{\sigma}_C = 0.012$ corresponding to a region of parameter space where the tumour-free, small and intermediate states are unstable and the large tumour state is stable (see Figure 2.6). Starting near the tumour-free state in the lower left corner, the trajectory in phase space leads to the large tumour steady state in the upper left corner. From the small tumour steady state the perturbation above takes a trajectory which also leads to the large tumour state, while the perturbation below first approaches the tumour-free state before also arriving at the large tumour state. For the intermediate tumour state the perturbation above directly leads to the large tumour state, while the perturbation below skirts by the tumour-free state before eventually arriving at the large tumour state. In summary, the perturbations above each state directly lead to the large tumour state (escape). The perturbations below first approach the tumour-free state before eventually arriving at the large tumour state.

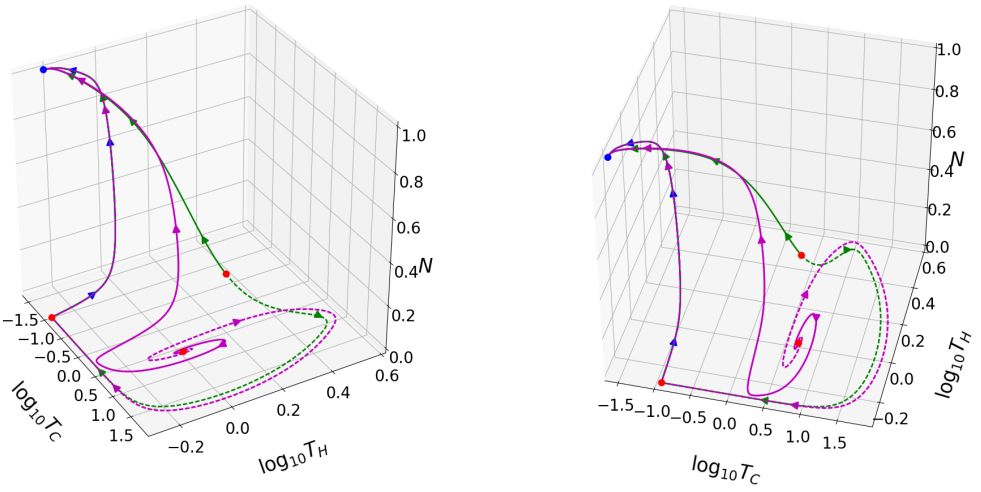

Figure 2.7: Confirmation of the predicted (linear) stability of the steady state solutions of equations (2.11)–(2.13) as depicted in Figures 2.8–2.10 when $\tilde{\sigma}_C = 0.012$ (and all other parameter values are held at their default values). A series of typical trajectories starting in different regions of the phase plane are presented. While all trajectories eventually evolve to the large tumour steady state (above left), in some cases they first approach close to the tumour-free steady state (below left). Note that perturbations about the small tumour steady state spiral outwards while perturbations about the intermediate tumour steady state (above right) either lead directly to the large tumour steady state or first skirt by the tumour-free steady state on route to the large tumour steady state. Red and blue circles denote unstable and stable steady states respectively. The continuous and dashed lines represent different initial conditions.

2.6 System bifurcations

We next scan over $\tilde{\sigma}_C$, holding all other parameters fixed at their default values in Table 2.2, to illustrate how the multiplicity and linear stability of the steady state solutions of equations (2.6)–(2.8) change as we vary $\tilde{\sigma}_C$. The results are presented in Figures 2.8–2.10 (qualitatively similar behaviour is observed when $\bar{\sigma}_H$ is varied; results not presented). We identify five distinct regions separated by four bifurcation points $\tilde{\sigma}_C^{\mathrm{F}}$, $\tilde{\sigma}_C^{\mathrm{T}}$, $\tilde{\sigma}_C^{\mathrm{Hopf}}$ and $\tilde{\sigma}_C^{\mathrm{Hom}}$. The qualitative behaviour in each region is summarised as follows

- $\tilde{\sigma}_C > \tilde{\sigma}_C^{\mathrm{F}}$: the system is monostable; all initial conditions evolve to the tumour-free steady state (tumour elimination).

- $\tilde{\sigma}_C = \tilde{\sigma}_C^{F}$: fold bifurcation at which two non-trivial steady states are created.

- $\tilde{\sigma}_C^T < \tilde{\sigma}_C < \tilde{\sigma}_C^F$: the system is bistable; an unstable steady state with intermediate tumour burden separates the stable, tumour-free steady state from a stable solution with a large tumour burden (tumour escape); as $\tilde{\sigma}_C$ decreases, the tumour burden on the upper branch of solutions increases towards its (dimensionless) carrying capacity.

- $\tilde{\sigma}_C = \tilde{\sigma}_C^T$: transcritical bifurcation at which a new branch of stable steady state solutions emerges from the tumour-free branch.

- $\tilde{\sigma}_C^{\text{Hopf}} < \tilde{\sigma}_C < \tilde{\sigma}_C^T$: bistability is preserved; the tumour-free steady state exchanges stability with the new branch of solutions characterised by a very small tumour burden.

- $\tilde{\sigma}_C = \tilde{\sigma}_C^{\text{Hopf}}$: Hopf bifurcation at which the branch of solutions characterised by a small tumour burden loses stability to oscillatory solutions.

- $\tilde{\sigma}_C^{\text{Hom}} < \tilde{\sigma}_C < \tilde{\sigma}_C^{\text{Hopf}}$: bistability between a stable limit cycle and the steady state with a large tumour burden; all other steady state solutions are unstable.

- $\tilde{\sigma}_C = \tilde{\sigma}_C^{\text{Hom}}$: the limit cycle disappears when it collides with the intermediate tumour steady state (see Figure 2.11 and below for details).

- $0 \leq \tilde{\sigma}_C < \tilde{\sigma}_C^{\text{Hom}}$: only the large tumour state is stable (i.e. tumour escape).

The bifurcation diagrams in Figures 2.8–2.10 indicate those values of $\tilde{\sigma}_C$ for which oscillatory solutions occur. The limit cycle emerges when $\tilde{\sigma}_C$ decreases through the critical value $\tilde{\sigma}_C^{\text{Hopf}}$ and disappears as $\tilde{\sigma}_C \to \tilde{\sigma}_C^{\text{Hom}}$. Numerical results which confirm these dynamics are presented in Figure 2.11. For $\tilde{\sigma}_C \gtrsim \tilde{\sigma}_C^{\text{Hom}}$, we observe periodic solutions for which tumour growth stimulates infiltration by helper T cells which, in turn, recruit large numbers of cytotoxic T cells. As the tumour increases in size, immunosuppression of the helper T cells becomes important and their rate of proliferation falls while levels of cytotoxic T cells continue to rise, causing the tumour burden to fall. As levels of helper T cells fall, the proliferation rate of the cytotoxic T cells falls, causing their levels also to decrease. The immunosuppressed tumour then resumes its growth until it reaches a size at which an effective immune response is again stimulated, levels of helper T cells rise, and the cycle repeats. As the rate $\tilde{\sigma}_C$ at which cytotoxic T cells infiltrate the tumour approaches $\tilde{\sigma}_C^{\text{Hom}}$ from above, the limit cycle period increases and the tumour spends increasingly longer periods around the tumour-free state. These periods correspond to the low flat regions in T_C shown in Figure 2.11(a).

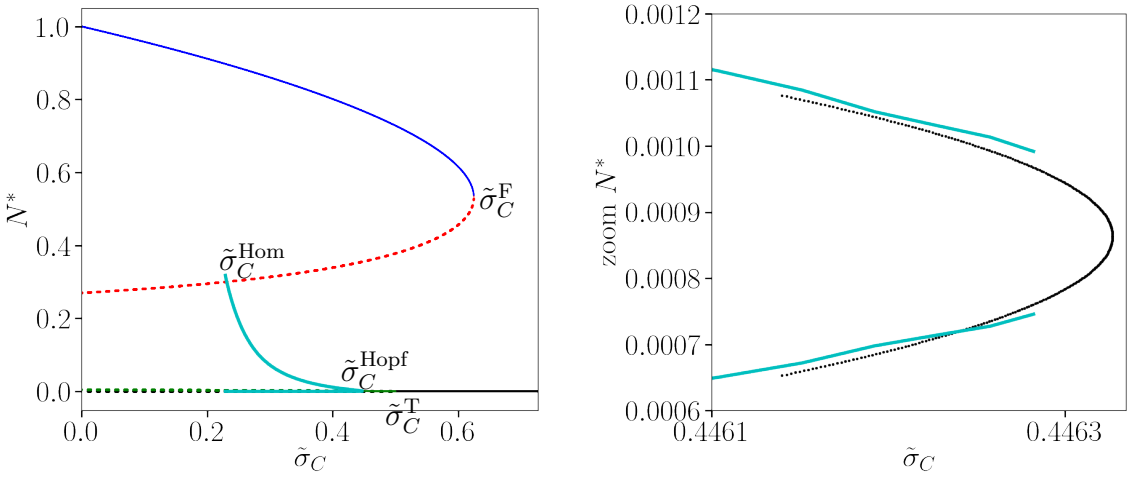

(a) tumour cell population, N^*

(b) zoom N^*

Figure 2.8: Domain of existence and linear stability of the steady state tumour population N^* as a function of $\tilde{\sigma}_C$, when all other parameters are fixed at their default values. Solution branches are distinguished by colour: the blue branch corresponds to the large tumour (escape) state; the red branch corresponds to the intermediate tumour state; the green branch corresponds to the small tumour state and the black branch corresponds to the tumour-free state. The small tumour state is nearly indistinguishable from the tumour-free state but can be distinguished when considering T_C^* versus $\tilde{\sigma}_C$ as done in Figure 2.9. The local stability of the steady states is distinguished by linestyle: solid and dashed curves correspond to stable and unstable solutions respectively. The cyan curves correspond to the maximum and minimum values of the limit cycle cell populations obtained from the numerical solutions. The zoom in panel (b) illustrates the good agreement between the numerical simulations (cyan curve) and the results of an asymptotic analysis in the neighbourhood of the Hopf bifurcation point (solid black curve; for details see Section 2.7.4). The discrepancy between the cyan and black curves is due to the difficulty in obtaining accurate numerical estimates for the amplitude of the limit cycle near its point of emergence. Exceedingly long integration times would be required to improve the match.

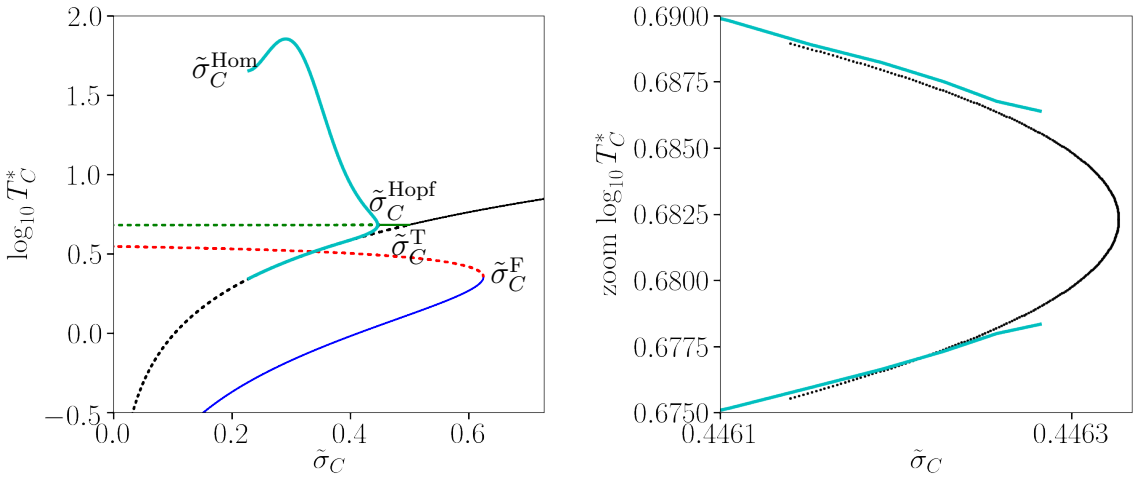

(a) cytotoxic T cell population, T_C^*

(b) zoom T_C^*

Figure 2.9: Domain of existence and linear stability of the steady state cytotoxic T cell population T_C^* as a function of $\tilde{\sigma}_C$, when all other parameters are fixed at their default values. The layout of the figures is the same as in Figure 2.8.

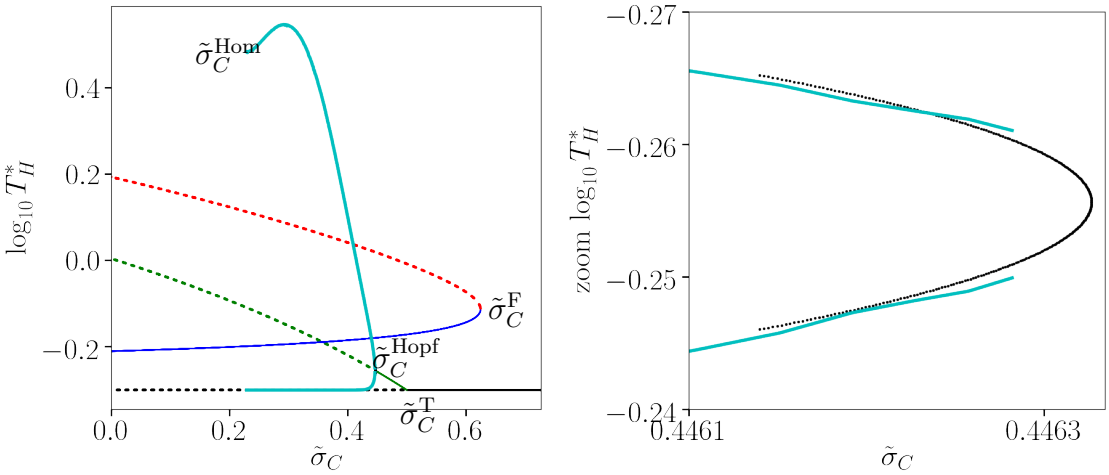

(a) helper T cell population, T_H^*

(b) zoom T_H^*

Figure 2.10: Domain of existence and linear stability of the steady state helper T cell population T_H^* as a function of $\tilde{\sigma}_C$, when all other parameters are fixed at their default values. The layout of the figures is the same as in Figure 2.8.

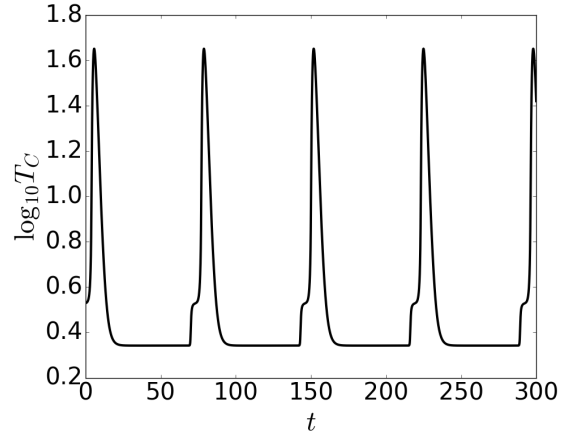

(a) $\tilde{\sigma}_C \gtrsim \tilde{\sigma}_C^{\mathrm{Hom}}$

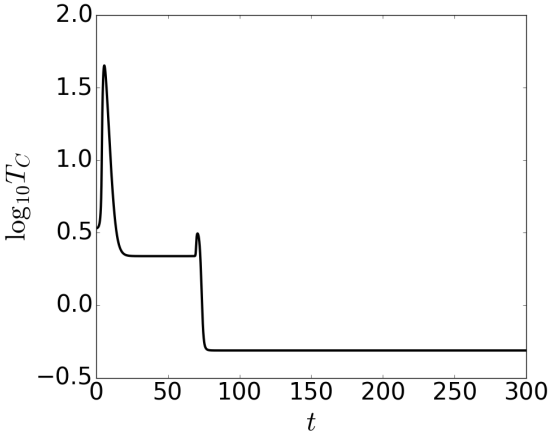

(b) $\tilde{\sigma}_C < \tilde{\sigma}_C^{\mathrm{Hom}}$

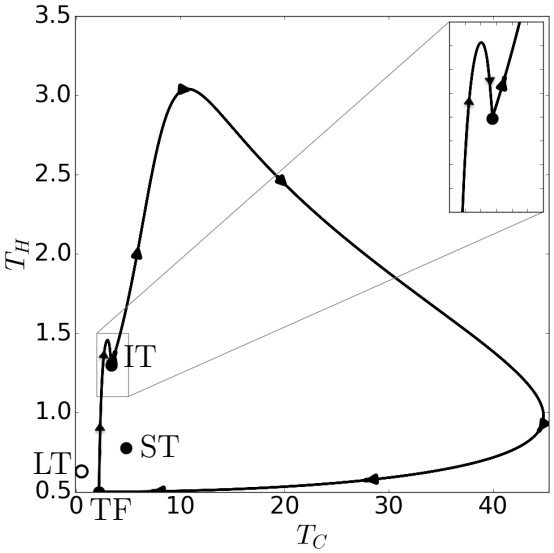

(c) $\tilde{\sigma}_C \gtrsim \tilde{\sigma}_C^{\mathrm{Hom}}$

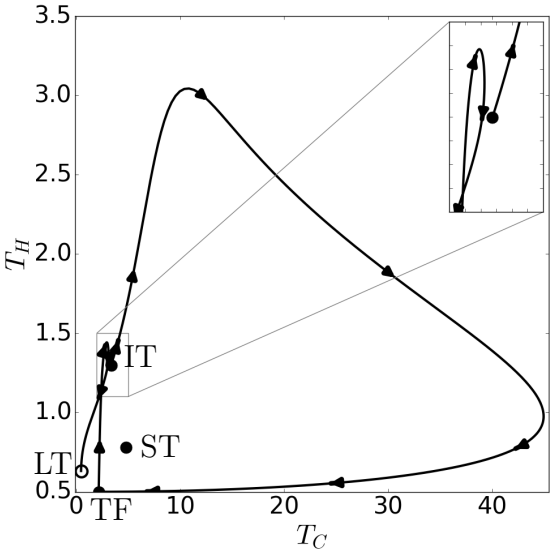

(d) $\tilde{\sigma}_C < \tilde{\sigma}_C^{\mathrm{Hom}}$

Figure 2.11: Confirmation that equations (2.6)–(2.8) admit limit cycles when $\tilde{\sigma}_C = 0.2281 \gtrsim \tilde{\sigma}_C^{\mathrm{Hom}}$, and that they cease to exist when $0 < 0.2263 = \tilde{\sigma}_C < \tilde{\sigma}_C^{\mathrm{Hom}}$ (all other parameters are fixed at their default values). The trajectories start near the intermediate tumour steady state (see red branch in Figures 2.8–2.10). Panels (a) and (b) show how the cytotoxic T cells $T_C(t)$ evolve when $\tilde{\sigma}_C \gtrsim \tilde{\sigma}_C^{\mathrm{Hom}}$ and $\tilde{\sigma}_C < \tilde{\sigma}_C^{\mathrm{Hom}}$ respectively. The corresponding trajectories in the (T_C, T_H) plane are presented in panels (c) and (d). Filled points represent unstable (tumour-free (TF), small tumour (ST) and intermediate tumour (IT)) steady states; the unfilled point represents the stable, large tumour steady state (LT).

As we approach the homoclinic bifurcation from above ($\tilde{\sigma}_C \gtrsim \tilde{\sigma}_C^{\mathrm{Hom}}$), the period of the limit cycle tends to infinity as it spends an increasing length of time near the

intermediate tumour state. As $\tilde{\sigma}_C \to \tilde{\sigma}_C^{\mathrm{Hom}}$ from above, the limit cycle approaches the unstable manifold of the intermediate tumour steady state, connecting with it (along its stable eigenvector) when $\tilde{\sigma}_C = \tilde{\sigma}_C^{\mathrm{Hom}}$ (see Figure 2.11 (c)). The trajectory then leaves the steady state along one of the unstable eigenvectors to complete the homoclinic orbit.

For $0 \leq \tilde{\sigma}_C < \tilde{\sigma}_C^{\mathrm{Hom}}$ the limit cycle no longer exists. Near but just below $\tilde{\sigma}_C^{\mathrm{Hom}}$ trajectories approach close to the intermediate tumour steady state before shooting off to the large tumour steady state (representing escape; see zoom in Figure 2.11 (d)). An initial condition starting near the intermediate tumour steady state first moves upwards and clockwise, as before. As the trajectory passes the tumour-free steady state and moves upwards in the unstable direction, it overshoots the intermediate tumour steady steady state and subsequently falls onto a stable manifold of the large tumour steady state (see insert of Figure 2.11 (d)). The trajectory is no longer a closed loop but terminates at the large tumour steady state.

2.7 Asymptotic behaviour for $\tilde{N}^2 \ll 1$

When $\tilde{N}^2 \ll 1$, immunosuppression occurs at small tumour sizes, and acts by reducing the proliferation rate of the helper T cells. We show below how, in this case, it is possible to construct asymptotic expressions for the large tumour steady state solutions representing tumour escape, and the small tumour steady state solutions from which oscillatory solutions emerge. In each case we determine an expression for the critical value of $\tilde{\sigma}_C$ where the fold point (giving rise to tumour escape) and the Hopf bifurcation point (giving rise to limit cycle solutions) occur respectively. In the neighbourhood of the Hopf bifurcation, we describe the amplitude of the limit cycle via a weakly nonlinear analysis.

2.7.1 The large tumour steady state (escape)

When $2\tilde{N} < \bar{\alpha} < 1 + \tilde{N}^2$ there exists two asymptotes in H_a at $N^* = N_-^*$ and $N^* = N_+^*$ (see equation (2.18) and Figure 2.4(b)). When H_a and H_b intersect tangentially near the asymptote $N^* = N_+^*$, a pair of steady state solutions emerge at a fold point $\tilde{\sigma}_C = \tilde{\sigma}_C^{\mathrm{F}}$. For $0 \leq \tilde{\sigma}_C < \tilde{\sigma}_C^{\mathrm{F}}$ two tumour equilibrium ($N^* > 0$) steady states exist which coalesce at $\tilde{\sigma}_C = \tilde{\sigma}_C^{\mathrm{F}}$ (see Figures 2.8–2.10)

We now construct approximate solutions for the steady state populations, N^*, T_H^* and T_C^* at the fold point, $\tilde{\sigma}_C = \tilde{\sigma}_C^{\mathrm{F}}$, when $\tilde{N}^2 \ll 1$ (the default case for our

parameters). Consider the following expansion for N^*, T_C^* and T_H^*:

$$N^* = N_0 + \tilde{N}^2 N_1 + \dots , \tag{2.23a}$$

$$T_C^* = T_{C0} + \tilde{N}^2 T_{C1} + \dots , \tag{2.23b}$$

$$T_H^* = T_{H0} + \tilde{N}^2 T_{H1} + \dots . \tag{2.23c}$$

To leading order, equation (2.16) for H_a reduces to $H_a = \bar{\sigma}_H N_0/(N_0 - \bar{\alpha})$. Likewise to leading order equation (2.17) for H_b reduces to, $H_b = 1 + \tilde{k}N_0 - \tilde{\sigma}_C/(1 - N_0)$. Equating the two leads to the cubic equation

$$\tilde{k}N_0^3 - (1 - \bar{\sigma}_H - \tilde{k}(1 + \bar{\alpha}))N_0^2 - (1 - \tilde{\sigma}_C - \bar{\sigma}_H + \bar{\alpha}(1 - \tilde{k}))N_0 + \bar{\alpha}(1 - \tilde{\sigma}_C) = 0 \,. \tag{2.24}$$

The fold bifurcation occurs when this cubic equation has a repeated root, specifically when equation (2.24) takes the form

$$\tilde{k}(N_0 - a)^2(N_0 - b) = 0 \,, \tag{2.25}$$

where a and b are constants and a corresponds to the leading order approximation for the tumour burden at the fold point. Equating the coefficients of equations (2.24) and (2.25) we find

$$\begin{aligned} N_0^2 :&\quad \tilde{k}(2a + b) = \bar{\sigma}_H + \tilde{k}(\bar{\alpha} + 1) - 1 \,, \\ N_0^1 :&\quad \tilde{k}a(a + 2b) = \bar{\sigma}_H + (\tilde{k} - 1)\bar{\alpha} - 1 + \tilde{\sigma}_C \,, \\ N_0^0 :&\quad \tilde{k}a^2 b = -\bar{\alpha}(1 - \tilde{\sigma}_C) \,. \end{aligned} \tag{2.26}$$

We can solve (2.26) to obtain the values of $\tilde{\sigma}_C$, $\bar{\sigma}_H$ and b at the fold point as a function of $a = N^{*F}$, the tumour population at the fold point. (We cannot solve directly for a or b since both a and b must satisfy the cubic equation for N_0 given in (2.24).) We denote the solutions by $\tilde{\sigma}_C^{\mathrm{F}}(a)$, $\bar{\sigma}_H^{\mathrm{F}}(a)$ and $b(a)$, given explicitly by

$$\tilde{\sigma}_C^{\mathrm{F}}(a) = 1 + \frac{\tilde{k}a^2 b}{\bar{\alpha}} \,, \tag{2.27}$$

$$\bar{\sigma}_H^{\mathrm{F}}(a) = 1 + \tilde{k}(2a + b - \bar{\alpha} - 1) \,, \tag{2.28}$$

$$b(a) = \frac{\bar{\alpha} + \tilde{k} - 1 - \tilde{k}a(2 - a)}{\tilde{k}(1 - 2a + a^2/\bar{\alpha})} \,. \tag{2.29}$$

Furthermore the leading order cytotoxic and helper T cell populations are given by

$$T_{C0} = \tilde{\gamma}(1 - a) \quad \text{and} \quad T_{H0} = \frac{\bar{\sigma}_H a}{a - \bar{\alpha}} \,. \tag{2.30}$$

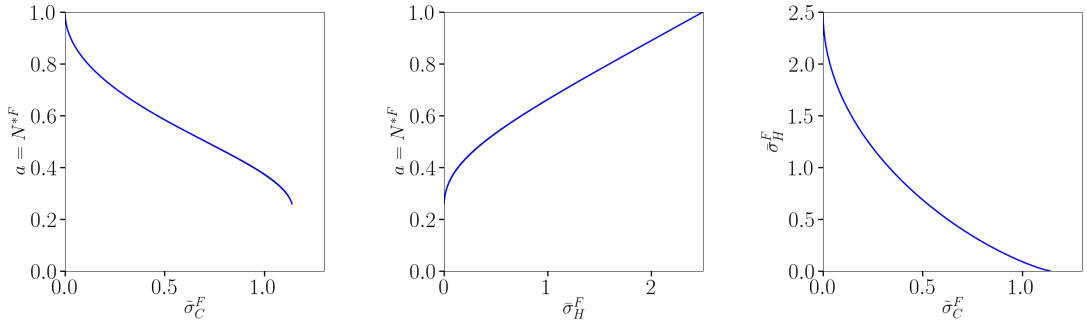

(a) (b) (c)

Figure 2.12: (a) The tumour population at the fold point, $a = N^{*\mathrm{F}}$ versus the infiltration rate of cytotoxic T cells, $\tilde{\sigma}_C^{\mathrm{F}}$ (from equation (2.27)), (b) $a = N^{*\mathrm{F}}$ versus the infiltration rate of helper T cells, $\bar{\sigma}_H^{\mathrm{F}}$ (from equation (2.28)), and (c) $\bar{\sigma}_H^{\mathrm{F}}$ versus $\tilde{\sigma}_C^{\mathrm{F}}$ (from equations (2.27) and (2.28)). The default values for $\tilde{k}$ and $\bar{\alpha}$ from equation (2.14) have been used. The plotted results depend only on these two parameter groupings. The exact solution for the fold point is shown by the black curves but this is largely obscured by the asymptotic solutions shown by the blue curves.

The asymptotic solutions for $\tilde{\sigma}_C^{\mathrm{F}}(a)$ and $\bar{\sigma}_H^{\mathrm{F}}(a)$, as well as $\bar{\sigma}_H^F(\tilde{\sigma}_C^{\mathrm{F}})$, are shown in Figure 2.12. In panels (a) and (b) we plot $a = N^{*\mathrm{F}}$ on the y-axis to show the inverse relationships $N^{*\mathrm{F}}(\tilde{\sigma}_C^{\mathrm{F}})$ and $N^{*\mathrm{F}}(\bar{\sigma}_H^{\mathrm{F}})$. These relationships cannot be directly inferred algebraically from (2.27)–(2.29) but nonetheless they are relatively simple. Similarly the relationship $\bar{\sigma}_H^{\mathrm{F}}(\tilde{\sigma}_C^{\mathrm{F}})$ is obtained parametrically by varying a over its range of permissible values. There are no solutions for $a < 0.26$ approximately, since in this range $T_H^* < 0$. In general $\bar{\sigma}_H^{\mathrm{F}}$ increases as $\tilde{\sigma}_C^{\mathrm{F}}$ decreases, reaching a value of $\bar{\sigma}_H^{\mathrm{F}} \approx 2.4$ when $\tilde{\sigma}_C^{\mathrm{F}} = 0$. The tumour population at the fold point $N^{*\mathrm{F}}$ increases from a relatively small value at the largest value of $\tilde{\sigma}_C^{\mathrm{F}}$ and approaches 1 (tumour escape) as $\tilde{\sigma}_C^{\mathrm{F}} \to 0$. The opposite relationship is found for $\bar{\sigma}_H^{\mathrm{F}}$, with $N^{*\mathrm{F}} \to 1$ as $\bar{\sigma}_H^{\mathrm{F}}$ approaches its largest value. With somewhat more algebra, the exact form of the fold point can be found without assuming $\tilde{N}^2 \ll 1$ (see Appendix C). The exact solutions are shown underneath the asymptotic solutions in Figure 2.12. For the parameters considered the exact and asymptotic solutions are too close to be distinguished.

2.7.2 The small tumour steady state

Consider $\tilde{N}^2 \ll \bar{\alpha}$, as holds for the default parameters. Then an asymptote in H_a occurs at $N_-^* = \tilde{N}^2/\bar{\alpha} = \delta \ll 1$ (assuming $\bar{\alpha} > 2\tilde{N}$), to leading order in δ (see equation (2.18)). We showed in the Section 2.4 that a tumour equilibrium steady state solution

occurs with $N^* < N^*_-$ for certain parameter groupings. We can explicitly calculate the form of this equilibrium to leading order in δ by assuming the expansions

$$(N^*, T^*_H, T^*_C) = (0, T^*_{H0}, T^*_{C0}) + \delta(N^*_1, T^*_{H1}, T^*_{C1}) + \delta^2 \dots . \tag{2.31}$$

Inserting these expansions into equations (2.16) and (2.17) gives

$$N^*_1 = 1 - \frac{\bar{\sigma}_H}{1-\tilde{\sigma}_C}, \quad T^*_{H0} = 1 - \tilde{\sigma}_C, \quad T^*_{C0} = \tilde{\gamma}\,, \tag{2.32}$$

and

$$T^*_{H1} = (\tilde{k} - \tilde{\sigma}_C)N^*_1, \quad T^*_{C1} = -\tilde{\gamma}N^*_1\,. \tag{2.33}$$

As anticipated from the analyses presented in Sections 2.4–2.6, a small tumour steady state exists where $0 < \tilde{\sigma}_C < 1 - \tilde{\sigma}_H$, which coincides with the domain of instability of the tumour-free steady state solution.

2.7.3 Linear Stability Analysis

Following the general linear stability analysis in Section 2.5, we next perturb the asymptotic solution for the small tumour steady state given by equations (2.32) and (2.33) by an infinitesimal time-dependent function proportional to $e^{\lambda t}$ (see equation (2.19)).

We deduce that the eigenvalues λ solve $|\mathcal{J} - \lambda I| = 0$ where the Jacobian is given by (see (2.20)):

$$\mathcal{J} = \begin{pmatrix} -\delta\gamma N^*_1 & 0 & -\delta pk N^*_1 \\ \dfrac{\delta_H(1-\tilde{\sigma}_C)}{\delta} & -\dfrac{\sigma_H}{(1-\tilde{\sigma}_C)} & 0 \\ -\dfrac{\gamma(1-p)}{p} & \tilde{\gamma} & -\tilde{\sigma}_C \end{pmatrix}.$$

Thus, the eigenvalues λ solve the following cubic

$$\lambda^3 + \left(\tilde{\sigma}_C + \frac{\sigma_H}{1-\tilde{\sigma}_C}\right)\lambda^2 + \frac{\tilde{\sigma}_C\sigma_H}{1-\tilde{\sigma}_C}\lambda + \gamma\left((1-\tilde{\sigma}_C)\delta_H - \sigma_H\right) = 0\,. \tag{2.34}$$

Periodic solutions emerge when two roots of equation (2.34) are purely imaginary, of the form $\lambda_{1,2} = \pm i\omega$, say. Hence we locate the Hopf bifurcation point by seeking solutions to equation (2.34) of the form

$$(\lambda^2 + \omega^2)(\lambda - \lambda_3) = 0\,, \tag{2.35}$$

where

$$\lambda_3 = -\left(\tilde{\sigma}_C + \frac{\sigma_H}{1-\tilde{\sigma}_C}\right), \quad \omega^2 = \frac{\sigma_H \tilde{\sigma}_C}{1-\tilde{\sigma}_C} \quad \text{and} \quad \lambda_3\omega^2 = -\gamma\left((1-\tilde{\sigma}_C)\delta_H - \sigma_H\right). \tag{2.36}$$

Eliminating λ_3 and ω^2 in (2.36) yields the following algebraic equation for $\tilde{\sigma}_C$ in terms of σ_H and other model parameters at the Hopf bifurcation point:

$$\tilde{\sigma}_C\sigma_H^2 + (1-\tilde{\sigma}_C)(\tilde{\sigma}_C^2 + \gamma(1-\tilde{\sigma}_C))\sigma_H - \gamma\delta_H(1-\tilde{\sigma}_C)^3 = 0\,. \tag{2.37}$$

Viewing equation (2.37) as a quadratic for σ_H rather than a cubic for $\tilde{\sigma}_C$, we can show where the small tumour steady state exists (i.e., where $0 < \tilde{\sigma}_C < 1 - \tilde{\sigma}_H$) there is a unique, positive root for σ_H:

$$\sigma_H = \sigma_H^{\text{Hopf}} = \frac{-\chi + \sqrt{\chi^2 + 4\gamma\delta_H\tilde{\sigma}_C(1-\tilde{\sigma}_C)^3}}{2\tilde{\sigma}_C}\,, \tag{2.38}$$

where $\chi = (1-\tilde{\sigma}_C)(\tilde{\sigma}_C^2 + \gamma(1-\tilde{\sigma}_C))$. The eigenvalue $\lambda_3 \leq 0$ over this range of $\tilde{\sigma}_C$, indicating stability of the oscillatory solutions where they exist.

The results of this analysis are verified below in Figure 2.13(a), showing $\bar{\sigma}_H$ versus $\tilde{\sigma}_C$ for both the asymptotic approximation using equation (2.38) and the numerical solution for the eigenvalues λ_i at the Hopf bifurcation point determined from $|\mathcal{J} - \lambda_i\mathcal{I}| = 0$ using $\mathcal{J}$ in (2.20). Close agreement is found for all values of $\bar{\sigma}_H$. In addition, Figure 2.13(b) shows how the frequency ω at the point of emergence of the limit cycle varies with $\tilde{\sigma}_C$. The frequency vanishes at $\tilde{\sigma}_C \to 0$ and $\tilde{\sigma}_C \to 1$, and peaks for $\tilde{\sigma}_C \approx 0.72$. Figure 2.13(c) shows how the real eigenvalue λ_3 is always negative (indeed $\lambda_3 < -1$) over the domain where Hopf bifurcations occur. Figure 2.13(d) shows how the leading order correction to the tumour population N_1 varies with $\tilde{\sigma}_C$. Notably $0 \leq N_1 \leq 1$. These results underpin and justify the weakly nonlinear analysis presented in the following subsection.

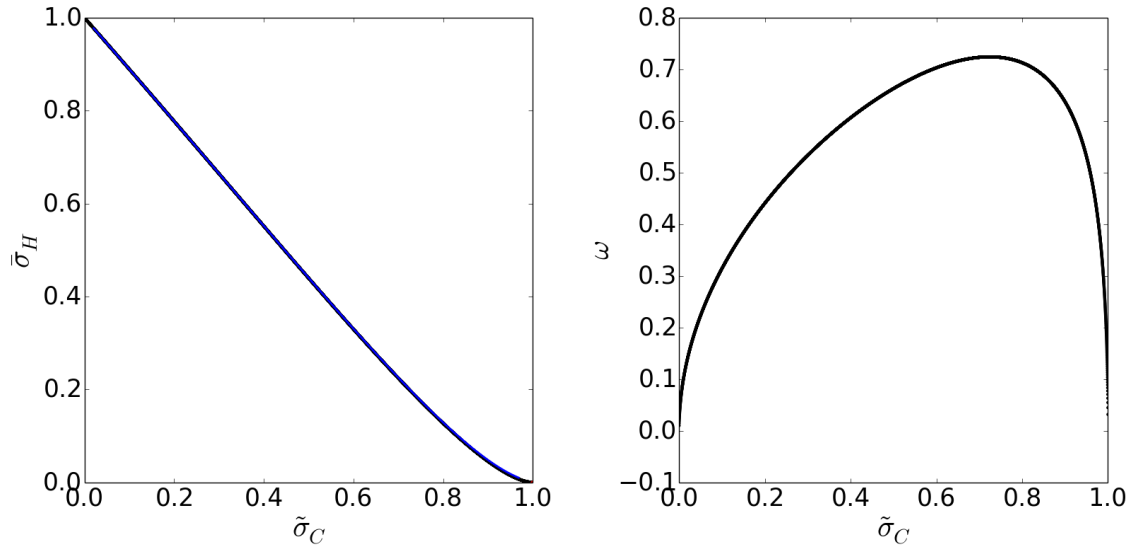

(a)

(b)

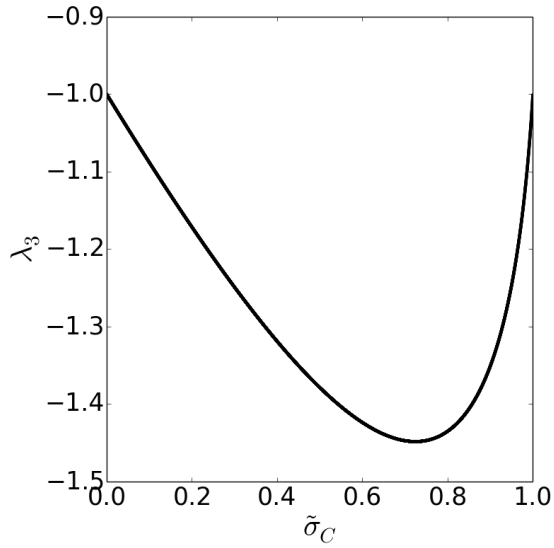

(c)

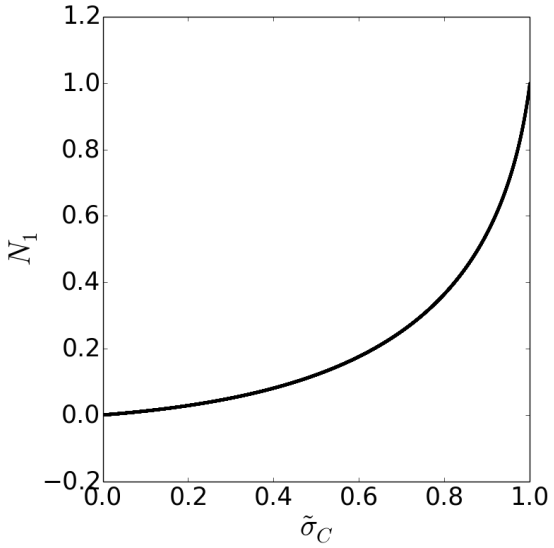

(d)

Figure 2.13: (a) Dependence of $\tilde{\sigma}_C$ on $\bar{\sigma}_H$ from equation (2.38) (black curve) compared with the numerical solution of $|\mathcal{J} - \lambda_i \mathcal{I}| = 0$ using $\mathcal{J}$ in (2.20) at the Hopf bifurcation point (blue curve). (b) Frequency ω associated with the eigenvalues $\lambda = \pm i\omega$ at the emergence of the limit cycle as $\tilde{\sigma}_C$ varies. Note $\omega \to 0$ as $\bar{\sigma}_H \to 0$ and 1. (c) The purely real eigenvalue, λ_3, associated with the small tumour steady state as $\tilde{\sigma}_C$ varies. (d) changes in the tumour population at the Hopf bifurcation point as $\tilde{\sigma}_C$ varies.

2.7.4 Weakly Nonlinear Analysis

In this section we perform a weakly nonlinear analysis in a neighbourhood of σ_C^{Hopf}, specifically $\sigma_C = \sigma_C^{\text{Hopf}} - \epsilon^2$ with $0 < \epsilon \ll 1$, in order to determine the amplitude of the limit cycle and confirm its local stability. Since the analysis is involved, results are summarised in the main text (see Appendix B for details).

For ease of presentation, we let $x = N$, $y = T_C$ and $z = T_H$. We introduce the long-time $\tau = \epsilon^2 t$ and proceed by expanding $\mathbf{x} = (x, y, z)^T$ as follows:

$$\mathbf{x} = \mathbf{x_0} + \epsilon \mathbf{x_1}(t, \tau) + \epsilon^2 \mathbf{x_2}(t, \tau) + \epsilon^3 \mathbf{x_3}(t, \tau) + \dots , \tag{2.39}$$

where the long time scale $\tau = \epsilon^2 t$ determines the limit cycle amplitude. Here $\mathbf{x_0}$ is the steady state solution with $N = \mathcal{O}(\tilde{N}^2)$ at $\sigma_C = \sigma_C^{\text{Hopf}}$. To obtain the amplitude equation for the limit cycle we substitute (2.39) into equations (2.6)–(2.8) and equate to zero terms of like orders of magnitude (full details are provided in Appendix B). At $\mathcal{O}(\epsilon)$, we recover the linear dynamics

$$\frac{\partial \mathbf{x_1}}{\partial t} = \mathcal{J}_0 \mathbf{x_1} \, , \tag{2.40}$$

where $\mathcal{J}_0 = \mathcal{J}(\mathbf{x_0})$. From the linear stability analysis, $\mathcal{J}_0 \mathbf{v_m} = \lambda_m \mathbf{v_m}$ where $\lambda_1 = i\omega$, $\lambda_2 = \lambda_1^* = -i\omega$ and $\lambda_3 \in \Re < 0$. Note $\mathbf{v_2} = \mathbf{v_1^*}$ while $\mathbf{v_3}$ is real. Let $\mathbf{v_m} = (v_{mx}, v_{my}, v_{mz})^T$ where $m = 1, 2, 3$. The most general solution of equation (2.40) is

$$\mathbf{x_1} = \phi(\tau)\mathbf{v_1} e^{i\omega t} + \phi^*(\tau)\mathbf{v_1^*} e^{-i\omega t} + \chi(\tau)\mathbf{v_3} e^{\lambda_3 t}. \tag{2.41}$$

Here, $\phi(\tau)$ is the amplitude of the first-order (linear) mode. The amplitude of the decaying mode, $\chi(\tau)$, plays no role in the subsequent analysis because it is non-secular. The equation for $\phi(\tau)$ is determined at $\mathcal{O}(\epsilon^3)$ by eliminating secular terms as discussed below.

At $\mathcal{O}(\epsilon^2)$ we find that $\mathbf{x_2}$ is given by

$$\mathbf{x_2} = \mathbf{x_{20}} + \mathbf{R_2^a}\phi^2(\tau)e^{2i\omega t} + c.c. + \mathbf{R_2^b}|\phi(\tau)|^2 + \mathbf{R_2^c}\phi(\tau)\chi e^{(\lambda_3 + i\omega)t} + c.c. + \mathbf{R_2^d}\chi^2 e^{2\lambda_3 t}. \tag{2.42}$$

where $\mathbf{x_{20}} = {\mathcal{J}_0}^{-1}(0, 1, 0)^T$ and $\mathbf{R_2^a}$ through $\mathbf{R_2^d}$ are constant vectors (see Appendix B). Notably, $\mathbf{x_{20}}$ arises from the $\mathcal{O}(\epsilon^2)$ correction to σ_C.

At $\mathcal{O}(\epsilon^3)$, the secularity condition supplies the following equation for the amplitude of the limit cycle

$$\frac{d\phi}{d\tau} = (\mu + \nu|\phi(\tau)|^2)\phi(\tau) \tag{2.43}$$

where $\mu = \mu_r + i\mu_i$ and $\nu = \nu_r + i\nu_i$ depend on the governing parameters.

Substituting $\phi(\tau) = r(\tau)\exp(i\vartheta(\tau))$ into equation (2.43) and equating real and imaginary parts yields

$$\frac{dr}{d\tau} = (\mu_r + \nu_r r^2)r \quad \text{and} \quad \frac{d\vartheta}{d\tau} = \mu_i + \nu_i r^2 \,. \tag{2.44}$$

The equation for r is independent of ϑ and has solution

$$r = \left(\frac{\mu_r}{(\mu_r/r^2(0) + \nu_r)\exp(-2\mu_r\tau) - \nu_r} \right)^{1/2} . \tag{2.45}$$

If $\mu_r > 0 > \nu_r$, as is typical for the parameter values considered (see Table 2.2), then $r \to \sqrt{-\mu_r/\nu_r} \equiv A$ (a constant) as $\tau \to \infty$ if $r(0) > 0$ (otherwise $r(\tau) \equiv 0 \; \forall \, t$). In such cases the limit cycle is a stable attractor.

We confirmed our weakly nonlinear analysis by computing the mean square amplitudes of $(x - x_0)/\epsilon$, $(y - y_0)/\epsilon$ and $(z - z_0)/\epsilon$ to time $t = t_{\max} = 20T(\epsilon^{-2} + 1)$ where $T = 2\pi/(\omega + \epsilon^2\omega_{nl})$ is the orbital period. Here ω_{nl} is the nonlinear correction to the frequency, given by $\omega_{nl} = \mu_i - \nu_i\mu_r/\nu_r$. The time $t_{\max}$ needs to be sufficiently long for the amplitude of the limit cycle to settle to a near constant value. Sampling the solution 3600 times over the last $20T$ time units yields estimates of the amplitude A which agree to within 0.4% when $\epsilon = 0.1$ and to within 0.016% when $\epsilon = 0.01$ (see zoomed regions in Figures 2.8(b)–2.10(b)). The sampling period chosen here is sufficiently long to minimise sampling errors, as the good agreement with the analysis confirms.

2.8 The effect of immunosuppression

We start by considering how changes in $\bar{\alpha}$, the (scaled) proliferation rate of the helper T cells upon encounter with tumour antigen, affect the bifurcation structure in $(\tilde{\sigma}_C, \bar{\sigma}_H)$ space. We focus on varying the (scaled) rates of T cell infiltration, $\bar{\sigma}_H$ and $\tilde{\sigma}_C$, as experiments have indicated large patient-to-patient variability in these parameters [141, 113, 98, 91]. Furthermore, high levels of infiltrating T cells correlate with good prognoses [113, 98, 91].

In Figure 2.14 we present results which show how the bifurcations that occur in $(\tilde{\sigma}_C, \bar{\sigma}_H)$ parameter space change as $\bar{\alpha}$ varies. We observe seven distinct regions:

1. Black shaded region: monostability of the tumour-free steady state (tumour elimination). Here no other steady states exist.

2. Region shaded with vertical lines: bistability between the tumour-free steady state and large tumour steady state solutions (depending on the initial conditions either the tumour is eliminated or it escapes).

3. Dark grey shaded region: bistability between the small and large tumour steady state solutions (depending on the initial conditions either tumour escape or equilibrium will occur).

4. Light grey shaded region: bistability between the limit cycle and large tumour steady state solutions.

5. White region: multiple unstable steady state solutions and stability of the large tumour steady state (tumour escape).

6. Region shaded by horizontal lines: instability of the tumour-free steady state and stability of the large tumour steady state (tumour escape).

7. Region shaded by crossings: instability of the tumour-free steady state and stability of the small tumour steady state (i.e. tumour equilibrium).

Features that are common for all values of $\bar{\alpha}$ can be summarised as follows:

- A stable tumour-free steady state exists for large values of $\tilde{\sigma}_C$ and $\bar{\sigma}_H$ (top right corner);

- An unstable tumour-free steady state and a stable large tumour steady state exists for small values of $\tilde{\sigma}_C$ and $\bar{\sigma}_H$ (lower left corner);

- The series of bifurcations that separate regions in which the tumour-free steady state is stable (large values of $\tilde{\sigma}_C$) from regions in which the large tumour state is stable (small values of $\tilde{\sigma}_C$) depend upon the value of $\bar{\alpha}$.

We now discuss the changes in the bifurcation structure that occur when $\bar{\alpha}$ is varied about its default value ($\bar{\alpha} = 0.19$). For smaller values of $\bar{\alpha}$ (e.g., $\bar{\alpha} = 0.06$, the small and intermediate steady state solutions coalesce at a fold bifurcation at a small value of $\tilde{\sigma}_C$ (see Figure 2.14(a,d)). Increasing $\bar{\alpha}$ increases the size of the region in which the tumour-free state is the only stable attractor (black region) and reduces the size of the region in which the tumour-free and large tumour states are stable (region shaded with vertical lines), with bistability disappearing altogether if $\bar{\alpha}$ is sufficiently large (see Figure 2.14 (c,f)). The size of the region characterised by bistability between the large and small tumour steady states disappears for large

values of $\bar{\alpha}$ (dark grey region). Comparison of Figure 2.14 (b,c) and (e,f) reveals that as $\bar{\alpha}$ increases the region in $(\tilde{\sigma}_C, \bar{\sigma}_H)$ parameter space in which only the large tumour steady state is stable decreases in size (white regions). Increasing $\bar{\alpha}$ increases the size of the region in which limit cycles exist (light grey region). We remark further that as $\bar{\alpha}$ increases the fold point at which the large and intermediate tumour steady states coalesce occurs at smaller values of $\tilde{\sigma}_C$. In particular, for $\bar{\alpha} > 1+\tilde{N}^2$, the intermediate and large tumour states disappear and only the small tumour and tumour-free steady state solutions exist (results not shown). In this case the tumour cells stimulate such a strong increase in the proliferation rate of the helper T cells that they increase to sufficient numbers that they can control or eliminate the tumour (see right hand panel of Figure 2.4(c)).

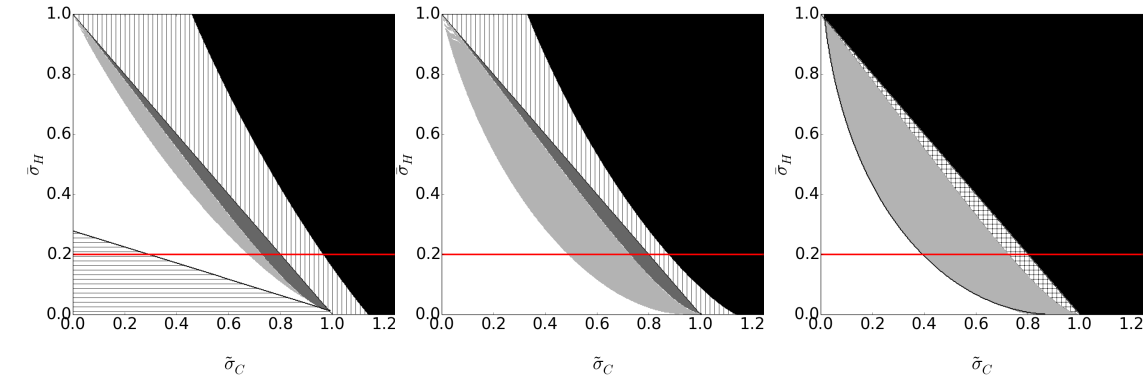

(a) $\bar{\alpha} = 0.06$ (b) default: $\bar{\alpha} = 0.19$ (c) $\bar{\alpha} = 0.6$

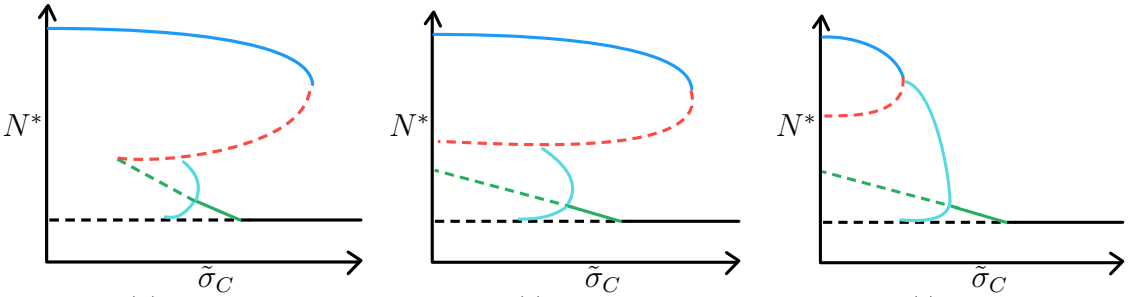

(d) $\bar{\alpha} = 0.06$ (e) $\bar{\alpha} = 0.19$ (f) $\bar{\alpha} = 0.6$

Figure 2.14: Bifurcation diagrams showing how the number of steady states (identified by continuous black lines), their stability, and the existence of the stable limit cycle change as σ_C and σ_H vary. Here the effects on the sizes and existence of these regions are examined for variations in $\bar{\alpha}$ with all remaining parameters fixed to their default values.

The results in Figure 2.14 provide a guide for potential treatment protocols for varying rates of helper T cell proliferation. In all cases, increasing $\tilde{\sigma}_C$ and $\bar{\sigma}_H$ in

equal amounts is most effective in driving the system away from tumour escape. However, the increase in either population must be limited to avoid an overzealous immune response. Targeting both populations in combination appears to be the most effective treatment. If only one population can be targeted alone, then targeting the cytotoxic T cell population appears to be most effective. The only exception occurs for an effective immune system (relatively high helper T cell proliferation, as in Figure 2.14(c)); in this case targeting either population is comparably effective.

In this section we have examined how the bifurcation structure in $(\tilde{\sigma}_C, \bar{\sigma}_H)$ space changes as we vary $\bar{\alpha}$, a parameter that reflects the extent to which the helper T cells increase their rate of cell proliferation on contact with tumour cells. We identified six distinct regions, distinguished by the existence and stability of steady states and the limit cycle. Variations in $\tilde{N}$ yield similar results and are, therefore, omitted. Variation of other model parameters (e.g., γ, k and p) affects the location of the fold point relative to the transcritical bifurcation, and the Hopf bifurcation. Our results show that changing the parameters $(\bar{\alpha}, \tilde{N})$ has a significant effect on the system's bifurcation structure in $(\tilde{\sigma}_C, \bar{\sigma}_H)$ parameter space. Taken together our results indicate the extent to which combination therapies which not only boost the immune system (by increasing $\bar{\sigma}_H$ and $\tilde{\sigma}_C$) but also block immunosuppressive effects may outperform monotherapies, with a single mode of action.

2.9 Discussion

We have proposed a new mathematical model of tumour-immune interactions in which helper and cytotoxic T cells interact with tumour cells. Our model captures the three Es of immunoediting — elimination, equilibrium and escape [52]. We have examined how the number and nature of the attractors (stable steady states and limit cycles) change as the infiltration rates of cytotoxic and helper T cells, σ_C and σ_H, are varied. Our focus on σ_C and σ_H is motivated by experimental observations which show high inter-patient variability in T cell infiltration rates and corresponding variability in observed outcomes [141, 66, 83, 5]. Specifically, high levels of tumour infiltrating T cells have been correlated with long-term progression free survival in a variety of different cancer types [153, 152, 91].

Our model exhibits three distinct behaviours as σ_C and σ_H vary. When σ_C and σ_H are both small the tumour always escapes. For intermediate values of σ_C and σ_H, two types of bistability can occur: either (a) bistability between tumour escape and elimination, or (b) bistability between tumour escape and tumour co-existence with

the immune system, the co-existence state representing either a finite equilibrium steady state or a time-dependent periodic solution. When σ_C and σ_H are both large, the tumour is always eliminated. Based upon these results, we propose that patients may be categorised into three main groups: immunocompromised patients have low rates of T cell infiltration and their tumours will escape; healthy patients have large rates of T cell infiltration and any nascent tumours will be eliminated; the tumours of patients with intermediate levels of T cell infiltration will either escape or be controlled, the outcome depending on the initial tumour size.

Stable limit cycles, characterised by periodic growth and suppression of the immune and tumour populations, have been observed both in other mathematical models of tumour-immune dynamics [102] and experimentally [38]. We confirmed that our model admits a stable limit cycle via a weakly nonlinear analysis which also yielded an equation for the amplitude of the limit cycle, valid near the Hopf bifurcation point.

To date, segregation of the T cell pool into helper and cytotoxic T cell populations, that can be targeted separately by immunotherapies, has received little attention. Which T cell population may elicit a stronger immune response is still widely debated [87, 51]. In this chapter we have developed a mathematical model which distinguishes their distinct roles as immune promoter and tumour killer respectively. We found that both T cell populations are important for tumour elimination. Given a sufficiently high rate of infiltration of either population, tumour elimination occurs. If, however, the rate of infiltration of helper T cells is low, then a large rate of infiltration of cytotoxic T cells is needed to eliminate the tumour. On the other hand, if the cytotoxic T cell infiltration rate is low, only a moderate increase in the helper T cell pool is required to eliminate the tumour. These findings suggest that targeting the helper T cell population may be more effective, and result in fewer immune-related adverse effects [72] than targeting the cytotoxic T cells directly.

Our model has also revealed that the immunosuppressive parameters α and $\tilde{N}$ play a major role in determining response outcomes. Specifically, increasing the proliferation rate of helper T cells, α, increases the size of the (σ_C, σ_H) region occupied by the stable tumour-free state. Increasing $\tilde{N}$, the size of the tumour at which immunosuppressive effects come into play, decreases the size of the region in which tumour escape occurs. These results suggest that manipulating α and $\tilde{N}$ may be effective therapies in cancer treatment. This could be achieved by blocking the PD-1/PD-L1 axis on T cells infiltrating the tumour [90], a therapy which has already shown significant promise [151].

In future work, it would be interesting to explore the effect of different treatment protocols for the different patient groups identified in this study. Immunotherapies that could be explored include: (a) treatment with an immune promoter cytokine such as IL-2, which stimulates the proliferation of cytotoxic T cells [164]; (b) adoptive T cell therapy which targets the infiltration of cytotoxic and helper T cells [131, 157]; (c) antibodies that block the PD-1/PD-L1 axis expressed by tumour and immune cells [145] affecting the size of the tumour at which immunosuppressive effects come into play; and (d) bi-specific antibodies that promote interactions between tumour and T cells [171]. Comparing different treatment strategies, both individually and in combination, may reveal effective treatment protocols that could be used to treat particular patient groups.

A limitation of the current model is the assumption of spatial homogeneity, and we neglect the spatial dynamics of interacting cytotoxic T cells, helper T cells and tumour cells. Future developments might extend our model to include random cell movement as well as movement driven by chemotactic effects leading to system ofs PDEs [130, 126]. Despite this limitation, our simplified model is able to capture the three Es of immunoediting and reveals distinct patient groups characterised by the levels of T cell infiltration into the tumour. Furthermore, interrogation of the model reveals how immunosuppressive effects and the rates of infiltration of the T cells might be manipulated to strengthen a weakened or ineffective immune system so that it can successfully eliminate any tumour.

To simplify yet retain key aspects of the complex model proposed by Robertson-Tessi *et al.* (2012) [160], we developed a system of three ODEs in the form of a predator-prey model, similar to Kuznetsov *et al.* (1994) [110], but with the addition of a helper T cell population. Our model enabled us to study, through a combination of analytical and numerical methods, the effectiveness of targeting helper and cytotoxic T cells in an anti-tumour immune response. Our model does not distinguish between the specific immunosuppressive effects that impact the tumour at various stages of development as in Robertson-Tessi *et al.* [160], but was nonetheless able to illustrate how the anti-tumour immune response varies with the level of infiltrating helper and cytotoxic T cells. Our results suggest that a combined therapy targeting the infiltration of both T cell populations may result in the best outcome for patients having a broad range of hindered immune systems. Nonetheless there is a preference for targeting the cytotoxic T cell population for highly hindered immune systems.

Chapter 3

A mathematical model of the progressive exhaustion of T cells in cancer

3.1 Introduction

In Chapter 2 we began exploring immune cell heterogeneity through subpopulations of T cells: helper and cytotoxic T cells. Specifically we proposed a simple extension of the model proposed by Kuznetsov *et al.* [110] to include a helper T cell population. Immunosuppression was also examined implicitly to account for the increasing resilience of the tumour to the immune system as the tumour grows. In this chapter we consider a new aspect of immune heterogeneity and focus exclusively on varying functional states (or states of exhaustion) of the cytotoxic T cells interacting with a tumour. Specifically we propose a distinct ODE model to address the following question:

- How do the rates of exhaustion of individual T cell functions, specifically their killing, infiltration and proliferation rates, suppress or facilitate tumour escape?

Through an array of immunosuppressive mechanisms, acting at different stages of tumour development, a pre-malignant neoplasm may evade immunosurveillance and develop into a clinically detectable tumour mass, ultimately metastasising. These immunosuppressive mechanisms act at all stages of the Cancer-Immunity Cycle [35] to break down an anti-tumour immune response, from the priming and activation stages in the lymph nodes (poor immunogenicity and antigenicity of the tumour cells) to the effector stages in the tumour microevironment (production of various cytokines such as TGF-β and IL-10 promoting up-regulation of various inhibitory

ligands such as PD-L1 by tumour cells and regulatory immune cells). A state of T cell exhaustion is induced and enhanced by the sustained exposure to high levels of tumour antigen [201, 199]. Increasingly exhausted T cells are identified by their highly diverse and dense expression of inhibitory receptors (IRs) [189, 171]. Other factors such as immunosuppressive cytokines produced by tumour cells and regulatory cells also contribute to the exhaustion state of the T cell [30, 208]. Here we study one stage of the cancer immunity cycle by developing a simple model of T cell exhaustion in the tumour microenvironment. We implicitly model the downstream effects on the T cell's function to kill, infiltrate and proliferate, accounting for all of these contributing suppressive pressures.

One of the mechanisms of immunosuppression used by the tumour is engagement of inhibitory receptors (IR) on the surface of the T cells with their matching ligands which activate the inhibitory pathways. Ligands expressed on the surface of tumour cells, as well as on the surface of antigen presenting cells (APCs), engage IRs up-regulated on the surface of T cells. Once engaged, these pathways signal to the T cell to dampen its function (e.g. hindered immunostimulatory cytokine production e.g. IL-2, proliferation and killing capacities). In cancer, T cells up-regulate their expression of IRs in response to soluble molecules (e.g. IL-10, TGF-β and adenoside) produced by tumour cells as well as regulatory immune cells (e.g. regulatory T cells (Tregs), myeloid derived suppressor cells (MDSCs) and tumour associated macrophages (TAMs)). As in chronic infections such as HIV and HPV where antigen levels persist, IR expression is sustained [199]. In a common acute infection, the expression of inhibitory receptors is transient and used to moderate the magnitude of the immune response. T cell exhaustion is characterised by the sustained co-expression of multiple IRs [201, 199].

The importance of T cell exhaustion in tumour growth was recognised recently through the success of monoclonal antibodies aimed at reversing or preventing T cell exhaustion in clinical trials. In these trials, monoclonal antibodies, known as checkpoint blockades, were designed to block the engagement of specific IR–ligand pathways on the surface of T cells, APCs and tumour cells. The two most well studied inhibitory receptors on the T cells are PD-1 and CTLA-4, and a number of antibodies that block these receptors have been FDA approved [150]. For a range of different cancers, such as breast cancer, colorectal cancer and advanced melanoma, clinical studies have found objective response rates when treated with checkpoint blockades for cohorts of patients [210]. However, such success is not uniform across all patients. In fact, a synthesis of the findings of a number of clinical trials found

that less than 50% of patients receiving these treatments exhibited durable responses [111, 84]. Despite this, the success of these immunotherapies in some patients has reinvigorated research into the role of the immune system in cancer progression, with specific focus on the state of exhaustion of the T cell [171].

There exist a number of ODE models designed specifically to examine the role of immunosuppressive effects in facilitating tumour escape. Some authors have singled out a specific immunosuppressive molecule or cell type, while others have sought to examine the combined effects of specific immunosuppressive pressures [160]. Other authors have included terms that only implicitly take immunosuppressive effects into account [22], through for example a biphasic term to describe T cell proliferation.

To explain the discrepancy in levels of regulatory T cells (Tregs) in experimental observations of different tumours, Leon *et al.* (2007) [114] developed a compartmentalised model to account for the immune activity in the lymph nodes and the tumour. They assumed that the immune activity in the lymph nodes (between Tregs, cytotoxic T cells and APCs) was occurring on a fast time scale compared to the activity within the tumour. This justified setting these populations to their equilibrium values, reducing the model to a system of three ordinary differential equations: tumour cells, cytotoxic T cells and regulatory T cells. Their model identified two mechanisms of tumour escape which were distinguished by the initial ratio of cytotoxic to regulatory T cell populations. Their results suggest that slow growing immunogenic tumours respond to T cell attack by recruiting/promoting the Treg population, ultimately enabling tumour cells to avoid destruction. In contrast, fast growing poorly immunogenic tumours do not recruit nearly as many Tregs.

Shariatpanahi *et al.* (2018) [177] developed a system of four ODEs consisting of two effector immune cell populations (cytotoxic T cells and natural killer cells), tumour cells, and MDSCs, a regulatory cell population of the innate immune response. In contrast to Leon *et al.* [114], their model was designed and validated to focus specifically on therapies targeting MDSCs in tumour eradication. They used their model to predict the optimal dosing regime of an anti-MDSC drug for tumours having various growth rates. They predicted that repeated dosages of an anti-MDSC drugs at low concentration would result in durable tumour-free responses, and identified that the frequency of dose administration is dependent on the growth rate of the tumour.

Other authors have gone further by including a range of immunosuppressive components in order to identify how the tumour orchestrates these components in tumour

escape. As discussed previously, Robertson-Tessi *et al.* (2012) [160] developed a system of twelve ODEs composed of nine cell populations and three cytokines. In this model they included what they argued to be the key immunosuppressive components, specifically Tregs and the cytokines IL-10 and TGF-β. Spatial limitations hindering the access of immune cells to the tumour were also accounted for. Their results identified the immunosuppressive factors primarily responsible for tumour escape for specific tumours characterised by their antigenicity and growth rate. They concluded that, irrespective of the tumour's antigenicity and growth rate, Tregs are a major component of the immunosuppressive network facilitating tumour escape. They further concluded that TGF-β becomes important only at large tumour sizes.

Instead of explicitly modelling regulatory immune cells (such as Tregs and MDSCs) and/or cytokines (such as IL-10 and TGF-β) other authors have implicitly accounted for immunosuppressive effects through terms damping the immune cell functions. This approach simplifies the underlying model. Clapp *et al.* (2015) [37] designed a model to capture the dynamical interactions between 'generic' cells of the immune system and four types of leukemic cells (quiescent, progenitor, cycling and mature). In their model they assumed that immunosuppressive effects acted in a biphasic manner on both the killing capacity of the T cells and their proliferative potential. They found there is an optimal number of tumour cells that elicits the strongest immune response. They used their model to explore how to drive a patient via immunotherapy into this optimum window to give the immune system the chance to work at its full potential, ultimately eliminating the tumour.

In this chapter we also adopt an implicit approach to model the downstream effects of immunosuppression on the T cell function mimicking the effects of T cell exhaustion. We are motivated by the recent experimental study of Thommen *et al.* (2015) [189] who observed time-dependency in IR expression in patients with non small lung cancer. We develop a simple predator-prey model for tumour and cytotoxic T cells to account for the continuous exposure of the T cells to the tumour, and the consequent impact on the functional state of the T cells. Variations in the rates at which the T cells lose their functionality and become exhausted are used to mimic additional immunosuppressive forces affecting the state of T cell exhaustion. How variations in these rates affect specific patients characterised by their T cell efficacy, defined as the ratio of the baseline T cell population (in the absence of a tumour) to the T cell population required to arrest tumour growth, is also examined. To our knowledge, this is the first model to attempt to model the effects of T cell exhaustion

and highlight the importance of specific T cell functions in preventing tumour escape. Ultimately these results may aid in the design of novel immunotherapies.

The structure of the chapter is as follows. In Section 3.2 we develop the model equations and discuss their underlying biological assumptions. In Section 3.3 the qualitative behaviour of the model is presented. In Section 3.4 we present the steady states together with their linear stability. In Section 3.5 we present the system bifurcations that arise as the T cell efficacy is varied as well as the rate at which tumour cells reduce the cytotoxicity, infiltration and proliferation of T cells, per tumour cell. In Section 3.6 we examine the effect of changing exponential tumour growth to logistic tumour growth in the model equations. In Section 3.7 the model equations are simplified in order to derive analytical approximations for the time-dependent limit cycle solutions observed in the full model. We derive analytical solutions describing the emergence, amplitude in the neighbourhood of the emergence point and disappearance of these limit cycle solutions. Section 3.8 concludes with a discussion of the main findings and their implications for potential immunotherapies.

3.2 The Mathematical Model

In the previous section the relevant biological context was described. Here the model equations together with their underlying assumptions are developed.

3.2.1 Model development

We propose a system of five ODEs focusing on interactions between tumour cells and cytotoxic T cells, where the T cells' rates of killing, infiltration and proliferation are continuously dampened due to sustained exposure to the tumour. With t denoting time, the dependent variables $N(t)$ and $T_C(t)$, represent numbers of tumour cells and cytotoxic T cells respectively. The parameters, $k(t)$, $\sigma(t)$ and $\alpha(t)$ evolve over time and represent respectively the rates of T cell killing, infiltration and proliferation in the presence of the tumour.

We suppose that the dominant processes regulating the dynamics of the tumour cells are cell proliferation and cell death caused by interactions with cytotoxic T cells. There is no clear consensus in the literature about how best to model tumour growth [76]. A number of different growth laws have been proposed including, for example, logistic, exponential, Gompertzian and power law growth [170]. In the previous chapter, we followed the approach of Kuznetov *et al.* (1994) [110], and assumed the tumour population grew logistically. In this chapter we assume that tumour cells grow

exponentially with growth rate γ (units: day^{-1}) and that tumour cells and cytotoxic T cells come into contact at a rate k (units: cells^{-1} day^{-1}) which is proportional to the product of their densities. Furthermore such contact leads to tumour cell death with probability $(1-\phi)$ (and cytotoxic T cell death with probability ϕ). Combining these effects we deduce that the tumour cell population evolves as follows,

$$\frac{dN}{dt} = \underbrace{\gamma N}_{\text{proliferation}} - \underbrace{k(t)(1-\phi)T_C N}_{\text{immune induced death}} . \tag{3.1}$$

This equation is similar to that proposed in Chapter 2, with terms accounting for tumour proliferation and death due to contact with the cytotoxic T cells. There are two main differences: (1) exponential growth of the tumour in place of the logistic growth, and (2) a time varying killing rate per T cell in place of a constant rate. This novelty enables us to explore in a simple way the effect of T cell exhaustion in tumour-immune dynamics.

We suppose that the physical processes that regulate the cytotoxic T cell population are infiltration from the lymph nodes, proliferation in response to tumour cells, cell death following contact with tumour cells and natural death. We assume cytotoxic T cells infiltrate the tumour tissue at rate σ (units: cells day^{-1}). In reality, T cells proliferate in response to indirect stimulation through the production of cytokines (e.g. IL-2) by the tumour cells (as well as other cells such as the helper T cells and APCs). For simplicity, we mimic this effect by assuming that direct contact with tumour cells stimulates the cytotoxic T cells to proliferate at a rate α (units: cells^{-1} day^{-1}) which is proportional to the product of their densities, or are killed with probability ϕ at rate k (units: cells^{-1}day^{-1}). Finally we assume that the cytotoxic T cells naturally decay at rate δ (units: day^{-1}), leading to

$$\frac{dT_C}{dt} = \underbrace{\sigma(t)}_{\text{infiltration}} + \underbrace{\alpha(t)T_C N}_{\text{proliferation}} - \underbrace{k(t)\phi T_C N}_{\text{tumour counter attack}} - \underbrace{\delta T_C}_{\text{natural death}} . \tag{3.2}$$

Here we propose a simple phenomenological description of T cell exhaustion and model the continuous progression of T cell exhaustion through the diminished rates of T cell killing, infiltration and proliferation proportional to the tumour population. In the absence of the tumour, the rates k, σ and α attain baseline values associated with a tumour-free state, $\breve{k}$, $\breve{\sigma}$ and $\breve{\alpha}$ (units: day^{-1}). In the presence of the tumour the rates of T cell killing, infiltration and proliferation are assumed to diminish at rates ξ_k, ξ_σ, ξ_α (units: cells^{-1} day^{-1}), respectively; they recover to their baseline values in the absence of the tumour at rate β (units: day^{-1}). This recovery rate of

the exhausted T cells mimics the influx of new, non-exhausted T cells. The rates of T cell killing, infiltration and proliferation are then described by the following equations

$$\frac{dk}{dt} = -\xi_k N k + \beta(\breve{k} - k)\,, \tag{3.3}$$

$$\frac{d\sigma}{dt} = -\xi_\sigma N \sigma + \beta(\breve{\sigma} - \sigma)\,, \tag{3.4}$$

$$\frac{d\alpha}{dt} = -\xi_\alpha N \alpha + \beta(\breve{\alpha} - \alpha)\,. \tag{3.5}$$

The model is completed by specifying the initial conditions

$$N(0) = N_0, \quad T_C(0) = T_{C0}, \quad k(0) = k_0, \quad \sigma(0) = \sigma_0 \quad \text{and} \quad \alpha(0) = \alpha_0\,, \tag{3.6}$$

where N_0, …, α_0 are given in specific cases examined in Section 3.3.

3.2.2 Non-dimensional system of equations

Before continuing we recast our model in dimensionless form. We scale time with δ^{-1}, the natural half-life of the cytotoxic T cells, therefore setting $t = \delta^{-1}\hat{t}$, where hats donate non-dimensional quantities. Setting $N = \breve{N}\hat{N}$, $T_C = \breve{T}_C\hat{T}_C$, $k = \breve{k}\hat{k}$, $\sigma = \breve{\sigma}\hat{\sigma}$ and $\alpha = \breve{\alpha}\hat{\alpha}$ in equations (3.1)–(3.5) gives

$$\breve{N} = \frac{\delta}{\breve{\alpha}} \quad \text{and} \quad \breve{T}_C = \frac{\gamma}{\breve{k}(1-\phi)}\,. \tag{3.7}$$

The typical population size of the cytotoxic T cells, $\breve{T}_C$, is given by balancing tumour proliferation and immune induced death in equation (3.1) assuming $\breve{k}$ is a characteristic size of $k(t)$. The typical tumour size, $\breve{N}$, represents a balance between T cell proliferation and natural death in equation (3.2), assuming $\breve{\alpha}$ is a characteristic value for $\alpha(t)$. The rates of T cell killing, infiltration and proliferation, $k(t)$, $\sigma(t)$ and $\alpha(t)$, are scaled by their baseline values $\breve{k}$, $\breve{\sigma}$, $\breve{\alpha}$. These scalings result in a dimensionless model with the fewest possible parameters given by

$$\frac{d\hat{N}}{d\hat{t}} = \hat{\gamma}\hat{N}\left(1 - \hat{k}\hat{T}_C\right)\,, \tag{3.8}$$

$$\frac{d\hat{T}_C}{d\hat{t}} = \hat{\nu}\hat{\sigma} + \hat{\alpha}\hat{T}_C\hat{N} - \hat{\kappa}\hat{k}\hat{T}_C\hat{N} - \hat{T}_C\,, \tag{3.9}$$

$$\frac{d\hat{k}}{d\hat{t}} = \hat{\beta}\left(1 - \hat{k}\left(\hat{\xi}_k\hat{N} + 1\right)\right)\,, \tag{3.10}$$

$$\frac{d\hat{\sigma}}{d\hat{t}} = \hat{\beta}\left(1 - \hat{\sigma}\left(\hat{\xi}_\sigma\hat{N} + 1\right)\right)\,, \tag{3.11}$$

$$\frac{d\hat{\alpha}}{d\hat{t}} = \hat{\beta}\left(1 - \hat{\alpha}\left(\hat{\xi}_\alpha \hat{N} + 1\right)\right), \tag{3.12}$$

where hatted quantities denote the following dimensionless parameter groups:

$$\begin{aligned} &\hat{\gamma} = \frac{\gamma}{\delta}, \quad \hat{\nu} = \frac{\breve{\sigma}\breve{k}(1-\phi)}{\delta\gamma}, \quad \hat{\kappa} = \frac{\breve{k}\phi}{\breve{\alpha}}, \\ &\hat{\xi}_k = \frac{\xi_k \delta}{\breve{\alpha}\beta}, \quad \hat{\xi}_\sigma = \frac{\xi_\sigma \delta}{\breve{\alpha}\beta}, \quad \hat{\xi}_\alpha = \frac{\xi_\alpha \delta}{\breve{\alpha}\beta} \quad \text{and} \quad \hat{\beta} = \frac{\beta}{\delta}. \end{aligned} \tag{3.13}$$

The dimensionless parameters are described in physical terms in Table 3.1.

Dimensionless parameter	**Physical interpretation**
$\hat{\gamma} = \frac{\gamma}{\delta}$	ratio of the typical life-span of a cytotoxic T cell to the tumour doubling time
$\hat{\nu} = \frac{\breve{\sigma}\breve{k}(1-\phi)}{\delta\gamma}$	ratio of the baseline T cell population (in the absence of a tumour) to the T cell population required to arrest tumour growth — herein after referred to as the 'T cell efficacy'
$\hat{\kappa} = \frac{\breve{k}\phi}{\breve{\alpha}}$	the ratio of the rate of tumour counter attack to the baseline rate of T cell proliferation
$\hat{\beta} = \frac{\beta}{\delta}$	rate at which non-exhausted T cells infiltrate the tumour over the typical life-span of a T cell
$\hat{\xi}_k = \frac{\xi_k \delta}{\breve{\alpha}\beta}$	the rate at which tumour cells reduce the cytotoxicity of T cells, per tumour cell
$\hat{\xi}_\sigma = \frac{\xi_\sigma \delta}{\breve{\alpha}\beta}$	the rate at which tumour cells reduce the infiltration of T cells, per tumour cell
$\hat{\xi}_\alpha = \frac{\xi_\alpha \delta}{\breve{\alpha}\beta}$	the rate at which tumour cells reduce the proliferation of T cells, per tumour cell

Table 3.1: Physical interpretation of the dimensionless parameters arising in equations (3.8)–(3.12).

In the definition of $\hat{\nu}$, we have estimated the baseline T cell population as $\breve{\sigma}/\delta$, taking $N = 0$ in equation (3.2) and using $\breve{\sigma}$ as a characteristic T cell infiltration. Whereas the T cell population required to arrest tumour growth, $\breve{T}_C$, is estimated by setting the tumour growth rate in equation (3.1) to 0, taking a characteristic value $\breve{k}$ for $k(t)$.

The model is closed by specifying initial conditions:

$$\hat{N}(0) = \hat{N}_0, \quad \hat{T}_C(0) = \hat{T}_{C0}, \quad \hat{k}(0) = \hat{k}_0, \quad \hat{\sigma}(0) = \hat{\sigma}_0 \quad \text{and} \quad \hat{\alpha}(0) = \hat{\alpha}_0. \tag{3.14}$$

In what follows both hats and tildes are omitted for clarity.

3.3 Qualitative behaviour

We next illustrate the range of behaviours exhibited by the model. In the absence of suitable data, the parameters in (3.13) are chosen such that the model exhibits the three Es of immunoediting: Elimination, Equilibrium and Escape [52]. We search for suitable values of the parameters by scanning over a 100-fold range of the parameters γ, ν, κ, β, ξ_k, ξ_σ and ξ_α (with 19 values taken between 0.1 to 10 and approximately equally spaced logarithmically). We choose default parameters that lie within a region in which tumour elimination, (finite) equilibrium and escape are possible. The default parameters used in the remaining analysis, unless otherwise stated, are given in Table 3.2. Note that due to the uncertainties in the dimensional parameters used in qualitatively similar models (see Table 2.1 in Chapter 2), the dimensionless parameters vary widely. As a result, a search through parameter space is necessary to find where the model exhibits expected behaviour.

Dimensionless parameter	**Default value**
γ	10
ν	1.5
κ	0.6
β	0.5
ξ_k	0.1
ξ_σ	1.0
ξ_α	0.15

Table 3.2: Summary of the default dimensionless parameter values used in equations (3.8)–(3.12) and defined in equation (3.13).

Figures 3.1 and 3.2 display the range of behaviours that the model exhibits as the T cell efficacy ν varies. To show how the tumour's growth dynamics are influenced by the initial functional state of the immune system, we fix the initial tumour population ($N_0 = 0.1$) and the initial cytotoxic T cell population ($T_{C0} = 1.0$), varying only the initial rates of T cell killing, infiltration and proliferation (k_0, σ_0 and α_0). The numerical method is the same as that used in Chapter 2 Section 2.3.

For the default value of $\nu = 1.5$ and all other parameters fixed at their default values, tumour elimination, equilibrium or escape are possible depending on the initial functional state of the immune system i.e. by the initial rates of T cell killing, infiltration and proliferation (see Figure 3.1(a)–3.2(a)). Escape occurs if the initial rates of T cell proliferation and infiltration, α_0 and σ_0 respectively, are small compared to their

baseline values of 1 (dotted black curve). In this case, even if the initial T cell kill rate k_0 is close to its baseline value of 1, the T cell population is unable to expand rapidly enough to prevent tumour growth. If instead the initial T cell infiltration rate σ_0 is close to its baseline value but k_0 and α_0 are reduced, the system settles to a tumour equilibrium state (solid dark grey curve). Elimination occurs when α_0 is close to its baseline value (dashed light grey curve). In this case the T cell population expands more rapidly than the tumour population and ultimately eliminates the tumour.

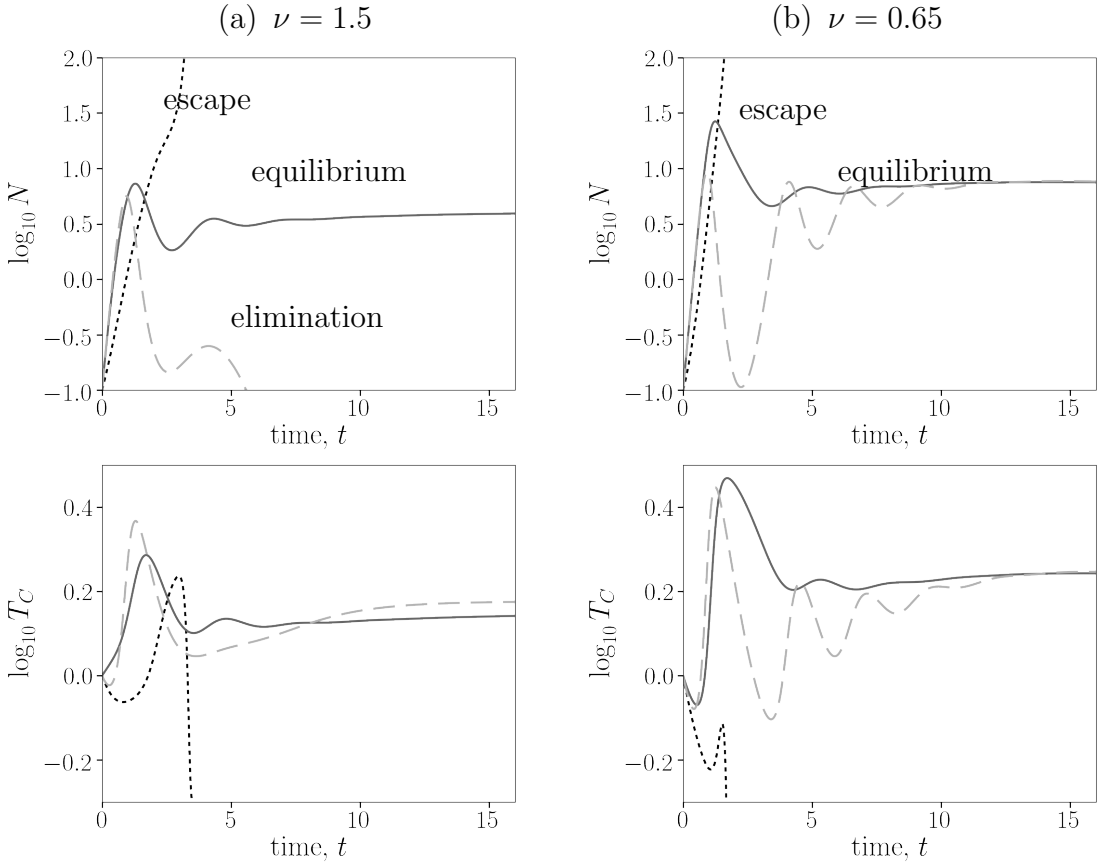

Figure 3.1: Illustration of the range of qualitative behaviours exhibited by equations (3.8)–(3.12). We plot the time evolution of the tumour population $N(t)$ and cytotoxic T cell population $T_C(t)$ for two different values of ν. In panel (a) for the default value of $\nu = 1.5$, we observe that the model exhibits states of tumour elimination, equilibrium and escape depending on initial conditions. In panel (b) for a smaller value of $\nu = 0.65$, we observe that for the initial conditions chosen, tumour elimination is no longer possible; instead the tumour settles either to an equilibrium or escapes. Parameter values: except for ν, all parameters are fixed at their default values. Initial conditions: $(N_0, T_{C0}, k_0, \sigma_0, \alpha_0) = (0.1, 1.0, 0.8, 0.4, 0.4)$ (dotted black curve), $(0.1, 1.0, 0.4, 0.8, 0.4)$ (solid dark grey curved) and $(0.1, 1.0, 0.4, 0.4, 0.8)$ (dashed light grey curve).

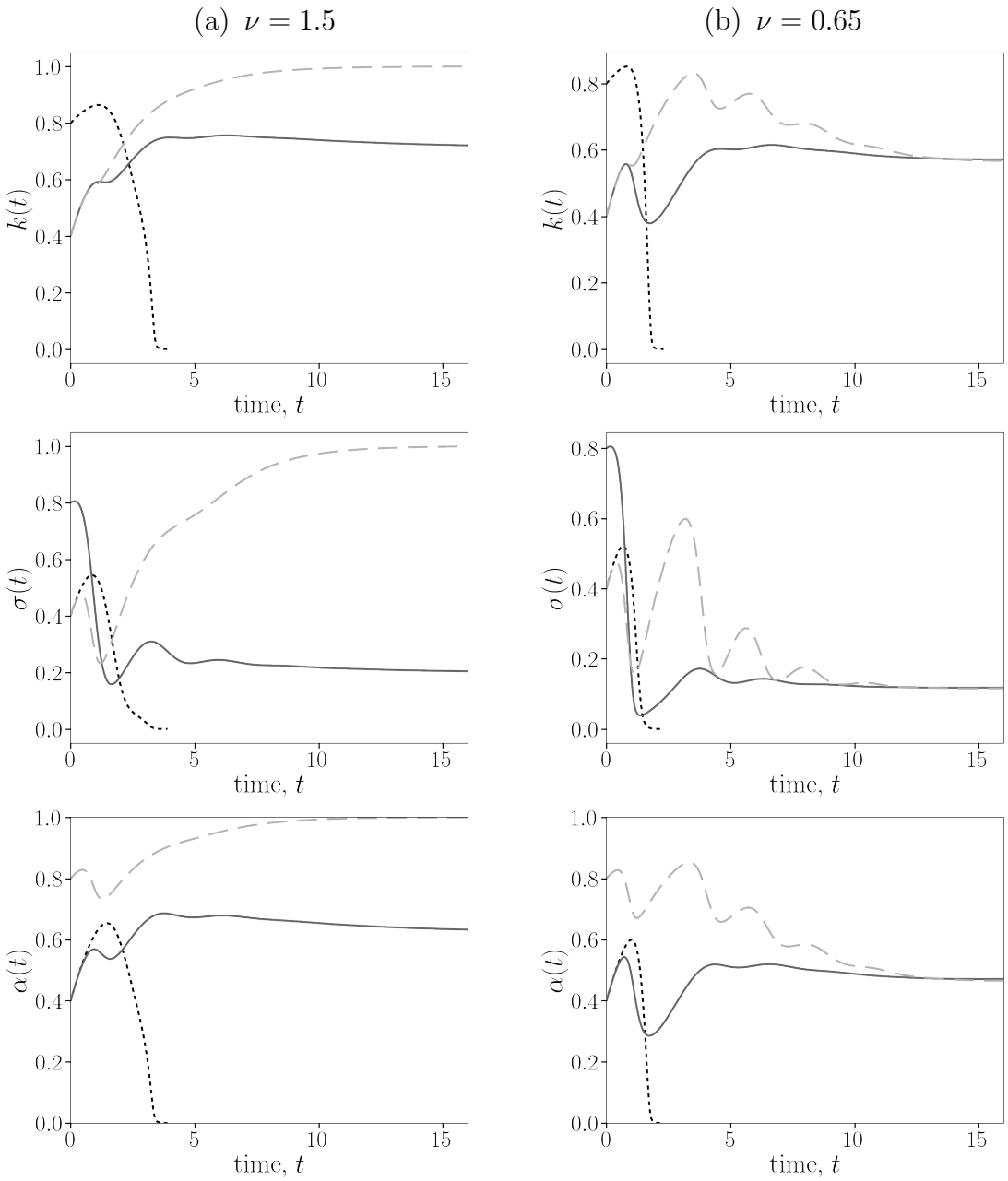

Figure 3.2: Evolution of the T cell functionalities corresponding to cases examined in Figure 3.1. Shown are the time evolution of T cell killing $k(t)$, T cell infiltration $\sigma(t)$ and T cell proliferation $\alpha(t)$ for two different values of ν. Key: as described in Figure 3.1.

By contrast when $\nu = 0.65$, tumour elimination is no longer observed for the initial conditions considered (in fact in Section 3.4 we find that the tumour-free state is linearly unstable for this choice of ν); only tumour equilibrium or escape is possible (see Figure 3.1(b) and 3.2(b)). As for $\nu = 1.5$, if σ_0 and α_0 are not close to their baseline values, then for the values of k_0 considered tumour escape is unavoidable

(dotted black curve).

In summary, starting with a small tumour population the model exhibits states of tumour elimination, equilibrium and escape [52]. The existence of such states appear to depend on ν, the T cell efficacy, in addition to the initial functional state of the cytotoxic T cell population (k_0, σ_0 and α_0). Provided ν is sufficiently large tumour elimination is possible. For the same choice of initial conditions but a smaller value of ν, tumour elimination is no longer possible and instead the system evolves to an equilibrium state. For both small and large values of ν, a high initial rate of T cell infiltration and/or proliferation is necessary to avoid escape. If such rates are not initially high then the T cells are unable to expand to match the exponential growth of the tumour and the tumour escapes. Our results suggest that if the initial state of a patient's immune system is exhausted, specifically if T cell infiltration and proliferation are hindered, the T cells are unable to effectively control the tumour.

3.3.1 Conditions for tumour escape

For the small and large value of ν considered in Figures 3.1 and 3.2, tumour escape occurs for the same choice of initial conditions in both cases. Due to our choice of an exponential law to describe tumour growth in the absence of an immune response, we wish to determine if there exists a bound on model parameters for which tumour escape is guaranteed irrespective of our initial conditions. We also determine whether the T cell population may escape.

For tumour escape to occur, examination of equation (3.8) reveals there must be a period in the early evolution when $kT_C < 1$ to allow the exponential growth of N over this time period. When $N(t)$ is sufficiently large then we can neglect 1 in equations (3.10)–(3.12) and therefore $k(t)$, $\sigma(t)$ and $\alpha(t)$ approach $(\xi_k N)^{-1}$, $(\xi_\sigma N)^{-1}$ and $(\xi_\alpha N)^{-1}$, respectively. If larger these quantities are pulled back to these values, while if smaller these quantities are pulled up to these values. Assuming T_C is growing in time, the leading order term in equation (3.9) namely $\nu\sigma$ may be neglected, allowing us to simplify this equation to

$$\frac{dT_C}{dt} = \Gamma T_C \quad \Longrightarrow \quad T_C(t) = Ae^{\Gamma t} \qquad \text{where} \qquad \Gamma = \frac{1}{\xi_\alpha} - \frac{\kappa}{\xi_k} - 1\,. \tag{3.15}$$

Therefore T_C grows if $\Gamma > 0$. Now according to equation (3.8) the tumour evolves according to

$$\frac{dN}{dt} = \gamma N - \frac{\gamma T_C}{\xi_k} \quad \Longrightarrow \quad N(t) = Be^{\gamma t} - \frac{\gamma A}{\Gamma \xi_k} e^{\Gamma t}\,.$$

Thus if $\gamma > \Gamma$ the tumour escapes. In this case $kT_C < 1$, which is assured provided Γ, the maximum growth rate of T_C, is less than γ, the maximum growth rate of N. In this case kT_C diminishes to zero as $t \to \infty$. In summary tumour escape occurs when

$$\gamma > \frac{1}{\xi_\alpha} - \frac{\kappa}{\xi_k} - 1\,. \tag{3.16}$$

This can be thought of as a necessary condition for tumour escape. It assumes N is large and $T_C < \xi_k N$.

The critical case $\gamma = \Gamma$ results in a secular term in the equation for N. The solution in this case is

$$N = \left(B - \frac{\gamma A}{\xi_k} t\right) e^{\gamma t}\,. \tag{3.17}$$

Since $\gamma A/\xi_k > 0$, N cannot grow indefinitely. This implies tumour escape only occurs when equation (3.16) is satisfied when N is sufficiently large.

This result helps us understand how the parameters controlling T cell exhaustion facilitate tumour escape. A low rate at which tumour cells reduce the proliferation of T cells per tumour cell helps to prevent tumour escape, as expected. On the other hand a low rate at which tumour cells reduce the killing of T cells per tumour cell (ξ_k) appears to favour tumour escape. This is because of the dual role that k plays in both the tumour and cytotoxic T cell evolution equations (3.8) and (3.9). Moreover as κ increases, corresponding to an increase in the ratio of the rate of tumour counter attack to the baseline rate of T cell proliferation, it becomes easier for the tumour to escape according to equation (3.16). This occurs because the tumour is killing the cytotoxic T cells needed to control the growth of the tumour.

3.4 Identification of steady states and their linear stability

To help interpret the behaviour observed in Section 3.3, we first identify the steady state solutions of equations (3.8)–(3.12) and examine their linear stability. The steady states are obtained by setting $d/dt = 0$ in equations (3.8)–(3.12) giving the algebraic system

$$0 = \gamma N^*(1 - k^* T_C^*)\,, \tag{3.18}$$

$$0 = \nu\sigma^* + T_C^*\left(\alpha^* N^* - \kappa k^* N^* - 1\right)\,, \tag{3.19}$$

$$0 = 1 - k^*(1 + \xi_k N^*)\,, \tag{3.20}$$

$$0 = 1 - \sigma^*(1 + \xi_\sigma N^*)\,, \tag{3.21}$$

$$0 = 1 - \alpha^*(1 + \xi_\alpha N^*)\,, \tag{3.22}$$

for the steady state variables, $(N^*, T_C^*, k^*, \sigma^*, \alpha^*)$.

Equation (3.18) suggests that steady state solutions may be either tumour-free (corresponding to $N^* = 0$) or tumour equilibrium states (with $N^* > 0$). The tumour-free state has the form

$$N^* = 0, \quad T_C^* = \nu \quad \text{and} \quad k^* = \sigma^* = \alpha^* = 1\,. \tag{3.23}$$

The tumour equilibrium states require $T_C^* = 1/k^*$ from equation (3.18) and

$$k^* = \frac{1}{1 + \xi_k N^*}, \quad \sigma^* = \frac{1}{1 + \xi_\sigma N^*}, \quad \alpha^* = \frac{1}{1 + \xi_\alpha N^*}\,, \tag{3.24}$$

from equations (3.20)–(3.22). Thus

$$T_C^* = 1/k^* = 1 + \xi_k N^*\,. \tag{3.25}$$

Using the expressions (3.24) and (3.25) in equation (3.19), the steady state tumour population N^* is determined by the roots of the cubic equation

$$C_3 N^{*3} + C_2 N^{*2} + C_1 N^* + C_0 = 0\,, \tag{3.26}$$

where

$$\begin{aligned} C_3 &= \xi_\sigma\left(\xi_k - \xi_\alpha(\kappa + \xi_k)\right)\,, \\ C_2 &= \xi_k + \xi_\sigma - \xi_\sigma\xi_\alpha - (\xi_\sigma + \xi_\alpha)(\kappa + \xi_k)\,, \\ C_1 &= 1 + \nu\xi_\alpha - (\kappa + \xi_k + \xi_\sigma + \xi_\alpha)\,, \\ C_0 &= \nu - 1\,. \end{aligned} \tag{3.27}$$

The roots of the cubic equation (3.26) are independent of γ and β. Hence tumour equilibria, where they exist, are independent of these parameters.

Note that as $C_3 \to 0$ a possible solution to (3.26) is $N^* \to \infty$. $C_3 = 0$ coincides with $\Gamma = 0$ where Γ was previously defined in equation (3.15), and occurs when the parameters satisfy

$$\xi_\alpha = \frac{\xi_k}{\kappa + \xi_k}\,. \tag{3.28}$$

With $C_3 = 0$, equation (3.26) reduces to a quadratic which is easily solved. Excluding the special case $C_2 = 0$, the roots of this quadratic are finite. Reintroducing C_3 but considering $C_3 = \epsilon \ll 1$, the two roots of the quadratic shift by $\mathcal{O}(\epsilon)$. However a third root may now exist (depending on the sign of N^*) having $N^* = \mathcal{O}(\epsilon^{-1})$. In fact to leading order in ϵ^{-1} this additional root is given by $-C_2/C_3$. This root is physical

therefore if C_2 and C_3 have opposite signs. As $\epsilon \to 0$ this solution terminates at the unbounded solution $N^* \to \infty$, as shown in Figure 3.3. The special case $C_2 = C_3 = 0$ requires a perturbation expansion in two small parameters and is not discussed here.

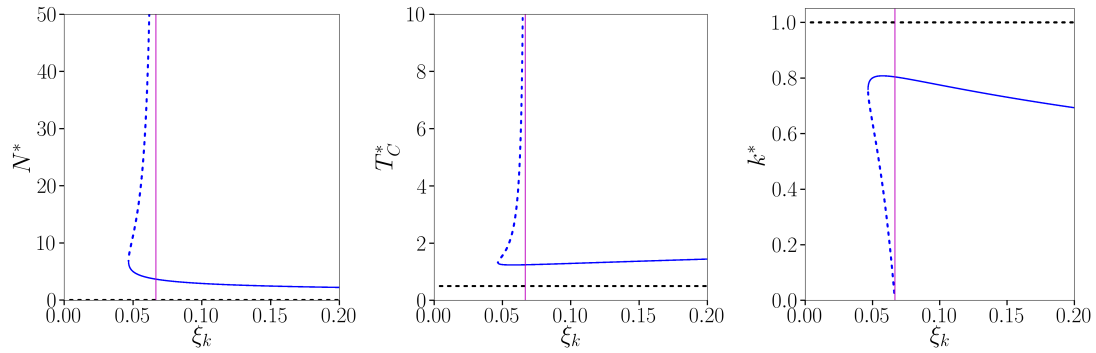

Figure 3.3: Bifurcation diagrams showing how the existence and (linear) stability of the steady state solutions vary with ξ_k for $\nu = 0.5$. Here we illustrate the fold bifurcation in which the upper branch of solutions terminates at unbounded populations in N^* and T_C^*, at $\Gamma = 0$. All remaining parameters are fixed at their default values. Key: solid lines indicate linear stability and dashed lines indicate linear instability; the horizontal magenta line represents the asymptote occurring when equation (3.28) is satisfied.

Linear stability of the steady states is studied by examining the growth rates associated with small time-dependent perturbations about $(N^*, T_C^*, k^*, \sigma^*, \alpha^*)$ (see Chapter 2 for further details). The growth rates associated with a given steady state are determined by calculating the eigenvalues λ_i, $i = 1, \ldots, 5$, from

$$|\mathcal{J}(N^*, T_C^*, k^*, \sigma^*, \alpha^*) - \lambda_i I| = 0\,, \tag{3.29}$$

where I is the identity matrix and $\mathcal{J}(N^*, T_C^*, k^*, \sigma^*, \alpha^*)$ is the Jacobian of equations (3.8)–(3.12):

$$\begin{pmatrix} \gamma(1-k^*T_C^*) & -\gamma k^* N^* & -\gamma N^* T_C^* & 0 & 0 \\ (\alpha^* - \kappa k^*)T_C^* & (\alpha^* - \kappa k^*)N^* - 1 & -\kappa T_C^* N^* & T_C^* N^* & \nu \\ -k^*\xi_k\beta & 0 & -(\xi_k N^* + 1)\beta & 0 & 0 \\ -\sigma^*\xi_\sigma\beta & 0 & 0 & -(\xi_\sigma N^* + 1)\beta & 0 \\ -\alpha^*\xi_\alpha\beta & 0 & 0 & 0 & -(\xi_\alpha N^* + 1)\beta \end{pmatrix}. \tag{3.30}$$

Linear stability is guaranteed provided $\max_i \Re(\lambda_i) < 0$. Otherwise if $\Re(\lambda_i) > 0$ for any i, the steady state is linearly unstable.

For the tumour-free state ($N^* = 0$) the eigenvalues can be determined analytically:

$$\lambda_1 = \gamma(1-\nu), \quad \lambda_2 = -1 \quad \text{and} \quad \lambda_3 = \lambda_4 = \lambda_5 = -\beta\,. \tag{3.31}$$

As $\beta > 0$ the linear stability of the tumour-free state is assured provided $\nu > 1$. When $\nu < 1$ the tumour-free state is linearly unstable.

The linear stability of the equilibrium states with $N^* > 0$ cannot generally be determined analytically. Their stability is instead examined numerically in Section 3.5.

3.5 System bifurcations

The qualitative behaviour in Section 3.3, for fixed rates at which tumour cells reduce the cytotoxicity, infiltration and proliferation of T cells per tumour cell (ξ_k, ξ_σ and ξ_α, respectively), suggests the model behaviour depends on the T cell efficacy, ν. Furthermore, the linear stability analysis in Section 3.4 reveals that there is a change in stability of the tumour-free steady state crossing $\nu = 1$, with instability for $\nu < 1$ and stability for $\nu > 1$, independent of the other model parameters, implying that tumour elimination is only possible in a region of parameter space where $\nu > 1$.

The dynamic process of T cell exhaustion is shaped by a number of forces in the tumour microenvironment. These range from soluble factors (e.g. IL-10 and IDO), regulatory immune cells (e.g. Tregs, TAMs and MDSCs), to changes in glucose levels and increased T cell expression of IRs [208]. Changes in the immunosuppressive pressures felt by the T cell during the growth of a tumour are encapsulated here through variations in the rates at which tumour cells reduce the cytotoxicity, infiltration and proliferation of T cells, per tumour cell, ξ_k, ξ_σ and ξ_α respectively. From herein we refer to these rates simply as the 'rates of exhaustion' of T cell killing, infiltration and proliferation, respectively. Another trait that may be used to identify and treat patients is the T cell efficacy, ν.

The appropriate way of treating a given patient, depending on their rates of T cell exhaustion and T cell efficacy, is explored in Figure 3.4. Here distinct states exhibiting qualitatively different behaviour are delineated. The results found here may be helpful in guiding immunotherapy treatment for a given patient.

The qualitative behaviours observed in Figure 3.4 are summarised next.

1. tumour elimination (white regions):
   (a) only the tumour-free state exists and is stable (uniform white region)
   (b) an additional unstable tumour equilibrium state exists (diagonal lines)
2. tumour elimination or equilibrium (white regions):

(a) bistability between a tumour-free and a tumour equilibrium state; no other steady states exist (horizontal lines)

(b) bistability between a tumour-free and an oscillatory solution; no other steady states exist (dotted region)

(c) bistability between a tumour-free and a tumour equilibrium characterised by an intermediate tumour load; two additional unstable tumour equilibria exist characterised by small and large tumour burdens (vertical lines)

3. tumour equilibrium (grey regions):

(a) bistability between two tumour equilibria characterised by small and large tumour burdens respectively; here the tumour-free state and an intermediate tumour equilibrium state exist but are unstable (grey shaded region)

(b) a stable oscillatory solution exists; the tumour-free state and a tumour equilibrium state exist but are unstable (dotted region)

(c) monostability of a tumour equilibrium state; the tumour-free state exists but is unstable (horizontal lines)

4. tumour escape; no stable steady states or oscillatory solutions exist (black regions). Note that when considering logistic growth in Section 3.6 this region corresponds to a large tumour equilibrium state at its carrying capacity, representing tumour escape.

We first discuss the overall structure in the panels shown in Figure 3.4. The dependence on ξ_σ (panel (b)) is seen to be considerably weaker than on either ξ_k or ξ_α (panels (a) and (c) respectively). This indicates that the role of infiltration is less important than either proliferation or tumour counter attack in equation (3.9). Mathematically, we conjecture that this is a consequence of the nonlinearity of the terms involving k and α in equations (3.10) and (3.12). Physically, the T cell killing and proliferation are strongly involved in the tumour-immune response while infiltration does not involve direct interaction with the tumour.

To better understand the changes in the qualitative behaviour as ξ_k, ξ_σ and ξ_α vary as a function of ν, a few representative cross sections are exhibited in Figure 3.5. There the rates of T cell exhaustion are fixed at specific values indicated by the red horizontal lines in Figure 3.4. The qualitative changes as we move through the regions for each cross section (a)–(f) are detailed next. In Figure 3.5(a), for $0 < \nu < \nu^{\mathrm{T}} = 1$ no stable steady states or limit cycles exist and the tumour escapes. When $\nu = \nu^{\mathrm{T}}$

there is a transcritical bifurcation at which the tumour-free state becomes stable and an unstable tumour equilibrium state emerges. For $\nu > \nu^{\mathrm{T}}$, either the tumour is eliminated or it escapes. Tumour elimination is only guaranteed if the initial tumour population is sufficiently small. Since here we lie in the region of parameter space below the critical curve $\Gamma = 0$ in equation (3.15) (see magenta line in Figure 3.4(a)), tumour escape is inevitable for all ν when the initial tumour population is large (see Section 3.3.1).

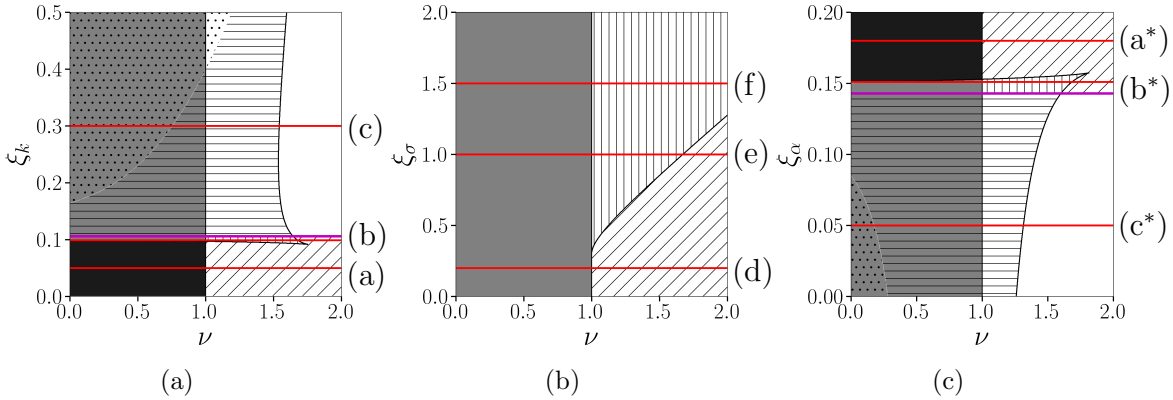

Figure 3.4: Plots showing how the qualitative behaviour of equations (3.8)–(3.12) varies with the parameters ν, ξ_k, ξ_σ and ξ_α. The remaining parameters are fixed at their default values. Shading and hatching is used to distinguish different behaviours according to the existence and stability of the model attractors (steady states and limit cycles). Key: white region: only the tumour-free state exists and is stable; white region with horizontal black lines: bistability between the tumour-free state and a tumour equilibrium state; white region with vertical black lines: bistability between the tumour-free state and a tumour equilibrium state, two additional tumour equilibria exist but are unstable; white region with diagonal black lines: the tumour-free state is stable and a tumour equilibrium state exists but is unstable; white region with black dots: bistability between the tumour-free state and an oscillatory solution, here an unstable tumour equilibrium state exists; grey region with black dots: a stable limit cycle solutions exists, here the tumour-free state and an intermediate tumour state exist but are unstable; grey region with black horizontal lines: a stable tumour equilibrium state exists, here the tumour-free state is unstable; grey region: bistability between two tumour equilibria characterised by small and large tumour burdens; here the tumour-free state and an intermediate tumour state exists but are unstable; black region: no stable solutions exist and therefore escape is inevitable. The horizontal red lines correspond to the cross sections (a)–(f) shown in Figure 3.5. The horizontal magenta lines in panels (a) and (c) correspond to $\Gamma = 0$ in equation (3.15) marking the termination of the solution branch originating from the fold point. Note Γ does not depend on either ξ_σ or ν and everywhere in panel (b) $\Gamma = 6$ and therefore $\Gamma < \gamma$, and a sufficiently large tumour escapes.

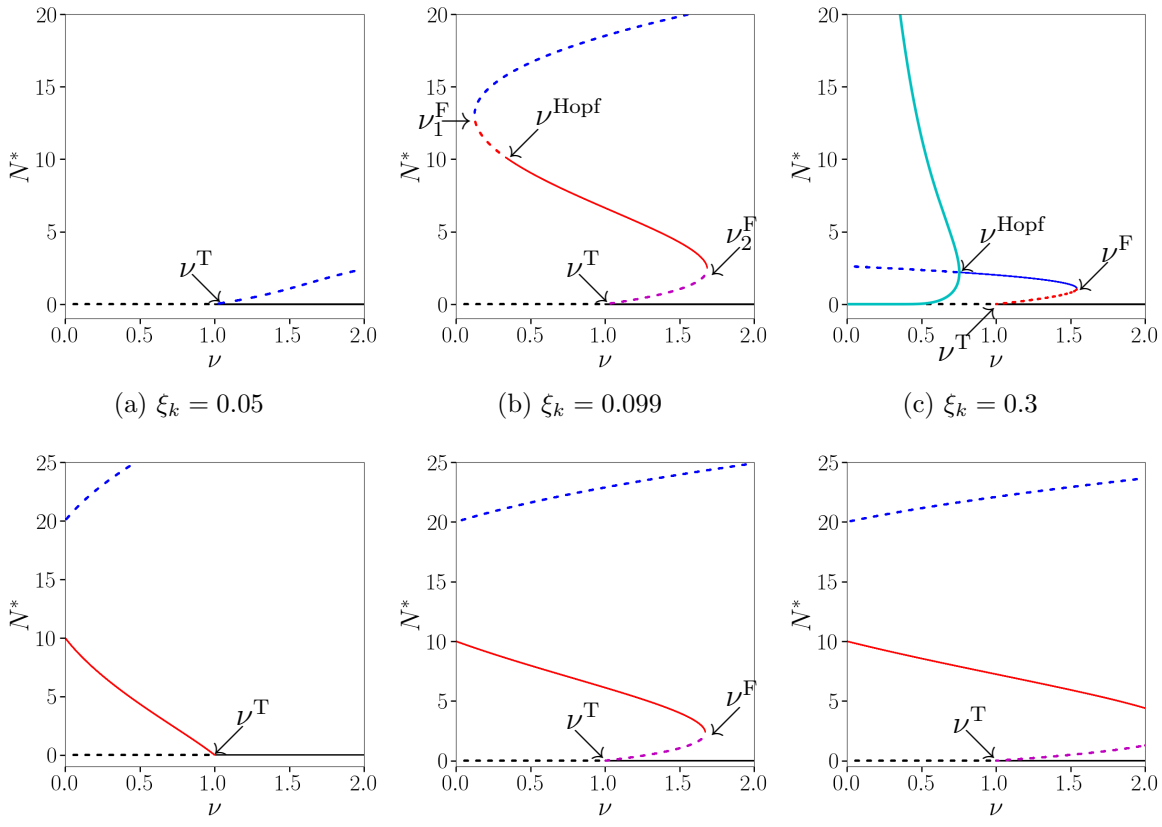

Figure 3.5: Bifurcation diagrams showing how the existence and (linear) stability of the tumour steady state solutions N^* change as ν is varied for the different values of ξ_k and ξ_σ indicated in panels 3.4. All remaining parameters are fixed at their default values. Key: line styles as in Chapter 2 Figure 2.8. The various bifurcations occurring are indicated.

Figure 3.5(b) differs substantially from Figure 3.5(a). Here in addition to the transcritical bifurcation, there are two fold bifurcations, ν_1^{F} and ν_2^{F} (with $\nu_1^{\mathrm{F}} < \nu_2^{\mathrm{F}}$), and a Hopf bifurcation at $\nu = \nu^{\mathrm{Hopf}}$. For $0 < \nu < \nu_1^{\mathrm{F}}$ no stable steady states or limit cycles exist, implying tumour escape is inevitable. For $\nu_1^{\mathrm{F}} \leq \nu < \nu^{\mathrm{Hopf}}$ two unstable tumour equilibria and an unstable limit cycle exist in addition to the tumour-free state which is also unstable. Likewise in this region tumour escape is inevitable. For $\nu^{\mathrm{Hopf}} \leq \nu < \nu^{\mathrm{T}}$ the tumour equilibrium, characterised by a small tumour burden, becomes stable. For $\nu \geq \nu^{\mathrm{T}}$, the tumour-free state becomes stable and an unstable tumour equilibrium state emerges at $\nu = \nu^{\mathrm{T}}$. We observe bistability between the tumour-free state and an intermediate tumour equilibrium state. At the fold point $\nu = \nu_2^{\mathrm{F}}$ two of the steady states collide and for $\nu > \nu_2^{\mathrm{F}}$ only the tumour-free state is stable. In the region $\nu > \nu^{\mathrm{Hopf}}$ there exists a stable tumour equilibrium and/or

tumour-free state. In this region tumour escape is only guaranteed if N is initially large enough. Otherwise the tumour will go to equilibrium or be eliminated (for $\nu > \nu^{\text{Hopf}}$).

In Figure 3.5(c) for $0 < \nu < \nu^{\text{Hopf}}$, a tumour-free steady state together with a tumour equilibrium state exist but both are unstable. Here there exists a stable limit cycle. The limit cycle exhibits increasingly large amplitude swings as $\nu \to 0$. This oscillation between near elimination and near escape is likely unfavourable for a patient in this condition. For $\nu^{\text{Hopf}} \leq \nu < \nu^{\text{T}}$ we pass through a Hopf bifurcation beyond which the limit cycle no longer exists. Here a stable tumour equilibrium exists but the tumour-free state remains unstable. For $\nu^{\text{T}} \leq \nu < \nu^{\text{F}}$ we pass through the transcritical bifurcation point where the tumour-free state becomes stable. Here an unstable tumour equilibrium state emerges into a region of bistability between the tumour-free state and the large tumour equilibrium state. (Note an unphysical 'stable' solution with $N^* < 0$ exists for $\nu < 1$ continuing the red branch of solutions — this behaviour in fact occurs in all cross sections shown). For $\nu \geq \nu^{\text{F}}$ we pass through a fold bifurcation where the stable tumour equilibrium state merges with the unstable tumour equilibrium state. In this region only the tumour-free state exists and is stable. These results suggest that when the rate of exhaustion of T cell killing is high, then even when $\nu < 1$, tumour escape may be avoided.

Further increases in ξ_k do not substantially alter the bifurcation structure shown in Figure 3.5(c), except that the region occupied by the stable limit cycle increases. As ξ_k increases ν^{Hopf} moves to the right, with $\nu^{\text{Hopf}} > \nu^{\text{T}}$ for $\xi_k > 0.4$. In this parameter range there is a small region of bistability between the tumour-free state and the limit cycle (results not shown).

Cross sections (a*), (b*) and (c*) in the (ν, ξ_α) plane in Figure 3.4 mirror those described above for cross sections (a), (b) and (c) in the (ν, ξ_k) plane (not shown). The dependence on ξ_α is inverted relative to ξ_k. For example the boundary of the limit cycle solutions moves downward in the (ν, ξ_α) plane and moves upwards in the (ν, ξ_k) plane. The main difference is that stable limit cycles are confined to smaller values of ν in the (ν, ξ_α) plane compared to the (ν, ξ_k) plane.

The remaining cross sections (d)–(f) in Figure 3.4(b) are more straightforward. In all three cross sections for $0 < \nu \leq \nu^{\text{T}}$, both the tumour-free and the large tumour equilibrium states are unstable. There exists however a stable intermediate tumour equilibrium. In Figure 3.5(d), for $\nu > \nu^{\text{T}}$ we lose the stable tumour equilibrium state but gain stability of the tumour-free state. In Figure 3.5(e), for $\nu^{\text{T}} < \nu < \nu^{\text{F}}$ an additional branch of unstable small tumour equilibrium states emerges. Here we have

a region of bistability between a tumour equilibrium state and a tumour-free state. For $\nu > \nu^{\mathrm{F}}$ a stable tumour-free state exists together with an unstable large tumour equilibrium state. In Figure 3.5(f) the behaviour observed is the same as shown in (e) except that the region of bistability extends over the entire range of $\nu > 1$ shown (a fold point still exists for $\nu > 2$). Note in cross sections (d)–(f), for the parameters chosen $\Gamma = 6$ (see equation (3.15)) which is less than $\gamma = 10$, and consequently a sufficiently large tumour population will escape everywhere in the (ν, ξ_σ) plane.

In summary, as the rate of exhaustion of T cell killing increases or the rate of exhaustion of T cell proliferation decreases, favourable outcomes are observed even when T cell efficacy is low ($\nu < 1$). Instead of tumour escape being the sole attractor, a tumour equilibrium state is also possible either in the form of a stable steady state or stable limit cycle. Here the T cells are able to control the tumour as they have the proliferative capacity to match the growth of the tumour without being overcome by tumour counter attack. However as $\nu \to 0$ the limit cycle exhibits increasingly large amplitude swings verging on tumour escape. When T cell efficacy is high ($\nu > 1$), tumour elimination is possible. As the rate of exhaustion of T cell killing increases or the rate of exhaustion of T cell proliferation decreases, there exists a region of bistability between a tumour equilibrium state and the tumour-free state. Increases in the rate of exhaustion of T cell infiltration extends the region of bistability. Then, even for high rates of exhaustion of T cell infiltration, a stable tumour equilibrium state remains. Taken together, these results indicate that T cell proliferation and killing both significantly affect tumour progression whereas T cell infiltration plays a less important role. These results are similar to those found in a distinct, agent based model looking at cytotoxic T cell and tumour cell interactions [121]. This suggests that manipulating T cell proliferation and killing may be effective in cancer treatment.

These results both compare to and contrast with the results in Chapter 2 where the rates of T cell killing, infiltration and proliferation were held fixed in time. In both models high infiltration rates lead to tumour elimination. Sufficiently high proliferation rates (which need to be sustained in the current model) also lead to more favourable outcomes (tumour elimination or control). A key difference in the current model is that the killing, infiltration and proliferation rates are affected by the tumour, leading to an additional competition in the model. We find that the initial rates of T cell functionality play a decisive role in tumour outcome.

An oscillatory tumour equilibrium solution with large amplitude may be less desirable than a stable steady state with a modest tumour burden. In Figure 3.5(c) as

$\nu \to 0$ the amplitude of the limit cycle solution rapidly increases. If the model dynamics is perturbed when the tumour population is at its peak, the tumour may escape. Further investigation is therefore needed to identify when in the cycle it is best to apply treatment to elicit promising outcomes avoiding tumour escape. However the question of when to target a patient with oscillations in tumour and immune cells is beyond the scope of this study. These oscillations are primarily found at moderate to large rates of exhaustion of T cell killing, consistent with clinical observations speculating that increasing immunosuppressive effects alter the existence and amplitude of oscillations [38].

3.6 Logistic tumour growth

As discussed in Section 3.2, their is much debate about the appropriate choice of tumour growth law. In Chapter 2 we used a logistic growth law. In this chapter we used an exponential growth law. The benefits of this choice are discussed next.

To this end, we extend the model in Section 3.2 to permit logistic growth. The only change to the model equations (3.8)–(3.12) occurs in the dimensionless tumour evolution equation (3.8) which becomes

$$\frac{dN}{dt} = \gamma N \left(1 - \frac{N}{\theta} - kT_C\right) , \tag{3.32}$$

where θ is the carrying capacity.

With this change, the steady state tumour populations N^* are given by the solutions of the quartic,

$$B_4 N^{*4} + B_3 N^{*3} + B_2 N^{*2} + B_1 N^* + B_0 = 0 , \tag{3.33}$$

where the coefficients B_i are given by

$$B_4 = \theta(\xi_k \xi_\sigma \xi_\alpha + \kappa \xi_\sigma \xi_\alpha - \xi_k \xi_\sigma) , \tag{3.34}$$

$$B_3 = \theta(\xi_k \xi_\alpha + \xi_\sigma(\xi_k + \xi_\alpha) + \kappa(\xi_\sigma + \xi_\alpha) - (\xi_k + \xi_\sigma)) + \xi_k \xi_\sigma - \xi_k \xi_\sigma \xi_\alpha , \tag{3.35}$$

$$B_2 = \theta(\kappa - 1 + \xi_k + \xi_\sigma + \xi_\alpha) + \xi_k + \xi_\sigma - \xi_k \xi_\alpha - \xi_\sigma(\xi_k + \xi_\alpha) , \tag{3.36}$$

$$B_1 = 1 - \kappa + \theta - (\xi_k + \xi_\sigma + \xi_\alpha) + \nu \xi_k , \tag{3.37}$$

$$B_0 = \nu - 1 . \tag{3.38}$$

We examine next the effects of logistic growth on model steady states and limit cycle solutions. We study the behaviour of the model for small, moderate and large values of the carrying capacity θ.

The results presented in Figure 3.6 show the qualitative behaviour as the parameters ν and ξ_k vary. This should be compared with Figure 3.4(a) for $\theta \to \infty$. We find that, provided the carrying capacity θ exceeds typical tumour steady state population sizes, the two models are in close agreement. There are however two differences. First of all, the region where no stable solutions exist and the tumour escapes is absent in the logistic growth law. This is the black region in Figure 3.4 for the exponential growth law. Secondly, the region containing a stable tumour-free state and unstable tumour equilibrium is absent. This is the white region with black diagonal lines in Figure 3.4. Moreover for the logistic growth law the tumour escape situation is replaced by a stable large tumour near the carrying capacity θ. This is the analogue of tumour escape.

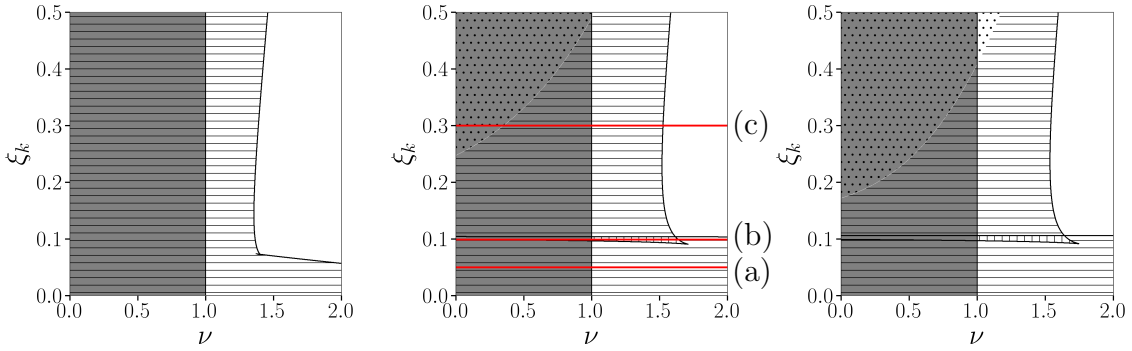

(a) $\theta = 10$ (b) $\theta = 100$ (c) $\theta = 1000$

Figure 3.6: Series of plots showing how the qualitative behaviour of equation (3.32) and equations (3.9)–(3.12) varies with the carrying capacity θ. The horizontal red lines correspond to the cross sections shown in Figure 3.7 below. The remaining parameters are fixed at their default values.

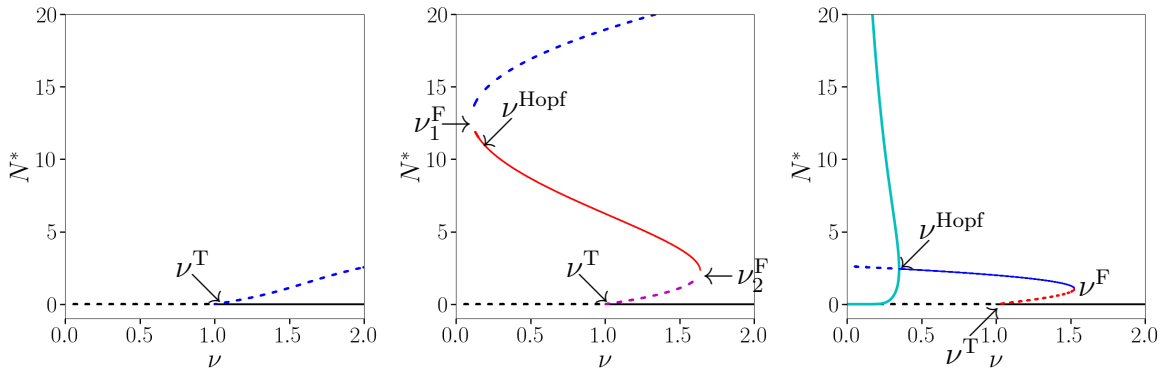

(a) $\xi_k = 0.05$ (b) $\xi_k = 0.099$ (c) $\xi_k = 0.3$

Figure 3.7: Bifurcation diagrams as a function of ν for a finite carrying capacity $\theta = 100$. These panels are the analogues of those shown in Figure 3.5(a)–(c) for $\theta \to \infty$ (for the exponential growth law).

Figure 3.7 shows several cross sections of ξ_k when $\theta = 100$. These cross sections closely compare to those shown for the exponential model in Figure 3.5(a)–(c). The primary difference is a reduced region of stable limit cycle solutions. At larger values of the carrying capacity the agreement between the logistic and exponential models improves further. However at lower carrying capacities (see Figure 3.6(a)) marked differences begin to appear. Notably, there are fewer possible outcomes and a complete absence of stable limit cycle solutions.

In summary if the carrying capacity is large, exponential and logistic growth laws result in similar qualitative behaviour. As we are interested in the effects of exhaustion which act before the tumour reaches its carrying capacity, this justifies our use of the exponential growth law and moreover simplifies the analysis to follow.

3.7 Time-dependent attractors

Oscillatory phenomena are observed throughout the biological sciences, from pattern formation, the circadian clock within cells to predator-prey interactions [77]. Fluctuations in the normal levels of immune cells have also been observed in healthy individuals [136]. Interactions involving tumour and immune cells may also exhibit oscillatory behaviour [38]. This behaviour is a characteristic feature of many mathematical models of tumour immune cell interactions [110, 160, 202, 55, 126].

Although such behaviour is commonly observed in mathematical models, the consensus in the experimental and clinical communities is less clear. A number of authors have obtained clinical evidence to suggest that the number of lymphocytes in cancer

patients fluctuates [197, 99, 38]. In their review article, Coventry *et al.* (2009) concluded that the amplitude of oscillatory cycles in C-Reactive Protein (CRP), which may be used as indicator of activation of the immune response, depends on the strength of the immune system and the aggressiveness of the cancer [38]. This finding is consistent with our results which indicate that the existence of oscillations depends on the degree of exhaustion of T cell killing and proliferation. The regulatory mechanisms of the T cell response weakens the immune system allowing the tumour to grow. Not all studies however have observed oscillations [123]. The inconsistency in experimental observations may in part be due to the difficulty in taking dynamic measurements at a frequency that captures such oscillations. It may also be that oscillations only exist in specific regions of parameter space, as our results suggest.

The bifurcation structure examined in Section 3.5 above reveals regions of parameter space in which Hopf bifurcations occur, giving rise to oscillatory solutions. Such solutions, formally known as limit cycle solutions, may be stable or unstable. Of interest are the stable solutions, mimicking a tumour equilibrium state that oscillates about a finite tumour population.

To make analytical progress, we simplify our model by assuming that the rates of exhaustion of T cell killing, infiltration and proliferation are all equal: $\xi_k = \xi_\sigma = \xi_\alpha = \xi$. In this case the variables $k(t)$, $\sigma(t)$ and $\alpha(t)$ rapidly converge to a common value which may be time-dependent in the case of oscillatory solutions. This occurs on a $\mathcal{O}(\beta^{-1})$ time-scale at the longest, as shown next.

Suppose the initial values k_0, σ_0 and α_0 in general differ. Define $q(t)$ to be the difference at subsequent times between any pair of the quantities $k(t)$, $\sigma(t)$ and $\alpha(t)$. Then $q(t)$ satisfies

$$\frac{dq}{dt} = -\beta q(\xi N + 1) \quad \text{with} \quad q(0) = q_0\,, \tag{3.39}$$

and general solution

$$q(t) = q_0 \exp\left(-\beta \int_0^t (\xi N(t') + 1) dt'\right) \leq q_0 \exp(-\beta t)\,, \tag{3.40}$$

demonstrating $q(t)$ decays to zero at a rate which is at least β. Hence $k(t)$, $\sigma(t)$ and $\alpha(t)$ converge to a common time-dependent function $F(t)$ say. With little loss of generality, we thus consider a simpler model governed by three variables $S(t) \equiv \xi N(t)$,

$T_C(t)$ and $F(t)$, satisfying

$$\frac{dS}{dt} = \gamma S(1 - FT_C)\,, \tag{3.41}$$

$$\frac{dT_C}{dt} = \nu F - \mu F T_C S - T_C\,, \tag{3.42}$$

$$\frac{dF}{dt} = \beta(1 - F(1 + S))\,, \tag{3.43}$$

where $\mu \equiv (\kappa - 1)/\xi$, and $F(t)$ is referred to as the 'functionality' of the cytotoxic T cell population, with $F(0) = F_0$. The rescaling performed above enables us to reduce the number of model parameters by one. Note that the parameter μ, in dimensional variables, has the form

$$\mu = \beta \frac{\check{k}\phi - \check{\alpha}}{\xi_\alpha \delta}$$

where on the right hand side of this equation all of the parameters are their original dimensional values. μ is therefore seen to reflect the difference between tumour counter attack ($\check{k}\phi$) and the baseline proliferative capacity of the T cells ($\check{\alpha}$) all divided by the exhaustion rate of T cell proliferation. Factors of β and δ also appear. We interpret μ, for negative values as a measure of the proliferative capacity to overcome tumour counter attack on a time-scale related to the exhaustion rate of T cell proliferation.

Dimensionless parameter	**Default value**
γ	1
β	1
ξ	0.4
κ	0.4
ν	1.1

Table 3.3: A summary of the default dimensionless parameter values used in equations (3.41)–(3.43). Note $\mu \equiv (1 - \kappa)/\xi = -1.5$ for the default dimensionless parameters.

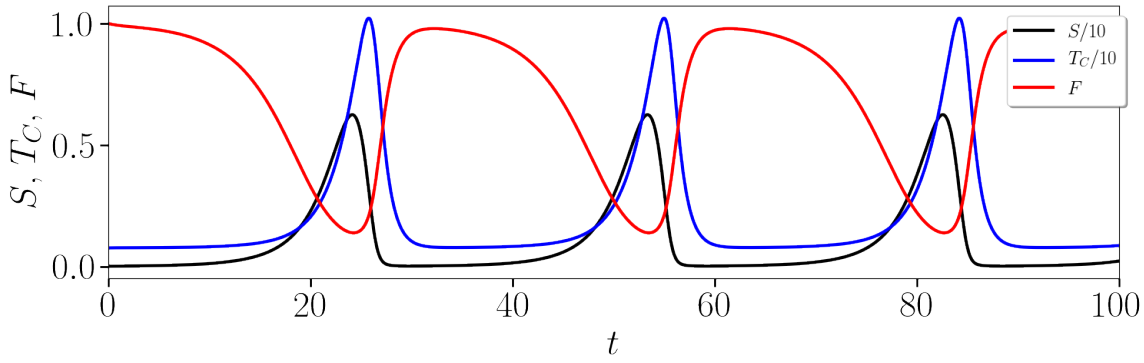

Figure 3.8: Dynamics arising from equations (3.41)–(3.43) for $\nu = 0.76$. We show the time evolution of the scaled tumour population $S(t)$ (black curve), cytotoxic T cell population $T_C(t)$ (blue curve), and functionality $F(t)$ (red curve) initialised with $(S_0, T_{C0}, F_0) = (0.004, \nu, 1.0)$. Parameter values: except ν, all parameters are fixed at their default values.

As in the original model, given by equations (3.8)–(3.12), the simplified model, given by equations (3.41)–(3.43), exhibits oscillatory solutions over extensive regions of parameter space. Figure 3.8 illustrates one such instance of this behaviour for the default parameters listed in Table 3.3. We show in Section 3.7.2 that this oscillatory solution is a stable limit cycle. The oscillation is characterised by a growing tumour population (black curve) which weakens the functionality of the T cells (red curve). The T cells (blue curve) nevertheless manage to increase to sufficient numbers to reverse the growth of the tumour and greatly reduce the tumour population. This enables the functionality of the T cell population to recover due to the influx of functional T cells, and the T cell population returns to its baseline value. This cycle then repeats because the baseline value of T cells is not sufficient to prevent the resurgence of the tumour.

The remainder of this section is devoted to explaining aspects of this limit cycle solution analytically. We first determine the steady state solutions and their linear stability, in order to locate Hopf bifurcations in (ν, μ) parameter space. Using a weakly nonlinear analysis near the Hopf bifurcation, we derive an amplitude equation for the limit cycle and determine its stability. We conclude with a discussion of the disappearance of the limit cycle at large amplitude, the full analysis of which is relegated to Appendix D.3.

3.7.1 Limit cycle emergence

Limit cycles typically emerge at Hopf bifurcations [81]. Our first task is therefore to locate the Hopf bifurcations in the present model. To do this we must first identify the steady state solutions of equations (3.41)–(3.43) and characterise their linear stability.

3.7.1.1 Identification of steady states

The tumour equilibria ($N^* > 0$) solve the quadratic

$$(1+\mu)S^2 + (2+\mu)S + 1 - \nu = 0\,, \tag{3.44}$$

with

$$T_C^* = 1 + S^* \quad \text{and} \quad F^* = \frac{1}{1+S^*}\,. \tag{3.45}$$

The simplicity of equation (3.44) enables us to determine where in (ν, μ) parameter space there exists zero, one or two positive roots of the quadratic equation:

(a) $\mu < -2$:

- one root provided $0 < \nu < 1$

(b) $-2 \leq \mu < -1$:

- one root provided $0 \leq \nu < 1$
- two roots provided $1 < \nu < \frac{-\mu^2/4}{1+\mu}$

(c) $\mu \geq -1$:

- one root provided $\nu > 1\,.$

Outside of these regions of parameter space no tumour equilibria with $N^* > 0$ exist. In these regions only the tumour-free state exists.

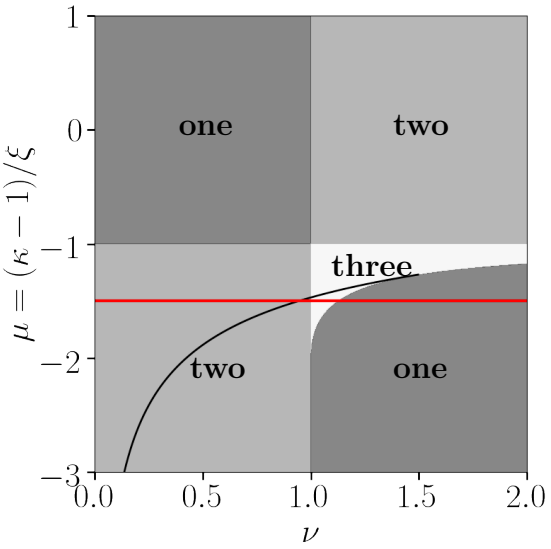

Figure 3.9: Solution domain showing the number of steady states (including the tumour-free state) over the (ν, μ) parameter space. The black curve represents Hopf bifurcation points where limit cycles emanate from (see equation (3.50) below); this curve is the 'emergence curve'.

Figure 3.9 summarises the multiplicity of steady states together with the curve of Hopf bifurcation points along which limit cycles arise within the (ν, μ) parameter space (see Section 3.7.1.4). The lines $\nu = 1$ and $\mu = -1$ divide the parameter space into four distinct regions. A transcritical bifurcation occurs at $\nu = 1$ for all values of μ. Here we either gain or lose an equilibrium depending on whether $\mu > -1$ or $\mu < -1$. When $\nu > 1$ a fold bifurcation occurs along the curve $4\nu(1 + \mu) + \mu^2 = 0$ between the dark grey and white region. As μ increases through -1 a solution is lost where $S^* \to \infty$. In the full model this occurs when $\Gamma = 0$ (see equation (3.15)).

Notably, the line $\nu = 1$ divides unstable tumour-free steady states ($\nu < 1$) from stable ones ($\nu > 1$). This change in stability is also associated with the emergence or disappearance of tumour equilibrium states.

3.7.1.2 Stability properties

In this subsection, we determine the linear stability of the steady states (S^*, T_C^*, F^*). In addition to the fold bifurcations and transcritical bifurcations giving rise to two or one tumour equilibrium solutions respectively, Figure 3.9 indicates Hopf bifurcation points from which oscillatory solutions are born. These Hopf bifurcations occur at an exchange in stability of the tumour equilibrium states ($S^* > 0$). We focus on how this varies with ν keeping the default value of μ indicated by the red line in Figure 3.9 fixed.

Linear stability is determined by the roots of the cubic equation

$$\lambda^3 + a_2\lambda^2 + a_1\lambda + a_0 = 0\,, \tag{3.46}$$

where λ is the eigenvalue (generally complex) and

$$\begin{aligned} a_0 &= -\beta\gamma(1 + \mu + \nu F^{*2})S^*, \\ a_1 &= \beta T_C^* + (\beta(\mu - \gamma) - \mu\gamma F^*)\, S^*, \\ a_2 &= 1 + \mu F^* S^* + \beta T_C^*\,, \end{aligned} \tag{3.47}$$

where $S^* \equiv \xi N^*$ and $\mu \equiv (\kappa - 1)/\xi$ as before.

While the steady states depend only on μ and ν, the additional parameters β and γ are required to determine the associated linear stability of the steady states. Although significantly simpler than in the full model equations (which required solving a fifth order polynomial), the roots of equation (3.46) involve complicated groupings of our parameters and therefore the roots are found numerically as a function of ν.

In Figure 3.10 bifurcation diagrams over ν illustrate how the existence and linear stability of the steady state solutions given by equations (3.44) and (3.45) vary. The bifurcation structure closely resembles Figure 3.5(c) of the full model with one distinction: in the simplified model a stable limit cycle solution does not extend to $\nu = 0$.

As a confirmation of the stability of the steady state solutions shown in Figure 3.10, trajectories in (S, T_C, F) space are presented for the full model given by equations (3.41)–(3.43) in Figure 3.11. Three values of ν are considered exhibiting different qualitative behaviour. The results were generated by perturbing each unstable steady state in the eigenvector directions associated with each unstable mode. This is done by multiplying the normalised eigenvector by ± 0.01 and adding it to the steady state population. Hence there are in general two directions for each unstable mode. An exception occurs for the tumour-free state where only one direction corresponds to $N_0 > 0$.

In Figure 3.11(a) where $\nu < \nu^{\mathrm{Hom}}$, all trajectories lead to tumour escape. In Figure 3.11(b) where $\nu^{\mathrm{Hom}} < \nu < \nu^{\mathrm{Hopf}}$, all trajectories evolve to the stable limit cycle solution. In Figure 3.11(c) where $\nu^{\mathrm{T}} < \nu < \nu^{\mathrm{F}}$, trajectories evolve to either a state of tumour elimination or equilibrium.

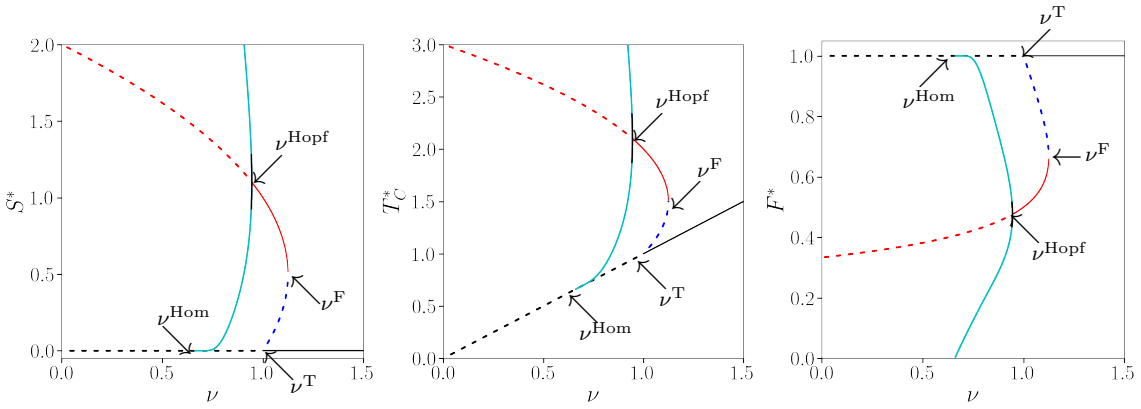

(a) (b) (c)

Figure 3.10: Bifurcation diagrams for the scaled tumour population S^*, cytotoxic T cell population T_C^* and its associated functionality F^* from equations (3.44) and (3.45) as ν is varied. Key: line styles as in Figure 2.8. Parameter values: except ν, all parameters are fixed at their default values.

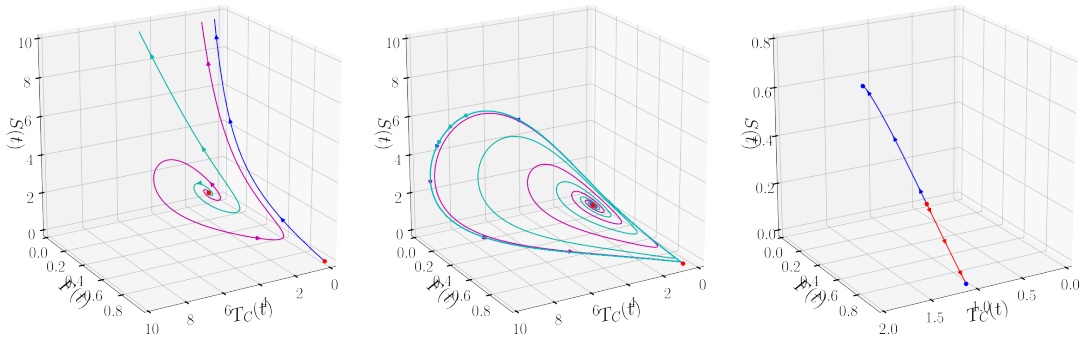

(a) escape ($\nu = 0.2$) (b) equilibrium ($\nu = 0.76$) (c) equilibrium/elimination ($\nu = 1.1$)

Figure 3.11: Confirmation of the attractors that emerge from equations (3.41)–(3.43) as ν is varied, corresponding to the regions delineated by the bifurcation points in Figure 3.10. The trajectories are solutions to the nonlinear equations starting at $(S^*, T_C^*, F^*) \pm 0.01\mathbf{v}_m$, where $\mathbf{v}_m$ is the normalised eigenvector associated with the unstable mode. For the unstable steady states illustrated there is only one mode of instability. Three values of ν are considered: (a) $\nu = 0.2$, (b) $\nu = 0.76$ and (c) $\nu = 1.1$. In (a) all trajectories rapidly escape; in (b) all trajectories starting close to the unstable tumour steady states collapse onto the stable limit cycle solution; in (c) trajectories starting close to the unstable tumour steady state evolve to either a tumour equilibrium or to the tumour-free state (elimination). Red and blue circles denote unstable and stable steady states respectively. Line colour represents different initial conditions. Parameter values: except ν, all parameters are fixed at their default values.

3.7.1.3 Basins of attraction

For all ν tumour escape is inevitable for $\mu > -1 - \gamma$, provided the initial tumour population is sufficiently large. The condition on μ is equivalent to the condition for tumour escape $\gamma > \Gamma$ found in the full model (see equation (3.16)). We next explore the initial conditions giving rise to tumour escape for fixed model parameters. Specifically we locate the basin of attraction in the initial condition space (S_0, T_{C0}, F_0) dividing tumour escape from equilibrium or elimination.

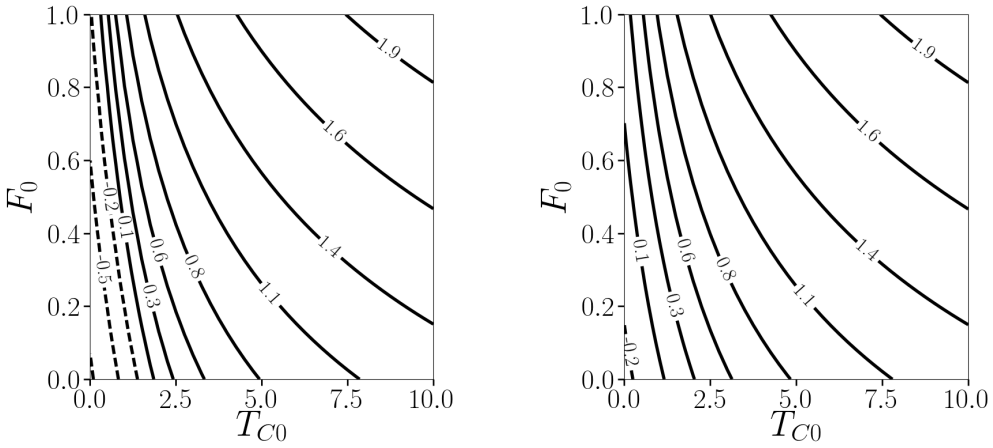

(a) $\nu = 1$ (b) $\nu = 2$

Figure 3.12: Contour lines of the initial (scaled) tumour population $\log_{10} S_0$ beyond which tumour escape is inevitable as a function of the initial cytotoxic T cell population T_{C0} and functionality F_0. Two values of ν are shown: (a) $\nu = 1$ and (b) $\nu = 2$. Parameter values: except ν, all parameters are fixed at their default values.

In Figure 3.12 the initial (scaled) tumour population S_0, beyond which tumour escape is inevitable, is contoured as a function of the initial T cell population T_{C0}, and functionality F_0. For small T_{C0} and F_0, tumour escape occurs for small N_0. When T_{C0} is small a larger F_0 is necessary to prevent tumour escape for a fixed initial tumour size. As T_{C0} increases, F_0 plays an increasingly important role. Comparing Figures 3.12(a) and (b), the only significant difference is seen at small T_{C0}. Overall we see that larger ν is beneficial in preventing tumour escape since the initial tumour population is larger for a given T_{C0} and F_0. The differences are slight for large T_{C0} and F_0 but become more significant for small T_{C0} and F_0. The results illustrate that a fully functioning large initial T cell population depends only negligibly on the T cell efficacy ν. Conversely a low functioning small initial population of T cells depends strongly on ν.

3.7.1.4 Location of Hopf bifurcation points

Hopf bifurcations occur at an exchange in stability for a complex conjugate pair of eigenvalues. Setting $\lambda = i\omega$ in equation (3.46) and equating real and imaginary parts gives

$$a_2\omega^2 = a_0, \quad \text{and} \quad \omega^3 = \omega a_1\,. \tag{3.48}$$

As $|\omega| > 0$, we have $\omega^2 = a_1$ and therefore $a_0 = a_1 a_2$. Using the definitions for a_0, a_1 and a_2 in (3.47) it is straightforward to show that this is equivalent to

$$\begin{aligned}&\left(\mu S^* + T_C^* + \beta T_C^{*2}\right)\left(\beta T_C^{*2} + \beta(\mu-\gamma)S^*T_C^* - \mu\gamma S^*\right)\\&+ \beta\gamma S^*\left(\nu + (1+\mu)T_C^{*2}\right) = 0\,,\end{aligned} \tag{3.49}$$

where $T_C^* = 1 + S^*$ and $S^*(\nu,\mu)$ is given by the quadratic equation (3.44). We view this equation as defining ν at the Hopf bifurcation, $\nu = \nu^{\text{Hopf}}(\mu)$. The steady state populations S^* and T_C^* depend only on ν and μ. Using $T_C^* = 1 + S^*$ together with S^* from equation (3.44) leads to the quartic

$$g_4C^4 + g_3C^3 + g_2C^2 + g_1C + g_0 = 0 \quad \text{where} \quad C = \frac{1-\nu}{1+\mu}\,, \tag{3.50}$$

whose single physical root determines the critical curve $\nu = \nu^{\text{Hopf}}(\mu)$ along which limit cycles emerge (see black curve in Figure 3.9). From our numerical investigations, all other solutions of the quartic equation have $\nu < 0$ or complex. The coefficients $g_0, \ldots g_4$ are provided in terms of model parameters in Appendix D.1.

Note that a Hopf bifurcation occurs along a branch of solutions stemming from a fold point as illustrated in Figure 3.10(b). It occurs specifically at the point where the solution branch changes stability. For the default parameters in Table 3.3 this happens for $\mu \lesssim -1.27$ (and $\nu \lesssim 1.5$). Otherwise this entire branch is unstable.

3.7.2 Limit cycle amplitude equation

Generically, near a Hopf bifurcation a finite amplitude limit cycle or periodic oscillation emerges [81]. In the previous subsection, we determined the point of emergence $\nu = \nu^{\text{Hopf}}(\mu)$, which exists for $\mu < -1.27$. The limit cycle can be described asymptotically near its point of emergence by an amplitude equation derived from a weakly nonlinear analysis which is essentially the same as that presented in Chapter 2 Section 2.7.4. Full details can be found in Appendix D.2; here we present the main results.

The limit cycle is described by the equation

$$\frac{d\phi}{d\tau} = (\eta + \zeta|\phi(\tau)|^2)\phi(\tau) \tag{3.51}$$

where $\phi(\tau)$ is proportional to the amplitude of the limit cycle, while $\eta = \eta_r + i\eta_i$ and $\zeta = \zeta_r + i\zeta_i$ are functions of the model parameters, and $\tau = \epsilon^2 t$ is the long time scale. Here ϵ^2 is the shift in η from ν^{Hopf}, i.e. $\nu = \nu^{\text{Hopf}} - \epsilon^2$. To leading order in ϵ, the model variables $(S, T_C, F) = (S_0, T_{C0}, F_0) + \epsilon\phi(\tau)\mathbf{v}_1 e^{i\omega t} + c.c.$, where $\mathbf{v}_1$ is the eigenvector of the unstable linear mode and ω is its frequency in the limit $\nu \to \nu^{\text{Hopf}}(\mu)$.

Equation (3.51) can be solved by taking $\phi(\tau) = r(\tau)\exp(i\vartheta(\tau))$, where r and ϑ are real functions of τ. They satisfy

$$\frac{dr}{d\tau} = (\eta_r + \zeta_r r^2)r \quad \text{and} \quad \frac{d\vartheta}{d\tau} = \eta_i + \zeta_i r^2 \,. \tag{3.52}$$

The equation for r can be solved directly to give

$$r^2(\tau) = \frac{\eta_r}{(\eta_r/r^2(0) + \zeta_r)\exp(-2\eta_r\tau) - \zeta_r} \,. \tag{3.53}$$

A stable limit cycle requires that η_r and ζ_r have opposite signs. In this case $r = \sqrt{-\eta_r/\zeta_r} \equiv A$ (a constant) is a solution of equation (3.53). This is the amplitude of the limit cycle at equilibrium. However only when $\eta_r > 0$ and $\zeta_r < 0$ is this a stable limit cycle. In this case all initial conditions with $r(0) > 0$ tend to $r = A$ as $\tau \to \infty$. By contrast when $\eta_r < 0$ and $\zeta_r > 0$ the limit cycle is unstable. The other situations in which η_r and ζ_r have the same sign do not correspond to limit cycles since r can never remain at a constant amplitude over τ. Either $r \to 0$ when η_r and ζ_r are negative or $r \to \infty$ when η_r and ζ_r are positive, for any finite value of $r(0)$.

For the default parameter values specified in Table 3.3, in Figure 3.13(a) we plot $\eta_r(\mu)$ and $\zeta_r(\mu)$, while in Figure 3.13(b) we plot the amplitude A of the limit cycle. We find that $\zeta_r < 0 < \eta_r$ for all values of μ considered, indicating that the limit cycle is stable where our weakly nonlinear theory is valid.

In summary, we have determined where stable limit cycles emerge via a Hopf bifurcation in the (ν, μ) plane and have derived an asymptotic solution for the amplitude of the limit cycle in the neighbourhood of $\nu = \nu^{\text{Hopf}}(\mu)$. Moreover we have shown that the limit cycle is stable for the parameters investigated near its point of emergence. Figure 3.14(b) shows how well the weakly nonlinear analysis (black curves) compares with the numerical estimates of the limit cycle amplitude (cyan curves). The discrepancy very near $\nu = \nu^{\text{Hopf}}$ is due to the difficulty in accurately estimating the amplitude of the limit cycle near its point of emergence within reasonable computing time.

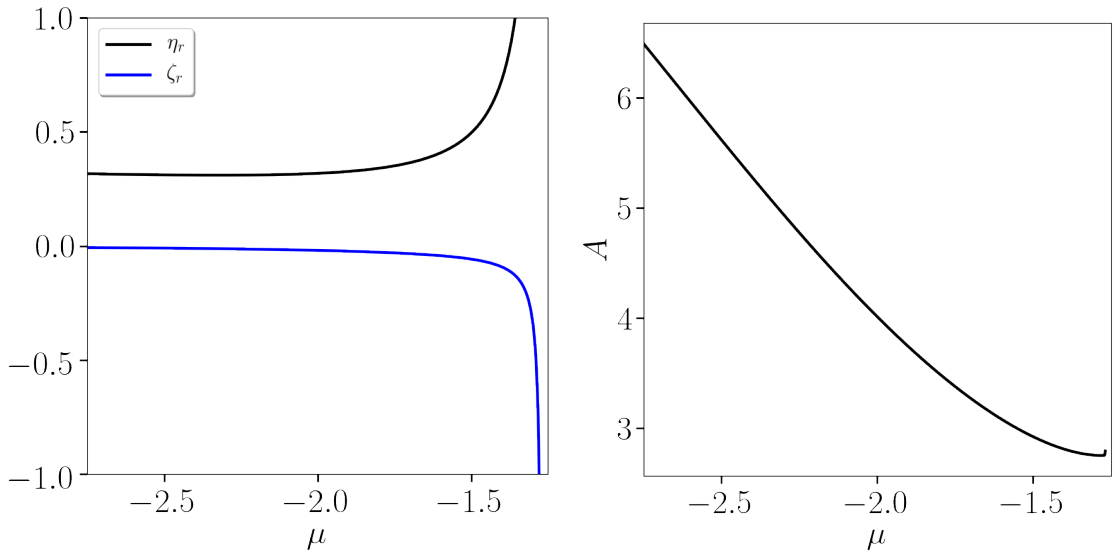

Figure 3.13: (a) η_r and ζ_r versus μ and (b) the amplitude $A = \sqrt{-\eta_r/\zeta_r}$ versus μ with all remaining parameters fixed at their default values.

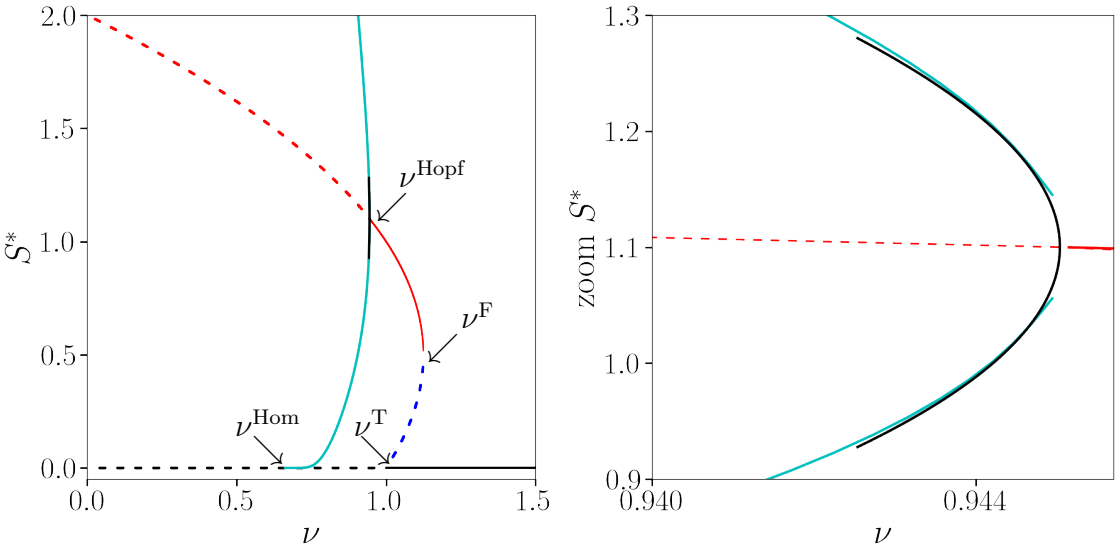

(a) scaled tumour population, S^*

(b) zoom S^*

Figure 3.14: Bifurcation diagram of the scaled steady state tumour population S^* together with the minimum and maximum amplitude of the limit cycle (cyan curve) as ν varies, with all remaining parameters are fixed at their default values. Here solid curves represent stable solutions and dashed curves represent unstable solutions. The right panel illustrates a zoom of the left panel in the neighbourhood of the Hopf bifurcation $\nu = \nu^{\text{Hopf}}$ showing the emergence of the limit cycle and the asymptotic predication (black lines, see equation (3.51)). That prediction uses equation (D.5) up to and including order ϵ^2 terms, where $\epsilon = \sqrt{\nu^{\text{Hopf}} - \nu}$.

3.7.3 Limit cycle disappearance

As ν decreases from ν^{Hopf}, the limit cycle amplitude and period grow, tending to infinity at the Homoclinic bifurcation $\nu = \nu^{\text{Hom}}$. Here the limit cycle merges into an infinite homoclinic orbit associated with the tumour-free steady state, and ceases to exist for $\nu < \nu^{\text{Hom}}$ (see Chapter 2 for a detailed description of this global bifurcation point). The simple form of equations (3.41)–(3.43) allows a largely analytical description of the approach to $\nu = \nu^{\text{Hom}}$. This analysis underpins the numerical results but also indicates more generally where the limit cycle terminates in equations (3.41)–(3.43). The limit cycle disappearance is a generic feature of this model and therefore is described in detail below and in Appendix D.3.

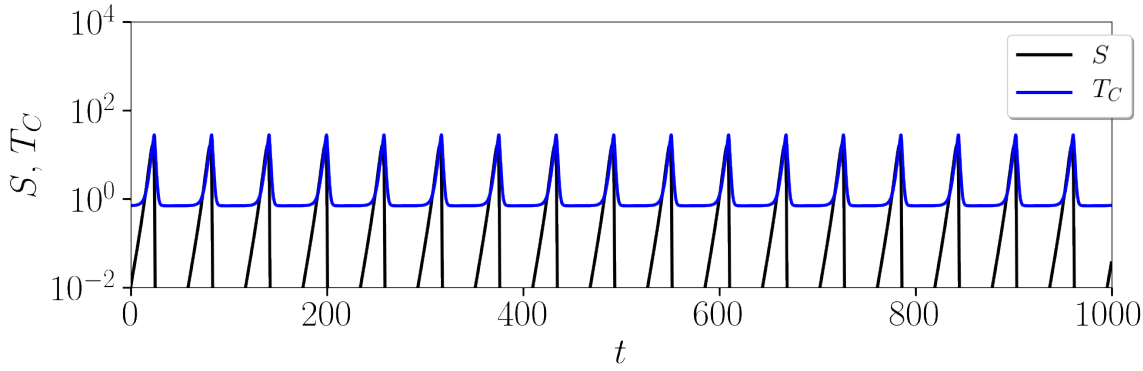

(a) $\nu = 0.7$

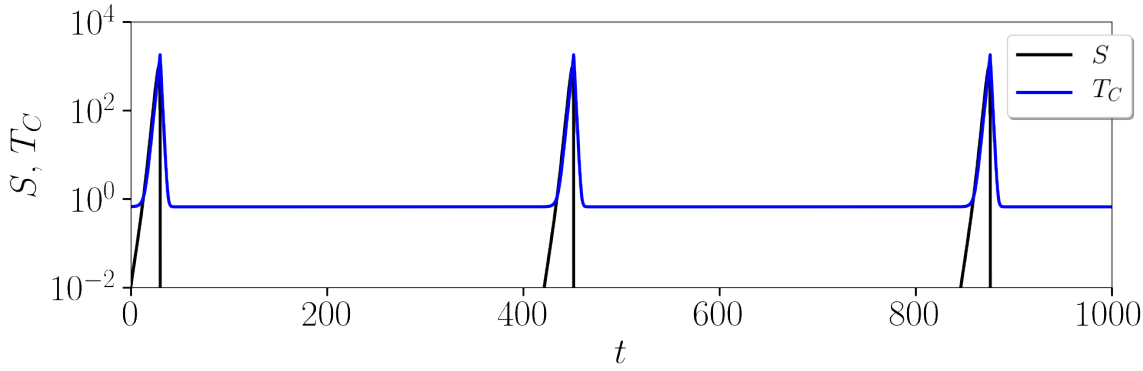

(b) $\nu = 0.66$

Figure 3.15: Time evolution of the scaled tumour population $S(t)$ and cytotoxic T cell population $T_C(t)$ arising from equations (3.41)–(3.43) for two values of ν approaching $\nu = \nu^{\text{Hom}}$: (a) $\nu = 0.7$ and (b) $\nu = 0.66$, to illustrate how the period and amplitude of the limit cycle increase with $\nu \to \nu^{\text{Hom}}$. Initial conditions: $(S_0, T_{C0}, F_0) = (0.01, \nu, 1)$ (about the tumour-free state). Parameter values: except ν, all parameters are fixed at their default values.

Near the disappearance of the limit cycle, both S and T_C periodically attain large values, tending to infinity as $\nu \to \nu^{\text{Hom}}$. The large amplitudes of S and T_C enable a matched asymptotic analysis describing the model variables both before, around and after the peaks in the amplitudes of S and T_C (see Figure 3.15).

Before the peaks in S and T_C, both populations exhibit an exponential increase in time while F remains approximately zero. In the vicinity of the peaks F obeys a Riccati equation which can be solved analytically. From this solution the populations of S and T_C can be determined. Finally to the right of the peaks $S \approx 0$ while F and T_C exponentially decay.

To confirm that the expressions describing the populations S, T_C and F in the vicinity of the peak are good approximations of equations (3.41)–(3.43), we next compare these analytical expressions with our numerical results. Figure 3.16 presents the analytical results in the regions to the left, right and about the peak in T_C together with the numerical results obtained by solving equations (3.41)–(3.43). This demonstrates how well our analytical approximations in each of the regions compare with our full numerical solutions about the peak in T_C.

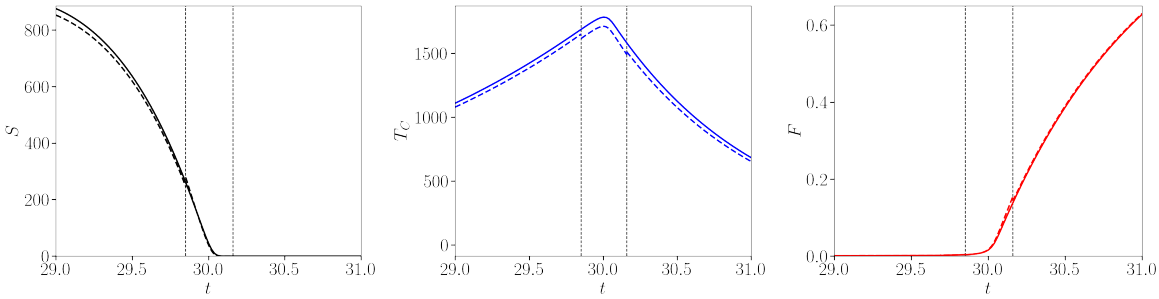

(a) scaled tumour cells (b) cytotoxic T cells (c) function of T cells

Figure 3.16: Time evolution of $S(t)$, $T_C(t)$ and $F(t)$ from equations (3.41)–(3.43) for $\nu = 0.66$ (solid curves), together with their asymptotic approximations (dashed curves). Here the asymptotic solution left of the first dashed vertical line is given by equations (D.85) and (D.86) for T_C and S respectively and $F = 1/S$. The asymptotic solution in the vicinity of the peak (between the two vertical dashed lines) is given by equations (D.82)–(D.84). The asymptotic solution to the right of the second vertical dashed line is given by equations (D.47) and (D.48). Parameter values: except ν, all parameters are fixed at their default values.

.

3.8 Discussion

In the present chapter we have developed a model that captures the dynamic interplay between tumour cells and cytotoxic T cells, accounting for the progressive exhaustion of T cells in the presence of a tumour. This model attempts to account for the fact that inhibitory receptor expression by T cells is time-dependent, a recent conclusion of Thommen *et al.* (2015) [189]. To our knowledge, this is the first ODE model exploring how tumour-immune dynamics change as the exhaustion rates of T cell killing, infiltration and proliferation vary with time. As discussed in the introduction in Chapter 1, there are many modelling approaches that could be used to address the question of T cell exhaustion. The present approach was adopted to explore how the rates of T cell exhaustion (or T cell functionality) affect tumour development. Arguably this is the first step in identifying the important mechanisms at play. The approach enables us to answer, in a relatively simple manner, how the rates of exhaustion of T cell killing, infiltration and proliferation facilitate or diminish tumour escape. More complex models such as agent based models may allow one to address additional aspects of this problem but may significantly increase complexity. Simple models enable a comprehensive exploration of parameter space, which is important for any initial study. Examination of the model revealed which T cell function is critical for tumour elimination, as well as how the initial functional capacity of the T cells affects outcomes. Such knowledge may help to inform future immunotherapies.

An initially small tumour mass in the presence of a moderate-sized cytotoxic T cell population, comparable in size to that found for a tumour-free state, evolves to either a tumour-free state (elimination), an equilibrium state (taking the form of a fixed finite tumour population or an oscillating tumour mass about a finite non-zero tumour population) or grows without bound (escapes). Such outcomes, expected in interactions of tumour and immune cells [52], were found to depend on the initial T cell killing, infiltration and proliferation rates. To avoid escape, a sufficient rate of proliferation and/or infiltration of the cytotoxic T cells is necessary; only if the initial proliferation rate of the cytotoxic T cell population is sufficiently high is tumour elimination possible. These results highlight the necessity of a strong immune system initially for effective tumour elimination or control. The model developed enables one to identify regions of parameter space where tumour escape is inevitable when the tumour is initially large.

Changes in the qualitative behaviour was then studied as a function of the rates of exhaustion of T cell killing, infiltration, and proliferation together with the T cell

efficacy, ν (summarised in Figures 3.4 and 3.5). Small variations in the exhaustion rate of T cell proliferation were found to have a significant effect on model outcome. With increasing rates of exhaustion of T cell proliferation, tumour escape becomes inevitable. Tumour escape in this situation is only avoided if the rate of exhaustion of T cell killing is sufficiently large to substantially hinder tumour counter attack on the small pool of existing T cells. In fact, our results suggest that there exists an optimum window of exhaustion of T cell killing. If too small, then tumour counter attack plays a dominant role in facilitating tumour escape, while if too large, then the killing capacity of the T cells is insufficient to prevent tumour escape. This analysis has allowed us to identify the aspects of T cell exhaustion that, if switched off or optimised, could lead to increasingly favourable outcomes for patients, therefore elucidating potential new treatment interventions.

Our results suggest that therapies that restore the proliferative capacity of T cells may be most effective. Furthermore our results suggest that therapies should be designed to drive the T cell killing capacity into the optimum window of 'exhaustion' so that the T cells can have the greatest effect on tumour killing without being overcome by tumour counter attack.

In the clinic, monoclonal antibodies (so called checkpoint blockades) have been designed and approved by the FDA to block specific inhibitory receptors (e.g. PD-1, CTLA-4). These inhibitory receptors are highly expressed by T cells in cancer. The checkpoint blockades appear to reverse the exhaustive effects of the T cells, thereby re-instating T cell function. These checkpoint blockades have shown remarkable success in a range of aggressive cancers [192]. Although such therapies have been designed to reverse some of the exhaustive effects of the T cells, our results suggest that the proliferative capacity of the T cells is an especially important factor limiting tumour escape. The model proposed here could also be used as a tool to examine how the kinetics of tumour exhaustion is affected by surgical removal of the tumour at different time points. Surgical removal would dampen the effects of T cell exhaustion and potential enable the T cell population to grow sufficiently large to eliminate the tumour.

The complexity of this model makes it difficult to understand its key features analytically. Therefore a simplified version of the model was constructed in which all exhaustion rates of T cell function are made equal. This simplification permits one to determine many features of the model analytically. In particular, as in Chapter 2, we used a multiple timescale analysis to derive an asymptotic approximation for the amplitude of the limit cycle in the neighbourhood of a Hopf bifurcation. Moreover

we could describe, through a matched asymptotic analysis, the limit cycle near its termination point. In the complete model, the additional degrees of freedom of varying rates of exhaustion of T cell killing, infiltration and proliferation make analytical progress unwieldy and therefore numerical methods to examine the model had to be used.

In conclusion a model composed of five ordinary differential equations was developed to study aspects of T cell exhaustion in tumour-immune interactions. This has allowed us to explore in a relatively simple way the progressive effects of T cell exhaustion in the presence of an evolving tumour and revealed which of the T cell's functions (to kill, infiltrate or proliferate) may be most important in preventing tumour escape.

Chapter 4

A mathematical model of T cell exhaustion in cancer with immunotherapy

4.1 Introduction

A common theme in this thesis is to explore aspects of heterogeneity specific to the tumour-immune system. The models in Chapters 2 and 3 consider different aspects of T cell heterogeneity. In Chapter 2 subpopulations of helper and cytotoxic T cells were distinguished. In Chapter 3 the effects of T cell exhaustion on T cell killing, infiltration and proliferation in the presence of an evolving tumour were modelled. In this chapter we investigate not only immune cell heterogeneity, including cytotoxic and exhausted T cells, but also tumour cell heterogeneity, including immune-resistant and immune-sensitive tumour cells. Specifically the model presented in this chapter is designed to address the following question:

- Given that infiltrating T cell populations exist in various functional states, how do the ratios of exhausted to functional T cells and immune-resistant to non-resistant tumour cells affect tumour escape?

Past research has shown that the strength of the immune response can explain, in part, the outcome of tumour-immune interactions [23]. The strength of the immune response depends upon a number of factors including:

- the mutational load of the tumour (the higher the load, the easier it is for the immune cells to recognise it) ,
- levels of inhibitory receptors/ligands (which inhibit the immune response) ,

- levels of tumour and immune cell derived cytokines (such as IL-10 and TGF-β which inhibit the immune response),
- the degree of antigenicity and immunogenicity of the tumour ,
- the degree of immune cell infiltration into the tumour .

It is well established that the number of tumour infiltrating lymphocytes (TILs) correlates with survival for a variety of cancers [188, 66]. Recent clinical studies have concluded that patient outcomes depend not only on the density of immune cells infiltrating into the tumour microenvironment, but also on their type and spatial location [68, 66, 74, 25]. To improve response outcomes, it is necessary to understand the clinical implications of an individual's 'immune contexture' [66, 67]. In a recent study, Chen *et al.* (2017) [36] classified tumours into three categories based on their immune cell composition: 'inflamed tumour', 'immune desert tumour' and 'immune-excluded tumour'. 'Immune-desert' tumours are devoid of immune cells in their stroma and core. Immune cells are unable to penetrate the core of 'immune-excluded' tumours and reside instead in the stroma. 'Immune-inflamed' tumours have cytotoxic and helper T cells in the tumour tissue adjacent to malignant cancer cells. Chen *et al.* (2017) find that immune-inflammed tumours respond better to checkpoint therapies. Other therapies have been designed to increase the activation and consequent infiltration of immune cells into the tumour. For example, a T cell bi-specific (TCB) antibody targets a chosen antigen and the CD3ϵ chain of the TCR. When the TCB antibody brings together the tumour and the T cell, it induces polyclonal activation of the T cell followed by potent killing of the tumour cell [189, 16]. In this model we mimic the effects of treatment with a TCB antibody on patients destined for tumour escape or living with a dormant tumour.

The established method of cancer staging, used for over 80 years, is tumour-node-metastasis (TNM) classification [79]. This method does not account for other cells and molecules in the tumour microenvironment. This may explain, at least in part, why patients diagnosed with the same stage and type of cancer often exhibit a wide range of outcomes [43]. It is evident that more accurate patient prognosis requires identification of components of the tumour microenvironment that can serve as biomarkers for cancer diagnosis and treatment [69, 36]. In colorectal cancer, Galon *et al.* [68, 71, 70] established that the densities of infiltrating immune cells, specifically CD3+ and CD8+ T cells in the tumour core and invasive tumour margin, are stronger predictors of overall patient survival than TNM classification. They termed

this biomarker the 'immunoscore', establishing it as a useful prognostic predictor in colorectal cancer patients. A similar biomarker has been identified for non-small lung cancer, and this has increased prognostic power when used in combination with TNM classification [25, 47]. Additionally, a large study is under way to establish an immunoscore for patients with melanoma [69]. Immunoscore biomarkers have also proved to be useful predictors for responses to chemotherapy and radiotherapy [45, 187].

It is now evident that understanding the tumour microenvironment in cancer diagnosis is key. Although much experimental and clinical work has focused on the presence of specific subpopulations of T cells in the tumour microenvironment, the implication of the presence of an exhausted T cell population in the tumour microenvironment for patient outcome has received less attention. T cell exhaustion results primarily from sustained exposure to high levels of tumour antigen, as discussed in Chapter 3. T cell exhaustion is characterised by reduced effector T cell functionality (e.g. reduced killing, proliferation and cytokine production capabilities). The degree of T cell exhaustion changes over time in response to an evolving tumour [189], and is associated with the variety and density of inhibitory receptor (IR) expression on the T cells [201]. These IRs bind to matching ligands (e.g. PD-L1) expressed by the tumour cells, as well as other cells such as tumour associated macrophages (TAMs), dendritic cells and myeloid-derived suppressor cells (MDSCs). When an IR is bound with its matching ligand, the inhibitory pathway is activated, damping the T cell response. Cancer is associated with high levels of expression of IRs on T cells as well as high levels of ligand expression by tumour cells and TAMs [145]. In a recent study, Schriener *et al.* (2016) [171] observed that patients with high levels of exhausted T cells appeared not to respond to treatment with combined monoclonal antibody and bispecific antibody therapies.

Both immune cell presence and tumour composition are important factors in patient prognosis. PD-L1 expression by tumour cells has been identified as an important biomarker in patient prognosis [188], and has been observed to correlate with tumour infiltrating lymphocytes (TILs) levels [186]. PD-L1 expression is used to moderate an immune response, damping the T cell response not only through the engagement of inhibitory receptor pathways but through the maintenance of the regulatory T cell response [64]. The expression of PD-L1 is believed to increase in response to an increasing immune response [186]. The relationship between PD-L1 expression by tumour cells and the presence of TILs is not clearly understood. The aim of this chapter is to investigate how heterogeneous populations of tumour and immune cells interact,

and how the relative levels of exhausted to cytotoxic T cells and immune-resistant to immune-sensitive tumour cells influence escape from a tumour dormant state.

Mathematical models have been developed to both identify and explore factors promoting tumour escape from a tumour dormancy state. A number of such models have tried to explain escape through tumour immunosuppression by identifying the components of the immunosuppressive network which are primarily responsible for tumour escape [160, 114, 100]. On the other hand, other authors have sought to capture these effects implicitly through, for example, the inclusion of immune-resistant tumour cells, a feature of the model presented in this chapter. Wilkie *et al.* (2013) [202] designed a model to examine two different mechanisms used by the tumour to escape from an equilibrium state: (1) a decrease in the cytotoxic T cell strength (through its infiltrative and killing capacities), and (2) the presence of a resistant tumour population. In both cases they found that the level of infiltrating T cells is critical for maintaining a tumour equilibrium state.

Instead of accounting for heterogeneity in the immune sensitivity of the tumour, other authors have studied different subpopulations of T cells. For example, Macnamara and Eftimie (2015) [122] developed a mathematical model for oncolytic viral therapy to study the role of effector and memory T cells on long term tumour control. They found that in the absence of viral therapy, a sufficiently large memory pool is required to slow tumour growth. On the other hand, in the presence of a virus (mimicking oncolytic viral therapy), they found that a smaller initial memory pool would have a similar effect. They concluded that for sustained tumour control, a large pool of effector T cells must be maintained, which requires a supporting memory population.

Mathematical models also have the potential to identify promising therapeutic regimes for an individual, for example the combination of therapies to be given and how they should be administered [107]. Kirschner and Panetta (1998) [102] were among the first researchers to examine the effects of immunotherapy using an ODE model of tumour cells, cytotoxic T cells and the cytokine IL-2. Two different immunotherapies, both designed to boost the immune system, were examined. IL-2 therapy (examined in this chapter) works by promoting the proliferation of both T cells and natural killer cells resulting, at least in some cases, in durable progression-free survival in a number of aggressive cancers, including renal cell carcinoma and metastatic melanoma [62, 104, 164]. Kirschner and Panetta (1998) also examined adoptive T cell therapy (this is not relevant to the present model but details can be found in Chapter 1). They found that IL-2 therapy alone could not drive the system

to a tumour-free state but, interestingly, adoptive T cell transfer alone or in combination with IL-2 therapy could. In this chapter we also examine IL-2 therapy but in combination with a TCB antibody.

The model developed in this chapter is analogous to the model of Kirschner and Panetta [102] in that it includes the effects of an IL-2 therapy. Here however we consider the effects of an IL-2 therapy alone or in combination with a TCB antibody. Moreover we incorporate aspects of the model developed by Wilkie *et al.* [202] by including heterogeneity through an immune-resistant tumour population. Finally, we follow Macnamara and Eftimie [122] by considering different functional states of cytotoxic T cells. Instead of considering the memory T cell population we consider the exhausted T cell population. The emphasis on the exhausted T cells is motivated by the work of Wherry and Kuarchi (2015) [201], who found that sustained exposure to tumour antigen hinders the differentiation of the cytotoxic T cells into a memory population.

The remainder of this chapter is organised as follows. We introduce the model equations in Section 4.2. In Section 4.3 we summarise the qualitative behaviour exhibited by the model and derive bounds on key parameters delineating regions of tumour escape. In Section 4.4 we identify steady state solutions and characterise their linear stability. In Section 4.5 we examine how the qualitative behaviour of the model changes with the infiltration rate of the cytotoxic T cells together with the tumour growth rate, the probability of the tumour becoming immune-resistant, the exhausted T cell kill rate and the rate of T cell exhaustion. In Section 4.6 an alternative approach to characterising tumour equilibria is proposed as a way of inferring patient specific model parameters. This approach starts with given fractions of the tumour and cytotoxic T cell populations, and deduce from these the associated tumour growth rate and T cell infiltration rate. We determine the long term outcome starting in the neighbourhood of tumour equilibria. Finally, in Section 4.7 the effects of two immunotherapies — a TCB antibody and IL-2 therapy — are simulated and used to suggest personalised treatments based upon the composition of the tumour and cytotoxic T cell populations. Attention is focused on tumours which are destined for escape or dormancy. We conclude in Section 4.8 with a summary of our main findings.

4.2 The Mathematical Model

In this section we develop an ODE model to study the effects of an exhausted T cell population in the presence of cytotoxic T cells, immune-resistant and immune-sensitive tumour cells. We begin by presenting the model equations and their underpinning assumptions. We next identify parameter ranges for which the model exhibits the three Es of immunoediting [52].

4.2.1 Model equations

We propose a system of four ODEs to model the interactions between populations of cytotoxic and exhausted T cells, and two populations, of immune-sensitive and immune-resistant tumour cells. In practice exhausted T cells are distinguished from cytotoxic T cells by their up-regulation of a variety of inhibitory receptors (e.g. PD-1) while immune-resistant tumour cells are distinguished by their expression of ligands (e.g. PD-L1). The dependent variables are the number of immune-sensitive tumour cells $N(t)$, immune-resistant tumour cells $N_R(t)$, cytotoxic T cells $T_C(t)$, and exhausted T cells $T_E(t)$, where t represents time in days.

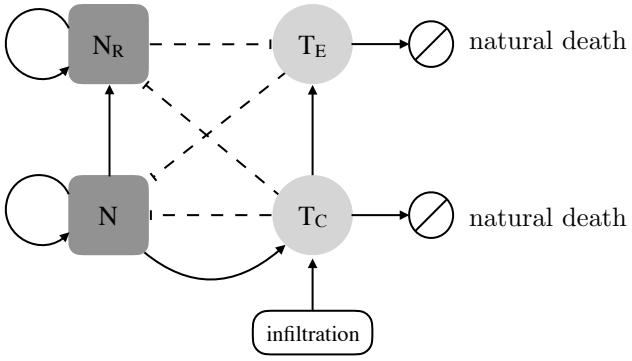

Figure 4.1: Schematic of the tumour-immune cell interactions included in our model. The circles indicate the cytotoxic and exhausted T cells, $T_C(t)$ and $T_E(t)$. The squares represent the immune-sensitive and immune-resistant tumour populations, $N(t)$ and $N_R(t)$. Interactions that directly increase a population are indicated by continuous lines while suppressive interactions are illustrated by dashed lines.

We assume that the evolution of the tumour populations, $N(t)$ and $N_R(t)$, are dominated by cell division and death, the latter being regulated by interactions with both cytotoxic and exhausted T cells. While several growth laws have been used to model tumour growth (e.g. logistic growth [110] or power-law growth [160]), we assume here for simplicity, as in Chapter 3, that in the absence of an immune response

the tumour grows exponentially, with growth rate γ (units: day^{-1}). We suppose that during cell division the tumour population N increases with probability $(1-\theta)$, or mutates to produce immune-resistant tumour cells N_R, with probability θ. We assume that cytotoxic T cells kill both populations of tumour cells at a rate which is proportional to the product of their densities, with kill rate k (units: cells^{-1}day^{-1}). Similarly, exhausted T cells, $T_E(t)$, kill immune-sensitive tumour cells at a rate proportional to the product of their densities, with kill rate k_E (units: cells^{-1}day^{-1}). Exhausted T cells are unable to kill immune-resistant tumour cells N_R; instead when immune-resistant tumour cells and exhausted T cells come into contact they are deleted. Combining these processes we propose the following ODEs to describe the evolution of the tumour populations N and N_R:

$$\frac{dN}{dt} = \underbrace{\gamma(1-\theta)N}_{\text{exponential growth}} - \underbrace{kT_CN - k_ET_EN}_{\text{immune induced death}}, \tag{4.1}$$

$$\frac{dN_R}{dt} = \underbrace{\gamma\theta N + \gamma_R N_R}_{\text{exponential growth}} - \underbrace{kT_CN_R}_{\text{immune induced death}}, \tag{4.2}$$

We assume that the evolution of cytotoxic T cells, $T_C(t)$, is dominated by infiltration from the lymph nodes at rate σ (units: cells day^{-1}), proliferation in response to the tumour population, exhaustion and natural cell death. Similarly, we assume that the evolution of the exhausted T cells, $T_E(t)$, is dominated by conversion of cytotoxic T cells into an exhausted state, deletion by immune-resistant tumour cells N_R and natural cell death. As in Chapter 2, cytotoxic T cells are assumed to proliferate at a rate which has biphasic dependence on the tumour cell density $N(t)$ with constant of proportionality α (units: day^{-1}). By contrast, exhausted T cells do not proliferate. We assume cytotoxic T cells become exhausted at a rate which is proportional to the number of immune-resistant tumour cells with constant of proportionality ν (units: cells^{-1}day^{-1}). We assume that cytotoxic and exhausted T cells die at rates δ_C and δ_E (units: day^{-1}), respectively. Combining these processes, we propose the following ODEs to describe the evolution of the two populations of T cells:

$$\frac{dT_C}{dt} = \underbrace{\sigma}_{\text{infiltration}} + \underbrace{\frac{\alpha T_C\tilde{N}N}{\tilde{N}^2+N^2}}_{\text{proliferation}} - \underbrace{\nu T_CN_R}_{\text{conversion from } T_C} - \underbrace{\delta_CT_C}_{\text{natural death}}, \tag{4.3}$$

$$\frac{dT_E}{dt} = \underbrace{\nu T_CN_R}_{\text{conversion from } T_C} - \underbrace{rN_RT_E}_{\text{deletion}} - \underbrace{\delta_ET_E}_{\text{natural death}}. \tag{4.4}$$

The model is completed by specifying the initial cell populations:

$$N(0) = N_0, \quad N_R(0) = N_{R0}, \quad T_C(0) = T_{C0}, \quad T_E(0) = T_{E0}\,. \tag{4.5}$$

Specific values for the initial conditions $(N_0, N_{R0}, T_{C0}, T_{E0})$ are examined in the qualitative behaviour presented in Section 4.3.

4.2.2 Non-dimensionalised equations

Before continuing it is convenient to non-dimensionalise the governing equations. We scale the tumour populations, N and N_R, with the tumour size at which suppressive effects come into play, $\tilde{N}$. We scale the T cell populations, T_C and T_E, by the parameter combination δ_C/k in order to minimise the number of dimensionless parameters in the dimensionless model. We scale time by the half-life of the cytotoxic T cell population, δ_C^{-1}. Hence, we take

$$N = \tilde{N}\hat{N}, \quad N_R = \tilde{N}\hat{N}_R, \quad T_C = \delta_C\hat{T}_C/k, \quad T_E = \delta_C\hat{T}_E/k \quad \text{and} \quad t = \hat{t}/\delta_C\,, \tag{4.6}$$

where hats denote dimensionless quantities. Substitution of (4.6) into equations (4.1)–(4.4) gives

$$\frac{d\hat{N}}{d\hat{t}} = \hat{N}\left(\hat{\gamma}(1-\theta) - \hat{T}_C - \hat{k}_E\hat{T}_E\right), \tag{4.7}$$

$$\frac{d\hat{N}_R}{d\hat{t}} = \hat{\gamma}\theta\hat{N} + \left(\hat{\gamma}_R - \hat{T}_C\right)\hat{N}_R\,, \tag{4.8}$$

$$\frac{d\hat{T}_C}{d\hat{t}} = \hat{\sigma} + \frac{\hat{\alpha}\hat{N}\hat{T}_C}{1+\hat{N}^2} - \hat{\nu}\hat{N}_R\hat{T}_C - \hat{T}_C\,, \tag{4.9}$$

$$\frac{d\hat{T}_E}{d\hat{t}} = \hat{\nu}\hat{T}_C\hat{N}_R - \hat{r}\hat{N}_R\hat{T}_E - \hat{\delta}_E\hat{T}_E\,, \tag{4.10}$$

with initial conditions

$$\hat{N}(0) = \hat{N}_0, \quad \hat{N}_R(0) = N_{R0}, \quad \hat{T}_C(0) = \hat{T}_{C0}, \quad \hat{T}_E(0) = \hat{T}_{E0}\,, \tag{4.11}$$

where

$$\begin{aligned} &\hat{\gamma} = \gamma/\delta_C, \quad \hat{\gamma}_R = \gamma_R/\delta_C, \quad \hat{k}_E = k_E/k, \quad \hat{\alpha} = \alpha/\delta_C, \\ &\hat{\sigma} = \sigma k/\delta_C^2, \quad \hat{r} = r\tilde{N}/\delta_C, \quad \hat{\delta}_E = \delta_E/\delta_C, \quad \hat{\nu} = \nu/k, \\ &\hat{N}_0 = \frac{N_0}{\tilde{N}}, \quad \hat{N}_{R0} = \frac{N_{R0}}{\tilde{N}}, \quad \hat{T}_{C0} = \frac{T_{C0}k}{\delta_C}, \quad \hat{T}_{E0} = \frac{T_{E0}k}{\delta_C}\,. \end{aligned} \tag{4.12}$$

As before, for ease of presentation, we drop the hats on all quantities. Interpretation of the dimensionless parameters in (4.12) is provided in Table 4.1.

For clarity we point out the features of the model (4.7)–(4.10) absent in the models previously considered in Chapters 2 and 3. The equations representing the tumour and cytotoxic T cell populations in the present model closely resemble those in Chapter 2 but using exponential tumour growth in place of logistic tumour growth. Equations (4.8) and (4.10) are unique to this model and account for the additional effects of an immune-resistant tumour population and an exhausted T cell population. This approach to modelling T cell exhaustion differs from the previous model where we were interested in studying how the specific T cell functions diminish in the presence of an increasing tumour mass. In the present model we mimic the effects of exhaustion by a distinct T cell population which feeds in from the cytotoxic T cell equation (4.9) through a mass action term. The growth rate for the tumour population in equation (4.7) has an additional term accounting for tumour cell killing by exhausted T cells. Moreover, as the tumour expands it now expands as both an immune-sensitive and immune-resistant tumour population.

4.2.3 Parameter values

Due to the lack of experimental data to obtain model parameters directly (a problem faced by many authors [102, 39]) and the difficulty of obtaining accurate measurements experimentally, we choose our parameters such that the model exhibits expected qualitative behaviour. Specifically we select the parameters such that the model captures the three Es of immunoediting [52]. Furthermore, as the death rate and kill rate of the exhausted T cells are lower than for the cytotoxic T cells [199], we constrain the parameters δ_E and k_E to be small compared to one.

To determine the default parameter values we looped over a range of logarithmically-spaced (dimensionless) parameter values extending over six orders of magnitude from 10^{-3} to 10^{3} (with 13 values). This search identified a small region of parameter space in which there exist up to four steady state solutions (including the tumour-free state). We also sought to keep as many of the parameters as possible near unity in magnitude. However since we expect the death rate of exhausted T cells to be low compared to the death rate of cytotoxic T cells (T_C), and the rate of T cell killing of the tumour by exhausted T cells (T_E) to be lower than that of cytotoxic T cells [199], we sought values of δ_E and k_E of the order 10^{-1}. The default parameter choices listed in Table 4.1 exhibit the three Es of immunoediting under the constraints that k_E and δ_E are small. Unless otherwise stated, the default parameters used throughout are given in Table 4.1.

Dimensionless parameter	Physical description	Default value
γ	immune-sensitive tumour growth rate	0.3
θ	probability of tumour becoming immune-resistant	0.3
γ_R	immune-resistant tumour growth rate	0.01
k_E	tumour population rate at which exhausted T cells kill immune-sensitive tumour cells	0.1
σ	rate of cytotoxic T cell infiltration	0.15
α	proliferation rate of cytotoxic T cells in the presence of the tumour	1
r	rate at which immune-resistant tumour cells kill exhausted T cells	0.1
ν	rate at which cytotoxic T cells become exhausted	0.3
δ_E	natural death rate of exhausted T cells	0.1

Table 4.1: Summary of the default dimensionless parameter values used in equations (4.7)–(4.10).

4.3 Qualitative behaviour

As in Chapters 2 and 3, to illustrate the range of behaviours exhibited by our model, equations (4.7)–(4.11) were solved numerically using the Dormand-Prince explicit adaptive time-stepping method in Python (dopri5) [49].

In Figure 4.2 we present simulation results for two values of the background infiltration rate of the cytotoxic T cells into the tumour, σ. The emphasis on σ is motivated by clinical observations which suggest that levels of tumour infiltrating lymphocytes (TILs) correlate with more favourable response outcomes and are patient specific [141, 188, 98, 91]. This figure illustrates the behaviour exhibited by equations (4.7)–(4.10) for the default parameters in Table 4.1. When the initial tumour and T cell populations are close to the tumour-free steady state (blue curves), the long time behaviour depends on σ, with elimination for large values of σ and equilibrium for small values of σ. On the other hand, if the tumour is initially large (black curves), then tumour escape is inevitable for both values of σ considered.

(1) $\sigma = 0.15$

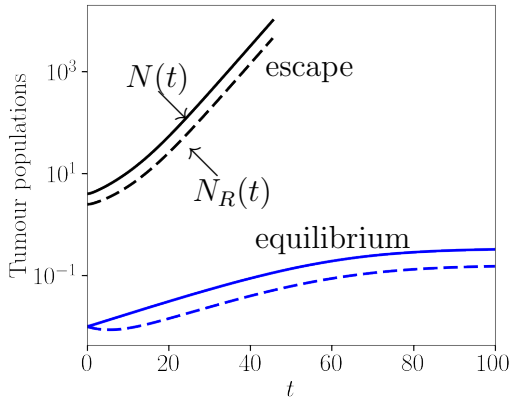

(a) tumour cells: $N(t)$ and $N_R(t)$

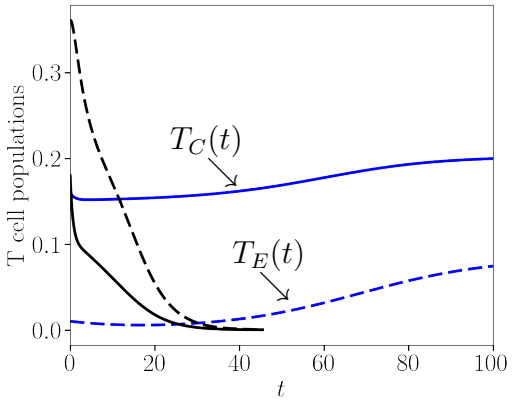

(b) cytotoxic T cells: $T_C(t)$ and $T_E(t)$

(2) $\sigma = 0.25$

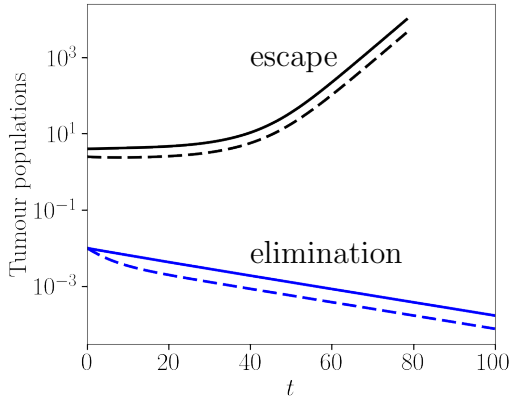

(c) tumour cells: $N(t)$ and $N_R(t)$

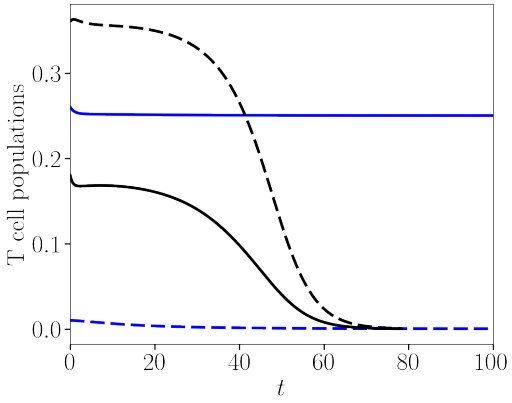

(d) cytotoxic T cells: $T_C(t)$ and $T_E(t)$

Figure 4.2: Series of plots illustrating the range of qualitative behaviours exhibited by equations (4.7)–(4.10). We plot the time evolution of the tumour populations $N(t)$ and $N_R(t)$ (solid and dashed curves respectively) and the T cell populations $T_C(t)$ and $T_E(t)$ (solid and dashed curves respectively) for different values of σ the rate of T cell infiltration. In panels (a) and (b), for the default value of $\sigma(= 0.15)$ we observe that the model exhibits states of tumour equilibrium and escape depending on initial conditions; in panels (c) and (d), when σ is increased from $\sigma = 0.15$ to $\sigma = 0.25$, we observe that tumour elimination is now possible. In both cases we observe bistability, and collectively we see that the model exhibits the three Es of Immunoediting. Parameter values: except for σ, all parameters are fixed at their default values. Initial conditions: $(N_0, N_{R0}, T_{C0}, T_{E0}) = (0.01, 0.01, \sigma + 0.01, 0.01)$ (blue curves) and $(N_0, N_{R0}, T_{C0}, T_{E0}) = (4, 2.5, 0.18, 0.36)$ (black curves).

4.3.1 Basins of attraction of tumour escape

The simulation results presented in Figure 4.2 illustrate possible outcomes but do not address the fate of the tumour-immune system starting from an arbitrary initial condition. Due to the use of an exponential tumour growth law, tumour escape is inevitable for sufficiently large initial tumour populations (for any choice of parameters). For our choice of parameters, to understand when tumour escape occurs as a function of initial conditions, we solve equations (4.7)–(4.10) for a range of initial immune-sensitive tumour populations N_0 to locate (by bisection) the critical initial immune-sensitive tumour population, N_0^{crit}, separating tumour escape from all other outcomes. This is done for varying initial populations T_{C0} and T_{E0}, keeping the ratio N_{R0}/N_0 fixed.

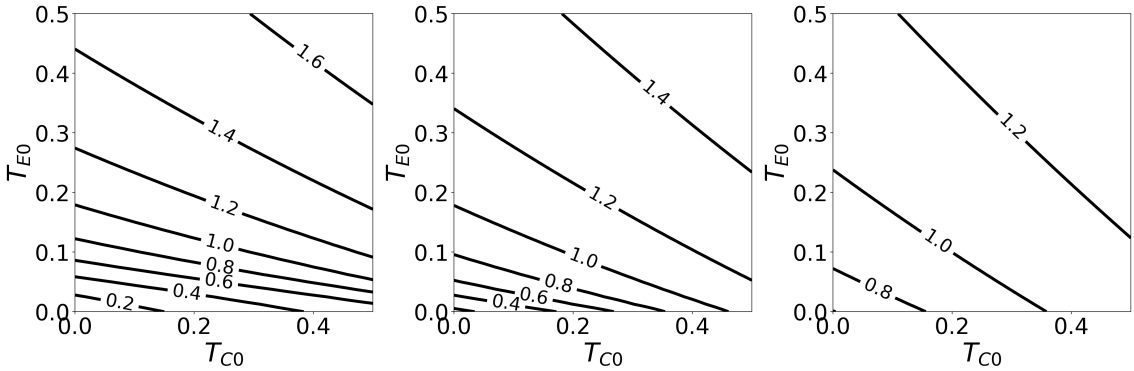

(a) $N_{R0}/N_0 = 0.5$ (b) $N_{R0}/N_0 = 1$ (c) $N_{R0}/N_0 = 2$

Figure 4.3: Series of plots delineating the basins of attraction of tumour escape over the (T_{C0}, T_{E0}) initial condition plane. Shown are contour lines of the log-scaled initial tumour population $\log_{10} N_0^{\text{crit}}$ dividing tumour escape from tumour elimination or equilibrium. Three ratios of N_{R0} to N_0 are considered: (a) $N_{R0}/N_0 = 0.5$, (b) $N_{R0}/N_0 = 1.0$ and (c) $N_{R0}/N_0 = 2$. Note that values of $\log_{10} N_0^{\text{crit}}$ larger than that shown for a particular T_{C0} and T_{E0} results in tumour escape. Parameter values: all model parameters are fixed at their default values.

Figure 4.3 presents our findings. As the ratio N_{R0}/N_0 increases, smaller initial immune-sensitive tumour populations escape for larger values of T_{C0} and T_{E0}. Conversely, larger initial tumour populations escape for smaller values of T_{C0} and T_{E0}. When T_{C0} and T_{E0} are simultaneously increased, the initial population of tumour cells has to be larger to escape, as expected. In summary the results presented in Figure 4.3 illustrate, for fixed model parameters, where in initial condition space tumour escape occurs.

4.3.2 Conditions for tumour escape

For given initial conditions and parameters, we have seen that the tumour may escape. In Section 4.3.1 we determined the basin of attraction of tumour escape depending on the initial T cell populations and the ratio N_{R0}/N_0 of the initial tumour populations. In Figure 4.2 we illustrated that model outcomes vary with the rate of T cell infiltration σ. For the values of σ considered, we observed bistability between escape and either elimination or equilibrium. We next determine a critical value of σ, as a function of model parameters, below which tumour escape is possible, *independent of initial conditions*.

A sufficient (but not necessary) condition for tumour escape is $dN/dt > 0$ for all time. To determine the region of parameter space in which this occurs, we first determine upper bounds on T_C and T_E for which the growth rate in equation (4.7) is positive. Likewise N_R will grow without bound if $dN_R/dt > 0$ for all time. The minimum value of $\gamma_R - T_C$ in equation (4.8) is attained when T_C reaches a maximum value. We thus ensure $dN_R/dt > 0$ for all time if $\gamma_R - T_{C,\max} > 0$. Therefore $\gamma_R > T_{C,\max}$ is a sufficient (but not necessary) condition for tumour escape. An upper bound for T_C occurs at a stationary point when $dT_C/dt = 0$. This is found by using the maximum value of the proliferation term in equation (4.9) and ignoring the decay term $-\nu T_C N_R$. The maximum proliferation rate of the cytotoxic T cells occurs when $N = 1$ and attains the value of $\alpha T_C/2$. Hence the maximum value of the growth terms in equation (4.9) is $(\sigma + \alpha T_C/2)$. Balancing this with the decay term $-T_C$ at the stationary point where $dT_C/dt = 0$, we obtain the estimate

$$T_{C,\max} = \frac{\sigma}{1 - \alpha/2}\,. \tag{4.13}$$

Notably an upper bound for T_C cannot be found in this way for $\alpha \geq 2$ (see below for this case), yet T_C can never become unbounded.

Returning to the growth of N in equation (4.7), N will continue to grow so long as $\gamma(1-\theta) > T_{C,\max} + k_E T_{E,\max}$. We next determine $T_{E,\max}$. This is determined from equation (4.10) where we use the maximum value of the growth term $\nu T_{C,\max} N_R$ and balance this with the decay term $-rT_E N_R$, ignoring the linear decay term $-\delta_E T_E$. Using the largest upper bound for T_E in equation (4.7) guarantees the continued growth of N. Hence we use

$$T_{E,\max} = \frac{\nu T_{C,\max}}{r} = \frac{\nu\sigma}{r(1-\alpha/2)}\,. \tag{4.14}$$

It follows therefore that N will continue to grow when

$$T_{C,\max} + k_E T_{E,\max} = \frac{\sigma(r + k_E\nu)}{r(1-\alpha/2)} < \gamma(1-\theta)\,. \tag{4.15}$$

Likewise N_R will continue to grow in equation (4.8) when

$$T_{C,\max} = \frac{\sigma}{1-\alpha/2} < \gamma_R\,. \tag{4.16}$$

Therefore tumour escape is guaranteed, independent of initial conditions, when

$$\sigma < \sigma_{\text{crit}} = (1-\alpha/2)\max\left(\gamma_R, \frac{r\gamma(1-\theta)}{r+k_E\nu}\right)\,. \tag{4.17}$$

(Note for the default parameters chosen, the second term in equation (4.17) is larger than the first term in the brackets.)

When the proliferation rate of the cytotoxic T cells α takes a value of $\alpha \geq 2$, the situation is different. We can no longer find a condition on parameters which guarantees tumour escape. For sufficiently large tumour populations initially, tumour escape is inevitable for all parameters (not shown). This follows because in the limit $N, N_R \to \infty$, regardless of parameters, both T_C and T_E are $\mathcal{O}(1/N_R) \ll 1$. Therefore the T cell populations are too small to arrest the growth of the tumour in equations (4.7) and (4.8).

On the other hand, it is possible to show that both T_C and T_E remain bounded when $\alpha \geq 2$. When $\alpha \geq 2$ the decay term $-\nu T_C N_R$ in equation (4.9) is responsible for ensuring that T_C is bounded. We prove that T_C remains bounded by contradiction. Supposing $T_C \gg \max(\sigma, \gamma(1-\theta))$, the decay rate in equation (4.7), $T_C + k_E T_E - \gamma(1-\theta) \gg 1$, since the T_C term dominates the decay. This implies that N is rapidly driven to zero. Likewise N_R is rapidly driven to zero since the production term $\gamma\theta N$ in equation (4.8) is negligible, and the largest-magnitude term on the right-hand side is $-T_C N_R$. Furthermore in equation (4.9) for T_C, the proliferation term is negligible in this case since it is proportional to N. Therefore

$$T_C \gg \sigma \quad \Rightarrow \quad \frac{dT_C}{dt} \approx \sigma - T_C \approx -T_C\,, \tag{4.18}$$

implying T_C decays exponentially. It follows therefore that T_C and T_E can never become unbounded.

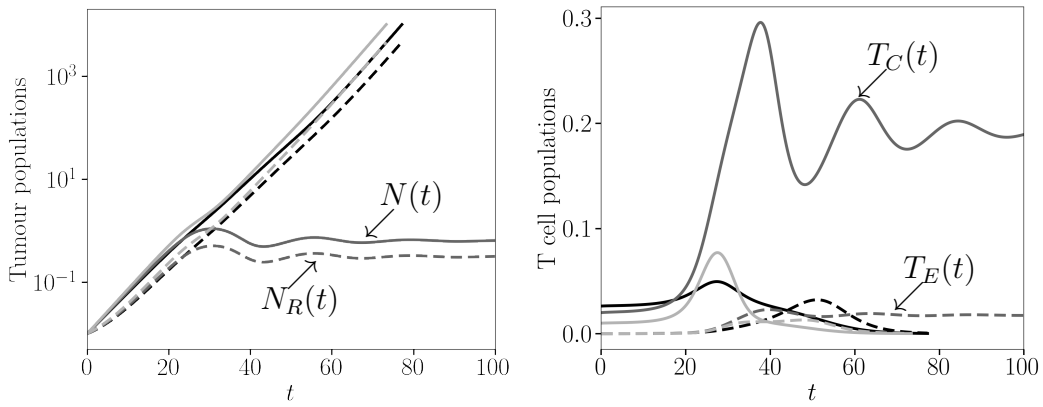

(a) $N(t)$ (solid) and $N_R(t)$ (dashed)

(b) $T_C(t)$ (solid) and $T_E(t)$ (dashed)

Figure 4.4: Verification of the condition (4.17) on σ for tumour escape. The results are obtained by solving equations (4.7)–(4.10) initialised around a small tumour population. We show the time evolution of (a) the tumour populations $N(t)$ and $N_R(t)$ (solid and dashed curves respectively) and, (b) the cytotoxic and exhausted T cell populations $T_C(t)$ and $T_E(t)$ (solid and dashed curves respectively) for three different pairs of parameters (α, σ). Parameter values: all parameters are fixed at their default values except for α and σ. Key: $(\alpha, \sigma) = (1.0, 0.02625)$ where the tumour escapes (black curves); $(\alpha, \sigma) = (2.0, 0.02)$ where the tumour settles to an equilibrium (dark grey curves); $(\alpha, \sigma) = (2.0, 0.01)$ where the tumour again escapes (light grey curves). Initial conditions: $(N_0, N_{R0}, T_{C0}, T_{E0}) = (0.01, 0.01, \sigma, 0)$.

To confirm the analysis for $\alpha < 2$ and $\alpha \geq 2$, in Figure 4.4 we consider the qualitative behaviour starting with an initially small tumour population for three choices of α and corresponding choices of σ. When $\alpha < 2$, σ is chosen to be σ_{crit} in equation (4.17). The case $(\alpha, \sigma) = (1, 0.02625)$ is shown in black and confirms that for this value of σ the tumour populations escape. When $\alpha = 2$, escape occurs if σ is sufficiently small ($\sigma = 0.01$, weak T cell infiltration); equilibrium occurs if σ is sufficiently large ($\sigma = 0.02$). When $\alpha > 2$ the results are qualitatively similar to that shown for $\alpha = 2$ and are therefore omitted. This analysis shows where tumour escape occurs as a function of σ and α, independent of initial conditions.

4.4 Steady state and linear stability analysis

The nonlinear dynamics described in Section 4.3 show that the model exhibits three distinct behaviours: elimination, equilibrium or escape. The observed behaviour is related to the existence of stable 'attractors' or steady states $(N^*, N_R^*, T_C^*, T_E^*)$. In Sections 4.3.1 and 4.3.2 we focused on 'escape' solutions for which N and N_R grow

without bound. In this section we characterise finite solutions by identifying the steady state solutions and characterising their linear stability.

Setting $d/dt = 0$ in equations (4.7)–(4.10) gives the following system of algebraic equations

$$[\gamma(1-\theta) - (T_C^* + k_E T_E^*)]\, N^* = 0\,, \tag{4.19}$$

$$\gamma\theta N^* = (T_C^* - \gamma_R) N_R^*\,, \tag{4.20}$$

$$\sigma + \frac{\alpha T_C^* N^*}{1 + N^{*2}} = (\nu N_R^* + 1) T_C^*\,, \tag{4.21}$$

$$\nu T_C^* N_R^* = (r N_R^* + \delta_E) T_E^*\,. \tag{4.22}$$

It is straightforward to see that there is a tumour-free steady state for which

$$N^* = N_R^* = T_E^* = 0 \quad \text{and} \quad T_C^* = \sigma\,. \tag{4.23}$$

Furthermore, if $\sigma > \gamma_R$ then there is a non-trivial fully immune-resistant tumour steady state for which

$$N^* = 0, \quad N_R^* = \frac{\sigma - \gamma_R}{\nu\gamma_R}, \quad T_C^* = \gamma_R \quad \text{and} \quad T_E^* = \frac{(\sigma - \gamma_R)\nu\gamma_R}{\delta_E \nu\gamma_R + r(\sigma - \gamma_R)}\,. \tag{4.24}$$

The remaining steady states have $(N^*, N_R^*, T_C^*, T_E^*) > 0$ which we determine as follows. With $N^* > 0$, equation (4.19) supplies an expression for T_E^* in terms of T_C^* of the form

$$T_E^* = a_0 - a_1 T_C^*\,, \tag{4.25}$$

where $a_0 = \gamma(1-\theta)/k_E$ and $a_1 = 1/k_E$. Substituting equation (4.25) into equation (4.22) yields an expression for T_C^* in terms of N_R^*,

$$T_C^* = \frac{b_0 + b_1 N_R^*}{c_0 + c_1 N_R^*}\,, \tag{4.26}$$

where $b_0 = \delta_E a_0$, $b_1 = r a_0$, $c_0 = \delta_E a_1$ and $c_1 = \nu + r a_1$. From equation (4.20) we obtain an expression for N^*, again in terms of N_R^*

$$N^* = N_R^* \frac{e_0 + e_1 N_R^*}{f_0 + f_1 N_R^*}\,, \tag{4.27}$$

where $e_0 = b_0 - \gamma_R c_0$, $e_1 = b_1 - \gamma_R c_1$, $f_0 = \gamma\theta c_0$ and $f_1 = \gamma\theta c_1$.

Finally, inserting equations (4.26) and (4.27) into equation (4.21) we obtain the following 6th order polynomial for N_R^*

$$m_0 + m_1 N_R^* + m_2 {N_R}^{*2} + m_3 N_R^{*3} + m_4 N_R^{*4} + m_5 N_R^{*5} + m_6 N_R^{*6} = 0\,, \tag{4.28}$$

where the coefficients $m_0, \ldots, m_6$ are combinations of the model parameters (see Appendix E for details).

The steady state analysis shows there exists a tumour-free state ($N^* = N_R^* = 0$), a immune-resistant tumour state ($N^* = 0$, $N_R^* > 0$) and up to six additional tumour equilibria ($N^*, N_R^* > 0$). In fact an intensive search through parameter space indicates that there are at most three physically realistic roots. We turn next to the linear stability of the steady states to understand which of these are model attractors.

As in Chapter 2 the linear stability analysis of the steady states $(N^*, N_R^*, T_C^*, T_E^*)$ is determined by considering small amplitude perturbations to the steady states leading to the Jacobian matrix $\mathcal{J}(N^*, N_R^*, T_C^*, T_E^*)$:

$$\mathcal{J} = \begin{pmatrix} \gamma(1-\theta) - T_C^* - k_E T_E^* & 0 & -N^* & -k_E N^* \\ \gamma\theta & \gamma_R - T_C^* & -N_R^* & 0 \\ \frac{\alpha T_C^*(1-N^{*2})}{(1+N^{*2})^2} & -\nu T_C^* & \frac{\alpha N^*}{1+N^{*2}} - \nu N_R^* - 1 & 0 \\ 0 & \nu T_C^* - r T_E^* & \nu N_R^* & -r N_R^* - \delta_E \end{pmatrix}. \quad (4.29)$$

From the Jacobian, the eigenvalues associated with the tumour-free steady state $(N^*, N_R^*, T_C^*, T_E^*) = (0, 0, \sigma, 0)$ are simply

$$\lambda_1 = -1, \quad \lambda_2 = -\delta_E, \quad \lambda_3 = \gamma_R - \sigma, \quad \lambda_4 = \gamma(1-\theta) - \sigma\,. \quad (4.30)$$

Linear stability of the tumour-free state is guaranteed provided the T cell infiltration rate surpasses the growth rates of immune-sensitive and immune-resistant tumour populations, $\gamma(1-\theta)$ and γ_R respectively. Specifically linear stability of the tumour-free state is guaranteed provided

$$\sigma \geq \max\left(\gamma_R, \gamma(1-\theta)\right)\,. \quad (4.31)$$

On the other hand, the eigenvalues associated with the non-trivial fully immune-resistant tumour steady state (see equation (4.24)) are given by:

$$\lambda_1 = \gamma(1-\theta) - \gamma_R - \frac{k_E(\sigma - \gamma_R)\nu\gamma_R}{\delta_E \nu\gamma_R + r(\sigma - \gamma_R)}, \quad (4.32)$$

$$\lambda_2 = \frac{r(\gamma_R - \sigma)}{\nu\gamma_R} - \delta_E, \quad (4.33)$$

$$\lambda_3, \lambda_4 = \frac{-\sigma/\gamma_R \pm \sqrt{(\sigma/\gamma_R)^2 + 4(\sigma - \gamma_R)}}{2}\,. \quad (4.34)$$

Since the non-trivial fully immune-resistant tumour steady state only exists for $\sigma > \gamma_R$ (see equation (4.24)) one of the pair of eigenvalues in equation (4.34) is always positive and therefore this steady state is always unstable where it exists.

The remaining steady states have $N^*, N_R^* > 0$. The existence and stability of these steady states cannot be determined analytically. Instead in Section 4.5 we examine the existence and stability of the steady states numerically as a function of the T cell infiltration rate σ.

4.5 System bifurcations

When varying model parameters, steady states may appear or disappear at bifurcation points. To examine how variations in the model parameters affect qualitative behaviour, in Figure 4.5 we identify parameter regions of tumour elimination, equilibrium and escape. Where elimination and equilibrium are possible we have bistability with tumour escape. We focus on varying parameters associated with the exhausted T cell population, specifically the exhausted T cell tumour kill rate, k_E, and the conversion rate of cytotoxic to exhausted T cells, ν, as well as the growth rate of the tumour, γ, and the probability of the tumour becoming immune-resistant, θ, as we vary the rate of infiltration of the cytotoxic T cells, σ. Note the remaining parameters γ_R, α, r and δ_E have virtually no effect on the regions of tumour elimination, equilibrium and escape, and therefore are not discussed further.

For the parameters k_E and ν associated with the exhausted T cell population T_E, we observe that model outcomes of tumour elimination, equilibrium and escape depend only weakly on σ. In Figure 4.5(a), as k_E decreases and the exhausted T cell's killing capacity weakens, the region of tumour escape (black) increases at the expense of the region in which tumour equilibrium occurs (grey). In Figure 4.5(b), a similar trend is seen with increases in the conversion rate of cytotoxic to exhausted T cells, ν. As ν increases so does the region of escape, eventually replacing the region occupied by a tumour equilibrium state entirely.

The region where tumour elimination is possible is unaffected by variations in k_E and ν as these parameters are absent from the model when $N^* = N_R^* = 0$ (see equation (4.31)). In Figure 4.5(c), increases in the tumour growth rate γ require corresponding increases in the infiltration rate σ of the cytotoxic T cells. Consequently if a patient has a particularly aggressive tumour with a large growth rate but a poor infiltration of cytotoxic T cells, as observed for example in prostrate cancer [18], then this model predicts that tumour escape is inevitable. As θ decreases (and the tumour proliferates primarily as the immune-sensitive tumour population) a tumour equilibrium region emerges, cutting into the region of tumour elimination. The region of escape also expands with decreasing θ, implying that a larger infiltration of T cells is necessary

to control the tumour. This occurs because the growth rate of N_R is less than the growth rate of N. Overall this implies that the tumour population as a whole grows faster as θ decreases for fixed σ. Note that the scan conducted over parameters to locate regions of parameter space exhibiting the three Es of immunoediting in no case found $\gamma_R > \gamma/10$.

In Figure 4.6 we illustrate the variations in the steady state populations N^*, N_R^*, T_C^* and T_E^*, with the T cell infiltration rate σ. The black line shows the tumour-free state, the magenta line shows the tumour-resistant state, while the blue and red lines show tumour equilibria. Decreasing σ from 0.5, we observe three distinct bifurcations: a transcritical bifurcation at $\sigma = \sigma^{\mathrm{T}} \approx 0.21$ where the tumour-free state exchanges stability with a tumour equilibrium state, a fold point at $\sigma = \sigma^{\mathrm{F}} \approx 0.12$ where there exists an exchange of stability with the emergence of a new branch of tumour equilibrium states, and the emergence of a fully immune-resistant tumour state from the tumour-free solution branch at $\sigma = \sigma^{\mathrm{E}} = \gamma_R$. This illustrates the generic bifurcation structure exhibited by the model with variations in σ over a wide range of model parameters.

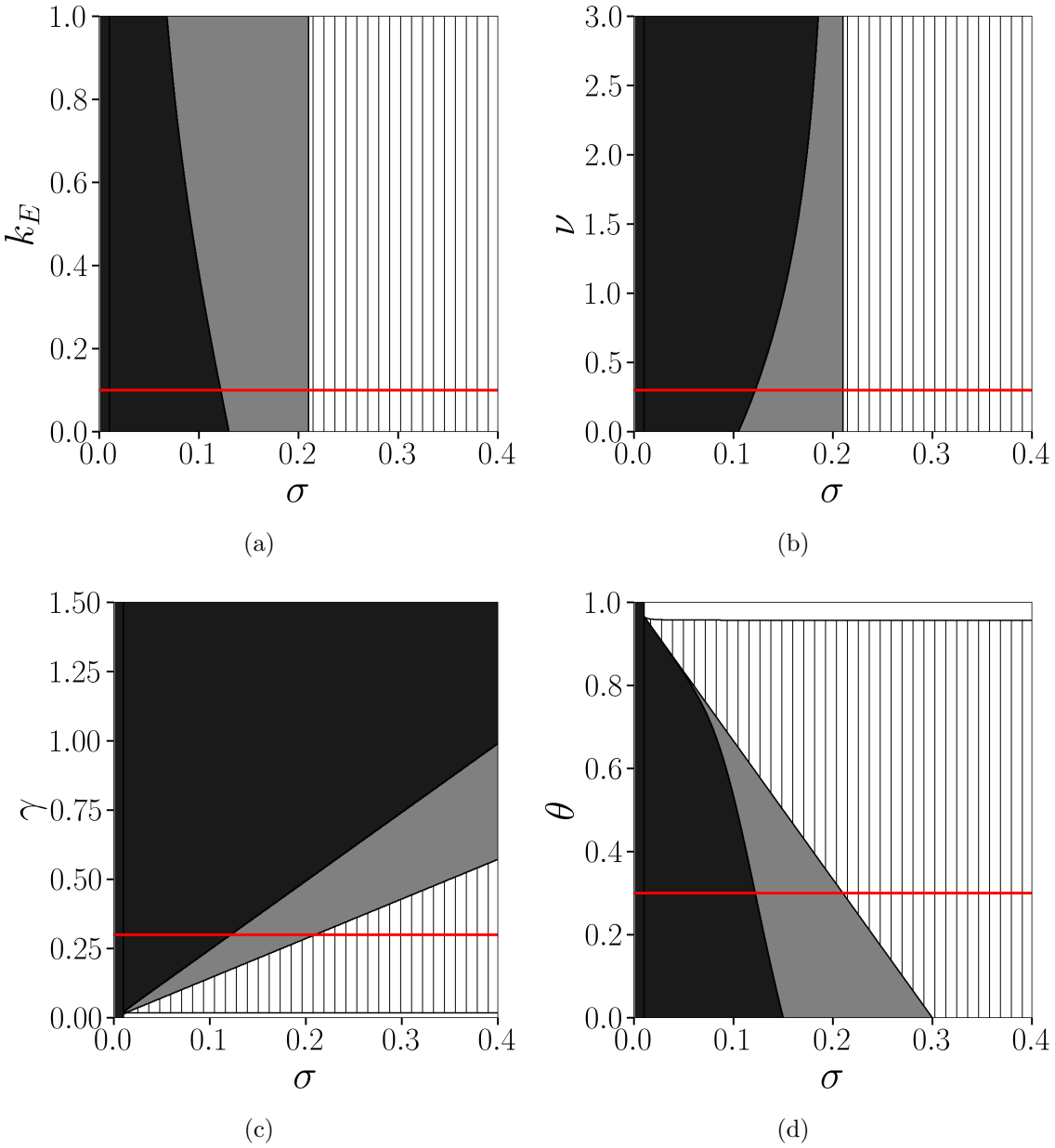

Figure 4.5: Dependence of the qualitative behaviour of equations (4.7)–(4.10) on the T cell infiltration rate σ versus: (a) the exhausted T cell tumour kill rate k_E, (b) the conversion rate ν of cytotoxic to exhausted T cells, (c) the tumour growth rate γ, and (d) the probability θ of the tumour becoming immune-resistant. Regions are distinguished by the existence and linear stability of the steady states. The red horizontal line indicates the cross-sections illustrated in Figure 4.6. Key: black region: tumour escape is the only attractor; grey region: bistability between a tumour equilibrium state and escape (here the tumour-free state, fully immune-resistant tumour state and an additional tumour equilibrium state exist but are unstable); white striped region: bistability between the tumour-free state and escape as well as instability of a tumour equilibrium state; white region: bistability between a tumour-free state and tumour escape — no other steady states exist. Parameter values: all remaining parameters are fixed at their default values.

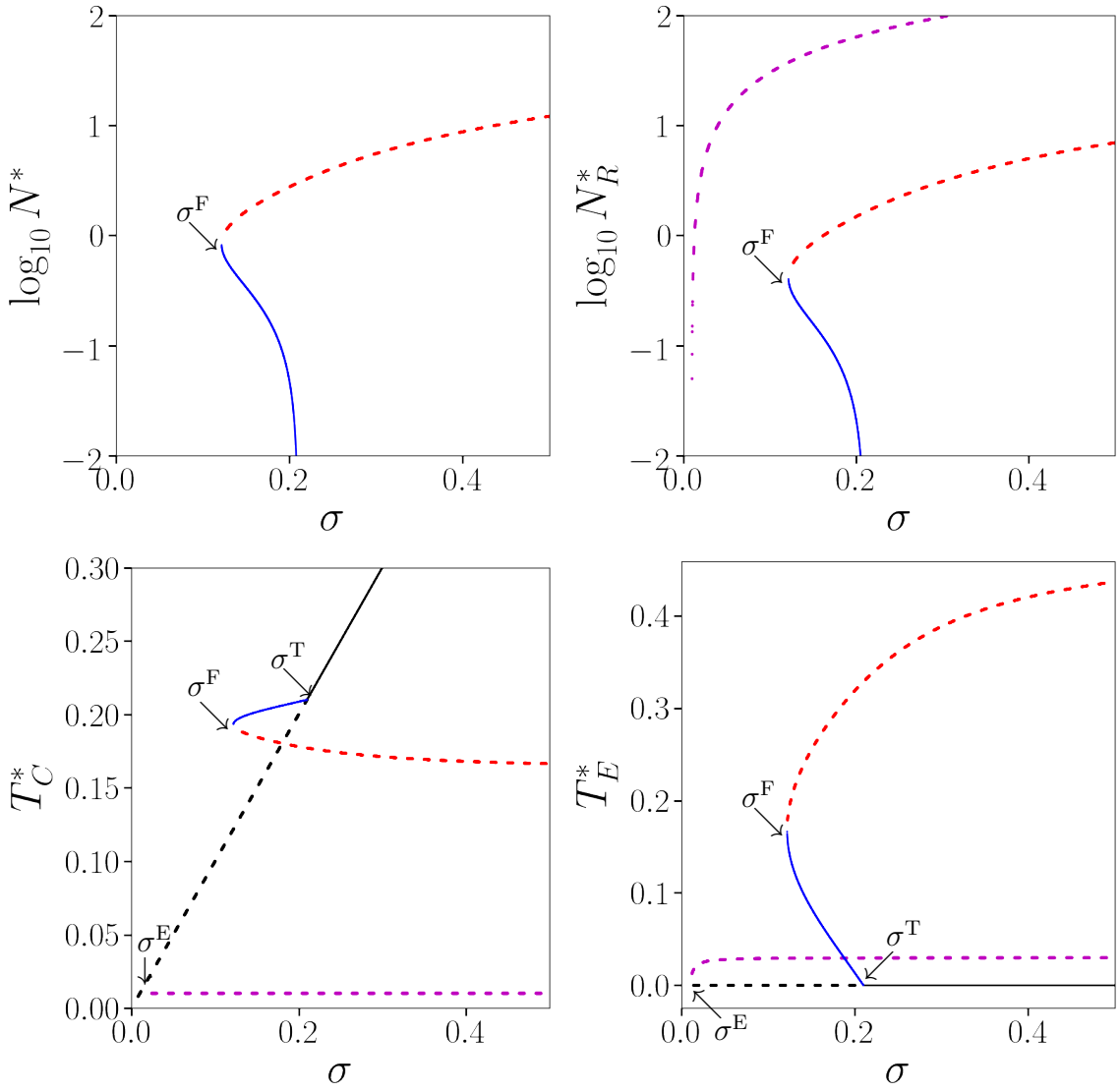

Figure 4.6: Existence and stability of the steady state solutions N^*, N_R^*, T_C^* and T_E^* arising from equations (4.19)–(4.22) as the infiltration rate σ is varied. These panels illustrate the bifurcation structure as we move along the horizontal red lines in Figure 4.5. Solution branches are distinguished by colour: the red branch corresponds to the large tumour state; the blue branch corresponds to the small tumour state; the magenta branch corresponds to the fully immune-resistant tumour state and the black branch corresponds to the tumour-free state. The local stability of the steady states is distinguished by linestyle: solid and dashed curves correspond to stable and unstable solutions respectively. Parameter values: except for σ all parameters are fixed at their default values.

The general features that emerge as σ decreases may be summarised as follows:

- $\sigma > \sigma^{\mathrm{T}}$: bistability between the tumour-free state and tumour escape. The immune-resistant tumour state and a tumour equilibrium state exist but are

both unstable.

- $\sigma = \sigma^{\mathrm{T}}$: the tumour-free state exchanges stability with the equilibrium tumour steady state.
- $\sigma^{\mathrm{F}} < \sigma < \sigma^{\mathrm{T}}$: bistability between tumour equilibrium and escape; the large tumour, tumour-free and immune-resistant tumour states exist but are all unstable.
- $\sigma = \sigma^{\mathrm{F}}$: the stable and unstable tumour equilibria coalesce.
- $\sigma^{\mathrm{E}} < \sigma < \sigma^{\mathrm{F}}$: tumour escape is the only outcome; the tumour-free and immune-resistant tumour states exist but are unstable.
- $\sigma = \sigma^{\mathrm{E}}$: the immune-resistant tumour state coalesces with the tumour-free state.
- $0 < \sigma < \sigma^{\mathrm{E}}$: tumour escape is the only outcome; the tumour-free state exists but is unstable.

In summary, in this section we have illustrated how the qualitative behaviour of the model changes with variations in the infiltration rate of the cytotoxic T cells, a trait recognised as being correlated with long term patient outcomes and treatment prognosis [68, 66, 74]. Due to the difficulty in estimating model parameters from clinical data, we have focused on the qualitative changes in model behaviour as the parameters k_E, ν, γ and θ vary. We find that for decreasing k_E and increasing ν, the region of tumour escape expands and occupies a progressively greater part of the tumour equilibrium region. This result makes sense since small k_E means that the T cells are not effective at killing tumour cells and large ν means that the functioning T cells are being rapidly converted into exhausted ones. We also find, as expected, that the more aggressive the tumour is (the higher the growth rate γ), the greater the rate of T cell infiltration required to prevent tumour escape.

4.5.1 Emergence of a tumour equilibrium at the transcritical bifurcation

As seen in Figure 4.6 a tumour equilibrium state emerges from the tumour-free branch at a critical $\sigma = \sigma^{\mathrm{T}}$. In this section we determine this point of emergence.

As the tumour equilibrium branch emerges from $N^* = 0$, we take N^* to be infinitesimally small in equations (4.19)–(4.22). We cannot simply put $N^* = 0$ in the

equations since then equation (4.19) is satisfied trivially. Instead from this equation we set the tumour growth rate, the term in brackets, to zero. In the remaining equations (4.20)–(4.22) we may put $N^* = 0$. The resulting equations are

$$\gamma(1-\theta) = T_C^* + k_E T_E^* \,, \tag{4.35}$$

$$0 = (T_C^* - \gamma_R) N_R^* \,, \tag{4.36}$$

$$\sigma = (\nu N_R^* + 1) T_C^* \,, \tag{4.37}$$

$$\nu T_C^* N_R^* = (r N_R^* + \delta_E) T_E^* \,. \tag{4.38}$$

Equations (4.35)–(4.37) are easily solved for the remaining populations:

$$T_C^* = \gamma_R, \quad N_R^* = \frac{\sigma - \gamma_R}{\nu \gamma_R} \quad \text{and} \quad T_E^* = \frac{\gamma(1-\theta) - \gamma_R}{k_E} \,. \tag{4.39}$$

Note for non-negative steady state populations both $\sigma \geq \gamma_R$ and $\gamma(1-\theta) \geq \gamma_R$ are required. (It is not consistent to take $N_R^* = 0$ in equation (4.36) since this leads to $T_E^* = 0$ and $T_C^* = \gamma(1-\theta)$ and $T_C^* = \sigma$, which can only be satisfied for a special choice of σ.) Inserting T_C^*, N_R^* and T_E^* from equation (4.39) into equation (4.38) provides the following expression for σ at the transcritical bifurcation

$$\sigma = \sigma^{\mathrm{T}} = \gamma_R \left(1 + \frac{\delta_E \nu (\gamma(1-\theta) - \gamma_R)}{\gamma_R (\nu k_E + r) - r\gamma(1-\theta)} \right) \,. \tag{4.40}$$

This solution branch only emerges over a restricted region of parameter space with γ_R lying in the range

$$\gamma_{R,\min} = \frac{r\gamma(1-\theta)}{\nu k_E + r} < \gamma_R \leq \gamma(1-\theta) = \gamma_{R,\max} \,. \tag{4.41}$$

For $\gamma_R < \gamma_{R,\min}$, $\sigma^{\mathrm{T}} < 0$ and thus a transcritical bifurcation does not occur. While for $\gamma_R > \gamma_{R,\max}$, $T_E^* < 0$, and here again a transcritical bifurcation does not occur. Note that $\sigma^{\mathrm{T}} > 0$ over the range given in equation (4.41), but $\sigma^{\mathrm{T}} \to \infty$ as γ_R approaches $\gamma_{R,\min}$ from above. The dependence of σ^{T} on γ_R is illustrated in Figure 4.7.

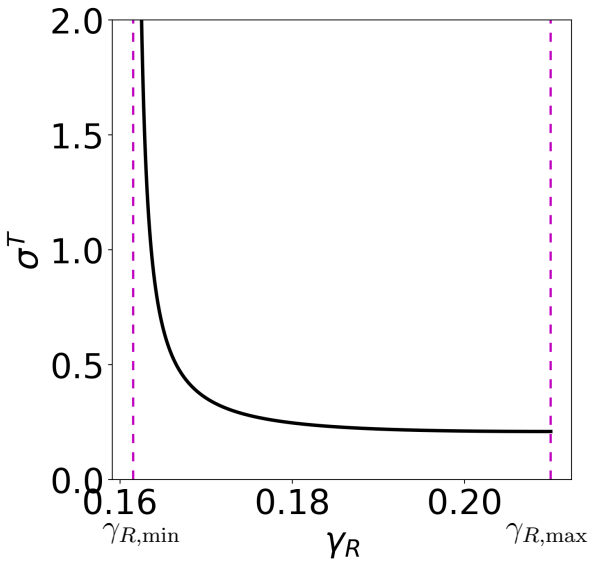

Figure 4.7: Dependence of the transcritical bifurcation σ^{T} on the immune-resistant tumour growth rate γ_R from equation (4.40), with all remaining parameters fixed at their default values. The vertical asymptotes (magenta, dashed) correspond to $\gamma_R = \gamma_{R,\min}$ and $\gamma_R = \gamma_{R,\max}$ in equation (4.41).

4.6 Parameter deduction based on model behaviour

One of the problems faced by mathematicians is inferring model parameters from available experimental data [116]. Experimental and clinical measurements rarely translate to specific model parameters. This motivates an approach whereby quantitative predications from the theoretical model are compared with experimental and clinical data to deduce model parameters. The interest in this approach is in part due to our industrial collaboration with Hoffman-La Roche. Here we propose a novel way of inferring two patient specific parameters based on quantitative predictions for the fractions of the immune-resistant tumour population to the total tumour population, and the exhausted T cells to the total T cell population at steady state. From a tumour equilibrium state determined in this way, we solve the fully nonlinear equations starting in the neighbourhood of this equilibrium to examine its long term outcome.

We next define the steady state population fractions as

$$f_N = \frac{N_R^*}{N^* + N_R^*} \quad \text{and} \quad f_T = \frac{T_E^*}{T_C^* + T_E^*} \quad \text{where} \quad 0 \leq f_N, f_T \leq 1\,, \tag{4.42}$$

and seek to characterise how variations in these population fractions affect whether the model evolves to a state of tumour elimination, equilibrium and escape. This approach provides an alternative view of parameter space. These fractions could be

used as a potential new biomarker to distinguish different classes of patients and consequently may allow appropriate treatment to be determined. A precedent for this approach is the recent clinical study by Schreiner *et al.* (2016) [171]. The goal of their study was to assess how the functional state of the T cells influences the efficacy of a TCB antibody. They found that patients with high densities of highly exhausted T cells did not appear to respond to treatment with a TCB antibody, even when it was combined with a PD-1 checkpoint blockade. By contrast, for patients with lower levels of highly exhausted T cells the therapy seemed to restore some of the functions of the T cells. This study motivates the need to understand what impact the ratio of exhausted to cytotoxic T cells has on response outcomes.

Prescribing the population fractions in equation (4.42) gives us the freedom to determine two of the model parameters. The two parameters chosen are σ and γ, since these control the T cell infiltration rate and the growth rate of the tumour which are arguably patient specific. In Section 4.4 we found that tumour equilibria were found by determining the roots of a sixth order polynomial and therefore we are constrained to numerical methods. This method reframes the steady states in order to gain an understanding of how the relative fraction of the different T cell populations and tumour populations relate to the parameters σ and γ explicitly. Inserting $N_R^* = f_N N^*/(1-f_N)$ and $T_E^* = f_T T_C^*/(1-f_T)$ into equations (4.19)–(4.22) we find

$$\begin{aligned} N^* &= \frac{\beta}{\phi}, \qquad & N_R^* &= \frac{\delta_E f_T}{\nu(1-f_T) - r f_T}, \\ T_C^* &= \gamma_R + \frac{\gamma\theta(1-f_N)}{f_N}, \qquad & T_E^* &= \frac{f_T}{1-f_T}\left(\gamma_R + \frac{\gamma\theta(1-f_N)}{f_N}\right), \end{aligned} \tag{4.43}$$

$$\gamma = \frac{\gamma_R f_N \kappa}{(1-\theta)f_N - \theta\kappa(1-f_N)}, \quad \sigma = T_C^*\left(1 + \frac{\beta\left(\nu f_N \beta^2 + (\nu f_N - \alpha(1-f_N))\phi^2\right)}{\phi\left(\beta^2+\phi^2\right)(1-f_N)}\right), \tag{4.44}$$

where

$$\kappa = 1 + \frac{k_E f_T}{1-f_T}, \quad \phi = \frac{f_N(\nu(1-f_T) - r f_T)}{(1-f_N)(1-f_T)} \quad \text{and} \quad \beta = \frac{\delta_E f_T}{1-f_T}. \tag{4.45}$$

Note that the tumour-free state corresponds to $f_T = 0$. In this case $\beta = 0$ and therefore $N^* = 0$ and $T_C^* = \sigma$ from equation (4.44). Likewise $T_E^* = f_T T_C^*/(1-f_T) = 0$. These are tumour-free steady state populations (see equation (4.23)).

4.6.1 Tumour elimination, equilibrium and escape

In the following we fix all parameters at their default values, apart from σ and γ which are defined in terms of the fractions f_N and f_T via equation (4.44). To predict the conditions necessary for tumour elimination, equilibrium and escape, we scan over these fractions. Permissible solutions with non-negative populations and parameters do not generally exist for all f_N and f_T. This is illustrated by the grey region in Figure 4.8. The upper limit of the grey region in Figure 4.8 corresponds to $f_T = \nu/(r+\nu)$ since any larger value would make $\phi < 0$ in equation (4.45) and therefore give negative tumour populations. (In fact $N^*, N_R^* \to \infty$ as $f_T \to \nu/(r+\nu)$ because $\phi \to 0$, and moreover $\sigma \to \infty$.) The limit on the left edge of the grey region in Figure 4.8 occurs where $\gamma \to \infty$ (where $T_C^*, T_E^* \to \infty$ as well), which according to equations (4.44) and (4.45) occurs when

$$\frac{(1-\theta)f_N}{1-f_N} = \frac{\theta(1-f_T+k_E f_T)}{1-f_T}\,. \tag{4.46}$$

(This equation can be directly solved to give f_N as a function of f_T or vice versa.) Where solutions exist, we determine their linear stability in order to predict whether tumour escape might be possible from a tumour equilibrium state.

Figure 4.8 illustrates how the tumour equilibria $(N^*, N_R^*, T_C^*, T_E^*)$ change as we vary the fractions f_N and f_T, while in Figure 4.9 we plot σ and γ as functions of f_N and f_T. The bold black curve shows the margin of stability for the tumour-free state for the parameters σ and γ given in equation (4.44). The bold red curve corresponds to the margin of stability of the tumour equilibrium state with instability found above this curve. It is important to note that for every tumour equilibrium state shown in these figures there is a distinct tumour-free state with the same values of σ and γ (see black curve in Figure 4.10). The tumour-free state is unstable below the bold black curve. Hence if the tumour equilibrium state is unstable, it cannot be attracted to the tumour-free state. It might appear that the only other possibility is tumour escape but in fact there may exist another tumour equilibrium state for the same parameters σ and γ which is stable. This is seen by overlaying the contour lines for σ (blue curves) and γ (red curves) over the (f_N, f_T) parameter space as illustrated in Figure 4.11. Here following a contour line for γ and another for σ the two curves cross twice representing two points in (f_N, f_T) space with the same values of σ and γ. This is illustrated by the black dots in Figure 4.11. This identifies the two equilibria to the right of the fold point, $\sigma = \sigma^{\mathrm{F}}$ in Figure 4.6, with one point lying below the bold red curve in the stable region, and other lying above it in the unstable region.

Figure 4.8(a)–(d) illustrates the size of the steady state populations N^*, N_R^* ,T_C^* and T_E^* as a function of f_N and f_T. The immune-sensitive tumour population generally increases with f_T but decreases with f_N, whereas the immune-resistant tumour population is purely dependent on f_T (see equation (4.43)). The cytotoxic T cell population mainly varies with f_N, increasing as f_N decreases. The exhausted T cell population generally increases with f_T but also with decreasing f_N. In general the largest populations are found in the upper left hand corner and the smallest populations are found in the lower right hand corner.

Note that the increase in N_R^* with f_T is expected since when f_T is large the T cells are dominantly in an exhausted state. This allows the immune-resistant tumour population to flourish as the immune-resistant tumour population is killed only by the cytotoxic T cells (see equation (4.8)). The tumour population $N^* = (1 - f_N)N_R^*/f_N$, and so is necessarily largest for small f_N. Note when $f_N < 0.5$, $N^* > N_R^*$. The T cell population T_C^* depends primarily on f_N, increasing as f_N decreases. This can be seen by returning to equations (4.7) and (4.9) for N and T_C. T_C kills off tumour cells which reduces the tumour population but the T cells also proliferate at a rate which depends in a biphasic way on the number of tumour cells. Finally, the exhausted T cell population T_E^* also depends primarily on f_N but shows a stronger dependence on f_T. This stronger dependence comes from the fact that $T_E^*/T_C^* = f_T/(1 - f_T)$, which increases with f_T as observed.

For clarity, a cross section at $f_T = 0.5$ is shown in Figure 4.10 for both N^* and T_C^*. The red curves in each panel correspond to the equilibrium populations plotted in Figure 4.8(a) and (c). In panel (b) for T_C^*, the black curve shows the tumour-free state while the magenta curve shows the non-trivial fully immune-resistant tumour state (for the parameters σ and γ determined by equation (4.44)). The tumour equilibria are unstable over a range of f_N extending from approximately 0.4 to 0.75 consistent with the region of instability below the bold red curve in Figure 4.8. The tumour-free state is unstable except for $f_N > 0.9$, again consistent with Figure 4.8. The non-trivial fully immune-resistant tumour state is always unstable (magenta curve).

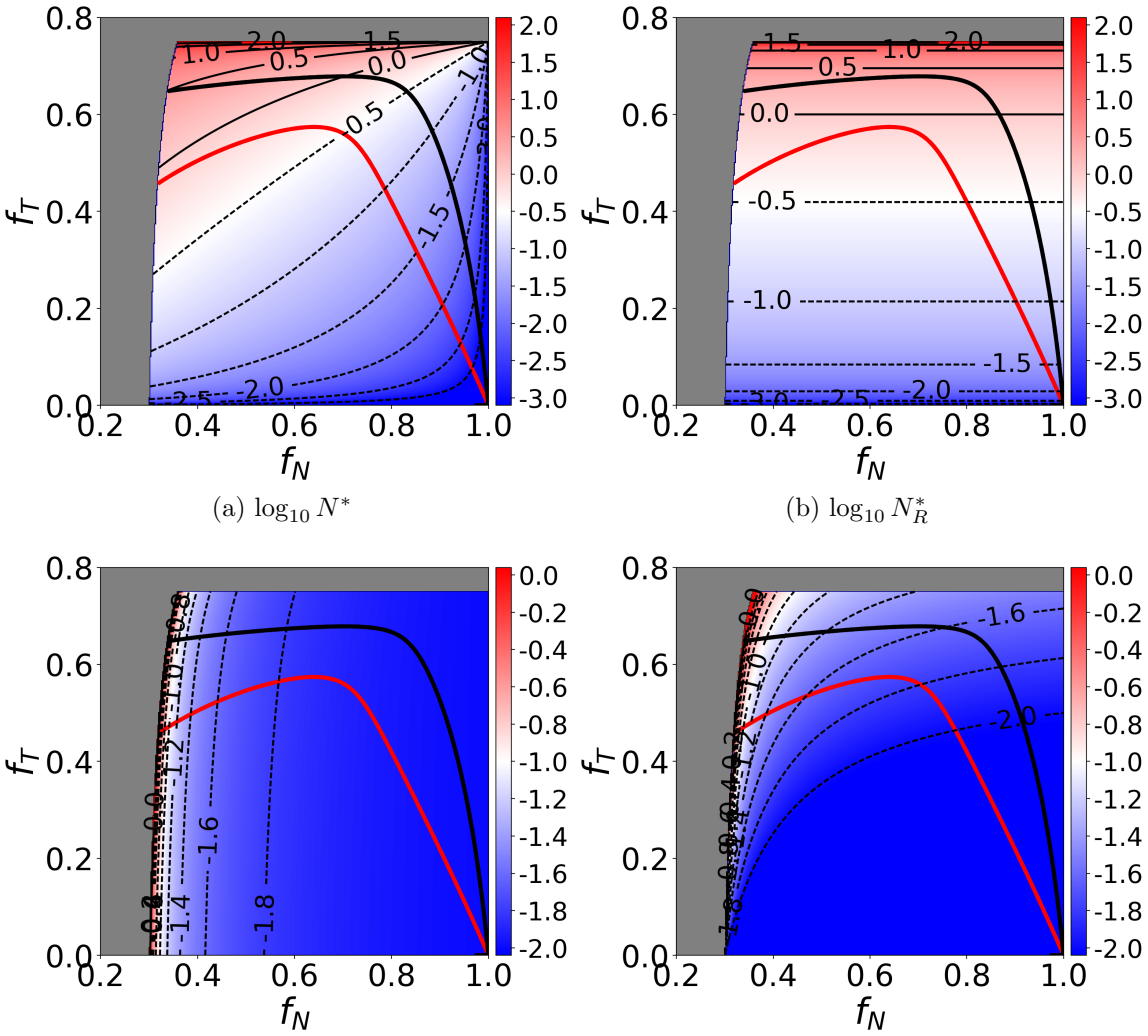

(a) $\log_{10} N^*$

(b) $\log_{10} N_R^*$

(c) $\log_{10} T_C^*$

(d) $\log_{10} T_E^*$

Figure 4.8: Equilibrium populations for the (a) immune-sensitive tumour cells N^*, (b) immune-resistant tumour cells N_R^*, (c) cytotoxic T cells T_C^*, and (d) exhausted T cells T_E^*, as a function of the total fraction of T cells f_T and tumour cells f_N (see equation (4.43)). Population sizes ($\log_{10}$ scaled) are indicated by contour lines with dashed lines corresponding to negative $\log_{10}$ values and solid lines corresponding to positive $\log_{10}$ values. Key: the bold red line represents the margin of stability of the tumour equilibrium state, with instability above this line; the bold black line represents the margin of stability of the tumour-free state, with instability below this line. Colour: low values indicated by blue and high values indicated by red. The grey region indicates where no tumour equilibrium solutions are possible. Parameter values: except for γ and σ all remaining parameters are fixed at their default values.

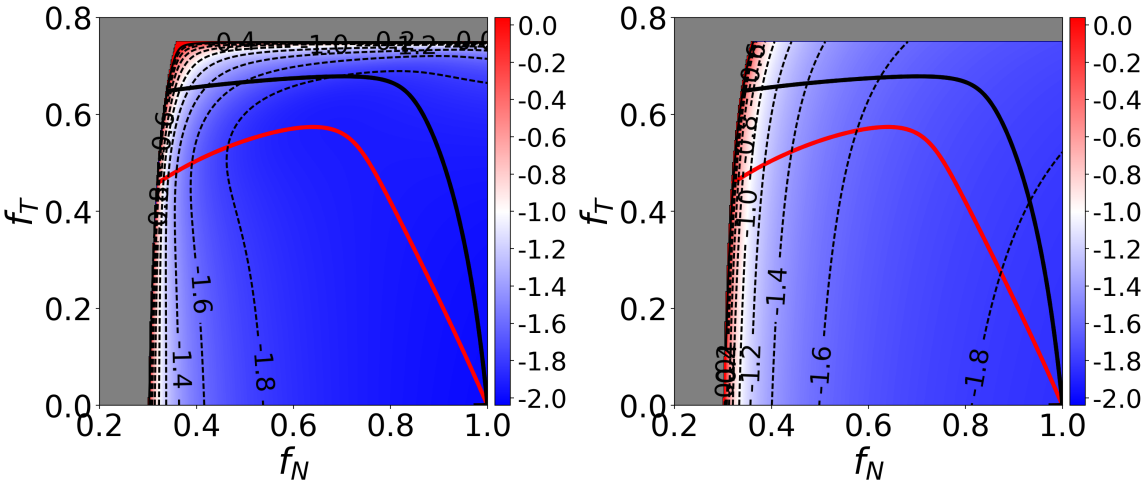

(a) $\log_{10}\sigma$ (b) $\log_{10}\gamma$

Figure 4.9: Parameters (a) σ and (b) γ as a function of f_N and f_T, as given by equation (4.44). Parameter values for γ and σ ($\log_{10}$ scaled) are indicated by contour lines. Key: as in Figure 4.8. Parameter values: except for γ and σ all remaining parameters are fixed at their default values.

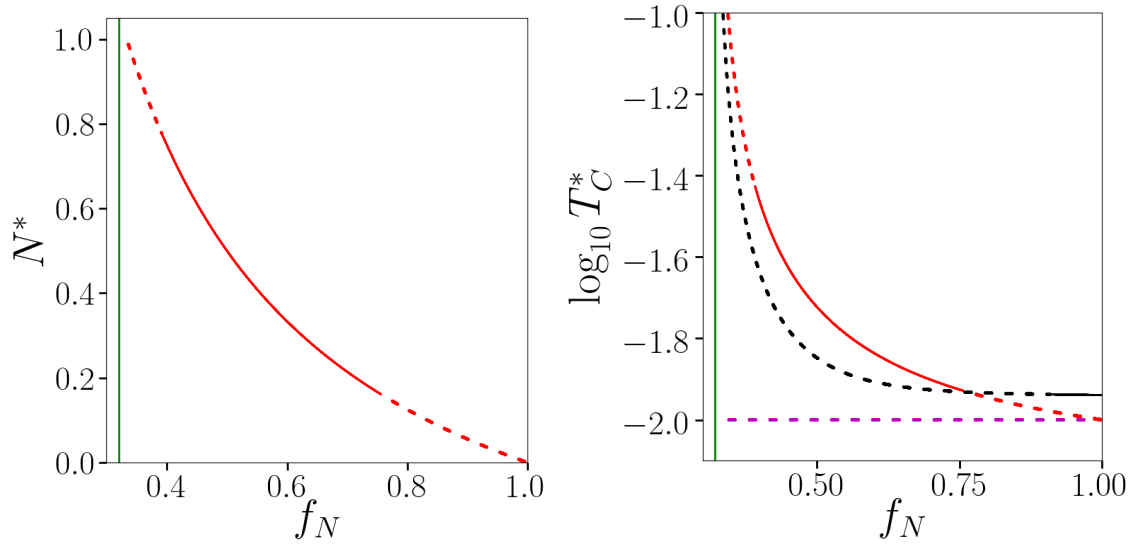

(a) N^* (b) $\log_{10} T_C^*$

Figure 4.10: Variation of (a) N^* and (b) $\log_{10} T_C^*$ with f_N for $f_T = 0.5$, as given by equation (4.43) together with the tumour-free state (black) and tumour-resistant state (magenta) determined from equations (4.23) and (4.24) for the same parameters σ and γ. The green vertical line indicates the minimum value of f_N at the left hand edge of the parameter space, determined from equation (4.46). Note that σ and γ vary with f_N in these figures. Parameter values: all other parameters are fixed at their default values.

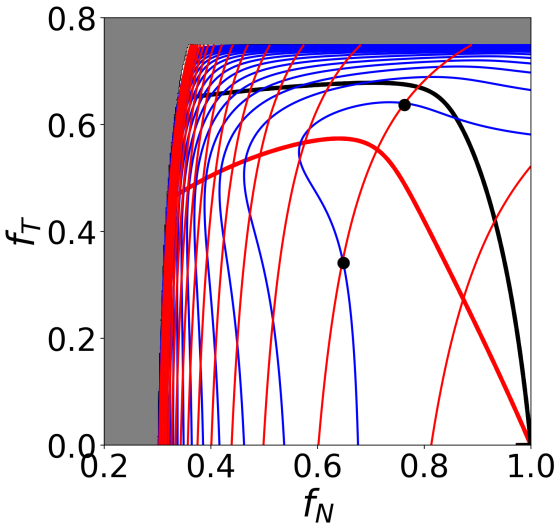

(a) Contour lines for $\log_{10}\sigma$ and $\log_{10}\gamma$

Figure 4.11: Crossings of contours for σ (blue curves) and γ (red curves) over the (f_N, f_T) parameter space to illustrate the double crossing of the same value of σ and γ, demonstrating the existence of two tumour equilibria one which is linearly stable and the other linearly unstable. Parameter values: apart from σ and γ which vary with f_N and f_T, all other parameters are fixed at their default values.

The dependence of σ and γ on f_N and f_T is illustrated in Figure 4.9. When the tumour population is predominantly composed of an immune-resistant tumour population ($f_N \to 1$) and/or the T cell population is predominantly composed of cytotoxic T cells ($f_T \to 0$), the rate of infiltration of the T cells is small. For small f_T, specifically when we are below the bold red curve, this state of equilibrium is stable. This implies that the infiltration of cytotoxic T cells is adequate to control the tumour in this state. However when f_N is nearly 1 (corresponding to a tumour population dominated by immune-resistant tumour cells) this state of equilibrium is unstable. The tumour growth rate is large when the tumour population is dominated by immune-sensitive tumour cells and depends only weakly on f_T. Here there is a balance between production of tumour cells and infiltration of cytotoxic T cells preserving the state of equilibrium. (Note the close correspondence between Figure 4.8(c) and Figure 4.9(b).)

4.6.2 Nonlinear stability

We turn next to the prognosis of a given patient defined by their fractions of T cells and tumour cells at steady state (f_N, f_T). To this end, in Figure 4.12 we show what happens to a perturbed equilibrium state in equations (4.7)–(4.10) over the

(f_N, f_T) parameter space. The model is initialised close to the tumour equilibrium corresponding to a specific f_N and f_T. Specifically, we increase the immune-sensitive tumour population by 10% and integrate the model equations for 20000 units of time. If at the end of the simulation, $N < N^*/10$, $N_R < N_R^*/10$, $T_E < T_E^*/10$ and $T_C - \sigma < \sigma/10$, we say the tumour is destined for elimination (note the tumour-free state has $N^* = N_R^* = T_E^* = 0$ and $T_C^* = \sigma$). On the other hand, if at the end of the simulation $N > 10N^*$ and $N_R > 10N_R^*$, we say that the tumour is destined for escape. There are two other possibilities. The first is that the tumour stays near its initial equilibrium. We say this occurs if at the end of the simulation $|N - N^*| < N^*/10$, $|N_R - N_R^*| < N_R^*/10$, $|T_C - T_C^*| < T_C^*/10$ and $|T_E - T_E^*| < T_E^*/10$. Otherwise, we say the tumour is approaching a *different* equilibrium, which is necessarily stable. Note the results shown in Figure 4.12, generated for approximately 16000 (f_N, f_T) points, took approximately one week of computer time on an Intel i7$-$3930k single processor.

Starting from a tumour equilibrium below the bold red curve in Figure 4.12 (light blue region) we remain in this state of equilibrium. In this region the T cell population is dominated by cytotoxic T cells ($f_T < 0.5$). As $f_N \to 1$ and the tumour population becomes dominated by immune-resistant tumour cells, the T cell population consists primarily of cytotoxic T cells ($f_T \to 0$) to remain in equilibrium. The small discrepancies between the stability boundary and the different shaded regions in Figure 4.12 are caused by the finite integration time taken and the exceedingly weak growth rates at small f_T and large f_N. In these cases the growth is too weak to lead to sufficient growth over the integration time. If integrations could be performed indefinitely the lower right red region is expected to dip down and occupy the region to the right of the bold red curve for $f_T < 0.5$ approximately. Similarly, the small blue region near the top of the bold red curve is due to the weak growth rates near the margin of stability. Above the bold red curve, where the tumour equilibrium is unstable, in most cases the tumour escapes (red regions). There is however, a wedge of stability encompassing the light red and blue regions, where the tumour either settles to another stable equilibrium or is eliminated altogether. Elimination can only occur when the tumour-free state itself is linearly stable and this only occurs in the region above and to the right of the bold black curve. In the region of elimination the tumour population is initially dominated by immune-resistant cells and the T cell population is initially dominated by exhausted cells. The rate of T cell infiltration however, is relatively large and the tumour growth rate relatively small in this region (see Figure 4.9), explaining why the dynamics leads to tumour elimination. Notably

starting from the upper part of the light blue equilibrium region and moving diagonally upwards towards the upper right corner of Figure 4.12, according to Figure 4.9 the T cell infiltration rate increases strongly beyond the upper black curve while the tumour growth rate remains approximately constant or decreases. In conclusion the increased rate of T cell infiltration favours tumour elimination, as expected.

In summary, we find that to remain in a dormant tumour equilibrium state, the T cell population must be dominated by cytotoxic T cells. This behaviour arises irrespective of the composition of the tumour population. On the other hand, when the T cell population is initially dominated by exhausted T cells or the tumour population is initially dominated by immune-resistant tumour cells, the tumour generally escapes. The exception is when both the exhausted T cell population and immune-resistant tumour population are initially relatively large. In this case the growth rate of the tumour is sufficiently small and the infiltration rate of cytotoxic T cells is sufficiently large to eliminate the tumour.

The results presented here provide a unique way of looking at the long time model behaviour as a function of the compositions of the tumour populations and the cytotoxic T cell populations to explain escape from a tumour equilibrium state. These results may be used as a guide to stratify patients according to the relative level of exhausted to cytotoxic T cell populations and immune-resistant to immune-sensitive tumour populations. Moreover, this approach enables one to determine patient specific parameters given experimental data on the steady state compositions of tumour and T cell populations.

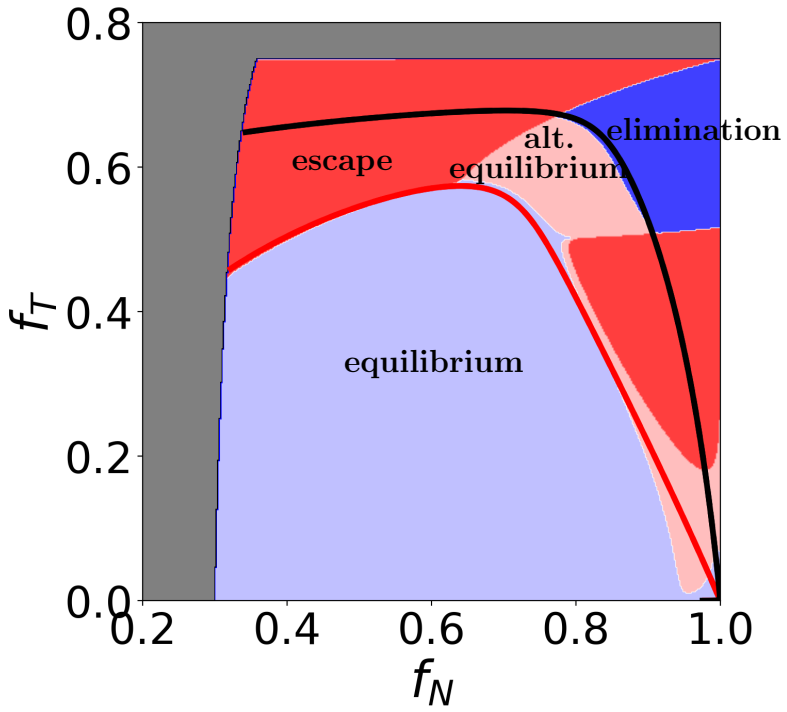

Figure 4.12: Long term outcome of the evolution from a perturbed tumour equilibrium state for given parameters f_N and f_T. The equilibrium is perturbed by increasing the steady state tumour population by 10%, leaving all other populations unchanged. Key: red region: the tumour escapes; blue region: the tumour is eliminated; light red region: the tumour settles to another tumour equilibrium; light blue region: the tumour stays in its original equilibrium state.

4.7 Immunotherapy

The analysis in Section 4.6 indicates that there are favourable regions of parameter space that can lead to elimination and that these regions depend on the relative proportion of the cytotoxic T populations and tumour populations as well as the parameters controlling the rate of T cell infiltration and tumour growth. Although several immunotherapies have shown promising results the responses are not uniform. In light of this there is a need to identify appropriate biomarkers to stratify patients according to their clinical response. As discussed in Section 4.1, a number of authors argue that a patient's 'immune contexture' in the tumour microenvironment could be used to predict a patient's response to treatment [195].

In this study we investigate how the initial ratios of exhausted to cytotoxic T cells and immune-resistant to immune-sensitive tumour cells affects a patient's response to treatment. We focus on an IL-2 therapy [105] and a TCB antibody [171, 16]. These

immunotherapies have shown recent success in pre-clinical studies especially when used in combination [88].

IL-2, a cytokine produced by activated helper T cells, modulates the immune response by expanding populations of innate and adaptive immune cells. Due to its potential to elicit an effective anti-tumour immune response by boosting the number of effector T cells available to target the infected cells, high-dose IL-2 (aldesleukin) therapy has been approved for treating renal cell carcinoma and malignant melanoma, showing long-term tumour-free survival for some patients [62, 104, 164]. However due to its dual role, promoting the differentiation and consequent expansion of the regulatory T cell population [127] and increasing the Fas/Fas-L induced death of the effector T cells, therapeutic outcomes are not consistently favourable [164]. Furthermore, standard delivery of this therapy often causes immune-adverse affects (e.g. cardiovascular, neurological and gastrointestinal problems) [164]. In a recent pre-clinical study [105], an IL-2 variant was designed to preferentially expand effector T cells over regulatory T cells and extend their half-life so that therapy need not be continuously injected to maintain a certain level of the drug in the blood serum.

More recently immunotherapy, a T Cell Bispecific (TCB) antibody has been designed to promote binding of T cells and tumour cells resulting in potent killing of the tumour cells by the T cells and in polyclonal activation of the T cells. A TCB antibody consists of two arms; one arm targets the non-specific part of the TCR, specifically the CD3ϵ chain (one of the four chains that make up the CD3 protein cluster found on the TCR) and the other arm targets a specific tumour antigen. In patients with healthy (i.e. non-exhausted T cells) such treatment enhances T cell activation, cytokine production and tumour cell killing [171, 16].

In this section we aim to identify the treatment (TCB antibody, IL-2 therapy, or both) that drives a patient destined for tumour escape to elimination (if possible). We assume that a TCB antibody acts by expanding the number of T cells infiltrating the tumour and enhancing the killing capacity of the exhausted T cells. We mimic these effects by amplifying the rates of T cell infiltration, σ, and tumour cell killing by the exhausted T cells, k_E. Similarly, we assume that IL-2 therapy increases the number of cytotoxic T cells, and we model this by increasing the proliferation rate of the cytotoxic T cells, α.

4.7.1 Model formulation

We propose a highly simplified model of drug treatment where the drug is added at an early time and decays before being re-introduced into the system (periodically

delivered). This is motivated by experimental observations from a pre-clinical study of the effects of a CEA-TCB antibody where the antibody concentration was measured over time [16]. Bacac *et al.* (2016) [16] (their supplementary Figure 2) show that the antibody concentration first rapidly decays then subsequently slowly decays back to small levels. To mimic this evolution, we propose the following model

$$k_E(t) = k_{E0} + \Delta k_E A(t)\,, \tag{4.47a}$$

$$\sigma(t) = \sigma_0 + \Delta\sigma A(t)\,, \tag{4.47b}$$

$$\alpha(t) = \alpha_0 + \Delta\alpha A(t)\,. \tag{4.47c}$$

where k_{E0}, α_0 and σ_0 are the rates in the absence of treatment, and the increments Δk_E, $\Delta\sigma$ and $\Delta\alpha$ mimic the drug treatment. The amplification factor $A(t)$ is taken to be

$$A(t) = \sum_{j=0}^{n} f(t - t_{\text{init}} - jP)\,, \tag{4.48}$$

where

$$f(\tau) = \begin{cases} 0 & \text{if } \tau < 0 \\ Ce^{-\delta_a \tau}\left(1 - e^{-\tau/\varepsilon}\right) & \text{if } \tau \geq 0\,, \end{cases} \tag{4.49}$$

and

$$C = \frac{1}{c^{\delta_a \varepsilon}(1-c)} \quad \text{where} \quad c = \frac{\delta_a \varepsilon}{\delta_a \varepsilon + 1}\,. \tag{4.50}$$

Here P is the period, n is the integer (floor) value of $(t - t_{\text{init}})/P$, δ_a is the rapid decay rate of the antibody, ε is the short time associated with the injection of the antibody, and t_{init} is the time at which the drug is first administered. Note: $n < 0$ when $t < t_{\text{init}}$. The form of $A(t)$ is shown in Figure 4.13 for the parameters $t_{\text{init}} = 0$, $\epsilon = 0.01$, $\delta_a = 0.5$ and $P = 7$.

The parameters k_{E0} and α_0 are taken to be their default values in the absence of treatment, i.e. $k_{E0} = 0.1$ and $\alpha_0 = 1$. The parameter σ_0 is taken to be the value corresponding to the equilibrium for a specific f_N and f_T value (see equation (4.44)). The changes Δk_E, $\Delta\sigma$ and $\Delta\alpha$ are taken proportional to k_{E0}, α_0 and σ_0, for simplicity.

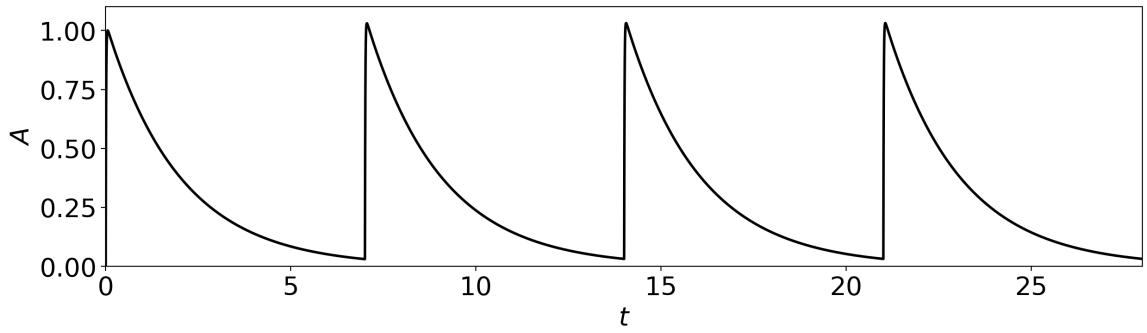

Figure 4.13: The scaled concentration of the antibody given in equation (4.49) introduced periodically to the system, following the observations and predictions made in [16], supplementary Figure 2.

4.7.2 Results

Here we consider the combined effects of a TCB antibody (through variations in k_E and σ) and high dose IL-2 therapy (through variations in α) for a patient destined for tumour escape or living with a dormant tumour (see Figure 4.12 in Section 4.6.2). We explore the response to treatment as a function of (a) the period of re-administration and (b) the fractions of tumour cells and cytotoxic T cells, f_N and f_T respectively.

Figure 4.14 examines the effect of the period over which the drug is administered. When the drug is repeatedly administered over short periods (black curve), the tumour is eliminated. Considering a period twice as long, repeated administration of the drug still manages to eliminate the tumour (grey curve). However for a longer period (light grey curve), the tumour escapes despite an early reduction in its size. Here we consider treatment after one unit of time $t_{\text{init}} = 1$. We find that the longer the time between initial detection and initial dosage, the higher the frequency of dosages are necessary to prevent tumour escape (not shown). In practice, the period of administration will likely depend also on the decay rate of the drug, δ_a. Therefore a careful examination of all of these factors is necessary to determine the appropriate period over which the drug should be re-administered.

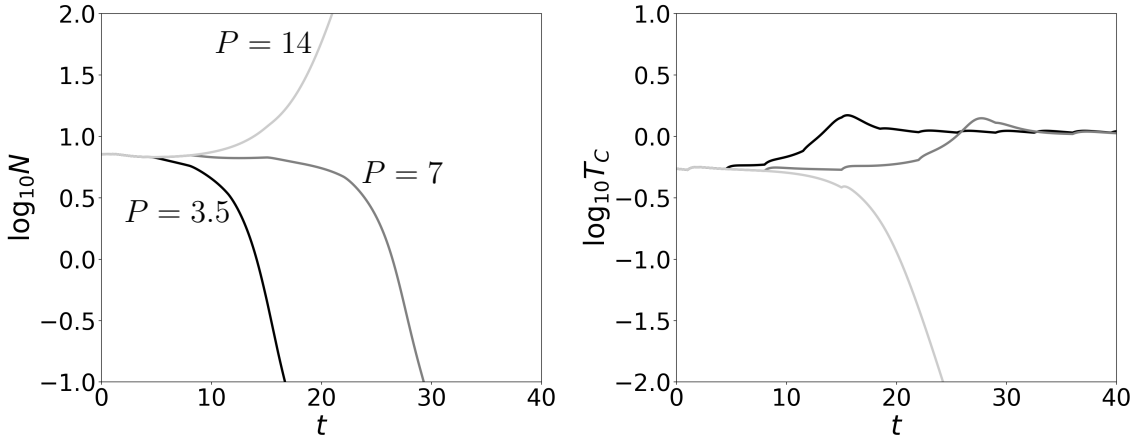

Figure 4.14: Evolution of the (a) tumour population $N(t)$ and (b) the cytotoxic T cell population $T_C(t)$ obtained by solving equations (4.7)–(4.10) with parameters k_E, σ and α evolving according to equation (4.47) for three different periods $P = 14$ (light grey), $P = 7$ (grey) and $P = 3.5$ (black). Here $t_{\text{init}} = 1$, $\delta_a = 0.5$, $\varepsilon = 0.01$, $k_{E0} = 0.1$, $\sigma_0 = 1.0$, $\alpha_0 = 1.0$, $\Delta k_E = 0.1 k_{E0}$, $\Delta\sigma = 0.1\sigma_0$, $\Delta\alpha = 0.1\alpha_0$. All remaining parameters are fixed to their default values. The system is initialised by increasing the N population by 10% relative to the tumour equilibrium state for $f_N = 0.35$ and $f_N = 0.7$.

Next we fix the period and explore the therapeutic outcomes of an IL-2 therapy and a TCB antibody, for three pairs of fractions f_N and f_T. In each case we present results for periodic variations of the parameters (see equation (4.47)) as well as the effect of maintaining the time average of each parameter. The latter situation mimics a scenario in which the drug increases the parameter to some value and keeps it fixed for $t > t_{\text{init}}$. As it is unclear how the drug directly affects the model parameters, it is important to consider contrasting scenarios.

In Figure 4.15 we summarise the combined effects of a TCB antibody and IL-2 therapy for patients characterised according to their fractions of tumour cells and T cells, f_N and f_T. For patients destined for tumour escape without treatment, we find that escape is only avoided if the drug is administered periodically at a sufficient frequency, which depends on the time after the initial tumour detection and treatment delivery. Notably if either therapy is administered alone tumour escape is unavoidable (results not shown). Hence the combined therapy appears to be necessary, echoing the findings of Kirschner and Panetta [102]. On the other hand, if the tumour is in a dormant tumour equilibrium state (black and light grey curves), repeated administration of the drug at this dosage is unable to perturb the system sufficiently to eliminate the tumour and instead the tumour remains close to its dormant state.

We next consider the effect of dosage size on a dormant tumour state. We consider the same case $f_N = f_T = 0.5$ considered in Figure 4.15 (black curve). In Figure 4.15 we chose a dosage to increase k_E, σ and α by 10% which was seen to have no appreciable effect on the dormant tumour equilibrium state. We next consider dosages of 20%, 100% and 500% and present the results in Figure 4.16. The smallest dosage leads to only a minor reduction in the tumour size over a long period of time (500 units of time). A more significant reduction is seen for a dosage which doubles the values of k_E, σ and α. At the highest dosage level the tumour has reduced to 1% of its original size after 150 units of time. These results show that the level of dosage has a direct impact on the reduction in size of dormant tumours.

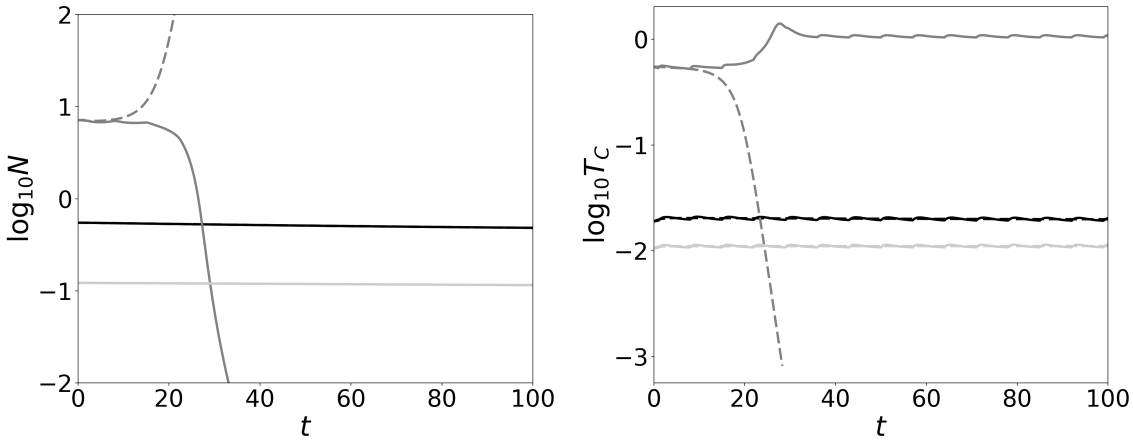

(a) tumour population $N(t)$

(b) cytotoxic T cell population $T_C(t)$

Figure 4.15: Evolution of the (a) tumour population $N(t)$ and (b) the cytotoxic T cell population $T_C(t)$ obtained by solving equations (4.7)–(4.10) with parameters k_E, σ and α evolving according to equation (4.47) for $(f_N, f_T) = (0.5, 0.5)$ (black curve), $(f_N, f_T) = (0.35, 0.7)$ (grey curve) and $(f_N, f_T) = (0.9, 0.6)$ (light grey curve). Continuous lines correspond to periodic administration of the drug while the dashed lines correspond to using the time average values of k_E, σ and α. Here $t_{\text{init}} = 1$, $\delta_a = 0.5$, $P = 7$, $\varepsilon = 0.01$, $k_{E0} = 0.1$, $\alpha_0 = 1$, and $\Delta k_E = 0.1k_{E0}$, $\Delta\sigma = 0.1\sigma_0$ and $\Delta\alpha = 0.1\alpha_0$ with σ_0 varying according to the pairs of fractions taken. Here all remaining parameters are fixed at their default values. The system is initialised by increasing the N population by 10% relative to the tumour equilibrium state for each (f_N, f_T) considered.

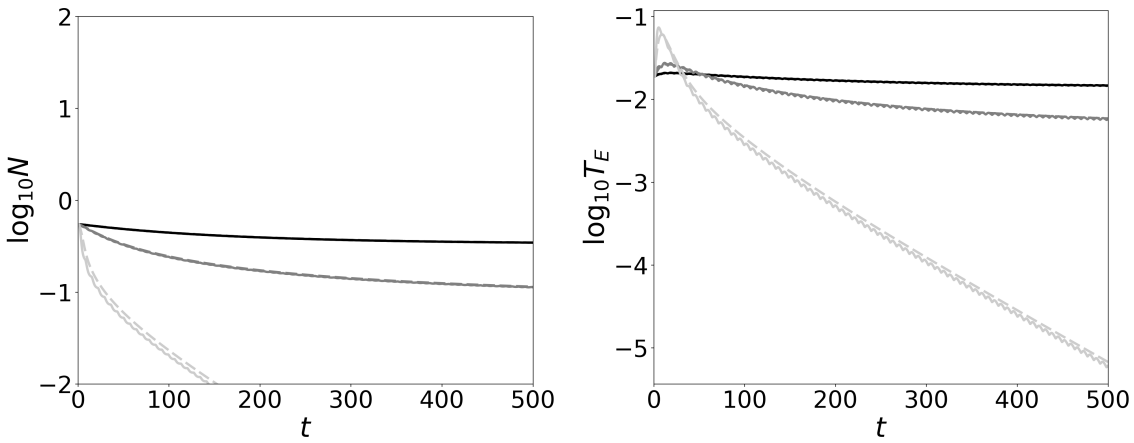

(a) tumour population $N(t)$ (b) exhausted T cell population $T_E(t)$

Figure 4.16: Evolution of the (a) tumour population $N(t)$ and (b) exhausted T cell population $T_E(t)$ obtained by solving equations (4.7)–(4.10) with parameters k_E, σ and α evolving according to equation (4.47) for $(f_N, f_T) = (0.5, 0.5)$ and for a variety of dosages which increase k_E, α and σ by 20% (black curve), 100% (grey curve), and 500% (light grey curve) respectively. All other parameters are the same as used in Figure 4.15.

In summary, combining IL-2 therapy and a TCB antibody can prevent escape provided the drug is delivered periodically. On the other hand, if either therapy is administered alone then tumour escape is inevitable. For tumours in a dormant equilibrium state, a sufficient shift in the parameters mimicking the drug is necessary to significantly reduce the size of the tumour.

4.8 Discussion

We have proposed a new mathematical model to examine the effects of T cell exhaustion on interactions between heterogeneous tumour cells and cytotoxic T cells. We have accounted for exhausted and cytotoxic T cells as well as immune-resistant and immune-sensitive tumour cells. The effects of T cell exhaustion have previously only been examined experimentally [171, 189]. To our knowledge, this is the first mathematical model designed to address how the composition of cytotoxic T cells and tumour cells dictates escape from a tumour equilibrium state. While idealised, our mathematical model provides more detailed information about the time evolution of the relevant cell populations than is currently available experimentally. We have used the model to reveal how the fractions of tumour cells and cytotoxic T cells can be used as a way of predicting response outcomes initialised about a dormant tumour

equilibrium. Based on these results, we used the model to explore two immunotherapies, a TCB antibody and IL-2 therapy, for different fractions of T cells and tumour cells.

From the simple design of the model, we have been able to comprehensively explore how the three Es of immunoediting arise as key model parameters vary. There have been numerous studies arguing that the infiltration of immune cells, specifically cytotoxic T cells, is associated with better outcomes [66]. We find that tumour elimination and equilibrium states exist independently, with a tumour equilibrium state arising for moderate rates of T cell infiltration and a tumour elimination state arising for high rates of T cell infiltration. Based on these findings we explored how variations in other model parameters affect the qualitative behaviour over changes in the infiltration rate of the cytotoxic T cells. We identified the tumour growth rate as an important parameter. Our results suggest that a fine balance must be achieved between the tumour and cytotoxic T cell populations in order to avoid tumour escape, as observed in aggressive, poorly immunogenic cancers such as pancreatic cancer [18]. This motivated an alternative approach examining tumour cell and T cell compositions (i.e. fractions) as a way of predicting tumour outcome.

Through this approach, we have been able to explicitly determine the regions where tumour elimination, equilibrium and escape may occur as a function of these population fractions. Moreover, this approach enables us to determine patient specific parameters, in particular the infiltration rate of the cytotoxic T cells and the growth rate of the tumour. Thus, while no classical biomarker exists, the present mathematical model may be regarded as such. Further model developments may provide greater confidence in our predications and may reveal new biomarkers. By examining the linear stability and nonlinear evolution of perturbed tumour equilibria, we have found that there are four possible outcomes. If the tumour equilibrium is linearly stable, it persists. When it is unstable and where the corresponding tumour-free state is also (linearly) unstable, either the tumour escapes or the system settles to another stable tumour equilibrium. When the tumour-free state is stable (this occurs only in the region where the tumour equilibrium is unstable), the tumour may either be eliminated or may escape. Elimination occurs when the initial population of T cells is dominated by exhausted T cells, and when the initial population of tumour cells is dominated by immune-resistant tumour cells. While this appears to be an unfavourable situation, the tumour equilibrium in this region is associated with both a small tumour growth rate and a relatively large T cell infiltration rate, evidently sufficient to lead to tumour elimination.

The final part of this chapter examines, in an idealised way, the effects of two immunotherapies: a T cell bispecific (TCB) antibody and IL-2 therapy. Our results suggest that for patients destined for tumour escape, repeated administration of combined TCB and IL-2 therapy is required for long-term progression-free survival. In fact, we find that the dosage frequency is dependent on the time between initial detection of the tumour and the first administration of therapy. For patients destined for tumour escape, both the frequency of dosage and the dosage size vary with the time lag between initial tumour detection and first administration, indicating that early diagnosis is beneficial. For patients having a dormant tumour the dosage size appears to bere important. A small to moderate dosage has no effect but a high dosage, equivalent to multiplying five times the various parameters enhancing T cell proliferation, infiltration and killing, leads to a substantial reduction in the tumour population.

A limitation of the model developed in this chapter is that it does not account for spatial distributions of cytotoxic and exhausted T cells in a tumour, as observed in a number of clinical studies [66, 71]. A natural extension of this model, therefore, would be to include spatial effects through chemotaxis and random motility. This would allow a study of how distributions of exhausted and cytotoxic T cells in the tumour mass affect model outcomes, and help elucidate the importance of these distributions on treatment. Another extension could be to combine aspects of the present model with those developed in Chapter 3, to explicitly account for the dynamical coupling between T cell functionality in tumour-immune dynamics.

Chapter 5

Conclusions

Tumours are by nature highly heterogeneous entities. They are composed of an array of different cell types such as fibroblasts, endothelial cells and immune cells. The malignant cancer cells form relationships with all of these various cell types in the tumour microenvironment, suppressing their normal function to allow for tumour growth. In this thesis we have considered different aspects of tumour and immune cell heterogeneity in the tumour micronevironment. Through a series of ordinary differential equation models we sought to examine how different aspects of heterogeneity in subpopulations of T cells, functional states of the cytotoxic T cells and subpopulations of tumour cells affect the ability of the immune system to cope in the presence of a tumour. Specifically we proposed three distinct ODE models to address the following three questions:

1. Given disagreement in the field about the importance of helper T cells in either facilitating or suppressing tumour growth, what is the relative effectiveness of cytotoxic versus helper T cells in controlling tumour growth?

2. How do the rates of exhaustion of individual T cell functions, specifically their killing, infiltration and proliferation rates, suppress or facilitate tumour escape?

3. Given that infiltrating T cell populations exist in various functional states, how do the ratios of exhausted to functional T cells and immune-resistant to non-resistant tumour cells affect tumour escape?

The manner in which these were addressed is discussed below after a general summary of the modelling approach adopted, and its potential for advancing cancer research.

Given the growing impact of cancer in today's society it is important to formulate predictive models that can provide insight into fundamental mechanisms and potential treatment [6]. Mathematical models have a distinct advantage over pre-clinical models

as they offer a comprehensive means to widely explore parameter space at low cost. Such models may not only be used as predictors but as potential biomarkers.

In a recent review article, Altrock *et al.* (2015) [6] have argued that while mathematical modelling of cancer is vital to efforts seeking to improve our understanding of this disease, due to a lack of high quality experimental data there remain problems fitting these models to available data. They suggest that a more integrated approach is needed first to acquire appropriate data and second to adjust the mathematical models to align with clinically observed behaviour. They attest that the mathematical models offer new, flexible, inexpensive tools to probe this disease in ways that were not previously possible. Such models may be used to help explain the variability exhibited by patients in their response to treatment, and in the longer term, save time and resources as well as improve the patient's quality of life through better targeting of treatment.

Models of increasing sophistication and complexity, although arguably closer to biological reality, require an increasing number of parameters. Under these circumstances, authors are forced to make estimates based on a wide range of different experimental and clinical studies [39]. As discussed in Chapter 2, estimates for the same parameters used across the modelling literature span wide ranges of values. The discrepancy in these estimates may be explained, at least in part, by the variability between species when drawing upon data acquired from different species, as well as variability in model design. Due to insufficient high quality time-series data, a theoretical approach has been adopted in this thesis. The relative simplicity of the models proposed permit significant analytical progress and allow one to identify important relationships between model parameters and variables. Such analytical approaches in combination with numerical solutions have enabled us to study, in detail, some of the fundamental interactions that contribute to observed tumour-immune dynamics. The conclusions from our theoretical studies may aid the identification of future biomarkers targeting aspects of heterogeneity of tumour and immune cells, and may also contribute to the design of novel patient-specific immunotherapies.

We have developed theoretical models to examine cancer progression in patients having a range of immune responses, focusing on aspects of heterogeneity in the T cells of the adaptive immune response. Past clinical studies looking at a variety of different cancer types have shown high inter-patient variability in the levels of T cell infiltration correlating with patient survival and rate of recurrence [66, 36]. The importance of the immune system in influencing the development of cancer has highlighted the need for a biomarker to classify patients according to the strength

of the immune system. In recent years a new score, termed the 'Immunoscore', has been proposed, which classifies colorectal cancer patients according to their levels of cytotoxic T cells and memory T cells residing in the core of the tumour as well as in the periphery [71, 70]. This method of patient categorisation has been found to be a better predictor of overall patient survival than other markers in this cancer type [134].

To understand how the tumour can escape the immune system, which in theory should be able to eliminate the tumour before it develops into a clinically detectable size [27], many clinicians and mathematicians have sought to understand the impact of immunosuppressive effects in the tumour microenvironment. In this thesis the aim has been to develop simple mathematical models to comprehensively explore key aspects of immunosuppression, with specific focus on T cell exhaustion. T cell exhaustion primarily occurs as a result of chronic exposure to tumour antigen leading to the gradual loss of function of effector cytotoxic T cells. A number of recent studies have illustrated how the density, as well as the degree of exhaustion correlates with patient outcomes [172, 189]. The models presented here examine T cell exhaustion in two ways: (1) how distinct T cell functions are implicated in tumour escape, and (2) how the composition of the immune population (specifically the relative levels of exhausted and cytotoxic T cells) affects model outcomes.

The three models developed in this thesis have been designed to capture the three Es of Immunoediting: Elimination, Equilibrium and Escape defined by Dunn *et al.* (2004) [52]. The three models considered different aspects of immune and tumour cell heterogeneity through (1) the inclusion of subpopulations of helper and cytotoxic T cells, (2) varying states of cytotoxic T cell exhaustion, (3) subpopulations of T cells (cytotoxic and exhausted) together with tumour cells (immune-sensitive and resistant). In each model we have quantified the impact of the strength of the immune system, characterised by either (a) the rate of infiltrating T cells or (b) the ratio of the baseline T cell population in the absence of the tumour to the T cell population required to arrest the growth of the tumour — the 'T cell efficacy'. The research carried out in this thesis has enabled us to better understand the conditions for tumour escape, and specifically how they depend on different subpopulations of T cells, their rates of exhaustion and the presence of immune resistant versus immune responsive tumour cells. In each model key parameters were identified which separate tumour escape from either tumour elimination or equilibrium. This is arguably the most important practical outcome of this thesis.

A common behaviour was observed throughout: provided the immune system is sufficiently strong and the initial number of tumour cells is sufficiently small, tumour elimination occurs. On the other hand, for a weak immune system, tumour escape is often the only possible outcome. But there is another possibility. We have often found a tumour equilibrium either in the form of a finite steady state or a stable limit cycle (oscillatory solution). Oscillatory solutions are a feature of a number of mathematical models of tumour-immune interactions [110, 160, 202, 55, 126]. Clinical findings are mixed however. Oscillations in the measured number of immune cells have been observed in patients with various different cancer types [99, 38]. Other authors have claimed there is no evidence of such oscillatory behaviour [123]. Mathematical models can be used to understand the nature and origin of oscillations as well as provide insights into the potential for oscillations to be observed clinically.

The finite tumour equilibrium steady state, often referred to as a dormant tumour, is of particular interest. It has been the focus of much experimental and clinical research, and mathematical models have been developed to better understand mechanisms responsible for tumour escape from a dormant state [160, 110, 121]. This state appears to be influenced by a number of factors in the tumour microenvironment [179]. The immune cells are believed to play a primary role. Experiments on mice have shown that if a tumour is in a dormant state for an extended period of time, the immune cells prune the tumour cells leaving behind those that are poorly immunogenic. In the models developed in this thesis, we find that a dormant state arises from a balance between tumour immunosuppression (damped T cell function in the presence of a tumour) and a moderately functioning immune response.

In Chapter 2 we extended a predator-prey model (Kuznetsov *et al.* [110]) of tumour and cytotoxic immune cell interactions to include an effector helper T cell population. (This work forms a paper which is now published in the special issue of Letters in Biomathematics: *Modeling Tumor-Immune Dynamics, Disease Progression, and Treatment* (2018) [50].) This model accounted for heterogeneity through subpopulations of cytotoxic and helper T cells. The extended model was also developed to account implicitly for the effects of immunosuppression with growing tumour size. This was done by including a biphasic term for the rate of helper T cell proliferation, which reaches a maximum at a critical tumour population. This term accounts for the fact that when the immune system is in the presence of a small amount of tumour antigen the proliferation rate of T cells is low. Likewise, the reduction in T cell proliferation in the presence of a large amount of tumour antigen captures the effect of immunosuppression. We found that increases in the infiltration rates of

either T cell population had similar effects on the long-time behaviour of the model, and a combination of both was beneficial for patients. We further found that the model outcomes could be predicted according to the rate of infiltration of the cytotoxic (or helper) T cells into the tumour. These results suggest that patients may be stratified according to their rate of T cell infiltration into three groups: immunocompromised, normal functioning and highly functioning immune systems. Due to the small number of model parameters, a comprehensive exploration across parameter space was feasible. This revealed the importance of the parameters controlling immunosuppression on model outcomes of elimination, equilibrium and escape. For the normal functioning group, the tumour equilibrium state was found to exist either as a stable (dormant) steady state or as a stable limit cycle (oscillation). Otherwise elimination more commonly occurs for the highly functioning group and escape for the immunocompromised group.

This relatively simple model, consisting of just three variables (helper and cytotoxic T cell populations and a tumour cell population), nonetheless reveals a rich bifurcation structure and permits significant analytical progress. For instance we were able to subdivide parameter space into regions associated with different numbers of steady states and their corresponding linear stability. By exploiting a small parameter we were able to obtain accurate expressions for both the small tumour equilibrium state as well as the fold point from which the large tumour state emerges (this state represents escape in the model). Furthermore from the small tumour steady state we could deduce the change in stability at which Hopf bifurcations occur and limit cycles arise. Having identified the point at which limit cycles emerge, a limit cycle amplitude equation in the neighbourhood of a Hopf bifurcation point was derived through a weakly non-linear analysis to cubic order in a small parameter representing the 'distance' from the Hopf bifurcation. This analysis was shown to accurately represent the fully nonlinear dynamics in the vicinity of the Hopf bifurcation point. The research in this chapter clarified the importance of immunosuppression in tumour-immune dynamics. Specifically, damping the rate of T cell proliferation increases the region of tumour escape at the expense of the stable tumour equilibrium state. These results highlight the need to study damping of all T cell functions (killing, infiltration and proliferation) collectively.

To this end, in Chapter 3 we formulated a novel approach to modelling the effects of T cell exhaustion on T cell killing, infiltration and proliferation in the presence of an evolving tumour. This was motivated by current experimental and clinical research, highlighting the role played by T cell exhaustion in an anti-tumour immune

response [189, 172, 146, 18]. Instead of accounting for distinct subpopulations of T cells, we modelled heterogeneity through the functional states of the cytotoxic T cells. In Chapter 3, progressive exhaustion of the T cell population was modelled by three separate ODEs describing the ability of the T cell population to kill, infiltrate and proliferate in the presence of an evolving tumour. These T cell 'functions' consisted of a recovery component to a baseline value, mimicking the influx of new non-exhausted T cells, and a degradation component proportional to the size of the tumour population. Our approach complements previous theoretical models in which immunosuppressive effects were examined through the inclusion of specific immunosuppressive components such as cells, molecules or size limitations mimicked through only a portion of T cells being able to interact with the total T cell population (see Robertson-Tessi *et al.* [160] and Leon *et al.* [114]).

Small variations in the parameters controlling the rates at which tumour cells reduce the proliferation and cytotoxicity of T cells per tumour cell, ξ_α and ξ_k respectively, were found to have the largest effect on model behaviour, particularly for immunocompromised patients characterised by their T cell efficacy. Increases in ξ_α reduce the region of parameter space where a tumour equilibrium state occurs, replacing it with escape. This is mirrored by decreases in ξ_k. Both such variations increase the likelihood of tumour escape. By contrast, variations in the rate at which tumour cells reduce the infiltration of T cells per tumour cell, ξ_σ, had a much less pronounced effect. Even when ξ_σ was high, an equilibrium state remained for immunocompromised patients (low T cell efficacy). A counter-intuitive finding of the model was the dual role played by the parameter controlling the exhaustion rate of T cell killing, ξ_k. We found that there was an optimum ξ_k for immunocompromised patients: when too low, the tumour is able to effectively counter attack the T cell population allowing tumour growth (as discussed above); when too high, the T cell population is unable to effectively kill the tumour. For patients with a high T cell efficacy, the range of ξ_k leading to favourable outcomes expands, though small ξ_k still leads to the least favourable outcomes.

The results of this research suggests that identification of the main inhibitory receptor pathways responsible for damping the proliferative capacity of the T cells is important for preventing tumour escape. Once identified, antibodies could be designed to target these pathways early on during tumour development. Our results indicate that excessive T cell killing may actually be unfavourable, and that some level of exhaustion is preferable. This unexpected feature of the model may be due to simultaneous decreases in the rate of T cell killing and tumour counter attack.

This requires further investigation. A potential way to address this in future research would be to have two separate rates for T cell killing and tumour counter attack, replacing $(1-\phi)k(t)$ and $\phi k(t)$ in equations (3.1) and (3.2).

As in Chapter 2 we observed that a tumour equilibrium state may exist either as a stable steady state (dormant) or as a stable limit cycle (oscillation). However the full model equations were too complex to make significant analytical headway, and therefore many of the results had to be obtained numerically. A simpler version of the model was therefore considered in which the rates of T cell killing, infiltration and proliferation were combined into a single variable termed 'T cell functionality'. This led to a system of three ODEs which was analytically tractable. Notably, analytical solutions for the amplitude of stable limit cycles near their point of emergence were derived. Moreover the disappearance of these limit cycles when their amplitude becomes unbounded was described by a matched asymptotic analysis. The simpler version of the model helped to clarify the global bifurcation structure present, providing a more complete understanding than is possible through numerical solutions of the full model. The two models provided a complementary view of the evolution of T cell function in the presence of a tumour.

The final model proposed in Chapter 4 combined key components of the models developed in Chapters 2 and 3, and accounted for heterogeneity by including subpopulations of T cells (exhausted and cytotoxic) and tumour cells (immune-sensitive and resistant). A number of authors have argued for using characteristic components of the tumour microenvironment, such as the level of cytotoxic T cells, as a biomarker for better patient prognosis than that presently achievable with conventional tumour node metastasis staging [68, 36]. Although a body of past research has identified how high levels of cytotoxic T cells are associated with favourable outcomes, little has been done to examine how the composition of functional and exhausted T cells, specifically the fraction of exhausted to the total T cell population, affects outcomes. This chapter was also motivated by the recent experimental study of Schreiner *et al.* [172] showing a large population of highly exhausted T cells was associated with a lack of response to treatment. There is thus a need to better understand the composition of T cells in the tumour microenvironment and its effect on tumour progression and treatment.

In Chapter 4 the aim was not to distinguish between the individual effects of T cell killing, infiltration and proliferation as in Chapter 3, but rather to understand the interplay between exhausted and cytotoxic T cells in combating tumour growth. The model in Chapter 2 was extended to include an immune-resistant tumour population

and an exhausted T cell population. We assumed that when the cytotoxic T cells come into contact with resistant tumour cells, the T cells become exhausted. These exhausted T cells retain some capacity to kill the immune-sensitive tumour cells, but this occurs at a reduced capacity compared to the functional T cells. The exhausted T cells have no capacity to kill resistant tumour cells. Instead, when exhausted T cells come into contact with resistant tumour cells, the exhausted T cells are removed. This approach offers new insights into how T cell exhaustion affects tumour-immune dynamics through explicit consideration of the composition of tumour and immune cell populations.

The model behaviour was first explored by varying the cytotoxic T cell infiltration rate together with other parameters which are likely to vary with both the patient and cancer type. These included the growth rate of the tumour, the probability of the tumour becoming immune-resistant, the conversion rate of functional T cells into exhausted T cells, and the rate at which exhausted T cells kill immune-sensitive tumour cells. We found as expected, the higher the tumour growth rate the higher the infiltration rate of cytotoxic T cells needed to combat the tumour. Notably, apart from the growth rate of the non-resistant tumour population, the parameters having the greatest impact are all associated with the resistant tumour population.

We next explored a means of extracting patient specific parameters when the ratios of exhausted to cytotoxic T cells and immune-resistant to sensitive tumour cells at steady state were prescribed. This represents a novel approach to exploring model behaviour, in particular the long-time evolution starting in a neighbourhood of a tumour equilibrium state. Fixing these steady state cell population ratios enabled us to determine two patient specific parameters: the tumour growth rate and the rate of T cell infiltration. By comprehensively exploring all permissible cell population ratios, we mapped out regions where a dormant tumour may either escape, settle to another stable dormant equilibrium state, cease to exist (elimination) or remain in the same (stable) equilibrium. A surprising finding was that tumour elimination occurs in a region of parameter space characterised by relatively large numbers of resistant tumour cells and exhausted T cells. The explanation for this behaviour is that, also in this region, the tumour growth rate is relatively low and the T cell infiltration rate is relatively high, and it is this infiltration of T cells that results in tumour elimination. These findings could aid patient prognosis by predicting patient outcomes based on their T cell and tumour cell compositions.

We next explored the effects of immunotherapy for patients destined either for tumour escape or living with a dormant tumour. Here two immunotherapies were

modelled: an IL-2 therapy designed to boost the functional T cells, and a T cell bispecific antibody designed to increase the killing capacity and infiltration of the T cells. For patients destined for tumour escape, we found that both the frequency of drug delivery, and the dosage, depends critically on the time between initial tumour detection and initial delivery of the drug. For patients with a dormant tumour, a high dosage level appears to be essential in reducing the tumour size, possibly leading to its elimination.

This thesis has set out to explore individual aspects of heterogeneity in the tumour microenvironment, focusing on the T cells of the adaptive immune response. Arguably for a biologically realistic framework a single model encapsulating all of these components of heterogeneity would be necessary. Such a model however would require estimates of many model parameters and therefore would be at the risk of over parametrisation. The approach adopted here instead attempts to build up layers of heterogeneity in the tumour with a focus on T cells of the immune system. By studying individually components of heterogeneity of an anti-tumour immune response, we were able to carry out a comprehensive analysis of salient aspects of tumour-immune dynamics using a combination of analytical and numerical techniques. A broad understanding of the various factors at play was achieved by retaining model simplicity at the expense of biological realism. The research presented in this thesis focused on the interactions occurring in the tumour microenvironment, and therefore considered only one portion of the Cancer-Immunity cycle illustrated by Chen and Mellman (2013) [35] (see Figure 1.4). In the future it would be beneficial to incorporate these models into larger modelling frameworks exploring the entire cycle.

All of the models exhibited the same qualitative behaviour: elimination, equilibrium and escape. How these vary with heterogeneity was explored. In Chapter 2 we found that variations in the rates of infiltration of both the helper and cytotoxic T cell populations gave rise to complementary behaviour, with elimination for high rates of infiltration and escape for low rates of infiltration. In Chapter 3 instead we measured the strength of the immune system by the T cell efficacy. As in Chapter 2 this measure of immune strength was important for determining the conditions for tumour escape, equilibrium and elimination. In Chapter 4 subpopulations of T cells (cytotoxic and exhausted) and tumour cells (resistant and sensitive) were modelled. Like in Chapter 2 we observed that escape is favoured for low infiltration, equilibrium for moderate infiltration and elimination for high infiltration. The main distinction between all three models occurs for a 'moderately' strong immune system as shown schematically in Figure 5.1. In this moderately strong region, for example in Figure

5.1(a) and (b), an equilibrium tumour state exists as either a stable limit cycle or as an equilibrium state (dormant state), whereas in Figure 5.1(c) an oscillatory solution does not exist. Furthermore, in (b) we have a region where elimination, equilibrium and escape can all occur. Collectively, these results suggest that when different aspects of heterogeneity are examined, the greatest differences occur for a moderately strong immune system.

In addition to aspects of heterogeneity, each model sought to examine immunosuppressive effects from different angles. Increasing immunosuppressive pressures were found to alter where elimination, equilibrium and escape occurs (see Figure 5.1). In Chapter 2 immunosuppressive effects were accounted for through two terms: a biphasic term to describe the proliferation of the helper T cells, and a term to account for tumour counter attack on the cytotoxic T cells. A thorough examination of model parameters revealed that those parameters controlling the proliferative potential of the helper T cells had the most notable effect on model behaviour. Following these results, Chapter 3 studied the effects of T cell exhaustion on T cell killing, infiltration and proliferation in the presence of an evolving tumour. This approach clarified the roles of individual T cell functions in tumour control. We found that variations in the rate the tumour dampens the individual T cell functions had a marked effect on the behaviours illustrated in Figure 5.1(b). In the final model presented in Chapter 4 we set out to examine how the composition of functional and exhausted T cell populations in the presence of a tumour population, consisting of immune resistant and non-resistant tumour cells, affects model outcomes. This model predicted that tumours in a dormant state either remain dormant, change to an alternative dormant state, escape or are eliminated. These outcomes were shown to be strongly dependent on two patient specific model parameters: the growth rate of the tumour cells and the infiltration rate of the cytotoxic T cells. We found that, if the rate of conversion of cytotoxic T cells to exhausted T cells is high, or if the kill rate of the exhausted T cells is low, the region of tumour equilibrium is replaced by escape (see Figure 5.1(c)).

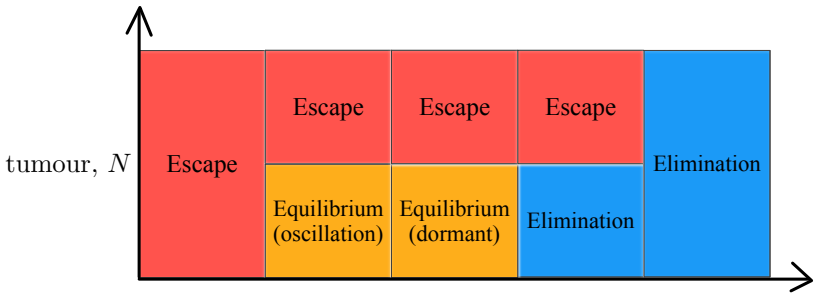

(a) Chapter 2 model

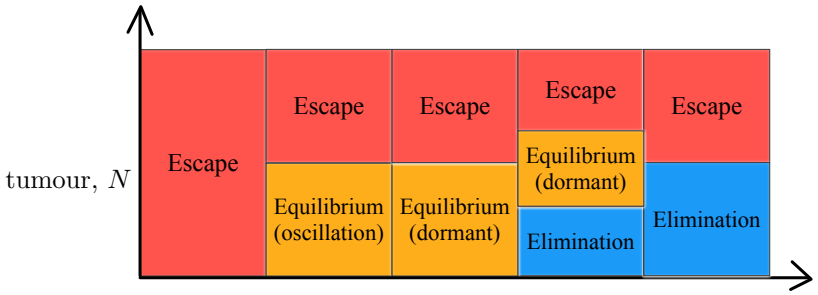

(b) Chapter 3 model

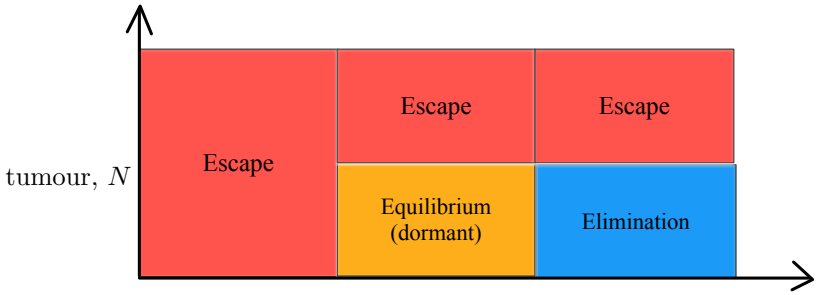

(c) Chapter 4 model

Figure 5.1: Schematic to compare the qualitative behaviours exhibited by the models in Chapters 2—4 with variations in the strength of the immune system captured by the rate of T cell infiltration (panels (a) and (c)) or the T cell efficacy (panel (b)).

There are a number of potentially promising avenues of future research. The research carried out in this thesis made the assumption of spatial homogeneity. This assumption, although an oversimplification of the underlying dynamics, facilitates analytical progress and is a necessary first step in understanding immunosuppression in tumour-immune interactions. Although the density of various immune cells is correlated with patient survival, the location of these cells is also implicated in response

outcomes [66, 45, 71]. Based on these clinical observations, the next step in this research would be to include spatial effects in each of these models. This could be achieved, for example, in a similar manner to that done in Matzavinos *et al.* (2004) [130], who accounted for spatial effects through random cell movement (diffusion) and movement directed by chemical gradients (chemotaxis). A spatial extension of the model presented in Chapter 2 would help elucidate how the location of helper and cytotoxic T cells relative to tumour cells influences model outcomes. A spatial extension of the model presented in Chapter 3 would permit study of the additional effect of the spatial distribution of T cells and tumour cells in T cell exhaustion. Finally, a spatial extension of the model in Chapter 4 would enable one to understand how the location of exhausted and cytotoxic T cells relative to immune-resistant and sensitive tumour cells alters model outcomes. Across all models we expect that the rich bifurcation structure found in ODE models translates into pattern formation, travelling waves, and (potentially) spatio-temporal chaos [129, 142].

In this thesis we have sought to keep the number of competing processes to a minimum while attempting to capture key aspects of tumour-immune interactions. A natural extension would be to include random fluctuations in source terms in order to represent effects not explicitly modelled. Those effects could represent natural variations in the tumour microenvironment. The random fluctuations could also be used to account for the missing detail in, for example, cell movements in a spatially homogeneous model. These fluctuations could be included by sampling from an appropriate probability distribution with prescribed means and variances. This would change the character of the models examined in this thesis substantially in that there would no longer be steady state solutions. Such a 'stochastic model' is inherently unsteady. Nonetheless, one can study where the model spends most of its time and how transitions between different behaviours occur. Stochastic effects may be beneficial in preventing an unrealistic tumour-free state when it is more likely that small tumours are developing and being eradicated by the immune system sporadically. This is the theory of immunosurveillance [27]. The main question here is the extent to which the immune system can maintain control over the sporadic development of small tumours.

Instead of considering spatial or stochastic effects individually, one may wish to consider their combined effects. For instance in a agent based model with probabilistic rules or in a stochastic PDE framework. In the context of tumour-immune interactions with a specific emphasis on T cell exhaustion, such approaches would only be

merited when there are commensurate improvements in data availability and quality. Undoubtedly with improvements in data, mathematical models of the underlying biological processes are likely to change.

Another extension would be to look beyond immunosuppressive effects to other mechanisms which enable tumour evasion of the immune system. There are a range of other ways in which pre-malignant cancer cells accumulate into a clinically detectable tumour mass (Hanahan and Weinberg [85] and [86]). For example angiogenesis and the immune system are believed to interact in a complex way; regulatory cells such as MDSC and TAMs induce the onset of angiogenesis but anti-angiogenic molecules targeting say VEGF are found to reverse immunosuppressive effects on the cells of the immune system [185]. In the present thesis we assumed avascular tumour growth, for simplicity. Such an extension would enable the study of how T cells infiltrate from blood vessels, and how this impacts tumour development. Including angiogenesis could be done either through a simple ODE model [168] or through the development of a spatial model to capture the formation of a blood vessel network [31]. Already some authors have examined the interactions of immune cells and angiogensis [117].

The evasion of the immune system by a tumour involves a cycle of mechanisms called the Cancer-Immunity Cycle (Chen and Mellman [35]) which is executed as long as tumour antigen is detected. We have yet to fully understand how stages in the cycle break down and how this break down propagates to further stages. A first step to achieve this would be to couple mathematical models looking at, for example, the activation stage (where naive T cells first encounter their antigen) via the migration stage (where the activated T cells move to the tumour site) to the development of the tumour microenvironment.

The research presented in this thesis addresses the three central questions posed at the beginning of this chapter. These target important aspects of tumour heterogeneity, and highlight potentially overlooked components of the T cell arm of the adaptive immune response. Instead of creating one model to incorporate a myriad of different components, simpler models were devised to study specific aspects of heterogeneity within tumour-immune cells interactions. This allowed one to widely explore parameter space and thereby gain a fuller understanding of the factors at play.

Mathematical models possess the means to identify key mechanisms involved in an anti-tumour immune response. These may reveal counter-intuitive and previously overlooked features. These models also have the potential to identify new therapeutic targets as well as effective treatment strategies (e.g. the window in time within which treatment may be most effective). Mathematical models used in combination with

experimental studies hold the key to the future of personalised medicine in cancer treatments.

Much work remains to be done to model the immune system's fight against cancer. The series of models proposed, while a simplification of the real biological system, have considered the role of heterogeneity and the effect of immunosuppresion by addressing three key questions. We have undertaken a comprehensive study of an anti-tumour immune response accounting for T cell exhaustion. Many questions however still remain that may help explain tumour escape. These include:

- Is it possible to avoid or reverse T cell exhaustion during chronic antigen exposure?
- How do the multiple inhibitory receptors upregulated on an exhausted T cell communicate and dampen key effector T cell functions?
- How long does it take for the TILs to become exhausted? Does this differ by cancer type?
- What role do other regulator factors play (such as the presence of Tregs) in T cell exhaustion?
- Why are some tumours heavily infiltrated by T cells while others are not?
- Is there an optimum level of antigenic diversity necessary to elicit an effective immune response against the tumour?

These are only a sample of the questions that still remain unanswered. However, as high quality time-series data becomes increasingly available, these models can be further developed or modified to incorporate more biological realism. This feedback between model development and data acquisition is crucial to the future of cancer research [6, 107]. The goal is to provide sufficiently accurate, predictive, quantitative models that are able to stratify patients and identify optimal treatment protocols.

Appendix A

Conditions for tumour equilibria in the helper and cytotoxic T cell model

In Chapter 2, Section 2.4, we introduced the functions $T_H = H_a(N)$ and $T_H = H_b(N)$ (see equations (2.16)–(2.17)) and showed that their positive intersections give rise to tumour equilibria. Figure 2.4 illustrates the ways in which these curves may intersect. In this appendix we detail how the qualitative behaviour of the functions $T_H = H_a(N)$ and $T_H = H_b(N)$ vary with model parameters and identify a region of parameter space in which four (positive) equilibria may occur.

For the curve $T_H = H_a(N)$, three cases may arise, depending on the values of $\bar{\alpha}$ and $\tilde{N}$:

(1) $\bar{\alpha} < 2\tilde{N}$: $T_H = H_a(N) > 0$ for $N \in (0, 1)$ and attains a finite (positive) maximum:

$$H_{a,\max} = H_a(\tilde{N}) = \frac{2\bar{\sigma}_H \tilde{N}}{2\tilde{N} - \bar{\alpha}}\,, \tag{A.1}$$

at $N = \tilde{N}$.

(2) $2\tilde{N} \leq \bar{\alpha} \leq 1 + \tilde{N}^2$: $T_H = H_a(N)$ has two asymptotes at

$$N_\pm = \frac{\bar{\alpha} \pm \sqrt{\bar{\alpha}^2 - 4\tilde{N}^2}}{2}\,. \tag{A.2}$$

Furthermore, $0 < N_- \leq N_+ \leq 1$, with $N_- = N_+ = \tilde{N}$ when $\bar{\alpha} = 2\tilde{N}$, and $N_- = \tilde{N}^2$ and $N_+ = 1$ when $\bar{\alpha} = 1 + \tilde{N}^2$.

(3) $\bar{\alpha} > 1 + \tilde{N}^2$: only the asymptote at $N = N_-$ lies in the interval $N \in [0, 1]$ (the other asymptote has $N_+ > 1$, and is therefore outside the range of feasible solutions).

When characterising the behaviour of $T_H = H_b(N)$ as defined by equation (2.17), we set $\tilde{k} = (1-p)k$ and $\tilde{\sigma}_C = \sigma_C pk/\gamma$, and write

$$T_H = H_b(N) = 1 + \tilde{k}N - \frac{\tilde{\sigma}_C}{1-N}. \tag{A.3}$$

This function attains a maximum when

$$N = 1 - \sqrt{\frac{\tilde{\sigma}_C}{\tilde{k}}}\,. \tag{A.4}$$

There are two cases to consider depending on the magnitude of $\tilde{\sigma}_C/\tilde{k}$:

(1) $\tilde{\sigma}_C/\tilde{k} > 1$: $H_{b,\max} = 1-\tilde{\sigma}_C$ occurs at $N^* = 0$. $H_b(N)$ is monotonically decreasing for $N \in [0,1]$. Hence if $\tilde{\sigma}_C > 1$, $H_b(N) < 0\ \forall N \in [0,1]$ and there can be no physically realistic tumour equilibria. If $0 < \tilde{\sigma}_C < 1$, $H_b(N) < 0$ for $N \in (0, N_c)$, where $N_c \in (0,1)$ is defined as follows:

$$N_c = \frac{(\tilde{k}-1) + \sqrt{(\tilde{k}+1)^2 - 4\tilde{k}\tilde{\sigma}_C}}{2\tilde{k}}\,, \tag{A.5}$$

and $H_{b,max} = H_b(0) = 1 - \tilde{\sigma}$. Hence, when $0 < \tilde{\sigma}_C < 1$, intersections with $T_H = H_a(N)$ (and, hence, tumour equilibria) may occur for $0 < N < N_c$.

(2) $\tilde{\sigma}_C/\tilde{k} \leq 1$: $T_H = H_b(N)$ attains a maximum $H_{b,\max} = 1 + \tilde{k} - 2\sqrt{\tilde{k}\tilde{\sigma}_C}$ at $N = 1-\sqrt{\tilde{\sigma}_C/\tilde{k}} \in (0,1)$. For physically realistic equilibria we require $H_{b,max} > 0$ or, equivalently,

$$\tilde{\sigma}_C < \frac{(1+\tilde{k})^2}{4\tilde{k}}\,. \tag{A.6}$$

These results are summarised in Figure A.1 where we indicate the region of $(\tilde{k}, \tilde{\sigma}_C)$ parameter space in which physically realistic tumour equilibria may occur.

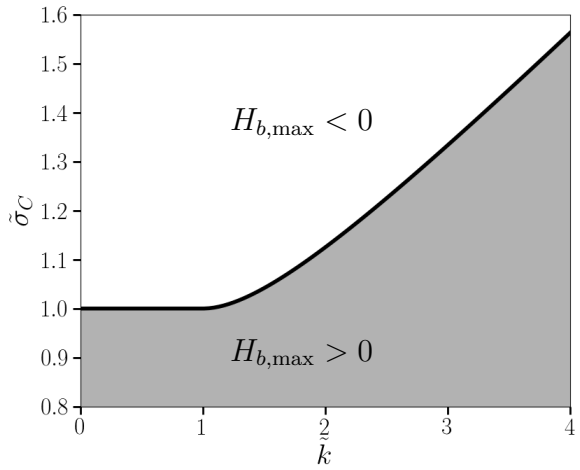

Figure A.1: The dividing line in $(\tilde{k}, \tilde{\sigma}_C)$ parameter space separating solutions which permit tumour equilibria ($H_{b,\max} > 0$) from those which do not permit tumour equilibria ($H_{b,\max} < 0$).

In Figure 2.4 we illustrated the possible intersections (and associated tumour equilibria) that occur as the qualitative behaviour of $H_a(N^*)$ and $H_b(N^*)$ vary. In practice, by a judicious choice of parameters, four intersections can occur. Further, for appropriate parameter choices, two of these intersections occur for $N^* \ll 1$, as we now investigate below.

For ease of presentation, we let $s = N^*/\tilde{N}$ and $a = \bar{\alpha}/\tilde{N}$. Values of s for which intersections between H_a and H_b occur are given by solutions to the following quartic equation:

$$p_4 s^4 + p_3 s^3 + p_2 s^2 + p_1 s + p_0 = 0, \tag{A.7}$$

where

$$p_4 = \tilde{k}\tilde{N}^2\,,\; p_3 = (1-\tilde{k})\tilde{N} - a\tilde{k}\tilde{N}^2 - \bar{\sigma}_H\tilde{N}\,,\; p_2 = (\tilde{\sigma}_C - 1) + \tilde{k}\tilde{N}^2 + a\tilde{N}(\tilde{k}-1) + \bar{\sigma}_H\,, \tag{A.8a}$$

$$p_1 = (1-\tilde{\sigma}_C)a + (1-\tilde{k})\tilde{N} - \bar{\sigma}_H\tilde{N}\,,\; p_0 = \tilde{\sigma}_C + \bar{\sigma}_H - 1. \tag{A.8b}$$

We fix parameter values as follows: $\bar{\sigma}_H = 0.25$, $\tilde{N} = 0.25$ and $\bar{\alpha} = 0.25$ (so that $a = 1$). We then consider $\tilde{\sigma}_C = 1 - \bar{\sigma}_H + \epsilon^2\tilde{\sigma}_{C2}$ and $\tilde{k} = 1 + (a/\tilde{N} - 1)\bar{\sigma}_H + \varepsilon\tilde{k}_1$, where $0 < \varepsilon \ll 1$. With this choice of parameters, we find $p_4 = p_3 = p_2 = O(1)$, $p_1 = O(\sqrt{\epsilon})$, $p_0 = O(\epsilon)$. Suppose we seek roots of the form $s = \epsilon s_1 \ll 1$. By considering leading-order terms in ε in equation (A.7), it is straightforward to show that s_1 satisfies the

quadratic equation $p_2 s_1^2 - \tilde{N}\tilde{k}_1 s_1 + \tilde{\sigma}_{C2} = 0$, and the two solutions for s_1 are given by the following

$$s_1 = \frac{\tilde{N}\tilde{k}_1 \pm \sqrt{\tilde{N}^2\tilde{k}_1^2 - 4\tilde{\sigma}_{C2}p_2}}{2p_2}\,, \tag{A.9}$$

where $p_2 = \bar{\sigma}_H a^2 + \tilde{\sigma}_C \tilde{N}^2 > 0$. For two real positive roots, we require

$$0 < \tilde{\sigma}_{C2} < \frac{\tilde{N}^2\tilde{k}_1^2}{4p_2}\,. \tag{A.10}$$

To show this works, consider the parameter choices $\varepsilon = 0.03$, $\tilde{\sigma}_{C2} = 0.33$ and $\tilde{k}_1 = 1.26$. With these choices, we have $\tilde{\sigma}_C \approx 0.75$ and $\tilde{k} \approx 1.79$. The intersections of $H_a(N^*)$ and $H_b(N^*)$ are shown on the left panel of Figure A.2, while the right panel zooms in on the two equilibria with $0 < N^* \ll 1$.

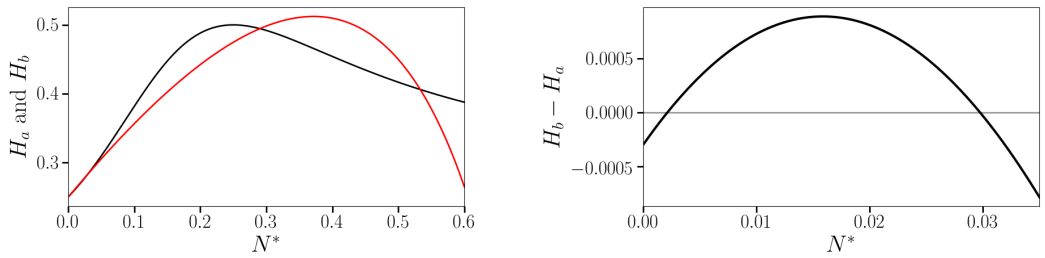

Figure A.2: Example showing that the curves $H_a(N)$ and $H_b(N)$ defined by equations (2.16) and (2.17) may intersect four times (see text for details). All four intersections are shown on the left panel, although the two intersections with $0 < N = N^* \ll 1$ are difficult to detect. The zoom on the right panel verifies that there are two intersections with $0 < N = N^* \ll 1$.

Appendix B

Limit cycle for helper and cytotoxic T cell model

Here we detail the weakly nonlinear analysis presented in Section 2.7.4. With $\mathbf{x} = (N, T_C, T_H)$ and $\mathbf{x} = x(t, \tau)$ where $\tau = \epsilon^2 t$, equations (2.6)–(2.8) expanded to order ϵ^3 are

$$\begin{aligned}
\dot{x} &= \epsilon\frac{\partial x_1}{\partial t} + \epsilon^2\frac{\partial x_2}{\partial t} + \epsilon^3\left(\frac{\partial x_3}{\partial t} + \frac{\partial x_1}{\partial \tau}\right) \\
&= \gamma(x_0 + \epsilon x_1 + \epsilon^2 x_2 + \epsilon^3 x_3) \\
&\quad - \gamma[x_0^2 + 2\epsilon x_0 x_1 + \epsilon^2(2x_0x_2 + x_1^2) + \epsilon^3(2x_0x_3 + 2x_1x_2)] \\
&\quad - p[x_0y_0 + \epsilon(x_0y_1 + x_1y_0) + \epsilon^2(x_0y_2 + y_0x_2 + x_1y_1) + \epsilon^3(x_0y_3 + y_0x_3 + x_1y_2 + y_1x_2)]\,,
\end{aligned} \tag{B.1}$$

$$\begin{aligned}
\dot{y} &= \epsilon\frac{\partial y_1}{\partial t} + \epsilon^2\frac{\partial y_2}{\partial t} + \epsilon^3\left(\frac{\partial y_2}{\partial t} + \frac{\partial x_1}{\partial \tau}\right) \\
&= \sigma_{C0} - \epsilon^2 \\
&\quad + [y_0z_0 + \epsilon(y_0z_1 + z_0y_1) + \epsilon^2(y_0z_2 + z_0y_2 + y_1z_1) + \epsilon^3(y_0z_3 + z_0y_3 + y_1z_2 + z_1y_2)] \\
&\quad + (p-1)[x_0y_0 + \epsilon(x_0y_1 + y_0x_1) + \epsilon^2(x_0y_2 + y_0x_2 + x_1y_1) + \epsilon^3(x_0y_3 + y_0x_3 + x_1y_2 + y_1x_2)] \\
&\quad - (y_0 + \epsilon y_1 + \epsilon^2 y_2 + \epsilon^3 y_3)\,,
\end{aligned} \tag{B.2}$$

$$\begin{aligned}
\dot{z} &= \epsilon\frac{\partial z_1}{\partial t} + \epsilon^2\frac{\partial z_2}{\partial t} + \epsilon^3\left(\frac{\partial z_2}{\partial t} + \frac{\partial x_1}{\partial \tau}\right) \\
&= \sigma_H + \alpha[z_0f_0 + \epsilon(z_0{f_0}'x_1 + f_0z_1) \\
&\quad + \epsilon^2(z_0{f_0}'x_2 + z_0{f_0}''x_1^2/2 + {f_0}'z_1x_1 + f_0z_2) \\
&\quad + \epsilon^3(z_0{f_0}'x_3 + z_0{f_0}''x_1x_2 + z_0{f_0}'''x_1^3/6 + z_1{f_0}'x_2 + z_1{f_0}''/2 + x_1^2 + {f_0}'x_1z_2 + f_0z_3)] \\
&\quad - \delta_H(z_0 + \epsilon z_1 + \epsilon^2 z_2 + \epsilon^3 z_3)\,,
\end{aligned} \tag{B.3}$$

where $f_0 = f(x_0)$ and $f(x) = x/(\tilde{N}^2 + x^2)$. Similarly, ${f_0}' = df(x_0)/dx$ etc.

At $\mathcal{O}(\epsilon)$ we obtain the linear dynamics described in Section 2.7.4, see in particular equation (2.41) for $\mathbf{x_1}$. Considering the $\mathcal{O}(\epsilon^2)$ terms in equations (B.1)–(B.3), we obtain:

$$\frac{\partial \mathbf{x_2}}{\partial t} = \mathcal{J}_0 \mathbf{x_2} - (0,1,0)^T + \mathbf{W_2} \tag{B.4}$$

where

$$\mathbf{W_2} = \begin{pmatrix} -\gamma x_1^2 - pkx_1y_1 \\ y_1z_1 + (p-1)kx_1y_1 \\ \alpha(f_0{}''z_0x_1^2/2 + f_0{}'x_1z_1) \end{pmatrix} \tag{B.5}$$

Plugging in equation (2.41) for $\mathbf{x_1}$ into equation (B.5) gives

$$\mathbf{W_2} = \mathbf{Q_2^a}\phi^2(\tau)e^{2i\omega t} + c.c. + \mathbf{Q_2^b}|\phi(\tau)|^2 + \mathbf{Q_2^c}\phi(\tau)\chi e^{(\lambda_3+i\omega)t} + c.c. + \mathbf{Q_2^d}\chi(\tau)^2 e^{2\lambda_3 t} \tag{B.6}$$

where $c.c.$ denotes the complex conjugate. The secular terms arising at $\mathcal{O}(\epsilon^3)$ involve only $e^{2i\omega t}$ and 1 terms. Thus only $\mathbf{Q_2^a}$ and $\mathbf{Q_2^b}$, shown in equations (B.7) and (B.8) are needed, and they are given explicitly by

$$\mathbf{Q_2^a} = \begin{pmatrix} -v_{1x}(\gamma v_{1x} + kpv_{1y}) \\ v_{1y}(v_{1z} + k(p-1)v_{1x}) \\ v_{1x}\alpha(f_0{}''z_0v_{1x} + f_0'v_{1z}) \end{pmatrix} \tag{B.7}$$

and

$$\mathbf{Q_2^b} = \begin{pmatrix} -v_{1x}^*(\gamma v_{1x} + kspv_{1y}) - v_{1x}(\gamma v_{1x}^* + pkv_{1y}^*) \\ v_{1y}^*(v_{1z} + k(p-1)v_{1x}) + v_{1y}(v_{1z}^* + k(p-1)v_{1x}^*) \\ v_{1x}^*\alpha(f_0{}''z_0v_{1x} + f_0{}'v_{1z}) + v_{1x}\alpha(f_0{}''z_0v_{1x}^* + f_0{}'v_{1z}^*) \end{pmatrix} \tag{B.8}$$

where v_{1x}, v_{1y} and v_{1z} are the components of the linear eigenvector in (2.41). The solution for $\mathbf{x_2}$ is given by

$$\mathbf{x_2} = \mathbf{x_{20}} + \mathbf{R_2^a}\phi^2(\tau)e^{2i\omega t} + c.c. + \mathbf{R_2^b}|\phi(\tau)|^2 + \mathbf{R_2^c}\phi(\tau)\chi e^{(\lambda_3+i\omega)t} + c.c. + \mathbf{R_2^d}\chi^2 e^{2\lambda_3 t}. \tag{B.9}$$

where

$$\mathbf{x_{20}} = \mathcal{J}_0{}^{-1}(0,1,0)^T, \quad \mathbf{R_2^a} = (2i\omega\mathcal{I} - \mathcal{J}_0)^{-1}\mathbf{Q_2^a}, \quad \mathbf{R_2^b} = -\mathcal{J}_0^{-1}\mathbf{Q_2^b}\,. \tag{B.10}$$

$\mathbf{R_2^c}$ and $\mathbf{R_2^d}$ are not required in the subsequent analysis as they belong to non-secular terms. Substituting $\mathbf{x_2}$ into (B.1)–(B.3), we obtain

$$\frac{\partial \mathbf{x_3}}{\partial t} + \frac{\partial \mathbf{x_1}}{\partial \tau} = \mathcal{J}_0 \mathbf{x_3} + \mathbf{W_3} \tag{B.11}$$

where

$$\mathbf{W_3} = \begin{pmatrix} -2\gamma x_1x_2 - pk(x_1y_2 + y_1x_2) \\ y_1z_2 + z_1y_2 + (p-1)k(x_1y_2 + y_1x_2) \\ \alpha(z_0f_0{}''x_1x_2 + z_0f_0{}'''x_1^3/6 + f_0{}'z_1x_2 + f_0{}''z_1x_1^2/2 + f_0{}'x_1z_2) \end{pmatrix}. \tag{B.12}$$

As before the homogeneous solution is already incorporated in $\mathbf{x_1}$. For the particular solution we must solve

$$\frac{\partial \mathbf{x_3}}{\partial t} - \mathcal{J}_0 \mathbf{x_3} + \frac{d\phi}{d\tau}\mathbf{v_1}e^{i\omega t} + c.c. = (\mathbf{B_l} + \mathbf{B_c}|\phi|^2)\phi e^{i\omega t} + c.c. + \mathbf{f}(t,\tau) + c.c. \tag{B.13}$$

where $\mathbf{f}(t,\tau)$ contains time dependencies other than $e^{i\omega t}$ and is therefore non-secular. The components of the vectors $\mathbf{B_l}$ and $\mathbf{B_c}$ are given by

$$\begin{aligned} B_{lx} &= -2\gamma v_{1x}x_{20} - kp(v_{1x}y_{20} + v_{1y}x_{20})\,, \\ B_{ly} &= (v_{1y}z_{20} + v_{1z}y_{20}) + k(p-1)(v_{1x}y_{20} + v_{1y}x_{20})\,, \\ B_{lz} &= \alpha[z_0 f_0{}'' v_{1x}x_{20} + f_0{}'(v_{1z}x_{20} + v_{1x}z_{20})]\,, \end{aligned} \tag{B.14}$$

and

$$\begin{aligned} B_{cx} &= -2\gamma(v_{1x}^* R_{2x}^a + v_{1x}R_{2x}^b) - kp(v_{1x}^* R_{2y}^a + v_{1x}R_{2y}^b + v_{1y}^* R_{2x}^a + v_{1y}R_{2x}^b)\,, \\ B_{cy} &= (v_{1y}^* R_{2z}^a + v_{1y}R_{2z}^b + v_{1z}^* R_{2y}^a + v_{1z}R_{2y}^b)\,, \\ &\quad + k(p-1)(v_{1x}^* R_{2y}^a + v_{1x}R_{2y}^b + v_{1y}^* R_{2x}^a + v_{1y}R_{2x}^b)\,, \\ B_{cz} &= \alpha[z_0 f_0{}''(v_{1x}^* R_{2x}^a + v_{1x}R_{2x}^b) + f_0{}'(v_{1z}^* R_{2x}^a + v_{1z}R_{2x}^b + v_{1x}^* R_{2z}^a + v_{1x}R_{2z}^b) \\ &\quad + f_0{}''' z_0 |v_{1x}|^2 v_{1x}/2 + f_0{}''(v_{1z}^* v_{1x}^2 + 2v_{1z}|v_{1x}|^2)/2]\,. \end{aligned} \tag{B.15}$$

The particular solution to equation (B.13) is

$$\mathbf{x_3}(t,\tau) = \mathbf{X_3}(t,\tau) + \mathbf{u}(\tau)e^{i\omega t} + c.c. \tag{B.16}$$

where $\mathbf{X_3}$ consists of non-secular terms coming from $\mathbf{f}(t,\tau) + c.c.$, while $\mathbf{u}$ accounts for all non-secular terms in $\mathbf{B_l}$ and $\mathbf{B_c}$. This means $\mathbf{u}$ must be a linear combination of $\mathbf{v_2}$ and $\mathbf{v_3}$:

$$\mathbf{u} = C_2(\tau)\mathbf{v_2} + C_3(\tau)\mathbf{v_3}$$

Moreover

$$\left(\frac{\partial}{\partial t} - \mathcal{J}_0\right)\mathbf{u}e^{i\omega t} = (i\omega\mathcal{I} - \mathcal{J}_0)\mathbf{u}e^{i\omega t} = (C_2\mathbf{r_2} + C_3\mathbf{r_3})e^{i\omega t} \tag{B.17}$$

where $\mathbf{r_j} = (i\omega\mathcal{I} - \mathcal{J}_0)\mathbf{v_j}$. Using this in equation (B.13) above, upon equating all potentially secular $e^{i\omega t}$ terms we obtain

$$\frac{d\phi}{d\tau}\mathbf{v_1} + C_2\mathbf{r_2} + C_3\mathbf{r_3} = (\mathbf{B_l} + \mathbf{B_c}|\phi|^2)\phi. \tag{B.18}$$

This can be regarded as a system of equations to determine the vector $(d\phi/d\tau, C_2, C_3)$. Define

$$\mathcal{M} = \begin{bmatrix} v_{1x} & r_{2x} & r_{3x} \\ v_{1y} & r_{2y} & r_{3y} \\ v_{1z} & r_{2z} & r_{3z} \end{bmatrix}$$

and let $\mathbf{s_l}$ and $\mathbf{s_c}$ be the solutions of $\mathcal{M}\mathbf{s_l} = \mathbf{B_l}$ and $\mathcal{M}\mathbf{s_c} = \mathbf{B_c}$ respectively. Then

$$\Big(d\phi/d\tau, C_2, C_3\Big)^T = (\mathbf{s_l} + |\phi|^2\mathbf{s_c})\phi\,. \tag{B.19}$$

Therefore the amplitude equation satisfied by the limit cycle is

$$\frac{d\phi}{d\tau} = (\mu + \nu|\phi(\tau)|^2)\phi(\tau)\,, \tag{B.20}$$

where $\mu = s_{lx}$ and $\nu = s_{cx}$.

Appendix C

Exact form of the fold point for helper and cytotoxic T cell model

In this appendix we derive the exact form of the fold point. This is done parametrically by finding $\tilde{\sigma}_C$ and $\bar{\sigma}_H$ as a function of the tumour population $a = N^{*\mathrm{F}}$ at the fold point. Setting $H_a = H_b$ leads to the quartic equation:

$$C_4 N^{*4} + C_3 N^{*3} + C_2 N^{*2} + C_1 N^* + C_0 = 0\,, \tag{C.1}$$

with coefficients

$$C_4 = \tilde{k}, \tag{C.2}$$

$$C_3 = -\bar{\sigma}_H + B_3; \quad B_3 = 1 - \tilde{k} - \bar{\alpha}\tilde{k}, \tag{C.3}$$

$$C_2 = (\tilde{\sigma}_C - 1) + \bar{\sigma}_H + B_2; \quad B_2 = \bar{\alpha}(\tilde{k} - 1) + \tilde{k}\tilde{N}^2, \tag{C.4}$$

$$C_1 = -\bar{\alpha}(\tilde{\sigma}_C - 1) - \tilde{N}^2\bar{\sigma}_H + B_1; \quad B_1 = (1 - \tilde{k})\tilde{N}^2, \tag{C.5}$$

$$C_0 = \tilde{N}^2(\tilde{\sigma}_C - 1) + \tilde{N}^2\bar{\sigma}_H\,. \tag{C.6}$$

For a double root which occurs at a fold point, equation (C.1) factorises as

$$(N^* - a)^2(C_4 N^{*2} + pN^* + q) = 0 \tag{C.7}$$

which can be expanded as another quartic equation. Eliminating p and q from the two quartic equations, (C.1) and (C.7), gives the following two expressions:

$$3C_4 a^4 + 2C_3 a^3 + C_2 a^2 - C_0 = 0\,, \tag{C.8}$$

$$4C_4 a^3 + 3C_3 a^2 + 2C_2 a + C_1 = 0\,. \tag{C.9}$$

Inserting the forms for C_0 to C_3 into equations (C.8) and (C.9) above allows us to determine $\bar{\sigma}_H$ and $\tilde{\sigma}_C - 1$ from the linear system:

$$(a^2 - \tilde{N}^2)(\tilde{\sigma}_C - 1) + (a^2 - \tilde{N}^2 - 2a^3)\bar{\sigma}_H = -3\tilde{k}a^4 - 2B_3 a^3 - B_2 a^2, \tag{C.10}$$

$$(2a - \bar{\alpha})(\tilde{\sigma}_C - 1) + (2a - \tilde{N}^2 - 3a^2)\bar{\sigma}_H = -4\tilde{k}a^3 - 3B_3 a^2 - 2B_2 a - B_1\,. \tag{C.11}$$

Solving these linear equations for $\bar{\sigma}_H$ and $\tilde{\sigma}_C$ provides the exact values $\bar{\sigma}_H^F$ and $\tilde{\sigma}_C^F$ at the fold point (details omitted).

Appendix D

Limit cycle for the continuous exhaustion model

D.1 Hopf bifurcation points and emergence of a limit cycle

Hopf bifurcations occur at points in parameter space where a complex conjugate pair of eigenvalues emerge with zero real part, $\lambda = \pm i\omega$ where $\omega \in \Re^+$. At such points equation (3.49) applies. We regard this as an equation for $\nu = \nu^{\text{Hopf}}(\mu)$, where $\mu = (\kappa - 1)/\xi$, with all other parameters fixed at their default values (see Table 3.3). We find ν first by substituting $T_C^* = 1 + S^*$ into equation (3.49), where $S^* = \xi N^*$ is the scaled steady state tumour population. Then using equation (3.44) for S^* this results in the following quartic equation for $C = (1 - \nu)/(1 + \mu)$,

$$g_4 C^4 + g_3 C^3 + g_2 C^2 + g_1 C + g_0 = 0\,, \tag{D.1}$$

with coefficients

$$\begin{aligned} g_0 &= s_0^2 - B^2 q_0^2, \\ g_1 &= q_0^2 + 2q_0 q_1 B^2 - 2s_0 s_1, \\ g_2 &= 2s_0 s_2 + s_1^2 - 2q_0 q_1 - B^2 q_1, \\ g_3 &= q_1^2 - 2s_1 s_2, \\ g_4 &= s_2^2\,, \end{aligned} \tag{D.2}$$

where

$$
\begin{aligned}
&2B = (2+\mu)/(1+\mu), \quad \bar{\beta} = 1+\beta, \quad \bar{\mu} = 1+\mu, \\
&p_0 = \beta(\bar{\mu}-\gamma), \quad s_0 = \bar{\beta}\beta - q_0 B, \quad q_0 = \bar{\beta}f_1 + \beta e_1 + \beta\gamma(1+\bar{\mu}) - 2Bh_0, \quad h_0 = e_1 f_1 + \beta\gamma\mu, \\
&e_1 = \bar{\mu} + \beta\mu/\bar{\mu}, \quad f_1 = \gamma(\beta/\bar{\mu} - \mu), \quad q_1 = \beta f_1 + p_0 e_1 + 2\beta\gamma\bar{\mu}, \\
&s_1 = \beta^2 + \bar{\beta}p_0 + h_0 - q_1 B, \quad s_2 = \beta p_0 \,.
\end{aligned}
\tag{D.3}
$$

For the parameters considered in this study only one root of this quartic is physically realistic. The other three roots are either complex or correspond to negative ν values. Having found C for a particular value of μ, ν is obtained from the definition

$$
\nu = \nu^{\mathrm{Hopf}}(\mu) = (1+\mu)C - 1 \,. \tag{D.4}
$$

D.2 Small amplitude form of the limit cycle

Next we conduct a weakly nonlinear analysis to derive an asymptotic solution for the limit cycle at small but finite amplitude. We start by renaming our variables as $x = \xi N$, $y = T_C$ and $z = F$, for ease of presentation.

We begin by expanding $\mathbf{x} = (x, y, z)^T$ as follows:

$$
\mathbf{x} = \mathbf{x_0} + \epsilon\mathbf{x_1}(t,\tau) + \epsilon^2\mathbf{x_2}(t,\tau) + \epsilon^3\mathbf{x_3}(t,\tau) + \ldots \,. \tag{D.5}
$$

Rewriting equations (3.41)–(3.43) and separating linear and nonlinear terms, we have

$$
\dot{x} = \gamma x - \gamma xyz \,, \tag{D.6}
$$

$$
\dot{y} = (\nu^{\mathrm{Hopf}} - \epsilon^2)z - y - \mu xyz \,, \tag{D.7}
$$

$$
\dot{z} = \beta\left(1 - z(1-x)\right) \,. \tag{D.8}
$$

Expanding nonlinear terms in equations (D.6)–(D.8), we have

$$
f = xz = \sum_{n=0}^{\infty} f_n \epsilon^n \quad \text{where} \quad f_n = \sum_{i=0}^{n} x_i z_{n-i} \,, \tag{D.9}
$$

and

$$
g = xyz = \sum_{n=0}^{\infty} g_n \epsilon^n \quad \text{where} \quad g_n = \sum_{i=0}^{n}\sum_{j=0}^{n-i} x_i y_j z_{n-i-j} \,. \tag{D.10}
$$

Note, $f_0 = x_0 z_0$ and $g_0 = x_0 y_0 z_0$. Substituting (D.9) and (D.10) into equations (D.6)–(D.8) and dropping terms of $\mathcal{O}(\epsilon^4)$ and higher leads to the following expanded

equations:

$$\epsilon\frac{\partial x_1}{\partial t}+\epsilon^2\frac{\partial x_2}{\partial t}+\epsilon^3\left(\frac{\partial x_3}{\partial t}+\frac{\partial x_1}{\partial \tau}\right)=\gamma\left(x_0-g_0+\epsilon(x_1-g_1)+\epsilon^2(x_2-g_2)+\epsilon^3(x_3-g_3)\right)\,, \tag{D.11}$$

$$\epsilon\frac{\partial y_1}{\partial t}+\epsilon^2\frac{\partial y_2}{\partial t}+\epsilon^3\left(\frac{\partial y_2}{\partial t}+\frac{\partial x_1}{\partial \tau}\right)=\nu^{\text{Hopf}}z_0-\mu g_0-y_0+\epsilon(\nu^{\text{Hopf}}z_1-\mu g_1-y_1) + \epsilon^2(\nu^{\text{Hopf}}z_2-z_0-\mu g_2-y_2)+\epsilon^3(\nu^{\text{Hopf}}z_3-z_1-\mu g_3-y_3)\,, \tag{D.12}$$

$$\epsilon\frac{\partial z_1}{\partial t}+\epsilon^2\frac{\partial z_2}{\partial t}+\epsilon^3\left(\frac{\partial z_2}{\partial t}+\frac{\partial x_1}{\partial \tau}\right)=\beta\left(1-z_0-f_0-\epsilon(z_1+f_1)-\epsilon^2(z_2+f_2)-\epsilon^3(z_3+f_3)\right)\,. \tag{D.13}$$

At leading order the equations above are satisfied by the small tumour population $\mathbf{x_0}$ at $\nu=\nu^{\text{Hopf}}$, i.e. $x_0=g_0$, $y_0=\mu g_0-\nu^{\text{Hopf}}(1-f_0)$, and $z_0=1-f_0$. At $\mathcal{O}(\epsilon)$ we recover the linear dynamics,

$$\frac{\partial \mathbf{x_1}}{\partial t}=\mathcal{J}_0\mathbf{x_1} \tag{D.14}$$

where

$$\mathcal{J}_0=\begin{pmatrix}\gamma(1-z_0y_0) & -\gamma z_0x_0 & -\gamma x_0y_0\\ -\mu y_0z_0 & -(\mu z_0x_0+1) & \nu^{\text{Hopf}}-\mu y_0x_0\\ -\beta z_0 & 0 & -\beta(x_0+1)\end{pmatrix}.$$

From the linear stability analysis, $\mathcal{J}_0\mathbf{v_m}=\lambda_m\mathbf{v_m}$ where $\lambda_1=i\omega$, $\lambda_2=\lambda_1^*=-i\omega$ and $\lambda_3<0$. Note $\mathbf{v_2}=\mathbf{v_1^*}$ while $\mathbf{v_3}$ is real. Let $\mathbf{v_m}=(v_{mx},v_{my},v_{mz})^T$ where $m=1,2,3$. The most general solution of equation (2.40) is

$$\mathbf{x_1}=\phi(\tau)\mathbf{v_1}e^{i\omega t}+\phi^*(\tau)\mathbf{v_1^*}e^{-i\omega t}+\chi(\tau)\mathbf{v_3}e^{\lambda_3 t}. \tag{D.15}$$

Here, $\phi(\tau)$ is the amplitude of the first-order (linear) mode evolving on the long time scale τ. The amplitude of the decaying mode $\chi(\tau)$ plays no role in the subsequent analysis because its non-secular. The equation for $\phi(\tau)$ is determined at $\mathcal{O}(\epsilon^3)$ by eliminating secular terms as detailed below.

Considering $\mathcal{O}(\epsilon^2)$ terms in equations (D.11)–(D.13), we obtain

$$\frac{\partial \mathbf{x_2}}{\partial t}=\mathcal{J}_0\mathbf{x_2}-(0,z_0,0)^T+\mathbf{W_2} \tag{D.16}$$

where

$$\mathbf{W_2}=-\begin{pmatrix}\gamma g_{2p}\\ \mu g_{2p}\\ \beta f_{2p}\end{pmatrix}\,, \tag{D.17}$$

$g_{2p}=x_0y_1z_1+x_1y_0z_1+x_1y_1z_0$ and $f_{2p}=x_1z_1$. Inserting $\mathbf{x_1}$ from equation (D.15) into equation (D.17) gives

$$\mathbf{W_2}=\mathbf{Q_2^a}\phi^2(\tau)e^{2i\omega t}+c.c.+\mathbf{Q_2^b}|\phi(\tau)|^2+\mathbf{Q_2^c}\phi(\tau)\chi e^{(\lambda_3+i\omega)t}+c.c.+\mathbf{Q_2^d}\chi(\tau)^2e^{2\lambda_3 t} \tag{D.18}$$

where *c.c.* denotes the complex conjugate. The secular terms arising at $\mathcal{O}(\epsilon^3)$ involve only $e^{2i\omega t}$ and 1 terms. Thus only $\mathbf{Q_2^a}$ and $\mathbf{Q_2^b}$ are needed, and they are given by

$$\mathbf{Q_2^a} = -\begin{pmatrix} \gamma\tilde{g}_{2p} \\ \mu\tilde{g}_{2p} \\ \beta\tilde{f}_{2p} \end{pmatrix} \quad ; \quad \mathbf{Q_2^b} = -\begin{pmatrix} \gamma\hat{g}_{2p} \\ \mu\hat{g}_{2p} \\ \beta\hat{f}_{2p} \end{pmatrix} \tag{D.19}$$

where

$$\begin{aligned} \tilde{g}_{2p} &= x_0 v_{1y} v_{1z} + y_0 v_{1x} v_{1z} + z_0 v_{1x} v_{1y}\,, \\ \tilde{f}_{2p} &= v_{1x} v_{1z}\,, \\ \hat{g}_{2p} &= x_0(v_{1y} v_{1z}^* + v_{1z} v_{1y}^*) + y_0(v_{1x} v_{1z}^* + v_{1z} v_{1x}^*) + z_0(v_{1x} v_{1y}^* + v_{1y} v_{1x}^*)\,, \\ \hat{f}_{2p} &= v_{1x} v_{1z}^* + v_{1z} v_{1x}^*\,. \end{aligned} \tag{D.20}$$

The solution to (D.16) for $\mathbf{x_2}$ consists of a homogeneous part which can be ignored since this is already part of $\mathbf{x_1}$, and a particular solution given by

$$\mathbf{x_2} = \mathbf{x_{20}} + \mathbf{R_2^a}\phi^2(\tau)e^{2i\omega t} + c.c. + \mathbf{R_2^b}|\phi(\tau)|^2 + \mathbf{R_2^c}\phi(\tau)\chi e^{(\lambda_3 + i\omega)t} + c.c. + \mathbf{R_2^d}\chi^2 e^{2\lambda_3 t} \tag{D.21}$$

where $\mathbf{x_{20}} = \mathcal{J}_0{}^{-1}(0, z_0, 0)^T$. Again only $\mathbf{R_2^b}$ and $\mathbf{R_2^b}$ are needed and are found by substituting (D.21) into (D.16) and equating terms with the same time dependencies:

$$\mathbf{R_2^a} = (2i\omega\mathcal{I} - \mathcal{J}_0)^{-1}\mathbf{Q_2^a} \quad ; \quad \mathbf{R_2^b} = -\mathcal{J}_0^{-1}\mathbf{Q_2^b}. \tag{D.22}$$

Finally considering terms of $\mathcal{O}(\epsilon^3)$ in expressions (D.11)–(D.13), we obtain

$$\frac{\partial \mathbf{x_3}}{\partial t} + \frac{\partial \mathbf{x_1}}{\partial \tau} = \mathcal{J}_0\mathbf{x_3} - (0, z_1, 0)^T + \mathbf{W_3} \tag{D.23}$$

where

$$\mathbf{W_3} = -\begin{pmatrix} \gamma g_{3p} \\ \mu g_{3p} \\ \beta f_{3p} \end{pmatrix}\,, \tag{D.24}$$

while $g_{3p} = x_1 y_1 z_1 + (x_1 y_2 + x_2 y_1) z_0 + (x_1 z_2 + x_2 z_1) y_0 + (y_1 z_2 + y_2 z_1) x_0$ and $f_{3p} = x_1 z_2 + x_2 z_1$.

Again the solution for $\mathbf{x_3}$ consists of a homogeneous part which can be ignored since this is already part of $\mathbf{x_1}$. The particular solution is found by solving

$$\frac{\partial \mathbf{x_3}}{\partial t} - \mathcal{J}_0\mathbf{x_3} + \frac{d\phi}{d\tau}\mathbf{v_1}e^{i\omega t} + c.c. = (\mathbf{B_l} + \mathbf{B_c}|\phi|^2)\phi e^{i\omega t} + c.c. + \mathbf{f}(t, \tau) + c.c. \tag{D.25}$$

where $\mathbf{f}(t, \tau)$ contains time dependencies other than $e^{i\omega t}$ and is therefore non-secular. The vectors $\mathbf{B_l}$ and $\mathbf{B_c}$ are given by

$$\mathbf{B_l} = -\begin{pmatrix} \gamma\tilde{g}_{3p} \\ v_{1z} + \mu\tilde{g}_{3p} \\ \beta\tilde{f}_{3p} \end{pmatrix} \quad ; \quad \mathbf{B_c} = -\begin{pmatrix} \gamma\hat{g}_{3p} \\ \mu\hat{g}_{3p} \\ \beta\hat{f}_{3p} \end{pmatrix} \tag{D.26}$$

where

$$
\begin{aligned}
\tilde{g}_{3p} &= x_0(y_{20}v_{1z} + z_{20}v_{1y}) + y_0(z_{20}v_{1x} + x_{20}v_{1z}) + z_0(y_{20}v_{1x} + x_{20}v_{1y})\,, \\
\tilde{f}_{3p} &= z_{20}v_{1x} + x_{20}v_{1z}\,, \\
\hat{g}_{3p} &= v_{1x}v_{1y}v_{1z}^* + v_{1x}v_{1y}^*v_{1z} + v_{1x}^*v_{1y}v_{1z} \\
&\quad + x_0(v_{1y}R_{2z}^b + v_{1y}^*R_{2z}^a + v_{1z}R_{2y}^b + v_{1z}^*R_{2y}^a) \\
&\quad + y_0(v_{1x}R_{2z}^b + v_{1x}^*R_{2z}^a + v_{1z}R_{2x}^b + v_{1z}^*R_{2x}^a) \\
&\quad + z_0(v_{1x}R_{2y}^b + v_{1x}^*R_{2y}^a + v_{1y}R_{2x}^b + v_{1y}^*R_{2x}^a)\,, \\
\hat{f}_{3p} &= v_{1x}^*R_{2z}^a + v_{1x}R_{2z}^b + v_{1z}^*R_{2x}^a + v_{1z}R_{2x}^b\,.
\end{aligned}
\tag{D.27}
$$

The particular solution to the above equation is

$$
\mathbf{x_3}(t,\tau) = \mathbf{X_3}(t,\tau) + \mathbf{u}(\tau)e^{i\omega t} + c.c. \tag{D.28}
$$

where $\mathbf{X_3}$ consists of non-secular terms coming from $\mathbf{f}(t,\tau) + c.c.$, while $\mathbf{u}$ accounts for all non-secular terms in $\mathbf{B_l}$ and $\mathbf{B_c}$. This means $\mathbf{u}$ must be a linear combination of $\mathbf{v_2}$ and $\mathbf{v_3}$:

$$
\mathbf{u} = C_2(\tau)\mathbf{v_2} + C_3(\tau)\mathbf{v_3}\,. \tag{D.29}
$$

The reason for proposing this form for $\mathbf{u}$ is because we have a non-normal matrix. Also note that the homogeneous solution is in the $\mathbf{v_1}$ direction and therefore we look for a particular solution in the other two eigenvector directions. Plugging in this proposed form of the particular solution for $\mathbf{x_3}$ into equation (D.23) and ignoring all non-secular terms, we obtain

$$
\left(\frac{\partial}{\partial t} - \mathcal{J}_0\right)\mathbf{u}e^{i\omega t} = (i\omega\mathcal{I} - \mathcal{J}_0)\mathbf{u}e^{i\omega t} = (C_2\mathbf{r_2} + C_3\mathbf{r_3})e^{i\omega t} \tag{D.30}
$$

where $\mathbf{r_j} = (i\omega\mathcal{I} - \mathcal{J}_0)\mathbf{v_j}$. Using this in equation (D.25) above and equating all potentially secular terms proportional to $e^{i\omega t}$ we obtain,

$$
\frac{d\phi}{d\tau}\mathbf{v_1} + C_2\mathbf{r_2} + C_3\mathbf{r_3} = (\mathbf{B_l} + \mathbf{B_c}|\phi|^2)\phi. \tag{D.31}
$$

This can be regarded as a system of equations to determine the vector $(d\phi/d\tau, C_2, C_3)^T$. Define

$$
\mathcal{M} = \begin{pmatrix} v_{1x} & r_{2x} & r_{3x} \\ v_{1y} & r_{2y} & r_{3y} \\ v_{1z} & r_{2z} & r_{3z} \end{pmatrix}
$$

and let $\mathbf{s_l}$ and $\mathbf{s_c}$ be the solutions of $\mathcal{M}\mathbf{s_l} = \mathbf{B_l}$ and $\mathcal{M}\mathbf{s_c} = \mathbf{B_c}$ respectively. Then

$$
\Big(d\phi/d\tau, C_2, C_3\Big)^T = (\mathbf{s_l} + |\phi|^2\mathbf{s_c})\phi.
$$

The first component of this vector gives the desired amplitude equation, namely

$$\frac{d\phi}{d\tau} = (\eta + \zeta|\phi(\tau)|^2)\phi(\tau) \tag{D.32}$$

where $\eta = s_{lx}$ and $\zeta = s_{cx}$.

D.3 Disappearance

As ν decreases the amplitude of the limit cycle increases ultimately without bound and disappears at an infinite Homoclinic orbit of the tumour-free state. We next describe the form of the limit cycle in this large amplitude limit. In particular we focus on the behaviour for $S = \xi N$, T_C and F near the vicinity of the peak of the limit cycle.

We illustrate what happens just before the limit cycle disappears by considering a value of $\nu = 0.66$ with all remaining parameters fixed at their default values given in Table 3.3. We initialise the simulation close to the tumour-free state, taking $T_C(0) = \nu$ and $F(0) = 1$ and perturb $S(0)$ to 0.01. The time evolution of the variables and particular combinations of them are shown in Figure D.1, focusing on the time near the peak amplitude in T_C (blue curve). The T_C population is seen to sharply peak near $t = 30$ though the zoom in (b) shows the peak is well resolved in time. Similarly F shows a rapid decrease at the same time T_C begins to decrease, and in fact F closely tracks the T_C population at this stage. The tumour population (black curve) peaks more than a unit of time before the peak in T_C and is essentially zero by the time T_C reaches its maximum and thereafter remains $\ll 1$. This behaviour then repeats periodically on a long time scale as a limit cycle oscillation (not shown).

The case illustrated above is used to motivate scaling the variables near the peak in T_C to describe asymptotically the behaviour near the peaks in both S and T_C. The zoom in panel (b) indicates there are two time scales. A slow time scale for the peaks to build up ($\sim \omega^{-1}$), followed by a relatively rapid time scale for them to diminish. We also see in panel (c) that the product FS is practically a step function going from 1 to 0 through the peak in T_C. In panel (d) we show the product FT_C since it is directly related to the increase or decrease of S: when $FT_C < 1$ then $dS/dt > 0$ from equation (3.41) and when $FT_C > 1$ then $dS/dt < 0$.

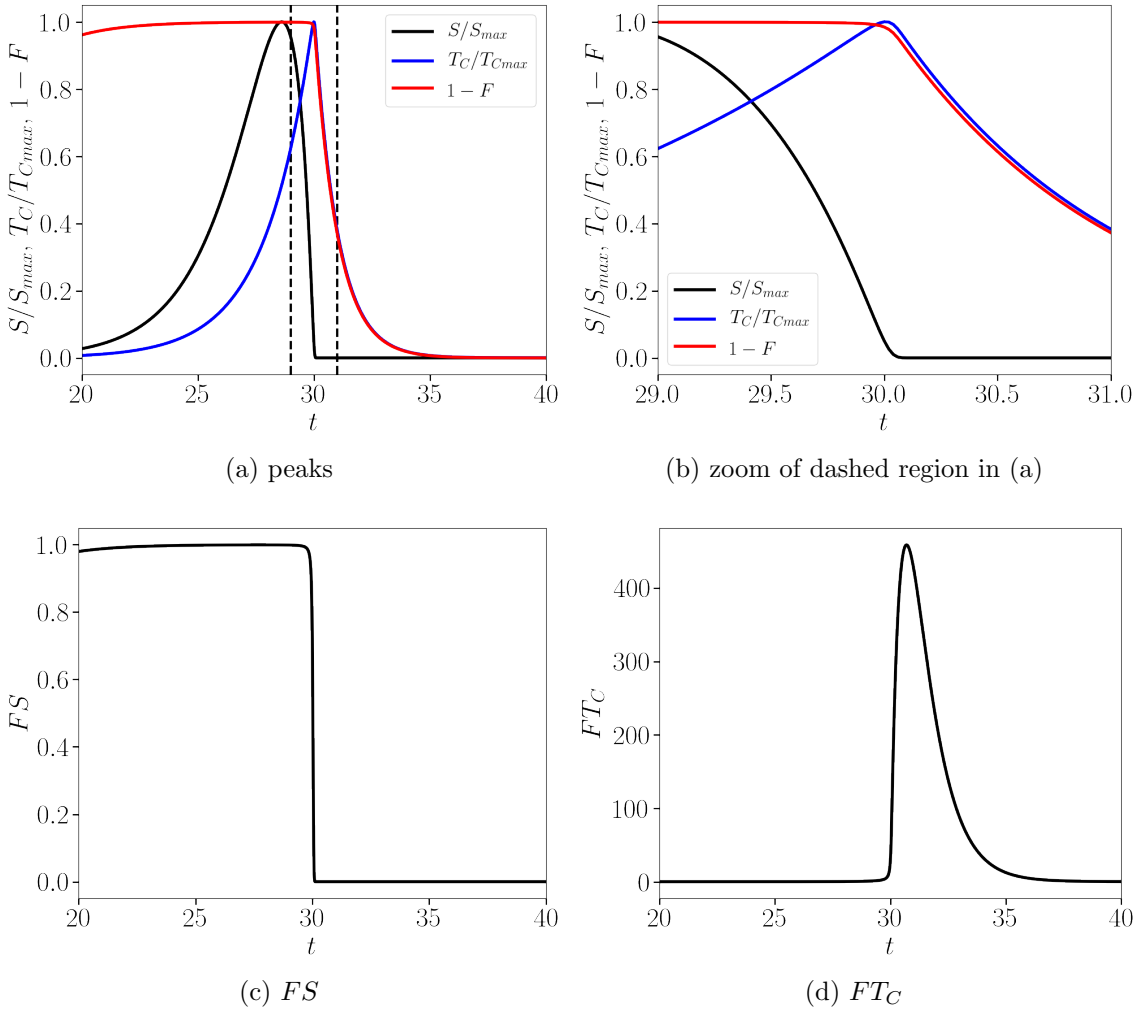

(a) peaks

(b) zoom of dashed region in (a)

(c) FS

(d) FT_C

Figure D.1: Time evolution arising from equations (3.41)–(3.43) centred about a peak of the stable limit cycle for $\nu = 0.66$ where a stable limit solution exists, and all remaining parameters fixed to their default values. Initially, $S(0) = 0.01$, $T_C(0) = \nu = 0.66$ and $F(0) = 1$. In (a) we show the scaled tumour and cytotoxic T cell populations, $S/S_{\max}$ (black curve) and $T_C/T_{C,\max}$ (blue curve), and one minus the functionality, $1 - F$ (red curve). In (b) we show a zoom of the region centred about the peak in T_C (blue curve) delineated by the two vertical dashed lines in (a). In (c) we show how the product of the functionality and the scaled tumour population, FS, evolves about the peak of the limit cycle. In (d) we show how the product of the functionality and the cytotoxic T cell population, FT_C, evolves about the peak of the limit cycle.

To better understand the time scale of the delay between the peaks in S and T_C, in Figure D.2 we show that this time difference tends to a constant as $\nu \to \nu^{\text{Hom}}$, where ν^{Hom} is value of ν for which the limit cycle ceases to exist (note for $\mu = -1.5$, $\nu^{\text{Hom}} \approx 0.6593$). As long as $\nu > \nu^{\text{Hom}}$, S reaches a maximum and decreases before T_C

reaches its maximum (see Figure D.1 (b)). For $\nu < \nu^{\text{Hom}}$, the limit cycle no longer exists and S instead diverges to infinity.

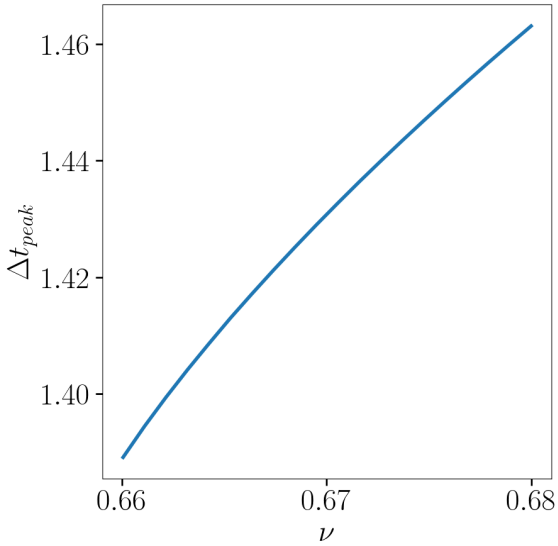

Figure D.2: Time difference Δt_{peak} between the peaks in S and T_C (black and blue curves in Figure D.1 (a)) over the range of ν values for which a limit cycle exists given the default parameters (see Table 3.3).

These observations from Figures D.1 and D.2 allow us to identify three significant times in the limit cycle evolution:

- t_0 = a time in which S is growing (e.g. $t_0 = 20$ in Figure D.1),
- t_1 = the time at which S reaches a maximum ($t_1 \approx 28.6$),
- t_2 = the time at which T_C reaches a maximum ($t_2 \approx 30.0$).

We next use the three times to develop an asymptotic approximation to the forms of $S(t)$, $T_C(t)$ and $F(t)$ near the peak in T_C.

D.3.1 To the left of the peak in T_C

To determine the leading order behaviour of the populations to the left of the peak in T_C we appeal to Figure D.1. From panel (a) we observe that $F \ll 1$ to the left of the peak in T_C. From panel (c) we observe that in this region, $FS \approx 1$ and therefore we infer that $S \gg 1$. By a similar argument, it follows that $T_C \gg 1$ (see panel (d)).

Taking $S \gg 1$, $T_C \gg 1$ and $F \ll 1$, and keeping only leading order terms, equations (3.41)–(3.43) simplify to

$$\frac{dS}{dt} \approx \gamma(S - T_C)\,, \tag{D.33}$$

$$\frac{dT_C}{dt} \approx -(\mu+1)T_C\,, \tag{D.34}$$

$$\frac{dF}{dt} \approx \beta(1-FN) \approx 0\,. \tag{D.35}$$

Equation (D.33) describes the evolution of S to the left of the peak. In this region S grows provided $S > T_C$ and decays when T_C exceeds S. As limit cycle solutions only emerge for $\mu < -1.27$ (see Figure 3.9), equation (D.34) describes the exponential growth of T_C here. Equation (D.35) reduces to an algebraic equation at leading order, giving the relationship $F \approx 1/S$, consistent with our numerical observations (see Figure D.1 (c)).

Analytical expressions for S and T_C and consequently F can be determined in this region. Equation (D.34) can be solved directly for T_C giving

$$T_C(t) = T_{CI}e^{-(\mu+1)(t-t_0)}\,, \tag{D.36}$$

where $T_{CI} = T_C(t_0)$. Using the solution for T_C in equation (D.33) we obtain the following solution for S:

$$S(t) = \left(S_I - \frac{\gamma T_{CI}}{\gamma+\mu+1}\right)e^{\gamma(t-t_0)} + \frac{\gamma T_{CI}}{\gamma+\mu+1}e^{-(\mu+1)(t-t_0)}\,, \tag{D.37}$$

where $S_I = S(t_0)$.

At the peak in S, $dS/dt = 0$ at some time $t = t_1$. This occurs when $S(t_1) = T_C(t_1)$:

$$e^{(\gamma+\mu+1)(t_1-t_0)} = \frac{-(\mu+1)T_{CI}}{\gamma T_{CI} - (\gamma+\mu+1)S_I}\,, \tag{D.38}$$

which gives us an expression for the time, t_1, where we reach the maximum in S. Provided S reaches a maximum, the trajectory remains on the stable limit cycle. However, if a maximum is not reached then the tumour population escapes. This tells us something about our initial conditions in S and T_C and how the limit cycle terminates. That is, provided

$$\frac{S_I}{T_{CI}} < \frac{\gamma}{\gamma+\mu+1}\,, \tag{D.39}$$

T_C will eventually overtake S, forcing S to reach a maximum before collapsing. If this inequality is breached, the system escapes ($S, T_C \to \infty$ and $F \to 0$).

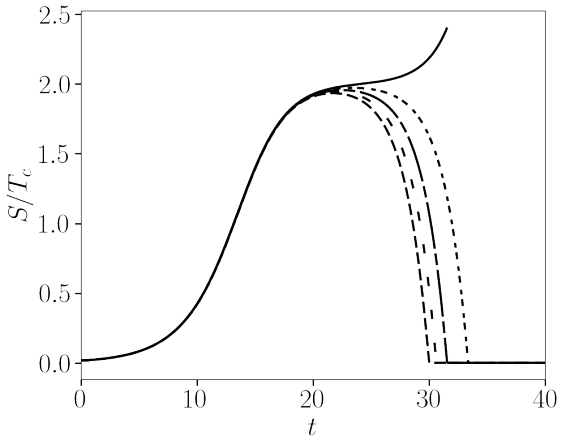

Figure D.3: Time evolution of $S(t)$, $T_C(t)$ and $F(t)$ from equations (3.41)–(3.43) of the ratio of the (scaled) tumour and cytotoxic T cell population, S/T_C, for five values of ν (distinguished by linestyle) about $\nu^{\text{Hom}} \approx 0.6593$ with all other parameters fixed at their default values (see Table 3.3). Here we initialise the system about the tumour-free state $(S(0), T_C(0), F(0)) = (0.01, \nu, 1.0)$ considering $\nu = 0.66$ (short dashes), $\nu = 0.6598$ (spaced dots), $\nu = 0.6596$ (dashed dots), $\nu = 0.6594$ (dots) and $\nu = 0.6592$ (solid curve).

Figure D.3 confirms that if the inequality given by equation (D.39) is breached, we lose the limit cycle and instead escape to infinity. For the parameters taken in the above simulation, the ratio $\gamma/(\gamma + \mu + 1) = 2$ and therefore, provided the ratio S/T_C lies below this value for a given value of ν, we remain on the limit cycle. Here decreasing ν towards ν^{Hom} increases the peak of the curve closer to the critical value of 2, eventually breaching this condition when $\nu < 0.6593$ (see solid curve).

D.3.2 After the peak in T_C

Following the peak in T_C, the appropriate scalings for S, T_C and F can be deduced from Figure D.1. The close tie between $1 - F$ (red curve) and $T_C/T_{C,\max}$ (blue curve) is seen in panel (a) where the two curves overlay one and other. In this region we see that $S \approx 0$ (see panels (a)–(c)) which simplifies equations (3.41)–(3.43) to

$$\frac{dT_C}{dt} \approx \nu F - T_C \,, \tag{D.40}$$

$$\frac{dF}{dt} \approx \beta(1 - F) \,, \tag{D.41}$$

which provide expressions for F and T_C to the right of the peak in T_C.

Using an integrating factor, equation (D.41) is solved directly giving

$$F = 1 - (1 - F_0)e^{-\beta(t - t_2)} \,, \tag{D.42}$$

where $F_0 = F(t_2)$. Substituting equation (D.42) for F into equation (D.40) we see that T_C evolves according to

$$\frac{dT_C}{dt} = \nu - \nu(1 - F_0)e^{-\beta(t-t_2)} - T_C\,, \tag{D.43}$$

which has two solutions depending on the value of β. Specifically,

$$T_C = \begin{cases} \nu + P_0 e^{-(t-t_2)} + P_1 e^{-\beta(t-t_2)}, & \text{if} \quad \beta \neq 1 \\ \nu + Q_0 e^{-(t-t_2)} + Q_1 t e^{-(t-t_2)}, & \text{if} \quad \beta = 1\,. \end{cases} \tag{D.44}$$

where P_0 and Q_0 are constants of integration and

$$P_1 = -\frac{\nu(1 - F_0)}{1 - \beta} \quad \text{and} \quad Q_1 = -\nu(1 - F_0)\,. \tag{D.45}$$

The constants of integration P_0 and Q_0 are determined from the value of T_C at the peak, $T_C(t_2) = T_{C,\max}$. That is, taking $t = t_2$ and $T(t_2) = T_{C,\max}$ in equation (D.44) gives

$$P_0 = T_{C,\max} - \nu - P_1 \quad \text{and} \quad Q_0 = T_{C,\max} - \nu - Q_1 t_2\,. \tag{D.46}$$

In summary, in the region to the right of the peak in T_C where $N \approx 0$, the cytotoxic T cell population T_C, and the functionality F, can be expressed as:

$$T_C = \begin{cases} \nu + P_0 e^{-(t-t_2)} - \frac{\nu(1-F_0)}{1-\beta} e^{-\beta(t-t_2)}, & \text{if} \quad \beta \neq 1 \\ \nu + Q_0 e^{-(t-t_2)} - \nu(1 - F_0) t e^{-(t-t_2)}, & \text{if} \quad \beta = 1\,, \end{cases} \tag{D.47}$$

$$F = 1 - (1 - F_0)e^{-\beta(t-t_2)}\,. \tag{D.48}$$

where P_0 and Q_0 are given in equation (D.46).

D.3.3 In the vicinity of the peak in T_C

We next deduce expressions for S, T_C and F near the peak in T_C. Figure D.1 (b) shows that the behaviour of the populations close to the peak in T_C occurs on a fast timescale

$$\tau = (t - t_2)/\epsilon^p\,, \tag{D.49}$$

where t_2 is the time at which the peak in T_C is reached, $\epsilon \ll 1$ and $p > 0$. To obtain the leading order scaling, we again appeal to Figure D.1 (b) where we observe that S, $T_C \gg 1$ with $S < T_C$, and $F \ll 1$. From these observations, the following expansions for S, T_C and F are assumed

$$S = \epsilon^{-1} S_0(\tau) + S_1(\tau) + \ldots \tag{D.50}$$

$$T_C = \epsilon^{-2} T_0(\tau) + \epsilon^{-1} T_1(\tau) + \dots \tag{D.51}$$

$$F = \epsilon F_0(\tau) + \epsilon^2 F_1(\tau) + \dots \tag{D.52}$$

The scaling exponent p is deduced by matching both sides of equation (3.41) at leading order:

$$\epsilon^{-(p+1)} \frac{dS_0}{d\tau} = -\gamma \epsilon^{-2} S_0 F_0 T_0 \,, \tag{D.53}$$

requiring $p = 1$. Therefore, in this region $\tau = (t - t_2)\epsilon^{-1}$. At the lowest non-trivial order equations (3.41)–(3.43) take the form

$$\frac{dS_0}{d\tau} = -\gamma S_0 F_0 T_0 \,, \tag{D.54}$$

$$\frac{dT_0}{d\tau} = 0, \quad \frac{dT_1}{d\tau} = -\mu S_0 F_0 T_0 - T_0 \,, \tag{D.55}$$

$$\frac{dF_0}{d\tau} = \beta(1 - F_0 S_0) \,. \tag{D.56}$$

Therefore we learn that T_0 is a constant (to be determined below). Eliminating $F_0 S_0$ in equations (D.54) and (D.56) we get

$$\beta \frac{dS_0}{d\tau} - \gamma T_0 \frac{dF_0}{d\tau} = -M \,, \tag{D.57}$$

where $M = \beta\gamma T_0$, a constant. We can integrate with respect to τ to get an expression for S_0:

$$\beta S_0 = \gamma T_0 F_0 - M\tau + C_0 \,, \tag{D.58}$$

where C_0 is an arbitrary constant of integration. Likewise, T_1 can be obtained by combining equations (D.55) and (D.56) to give

$$\beta\gamma T_1 = \frac{\mu}{\beta} F_0 - (\mu + 1)\tau + C_1 \,, \tag{D.59}$$

where C_1 is another constant of integration. Using expression (D.58) in equation (D.56) gives us an equation describing the leading order evolution of F,

$$\frac{dF_0}{d\tau} = \beta + (M\tau - C_0)F_0 - \gamma T_0 F_0^2 \,. \tag{D.60}$$

This is a Riccati equation which has the general form

$$\frac{dy}{dx} = q_0(x) + q_1(x)y(x) + q_2(x)y^2(x) \,, \tag{D.61}$$

which can be reduced to a second order linear equation of the form

$$u'' - R_1(x)u' + R_0(x)u = 0 \,, \tag{D.62}$$

where $u'/u = -yq_2$, $R_0 = q_2 q_0$ and $R_1 = q_1 + q_2'/q_2$. In our notation we have, $y = F_0$, $x = \tau$, $q_0 = \beta$, $q_1 = M\tau - C_0$ and $q_2 = -\gamma T_0$. Here $R_0 = -M$ and $R_1 = M\tau - C_0$, and therefore equation (D.60) may be re-expressed as the following second-order linear differential equation:

$$u'' - (M\tau - C_0)u' - Mu = 0\,. \tag{D.63}$$

Taking $z = M^{1/2}(\tau - C_0/M)$ reduces equation (D.63) to the following parameter free equation:

$$\frac{d^2u}{dz^2} - z\frac{du}{dz} - u = 0\,. \tag{D.64}$$

This is a second-order differential equation with non-constant coefficients. By inspection one solution to equation (D.64) is

$$u = e^{z^2/2}\,. \tag{D.65}$$

The constant of proportionality (here taken to be one) does not matter since the solution we seek is $F_0 = u'/(u\gamma T_0)$. The other solution has the form $u = e^{z^2/2}w(z)$, where $w(z)$ is a function of z which is determined by substitution into equation (D.64), leading to

$$\frac{dw}{dz} = e^{-z^2/2} \quad \Rightarrow \quad w(z) = \sqrt{\frac{\pi}{2}}\mathrm{erfc}(z/\sqrt{2})\,, \tag{D.66}$$

taking the arbitrary but convenient scaling $\sqrt{\pi/2}$ in the solution. Therefore the most general solution for u satisfying equation (D.64) consists of a linear combination of the above two solutions:

$$u = e^{z^2/2}\left(A_1 + A_2\sqrt{\frac{\pi}{2}}\mathrm{erfc}\left(\frac{z}{\sqrt{2}}\right)\right) \tag{D.67}$$

where A_1 and A_2 are arbitrary constants. Recall the solution to the Riccati equation for F_0 is related to u as follows

$$\hat{F} \doteq \gamma T_0 F_0 = \frac{u'}{u}\,. \tag{D.68}$$

We choose the ratio A_1/A_2 such that the following conditions are satisfied to the left and right of the peak in T_C:

$$\begin{aligned} z \ll -1: &\quad \text{left of peak} \quad \Rightarrow \quad \hat{F} \to 0, \\ z \gg 1: &\quad \text{right of peak} \quad \Rightarrow \quad \hat{F} \propto z\,. \end{aligned} \tag{D.69}$$

First consider the solution for F_0 to the right of the peak in T_C where $z \gg 1$. In this limit we can approximate the complimentary error function, erfc, by the Taylor series expansion

$$\mathrm{erfc}(z/\sqrt{2}) = \sqrt{\frac{2}{\pi}}\frac{e^{-z^2}}{z}\left(1 - \frac{1}{z^2} + \ldots\right)\,. \tag{D.70}$$

Using this expression in equation (D.67), we obtain

$$u = A_1 e^{z^2/2} + A_2(z^{-1} - z^{-3} + \dots) \approx A_1 e^{z^2/2}\,. \tag{D.71}$$

Substituting this expression for u in equation (D.68) gives $\hat{F} = z$.

Now consider the solution for F_0 to the left of the peak in T_C where $z \ll -1$ where erfc is again expanded as a Taylor series:

$$\begin{aligned} \mathrm{erfc}(z/\sqrt{2}) &= 2 - \mathrm{erfc}\underbrace{(-z/\sqrt{2})}_{+\mathrm{ve}} \\ &= 2 + \sqrt{\frac{2}{\pi}}\frac{e^{-z^2}}{z}\left(1 - \frac{1}{z^2} + \dots\right) < 2\,. \end{aligned} \tag{D.72}$$

Therefore when $z \ll -1$, u may be approximated by

$$u = (A_1 + \sqrt{2\pi}A_2)e^{z^2/2} + A_2(z^{-1} - z^{-3} + \dots)\,. \tag{D.73}$$

One of the restrictions required is $F_0 > 0$ which only holds provided $A_1 + \sqrt{2\pi}A_2 = 0$. This follows because the derivative of $e^{z^2/2}$ divided by $e^{z^2/2}$ itself is z which is less than zero in this region. Hence the ratio

$$\frac{A_1}{A_2} = -\sqrt{2\pi}\,. \tag{D.74}$$

Therefore to left of the peak, in the limit $z \ll -1$, $\hat{F} = -z^{-1}$. This solution must be greater than zero which requires $C_0 > 0$ in the definition $z = M^{1/2}(\tau - C_0/M)$ (as $\tau < 0$). On the other hand, the solution for $z \gg 1$ is positive provided $C_0 < 0$. Hence for both of these to be true C_0 must be identically zero.

About the peak in T_C we have obtained an exact solution for the leading order solution of the functionality, F_0, which allows us to determine the solutions for S_0 and T_1 from equations (D.54) and (D.55). Using the relationship between A_1 and A_2 found above and taking $A_1 = 1$ (w.l.o.g.) we find $A_2 = -1/\sqrt{2\pi}$ and therefore

$$u = e^{z^2/2}\left(1 - \frac{1}{2}\mathrm{erfc}\left(\frac{z}{\sqrt{2}}\right)\right) \tag{D.75}$$

Using this in equation (D.68), we obtain the leading order approximation for F about the peak in T_C:

$$F_0 = \frac{1}{\gamma T_0}\frac{z(1 - \frac{1}{2}\mathrm{erfc}(z/\sqrt{2})) + \frac{1}{\sqrt{2\pi}}e^{-z^2/2}}{1 - \frac{1}{2}\mathrm{erfc}(z/\sqrt{2})}\,. \tag{D.76}$$

The constant T_0 is determined by matching equation (D.76) to the solution for F_0 to the right of the peak in T_C. Here we use equation (D.76) in the limit $z \gg 1$, i.e.

$\tau \gg 1$. Then $F_0 \approx z/(\gamma T_0)$ where $z = M^{1/2}\tau$ and $M = \beta\gamma T_0$, which can be written in our original variables as follows

$$F_0 = \sqrt{\frac{\beta}{\gamma T_0}}\tau \quad \Rightarrow \quad F = \sqrt{\frac{\beta}{\gamma T_0}}(t - t_2)\,, \tag{D.77}$$

to leading order using $\tau = (t - t_2)/\epsilon$. This is consistent with our numerical results presented in Figure D.1 (b) where we see that to the right of the peak in T_C, F scales linearly with time. To determine the constant T_0 we match the solution above near the peak with that to the right of the peak in the limit $t - t_2 \ll 1$. Consider equation (D.48) which describes the solution of F to the left of the peak in T_C. We must take $F_0 = 0$ so that the leading order term in the Taylor series expansion for F is zero at $t = t_2$ (e.g. $F(t_2) = 0$). Near $t = t_2$ we can linearise the equation for F as follows

$$F = \beta(t - t_2) + H.O.T. \tag{D.78}$$

which we equate with the solution at the peak given in equation (D.77). This determines T_0 as follows:

$$T_0 = \frac{1}{\beta\gamma}\,. \tag{D.79}$$

Furthermore, this implies $M = \beta\gamma T_0 = 1$. Using T_0, the expressions for S_0 and T_1 near the peak in T_C:

$$S_0 = \frac{F_0}{\beta^2} - \tau\,, \tag{D.80}$$

and

$$T_1 = \frac{1}{\beta\gamma}\left(\frac{\mu}{\beta}F_0 - (\mu + 1)\tau\right)\,. \tag{D.81}$$

where the exact solution for F_0 near the peak is given by equation (D.76).

To summarise, we have found the exact solutions for the leading order approximations for S, T_C and F about the peak in T_C in terms of known parameters. The equations describing S, T_C and F in the vicinity of the peak are:

$$F = \epsilon F_0 = \epsilon\beta\frac{z\left(1 - \frac{1}{2}\mathrm{erfc}(z/\sqrt{2})\right) + \frac{1}{\sqrt{2\pi}}e^{-z^2/2}}{1 - \frac{1}{2}\mathrm{erfc}(z/\sqrt{2})}\,. \tag{D.82}$$

$$S = \epsilon^{-1}S_0 = \epsilon^{-1}\left(\frac{F_0}{\beta^2} - \tau\right) \tag{D.83}$$

$$T_C = \epsilon^{-2}T_0 + \epsilon^{-1}T_1 = \frac{1}{\beta\gamma}\left(\epsilon^{-2} + \epsilon^{-1}\left(\frac{\mu F_0}{\beta} - (\mu + 1)\tau\right)\right) \tag{D.84}$$

To constrain the solution fully we need to determine the value of ϵ used in the above scaling. This is done by calculating the unknown parameters associated with

the solutions to the left of the peak in T_C. Determining ϵ relies on the full nonlinear dynamics but can be found from the observed numerical value of $T_{C,\max}$.

Let us first return to the equations describing the evolution of S and T_C to the left of $T_{C,\max}$ about $t = t_2$. Equations (D.33) and (D.34) can be solved generally with solutions

$$T_C = B_1 e^{\gamma(t-t_2)}\,, \tag{D.85}$$

and

$$S = B_2 e^{\gamma(t-t_2)} + \frac{\gamma B_1}{\gamma+\mu+1} e^{-(\mu+1)(t-t_2)}\,, \tag{D.86}$$

where B_1 and B_2 are unknown constants of integration. We can determine a relationship between B_1 and B_2 by noting that at $t = t_2$, $S \approx 0$ (see black curve panel (a) of Figure D.1). Setting $S = 0$ at $t = t_2$ in equation (D.86) we get

$$B_2 = \frac{-\gamma B_1}{\gamma+\mu+1}\,. \tag{D.87}$$

Now we only have one unknown constant to determine here. Close to the peak, where $t - t_2 \ll 1$, we can expand equation (D.85) as a Taylor series about $t = t_2$:

$$T_C = B_1\left(1 + \gamma(t-t_2) + \dots\right)\,. \tag{D.88}$$

As $t - t_2 \ll 1$, we only need to match the leading order solution to the approximation for T_C at the peak giving

$$B_1 = T_C(t_2)\,. \tag{D.89}$$

Hence both B_1 and B_2 are determined by $T_C(t_2)$.

The remaining task is to determine ϵ using the actual value of T_C at t_2 together with its asymptotic approximation at $\tau = 0$. This implies that ϵ is determined by

$$T_C(t_2) = \frac{1}{\beta\gamma\epsilon^2}\,. \tag{D.90}$$

For the parameters taken in our model at $\nu = 0.66$, we find that $T_C(t_2) \approx 1782.35$ implying $\epsilon \approx 0.0237$.

In Section 3.7.3 we confirm this analysis against the full numerical results in Figure 3.16.

Appendix E

Derivation of the tumour equilibrium steady states in the T cell exhaustion model

Here we provide details for the algebra leading to equation (4.28) which provides the possible steady state populations of N_R^*. We start by substituting equation (4.26) for $T_C^*(N_R^*)$ into equation (4.21). This results in

$$(b_0 + b_1 N_R^*)N^* = (1 + N^{*2})(g_0 + g_1 N_R^* + g_2 N_R^{*2}) \,, \tag{E.1}$$

where $g_0 = (b_0 - \sigma c_0)/\alpha$, $g_1 = (b_0\nu + b_1 - \sigma c_1)/\alpha$ and $g_2 = b_1\nu/\alpha$. Next replacing $N^*(N_R^*)$ above using equation (4.27), we obtain

$$N_R^*(b_0 + b_1 N_R^*)(e_0 + e_1 N_R^*)(f_0 + f_1 N_R^*) = \tag{E.2}$$

$$(h_0 + h_1 N_R^* + h_2 N_R^{*2} + h_3 N_R^{*3} + h_4 N_R^{*4})(g_0 + g_1 N_R^* + g_2 N_R^{*2}) \,, \tag{E.3}$$

where $h_0 = f_0^2$, $h_1 = 2f_0 f_1$, $h_2 = f_1^2 + e_0^2$, $h_3 = 2e_0 e_1$ and $h_4 = e_1^2$. Expanding out the above expression yields a sixth order equation of the form with coefficients

$$m_0 = h_0 g_0 \,, \tag{E.4}$$

$$m_1 = h_0 g_1 + h_1 g_0 - b_0 e_0 f_0 \,, \tag{E.5}$$

$$m_2 = h_0 g_2 + h_1 g_1 + h_2 g_0 - b_0 e_0 f_1 - b_1 e_0 f_0 \,, \tag{E.6}$$

$$m_3 = h_1 g_2 + h_2 g_1 + h_3 g_0 - b_0 e_1 f_1 - b_1 e_0 f_1 - b_1 e_1 f_0 \,, \tag{E.7}$$

$$m_4 = h_2 g_2 + h_3 g_1 + h_4 g_0 - b_1 e_1 f_1 \,, \tag{E.8}$$

$$m_5 = h_3 g_2 + h_4 g_1 \,, \tag{E.9}$$

$$m_6 = h_4 g_2 \,. \tag{E.10}$$

Bibliography

[1] J. Adam and N. Bellomo. *A survey of models for tumor-immune system dynamics*. Springer Science & Business Media, 2012.

[2] I. Akhmetzyanova, G. Zelinskyy, S. Schimmer, S. Brandau, P. Altenhoff, T. Sparwasser, and U. Dittmer. Tumor-specific CD4+ T cells develop cytotoxic activity and eliminate virus-induced tumor cells in the absence of regulatory T cells. *Cancer Immunology, Immunotherapy*, 62(2):257–271, 2013.

[3] M. Al-Tameemi, M. Chaplain, and A. d'Onofrio. Evasion of tumours from the control of the immune system: consequences of brief encounters. *Biology Direct*, 7:31, 2012.

[4] D. Alemani, F. Pappalardo, M. Pennisi, S. Motta, and V. Brusic. Combining cellular automata and lattice Boltzmann method to model multiscale avascular tumor growth coupled with nutrient diffusion and immune competition. *Journal of Immunological Methods*, 376(1):55–68, 2012.

[5] H.R. Ali, L. Chlon, P.D.P. Pharoah, F. Markowetz, and C. Caldas. Patterns of immune infiltration in breast cancer and their clinical implications: A gene-expression-based retrospective study. *PLoS Medicine*, 13(12):e1002194, 2016.

[6] P.M. Altrock, L.L. Liu, and F. Michor. The mathematics of cancer: integrating quantitative models. *Nature Reviews Cancer*, 15(12):730–745, 2015.

[7] A.C. Anderson, N. Joller, and V.K. Kuchroo. Lag-3, Tim-3, and TIGIT: co-inhibitory receptors with specialized functions in immune regulation. *Immunity*, 44(5):989–1004, 2016.

[8] A.R.A. Anderson. A hybrid mathematical model of solid tumour invasion: the importance of cell adhesion. *Mathematical medicine and biology: a journal of the IMA*, 22(2):163–186, 2005.

[9] A.R.A. Anderson, C.J. Tomlin, J. Couch, and D. Gallahan. Mathematics of the integrative cancer biology program. *Interface Focus*, 3(4), 2013.

[10] A.R.A. Anderson, A.M. Weaver, P.T. Cummings, and V. Quaranta. Tumor morphology and phenotypic evolution driven by selective pressure from the microenvironment. *Cell*, 127(5):905–915, 2006.

[11] R.M. Anderson and R.M. May. Coevolution of hosts and parasites. *Parasitology*, 85(02):411–426, 1982.

[12] J.C. Arciero, T.L. Jackson, and D.E. Kirschner. A mathematical model of tumor-immune evasion and siRNA treatment. *Discrete and Continuous Dynamical Systems Series B*, 4(1):39–58, 2004.

[13] L. Arlotti, N. Bellomo, and E. De Angelis. Generalized kinetic (Boltzmann) models: mathematical structures and applications. *Mathematical Models and Methods in Applied Sciences*, 12(04):567–591, 2002.

[14] J. Attanasio and E.J. Wherry. Costimulatory and coinhibitory receptor pathways in infectious disease. *Immunity*, 44(5):1052–1068, 2016.

[15] M. Baar, L. Coquille, H. Mayer, M. Hölzel, M. Rogava, T. Tüting, and A. Bovier. A stochastic model for immunotherapy of cancer. *Scientific reports*, 6, 2016.

[16] M. Bacac, T. Fauti, J. Sam, S. Colombetti, T. Weinzierl, D. Ouaret, W. Bodmer, S. Lehmann, T. Hofer, R.J. Hosse, et al. A novel carcinoembryonic antigen T-cell bispecific antibody (CEA TCB) for the treatment of solid tumors. *Clinical Cancer Research*, 22(13):3286–3297, 2016.

[17] C. Badoual, S. Hans, J. Rodriguez, S. Peyrard, C. Klein, N.E.H. Agueznay, V. Mosseri, O. Laccourreye, P. Bruneval, W. Fridman, et al. Prognostic value of tumor-infiltrating CD4+ T-cell subpopulations in head and neck cancers. *Clinical Cancer Research*, 12(2):465–472, 2006.

[18] C. Bauer, B. Kühnemuth, P. Duewell, S. Ormanns, T. Gress, and M. Schnurr. Prevailing over T cell exhaustion: New developments in the immunotherapy of pancreatic cancer. *Cancer letters*, 2016.

[19] N. Bellomo and M. Delitala. From the mathematical kinetic, and stochastic game theory to modelling mutations, onset, progression and immune competition of cancer cells. *Physics of Life Reviews*, 5(4):183–206, 2008.

[20] N. Bellomo and G. Forni. Dynamics of tumor interaction with the host immune system. *Mathematical and computer modelling*, 20(1):107–122, 1994.

[21] N. Bellomo and L. Preziosi. Modelling and mathematical problems related to tumor evolution and its interaction with the immune system. *Mathematical and Computer Modelling*, 32(3-4):413–452, 2000.

[22] A. Besse, G.D. Clapp, S. Bernard, F.E. Nicolini, D. Levy, and T. Lepoutre. Stability analysis of a model of interaction between the immune system and cancer cells in chronic myelogenous leukemia. *Bulletin of Mathematical Biology*, pages 1–27, 2017.

[23] C.U. Blank, J.B. Haanen, A. Ribas, and T.N. Schumacher. The cancer immunogram. *Science*, 352(6286):658–660, 2016.

[24] I. Bozic, T. Antal, H. Ohtsuki, H. Carter, D. Kim, S. Chen, R. Karchin, K.W. Kinzler, B. Vogelstein, and M.A. Nowak. Accumulation of driver and passenger mutations during tumor progression. *Proceedings of the National Academy of Sciences*, 107(43):18545–18550, 2010.

[25] R.M. Bremnes, L.T. Busund, T.L. Kilvær, S. Andersen, E. Richardsen, E.E. Paulsen, S. Hald, M.R. Khanehkenari, W.A. Cooper, S.C. Kao, et al. The role of tumor-infiltrating lymphocytes in development, progression, and prognosis of non–small cell lung cancer. *Journal of Thoracic Oncology*, 11(6):789–800, 2016.

[26] C.J.W. Breward, H.M. Byrne, and C.E. Lewis. A multiphase model describing vascular tumour growth. *Bulletin of mathematical biology*, 65(4):609–640, 2003.

[27] F.M. Burnet. The concept of immunological surveillance. In *Immunological Aspects of Neoplasia*, volume 13, pages 1–27. Karger Publishers, 1970.

[28] H.M. Byrne, T. Alarcon, M.R. Owen, S.D. Webb, and P.K. Maini. Modelling aspects of cancer dynamics: a review. *Philosophical Transactions of the Royal Society of London A: Mathematical, Physical and Engineering Sciences*, 364(1843):1563–1578, 2006.

[29] M.K. Callahan and J.D. Wolchok. At the bedside: CTLA-4-and PD-1-blocking antibodies in cancer immunotherapy. *Journal of leukocyte biology*, 94(1):41–53, 2013.

[30] K. Catakovic, E. Klieser, D. Neureiter, and R. Geisberger. T cell exhaustion: from pathophysiological basics to tumor immunotherapy. *Cell Communication and Signaling*, 15(1):1, 2017.

[31] M. Chaplain and A. Matzavinos. Mathematical modelling of spatio-temporal phenomena in tumour immunology. *Tutorials in Mathematical Biosciences III*, pages 131–183, 2006.

[32] M.A.J. Chaplain. Avascular growth, angiogenesis and vascular growth in solid tumours: The mathematical modelling of the stages of tumour development. *Mathematical and computer modelling*, 23(6):47–87, 1996.

[33] M.A.J. Chaplain. Mathematical modelling of angiogenesis. *Journal of Neuro-oncology*, 50(1-2):37–51, 2000.

[34] J.M. Chauvin, O. Pagliano, J. Fourcade, Z. Sun, H. Wang, C. Sander, J.M. Kirkwood, T.T. Chen, M. Maurer, A.J. Korman, et al. TIGIT and PD-1 impair tumor antigen–specific CD8+ T cells in melanoma patients. *The Journal of clinical investigation*, 125(5):2046, 2015.

[35] D.S. Chen and I. Mellman. Oncology meets immunology: the cancer-immunity cycle. *Immunity*, 39(1):1–10, 2013.

[36] D.S. Chen and I. Mellman. Elements of cancer immunity and the cancer-immune set point. *Nature*, 541(7637):321–330, 2017.

[37] G.D. Clapp, T. Lepoutre, R. El Cheikh, S. Bernard, J. Ruby, H. Labussière-Wallet, F.E. Nicolini, and D. Levy. Implication of the autologous immune system in BCR–ABL transcript variations in chronic myelogenous leukemia patients treated with Imatinib. *Cancer research*, 75(19):4053–4062, 2015.

[38] B.J. Coventry, M.L. Ashdown, M.A. Quinn, S.N. Markovic, S.L. Yatomi-Clarke, and A.P. Robinson. CRP identifies homeostatic immune oscillations in cancer patients: a potential treatment targeting tool? *Journal of translational medicine*, 7(1):102, 2009.

[39] R.J. De Boer and A.S. Perelson. Quantifying T lymphocyte turnover. *Journal of theoretical biology*, 327:45–87, 2013.

[40] L.G. de Pillis, W. Gu, and A.E. Radunskaya. Mixed immunotherapy and chemotherapy of tumors: modeling, applications and biological interpretations. *Journal of Theoretical Biology*, 238(4):841–862, 2006.

[41] L.G. de Pillis, A.E. Radunskaya, and C.L. Wiseman. A validated mathematical model of cell-mediated immune response to tumor growth. *Cancer research*, 65(17):7950–7958, 2005.

[42] H.P. de Vladar and J.A. González. Dynamic response of cancer under the influence of immunological activity and therapy. *Journal of Theoretical Biology*, 227(3):335–348, 2004.

[43] C. Dehing-Oberije, S. Yu, D. De Ruysscher, S. Meersschout, K. Van Beek, Y. Lievens, J. Van Meerbeeck, W. De Neve, B. Rao, H. van der Weide, et al. Development and external validation of prognostic model for 2-year survival of non–small-cell lung cancer patients treated with chemoradiotherapy. *International Journal of Radiation Oncology Biology Physics*, 74(2):355–362, 2009.

[44] T.S. Deisboeck, Z. Wang, P. Macklin, and V. Cristini. Multiscale cancer modeling. *Annual review of biomedical engineering*, 13:127–155, 2011.

[45] D.G. DeNardo, D.J. Brennan, E. Rexhepaj, B. Ruffell, S.L. Shiao, S.F. Madden, W.M. Gallagher, N. Wadhwani, S.D. Keil, S.A. Junaid, et al. Leukocyte complexity predicts breast cancer survival and functionally regulates response to chemotherapy. *Cancer discovery*, 1(1):54–67, 2011.

[46] Y. Dong, G. Huang, R. Miyazaki, and Y. Takeuchi. Dynamics in a tumor immune system with time delays. *Applied Mathematics and Computation*, 252:99–113, 2015.

[47] T. Donnem, S.M. Hald, E.E. Paulsen, E. Richardsen, S. Al-Saad, T.K. Kilvaer, O.T. Brustugun, A. Helland, M. Lund-Iversen, M. Poehl, et al. Stromal CD8+ T-cell densitya promising supplement to TNM staging in non–small cell lung cancer. *Clinical Cancer Research*, 21(11):2635–2643, 2015.

[48] A. d'Onofrio. A general framework for modeling tumor-immune system competition and immunotherapy: Mathematical analysis and biomedical inferences. *Physica D: Nonlinear Phenomena*, 208(3):220–235, 2005.

[49] J. Dormand and P. Prince. A family of embedded Runge-Kutta formulae. *Journal of Computational and Applied Mathematics*, 6(1):19–26, 1980.

[50] H. Dritschel, S.L. Waters, A. Rollers, and H.M. Byrne. A mathematical model of cytotoxic and helper T cell interactions in a tumour microenvironment. *Letters in Biomathematics: Modeling Tumor-Immune Dynamics, Disease Progression, and Treatment*, 2018.

[51] M. Dudley, J. Wunderlich, P. Robbins, J. Yang, P. Hwu, D. Schwartzentruber, S. Topalian, R. Sherry, N. Restifo, A. Hubicki, et al. Cancer regression and autoimmunity in patients after clonal repopulation with antitumor lymphocytes. *Science*, 298(5594):850–854, 2002.

[52] G.P. Dunn, L.J. Old, and R.D. Schreiber. The three Es of cancer immunoediting. *Annual Review Immunology*, 22:329–360, 2004.

[53] M. DuPage, C. Mazumdar, L.M. Schmidt, A.F. Cheung, and T. Jacks. Expression of tumour-specific antigens underlies cancer immunoediting. *Nature*, 482(7385):405–409, 2012.

[54] R. Durrett. Branching process models of cancer. In *Branching Process Models of Cancer*, pages 1–63. Springer, 2015.

[55] A. dOnofrio, F. Gatti, P. Cerrai, and L. Freschi. Delay-induced oscillatory dynamics of tumour–immune system interaction. *Mathematical and Computer Modelling*, 51(5-6):572–591, 2010.

[56] R. Eftimie, J.L. Bramson, and D.J.D. Earn. Interactions between the immune system and cancer: a brief review of non-spatial mathematical models. *Bulletin of mathematical biology*, 73(1):2–32, 2011.

[57] P. Ehrlich. *Ueber den jetzigen Stand der Karzinomforschung.*

[58] P. Ehrlich. *Die Wertbemessung des Diphtherieheilserums und deren theoretische Grundlagen.* G. Fischer, 1897.

[59] Paul Ehrlich. Croonian lecture: on immunity with special reference to cell life. *Proceedings of the royal Society of London*, 66(424-433):424–448, 1899.

[60] D.L. Farber, N.A. Yudanin, and N.P. Restifo. Human memory T cells: generation, compartmentalization and homeostasis. *Nature Reviews Immunology*, 14(1):24, 2014.

[61] S. Farkona, E.P. Diamandis, and I.M. Blasutig. Cancer immunotherapy: the beginning of the end of cancer? *BMC medicine*, 14(1):73, 2016.

[62] R.I. Fisher, S.A. Rosenberg, and G. Fyfe. Long-term survival update for high-dose recombinant interleukin-2 in patients with renal cell carcinoma. *The cancer journal from Scientific American*, 6:S55–7, 2000.

[63] J. Fourcade, Z. Sun, O. Pagliano, P. Guillaume, I.F. Luescher, C. Sander, J.M. Kirkwood, D. Olive, V. Kuchroo, and H.M. Zarour. CD8+ T cells specific for tumor antigens can be rendered dysfunctional by the tumor microenvironment through upregulation of the inhibitory receptors BTLA and PD-1. *Cancer research*, 2011.

[64] L.M. Francisco, V.H. Salinas, K.E. Brown, V.K. Vanguri, G.J. Freeman, V.K. Kuchroo, and A.H. Sharpe. Pd-L1 regulates the development, maintenance, and function of induced regulatory T cells. *Journal of Experimental Medicine*, 206(13):3015–3029, 2009.

[65] F. Frascoli, P.S. Kim, B.D. Hughes, and K.A. Landman. A dynamical model of tumour immunotherapy. *Mathematical biosciences*, 253:50–62, 2014.

[66] W.H. Fridman, F. Pagès, C. Sautès-Fridman, and J. Galon. The immune contexture in human tumours: impact on clinical outcome. *Nature Reviews Cancer*, 12(4):nrc3245, 2012.

[67] W.H. Fridman, L. Zitvogel, C. Sautès-Fridman, and G. Kroemer. The immune contexture in cancer prognosis and treatment. *Nature Reviews Clinical Oncology*, 14(12):717, 2017.

[68] J. Galon, A. Costes, F. Sanchez-Cabo, A. Kirilovsky, B. Mlecnik, C. Lagorce-Pagès, M. Tosolini, M. Camus, A. Berger, P. Wind, et al. Type, density, and location of immune cells within human colorectal tumors predict clinical outcome. *Science*, 313(5795):1960–1964, 2006.

[69] J. Galon, B.A. Fox, C.B. Bifulco, G. Masucci, T. Rau, G. Botti, F.M. Marincola, G. Ciliberto, F. Pages, P.A. Ascierto, et al. Immunoscore and immunoprofiling in cancer: an update from the melanoma and immunotherapy bridge 2015. *Journal of Translational Medicine*, 14, 2016.

[70] J. Galon, B. Mlecnik, G. Bindea, H.K. Angell, A. Berger, C. Lagorce, A. Lugli, I. Zlobec, A. Hartmann, C. Bifulco, et al. Towards the introduction of the Immunoscorein the classification of malignant tumours. *The Journal of pathology*, 232(2):199–209, 2014.

[71] J. Galon, F. Pagès, F.M. Marincola, M. Thurin, G. Trinchieri, B.A. Fox, T.F. Gajewski, and P.A. Ascierto. The immune score as a new possible approach for the classification of cancer. *Journal of translational medicine*, 10(1):1, 2012.

[72] T.C. Gangadhar and R.H. Vonderheide. Mitigating the toxic effects of anticancer immunotherapy. *Nature Reviews Clinical Oncology*, 11(2):91–99, 2014.

[73] G. Gasteiger and A.Y. Rudensky. Interactions between innate and adaptive lymphocytes. *Nature Reviews Immunology*, 14(9):631–639, 2014.

[74] A.J. Gentles, A.M. Newman, C.L. Liu, S.V. Bratman, W. Feng, D. Kim, V.S. Nair, Y. Xu, A. Khuong, C.D. Hoang, et al. The prognostic landscape of genes and infiltrating immune cells across human cancers. *Nature medicine*, 21(8):938, 2015.

[75] A. Gerisch and M.A.J. Chaplain. Mathematical modelling of cancer cell invasion of tissue: local and non-local models and the effect of adhesion. *Journal of Theoretical Biology*, 250(4):684–704, 2008.

[76] P. Gerlee. The model muddle: in search of tumor growth laws. *Cancer research*, 73(8):2407–2411, 2013.

[77] A. Goldbeter. *Biochemical oscillations and cellular rhythms: the molecular bases of periodic and chaotic behaviour*. Cambridge University Press, 1997.

[78] D.C. Gondek, L.F. Lu, S.A. Quezada, S. Sakaguchi, and R.J. Noelle. Cutting edge: contact-mediated suppression by CD4+ CD25+ regulatory cells involves a granzyme B-dependent, perforin-independent mechanism. *The Journal of Immunology*, 174(4):1783–1786, 2005.

[79] F.L. Greene, C.M. Balch, I.D. Fleming, A. Fritz, D.G. Haller, M. Morrow, and D.L. Page. *AJCC cancer staging handbook: TNM classification of malignant tumors*. Springer Science & Business Media, 2002.

[80] N.H. Gruener, F. Lechner, M.C. Jung, H. Diepolder, T. Gerlach, G. Lauer, B. Walker, J. Sullivan, R. Phillips, G.R. Pape, et al. Sustained dysfunction of antiviral CD8+ lymphocytes after infection with hepatitis C virus. *Journal of virology*, 75(12):5550–5558, 2001.

[81] J. Guckenheimer and P. Holmes. *Nonlinear oscillations, dynamical systems, and bifurcations of vector fields*, volume 42. Springer Science & Business Media, 2013.

[82] W.C. Hahn and R.A. Weinberg. Rules for making human tumor cells. *New England Journal of Medicine*, 347(20):1593–1603, 2002.

[83] N. Halama, S. Michel, M. Kloor, I. Zoernig, A. Benner, A. Spille, T. Pommerencke, D.M. von Knebel, G. Folprecht, B. Luber, et al. Localization and density of immune cells in the invasive margin of human colorectal cancer liver metastases are prognostic for response to chemotherapy. *Cancer research*, 71(17):5670–5677, 2011.

[84] O. Hamid, C. Robert, A. Daud, F.S. Hodi, W.L. Hwu, R. Kefford, J.D. Wolchok, P. Hersey, R.W. Joseph, J.S. Weber, et al. Safety and tumor responses with lambrolizumab (anti–PD-1) in melanoma. *New England Journal of Medicine*, 369(2):134–144, 2013.

[85] D. Hanahan and R.A. Weinberg. The hallmarks of cancer. *Cell*, 100(1):57–70, 2000.

[86] D. Hanahan and R.A. Weinberg. Hallmarks of cancer: the next generation. *Cell*, 144(5):646–674, 2011.

[87] H. Hanson, D. Donermeyer, H. Ikeda, M. White, V. Shankaran, L. Old, H. Shiku, R. Schreiber, and P. Allen. Eradication of established tumors by CD8+ T cell adoptive immunotherapy. *Immunity*, 13(2):265–276, 2000.

[88] S. Herter, L. Morra, R. Schlenker, J. Sulcova, L. Fahrni, I. Waldhauer, S. Lehmann, T. Reisländer, I. Agarkova, J.M. Kelm, et al. A novel three-dimensional heterotypic spheroid model for the assessment of the activity of cancer immunotherapy agents. *Cancer Immunology, Immunotherapy*, 66(1):129–140, 2017.

[89] K. Hiom, M. Melek, and M. Gellert. DNA transposition by the RAG1 and RAG2 proteins: a possible source of oncogenic translocations. *Cell*, 94(4):463–470, 1998.

[90] F. Hirano, K. Kaneko, H. Tamura, H. Dong, S. Wang, M. Ichikawa, C. Rietz, D.B. Flies, J.S. Lau, G. Zhu, et al. Blockade of B7-H1 and PD-1 by monoclonal antibodies potentiates cancer therapeutic immunity. *Cancer research*, 65(3):1089–1096, 2005.

[91] K. Hiraoka, M. Miyamoto, Y. Cho, M. Suzuoki, T. Oshikiri, Y. Nakakubo, T. Itoh, T. Ohbuchi, S. Kondo, and H. Katoh. Concurrent infiltration by CD8+ T cells and CD4+ T cells is a favourable prognostic factor in non-small-cell lung carcinoma. *British Journal of Cancer*, 94(2):275–280, 2006.

[92] K. Hung, R. Hayashi, A. Lafond-Walker, C. Lowenstein, D. Pardoll, and H. Levitsky. The central role of CD4+ T cells in the antitumor immune response. *The Journal of experimental medicine*, 188(12):2357–2368, 1998.

[93] A. Iwasaki and R. Medzhitov. Regulation of adaptive immunity by the innate immune system. *Science*, 327(5963):291–295, 2010.

[94] C.A. Janeway and R. Medzhitov. Innate Immune Recognition. 20(1):197–216.

[95] C.A. Janeway, P. Travers, M. Walport, and M.J. Shlomchik. Immunobiology. 2001.

[96] B. Joshi, S. Wang, X.and Banerjee, H. Tian, A. Matzavinos, and M.A.J. Chaplain. On immunotherapies and cancer vaccination protocols: a mathematical modelling approach. *Journal of theoretical biology*, 259(4):820–827, 2009.

[97] P.W. Kantoff, C.S. Higano, N.D. Shore, E.R. Berger, E.J. Small, D.F. Penson, C.H. Redfern, A.C. Ferrari, R. Dreicer, R.B. Sims, et al. Sipuleucel-T immunotherapy for castration-resistant prostate cancer. *New England Journal of Medicine*, 363(5):411–422, 2010.

[98] O. Kawai, G. Ishii, K. Kubota, Y. Murata, Y. Naito, T. Mizuno, K. Aokage, N. Saijo, Y. Nishiwaki, A. Gemma, et al. Predominant infiltration of macrophages and CD8+ T cells in cancer nests is a significant predictor of survival in stage IV nonsmall cell lung cancer. *Cancer*, 113(6):1387–1395, 2008.

[99] B.J. Kennedy. Cyclic leukocyte oscillations in chronic myelogenous leukemia during hydroxyurea therapy. *Blood*, 35(6):751–760, 1970.

[100] K.S. Kim, G. Cho, and I.H. Jung. Optimal treatment strategy for a tumor model under immune suppression. *Computational and mathematical methods in medicine*, 2014, 2014.

[101] P.S. Kim and P.P. Lee. Modeling protective anti-tumor immunity via preventative cancer vaccines using a hybrid agent-based and delay differential equation approach. *PLoS computational biology*, 8(10):e1002742, 2012.

[102] D. Kirschner and J. Panetta. Modeling immunotherapy of the tumor immune interaction. *Journal of Mathematical Biology*, 37(3):235–252, 1998.

[103] D. Kirschner and A. Tsygvintsev. On the global dynamics of a model for tumor immunotherapy. *Mathematical Biosciences and Engineering*, 6(3):573–583, 2009.

[104] J.A. Klapper, S.G. Downey, F.O. Smith, J.C. Yang, M.S. Hughes, U.S. Kammula, R.M. Sherry, R.E. Royal, S.M. Steinberg, and S. Rosenberg. High-dose interleukin-2 for the treatment of metastatic renal cell carcinoma. *Cancer*, 113(2):293–301, 2008.

[105] C. Klein, I. Waldhauer, V.G. Nicolini, A. Freimoser-Grundschober, T. Nayak, D.J. Vugts, C. Dunn, M. Bolijn, J. Benz, M. Stihle, et al. Cergutuzumab amunaleukin (CEA-IL2v), a CEA-targeted IL-2 variant-based immunocytokine for combination cancer immunotherapy: Overcoming limitations of aldesleukin and conventional IL-2-based immunocytokines. *OncoImmunology*, 6(3):e1277306, 2017.

[106] A.H. Knoll. *Life on a young planet: the first three billion years of evolution on earth*. Princeton University Press, 2003.

[107] A. Konstorum, A.T. Vella, A.J. Adler, and R.C. Laubenbacher. Addressing current challenges in cancer immunotherapy with mathematical and computational modelling. *Journal of The Royal Society Interface*, 14(131):20170150, 2017.

[108] N. Kronik, Y. Kogan, M. Elishmereni, K. Halevi-Tobias, S. Vuk-Pavlović, and Z. Agur. Predicting outcomes of prostate cancer immunotherapy by personalized mathematical models. *PLoS One*, 5(12):e15482, 2010.

[109] H. Kumar, T. Kawai, and S. Akira. Pathogen recognition by the innate immune system. *International reviews of immunology*, 30(1):16–34, 2011.

[110] V.A. Kuznetsov, I.A. Makalkin, M.A. Taylor, and A.S. Perelson. Nonlinear dynamics of immunogenic tumors: parameter estimation and global bifurcation analysis. *Bulletin of Mathematical Biology*, 56(2):295–321, 1994.

[111] J. Larkin, C.D. Lao, W.J. Urba, D.F. McDermott, C. Horak, J. Jiang, and J.D. Wolchok. Efficacy and safety of nivolumab in patients with BRAF V600 mutant and BRAF wild-type advanced melanoma: a pooled analysis of 4 clinical trials. *JAMA Oncology*, 1(4):433–440, 2015.

[112] P.P. Lee, C. Yee, P.A. Savage, L. Fong, D. Brockstedt, J.S. Weber, D. Johnson, S. Swetter, J. Thompson, P.D. Greenberg, et al. Characterization of circulating T cells specific for tumor-associated antigens in melanoma patients. *Nature medicine*, 5(6):677–685, 1999.

[113] T.K. Lee, R.D. Horner, J.F. Silverman, Y.H. Chen, C. Jenny, and C.W. Scarantino. Morphometric and morphologic evaluations in stage III non-small cell lung cancers. prognostic significance of quantitative assessment of infiltrating lymphoid cells. *Cancer*, 63(2):309, 1989.

[114] K. Leon, K. Garcia, J. Carneiro, and A. Lage. How regulatory CD25+ CD4+ T cells impinge on tumor immunobiology: the differential response of tumors to therapies. *The Journal of Immunology*, 179(9):5659–5668, 2007.

[115] N.M. Lerret and A.L. Marzo. Adoptive T-cell transfer combined with a single low dose of total body irradiation eradicates breast tumors. *OncoImmunology*, 2(2):e22731, 2013.

[116] J. Lessler, W.J. Edmunds, M.E. Halloran, T.D. Hollingsworth, and A.L. Lloyd. Seven challenges for model-driven data collection in experimental and observational studies. *Epidemics*, 10:78–82, 2015.

[117] K.L. Liao, X.F. Bai, and A. Friedman. Mathematical modeling of interleukin-35 promoting tumor growth and angiogenesis. *PloS One*, 9(10):e110126, 2014.

[118] H.G. Ljunggren and K.J. Malmberg. Prospects for the use of nk cells in immunotherapy of human cancer. *Nature Reviews Immunology*, 7(5):329, 2007.

[119] Á. López, J. Seoane, and M. Sanjuán. A validated mathematical model of tumor growth including tumor–host interaction, cell-mediated immune response and chemotherapy. *Bulletin of Mathematical Biology*, 76(11):2884–2906, 2014.

[120] J.S. Lowengrub, H.B. Frieboes, F. Jin, Y.L. Chuang, X. Li, P. Macklin, S.M. Wise, and V. Cristini. Nonlinear modelling of cancer: bridging the gap between cells and tumours. *Nonlinearity*, 23(1):R1, 2009.

[121] F.R. Macfarlane, T. Lorenzi, and M.A.J. Chaplain. Modelling the immune response to cancer: An individual-based approach accounting for the difference in movement between inactive and activated t cells. *Bulletin of mathematical biology*, pages 1–24, 2018.

[122] C. Macnamara and R. Eftimie. Memory versus effector immune responses in oncolytic virotherapies. *Journal of theoretical biology*, 377:1–9, 2015.

[123] M.T. Madondo, S. Tuyaerts, B.B. Turnbull, A. Vanderstraeten, H. Kohrt, B. Narasimhan, F. Amant, M. Quinn, and M. Plebanski. Variability in CRP, regulatory T cells and effector T cells over time in gynaecological cancer patients: a study of potential oscillatory behaviour and correlations. *Journal of translational medicine*, 12(1):179, 2014.

[124] G. Magombedze, P. Reddy, S. Eda, and V. Ganusov. Cellular and population plasticity of helper CD4+ T cell responses. *Frontiers in Physiology*, 4, 2013.

[125] K.M. Mahoney, P.D. Rennert, and G.J. Freeman. Combination cancer immunotherapy and new immunomodulatory targets. *Nature Reviews Drug discovery*, 14(8):561–584, 2015.

[126] D.G. Mallet and L.G. De Pillis. A cellular automata model of tumor–immune system interactions. *Journal of Theoretical Biology*, 239(3):334–350, 2006.

[127] K.J. Maloy and F. Powrie. Fueling regulation: IL-2 keeps CD4+ Treg cells fit. *Nature immunology*, 6(11):1071–1072, 2005.

[128] F.O. Martinez, L. Helming, and S. Gordon. Alternative activation of macrophages: an immunologic functional perspective. *Annual review of immunology*, 27:451–483, 2009.

[129] A. Matzavinos and M.A.J. Chaplain. Travelling-wave analysis of a model of the immune response to cancer. *Comptes rendus biologies*, 327(11):995–1008, 2004.

[130] A. Matzavinos, M.A.J. Chaplain, and V.A. Kuznetsov. Mathematical modelling of the spatio-temporal response of cytotoxic T-lymphocytes to a solid tumour. *Mathematical Medicine and Biology*, 21(1):1–34, 2004.

[131] M.V. Maus, J.A. Fraietta, B.L. Levine, M. Kalos, Y. Zhao, and C.H. June. Adoptive immunotherapy for cancer or viruses. *Annual review of immunology*, 32:189–225, 2014.

[132] I. Mellman, G. Coukos, and G. Dranoff. Cancer immunotherapy comes of age. *Nature*, 480(7378):480, 2011.

[133] E. Metschnikoff. Ueber eine Sprosspilzkrankheit der Daphnien. Beitrag zur Lehre über den Kampf der Phagocyten gegen Krankheitserreger. *Virchows Archiv*, 96(2):177–195, 1884.

[134] B. Mlecnik, G. Bindea, H.K. Angell, P. Maby, M. Angelova, D. Tougeron, S.E. Church, L. Lafontaine, M. Fischer, T. Fredriksen, et al. Integrative analyses of colorectal cancer show immunoscore is a stronger predictor of patient survival than microsatellite instability. *Immunity*, 44(3):698–711, 2016.

[135] A.M. Monjazeb, A.E. Zamora, S.K. Grossenbacher, A. Mirsoian, G.D. Sckisel, and W.J. Murphy. Immunoediting and antigen loss: overcoming the achilles heel of immunotherapy with antigen non-specific therapies. *Frontiers in Oncology*, 3, 2013.

[136] A.A. Morley. A neutrophil cycle in healthy individuals. *The Lancet*, 288(7475):1220–1222, 1966.

[137] T.R. Mosmann and R.L. Coffman. Th1 and Th2 cells: different patterns of lymphokine secretion lead to different functional properties. *Annual Review of Immunology*, 7(1):145–173, 1989.

[138] P.A.H. Moss, W.M.C. Rosenberg, and J.I. Bell. The human T cell receptor in health and disease. *Annual Review of Immunology*, 10(1):71–96, 1992.

[139] D.L. Mueller, M.K. Jenkins, and R.H. Schwartz. Clonal expansion versus functional clonal inactivation: a costimulatory signalling pathway determines the outcome of T cell antigen receptor occupancy. *Annual review of immunology*, 7(1):445–480, 1989.

[140] F. Nani and H.I. Freedman. A mathematical model of cancer treatment by immunotherapy. *Mathematical biosciences*, 163(2):159–199, 2000.

[141] C. Oelkrug and J.M. Ramage. Enhancement of T cell recruitment and infiltration into tumours. *Clinical & Experimental Immunology*, 178(1):1–8, 2014.

[142] M.R. Owen and J.A. Sherratt. Pattern formation and spatiotemporal irregularity in a model for macrophage–tumour interactions. *Journal of theoretical biology*, 189(1):63–80, 1997.

[143] M.R. Owen and J.A. Sherratt. Mathematical modelling of macrophage dynamics in tumours. *Mathematical Models and Methods in Applied Sciences*, 9(04):513–539, 1999.

[144] M.R. Owen, I.J. Stamper, M. Muthana, G.W. Richardson, J. Dobson, C.E. Lewis, and H.M. Byrne. Mathematical modeling predicts synergistic antitumor effects of combining a macrophage-based, hypoxia-targeted gene therapy with chemotherapy. *Cancer research*, 71(8):2826–2837, 2011.

[145] D. Pardoll. The blockade of immune checkpoints in cancer immunotherapy. *Nature Reviews Cancer*, 12(4):252–264, 2012.

[146] K.E. Pauken and J.E. Wherry. Overcoming T cell exhaustion in infection and cancer. *Trends in Immunology*, 36(4):265–276, 2015.

[147] M. Piotrowska, M. Bodnar, J. Poleszczuk, and U. Foryś. Mathematical modelling of immune reaction against gliomas: sensitivity analysis and influence of delays. *Nonlinear Analysis: Real World Applications*, 14(3):1601–1620, 2013.

[148] S.A. Plotkin and S.L. Plotkin. The development of vaccines: how the past led to the future. *Nature Reviews Microbiology*, 9(12):889–893, 2011.

[149] A. Poltorak, X. He, I. Smirnova, M.Y. Liu, C. Van Huffel, X. Du, D. Birdwell, E. Alejos, M. Silva, C. Galanos, M. Freudenberg, P. Ricciardi-Castagnoli, B. Layton, and B. Beutler. Defective LPS signaling in C3H/HeJ and C57BL/10ScCr mice: mutations in Tlr4 gene. *Science*, 282(5396):2085–2088, 1998.

[150] M.A. Postow, M.K. Callahan, and J.D. Wolchok. Immune checkpoint blockade in cancer therapy. *Journal of Clinical Oncology*, 33(17):1974–1982, 2015.

[151] T. Powles, J. Eder, G. Fine, F. Braiteh, Y. Loriot, C. Cruz, J. Bellmunt, H. Burris, D. Petrylak, S.L. Teng, et al. MPDL3280A (anti-PD-L1) treatment leads to clinical activity in metastatic bladder cancer. *Nature*, 515(7528):558–562, 2014.

[152] C. Preston, M. Maurer, A. Oberg, D. Visscher, K. Kalli, L. Hartmann, E. Goode, and K. Knutson. The ratios of CD8+ T cells to CD4+ CD25+ FOXP3+ and FOXP3-T cells correlate with poor clinical outcome in human serous ovarian cancer. *PloS One*, 8(11):e80063, 2013.

[153] F. Rad, S. Ajdary, R. Omranipour, M. Alimohammadian, and Z. Hassan. Comparative analysis of CD4+ and CD8+ T cells in tumor tissues, lymph nodes and the peripheral blood from patients with breast cancer. *Iranian Biomedical Journal*, 19(1):35, 2015.

[154] S. Reignat, G.J.M. Webster, D. Brown, G.S. Ogg, A. King, S.L. Seneviratne, G. Dusheiko, R. Williams, M.K. Maini, and A. Bertoletti. Escaping high viral load exhaustion. *Journal of Experimental Medicine*, 195(9):1089–1101, 2002.

[155] K.A. Rejniak and A.R.A. Anderson. Hybrid models of tumor growth. *Wiley Interdisciplinary Reviews: Systems Biology and Medicine*, 3(1):115–125, 2011.

[156] Cancer Research UK. Key facts: Cancer Research UK, December 2014.

[157] N. Restifo, M. Dudley, and S. Rosenberg. Adoptive immunotherapy for cancer: harnessing the T cell response. *Nature Reviews Immunology*, 12(4):269–281, 2012.

[158] T. Reya, S.J. Morrison, M.F. Clarke, and Irving L Weissman. Stem cells, cancer, and cancer stem cells. *nature*, 414(6859):105, 2001.

[159] F.A. Rihan, D.H.A. Rahman, S. Lakshmanan, and A.S. Alkhajeh. A time delay model of tumour–immune system interactions: Global dynamics, parameter estimation, sensitivity analysis. *Applied Mathematics and Computation*, 232:606–623, 2014.

[160] M. Robertson-Tessi, A. El-Kareh, and A. Goriely. A mathematical model of tumor–immune interactions. *Journal of theoretical biology*, 294:56–73, 2012.

[161] K. Roesch, D. Hasenclever, and M. Scholz. Modelling lymphoma therapy and outcome. *Bulletin of mathematical biology*, 76(2):401–430, 2014.

[162] T. Roose, S.J. Chapman, and P.K. Maini. Mathematical models of avascular tumor growth. *Siam Review*, 49(2):179–208, 2007.

[163] S. Rosenberg, N. Restifo, J. Yang, R. Morgan, and M. Dudley. Adoptive cell transfer: a clinical path to effective cancer immunotherapy. *Nature Reviews Cancer*, 8(4):299–308, 2008.

[164] S.A. Rosenberg. Il-2: the first effective immunotherapy for human cancer. *The Journal of Immunology*, 192(12):5451–5458, 2014.

[165] M. Ruella and M. Kalos. Adoptive immunotherapy for cancer. *Immunological reviews*, 257(1):14–38, 2014.

[166] S.J. Russell and K.W. Peng. Viruses as anticancer drugs. *Trends in pharmacological sciences*, 28(7):326–333, 2007.

[167] S.J. Russell, K.W. Peng, and J.C. Bell. Oncolytic virotherapy. *Nature biotechnology*, 30(7):658–670, 2012.

[168] R.K. Sachs, L.R. Hlatky, and P. Hahnfeldt. Simple ODE models of tumor growth and anti-angiogenic or radiation treatment. *Mathematical and Computer Modelling*, 33(12-13):1297–1305, 2001.

[169] F. Sallusto and A. Lanzavecchia. Heterogeneity of CD4+ memory T cells: functional modules for tailored immunity. *European journal of immunology*, 39(8):2076–2082, 2009.

[170] E.A. Sarapata and L.G. de Pillis. A comparison and catalog of intrinsic tumor growth models. *Bulletin of mathematical biology*, 76(8):2010–2024, 2014.

[171] J. Schreiner, D.S. Thommen, P. Herzig, M. Bacac, C. Klein, A. Roller, A. Belousov, V. Levitsky, S. Savic, W. Moersig, et al. Expression of inhibitory receptors on intratumoral T cells modulates the activity of a T cell-bispecific antibody targeting folate receptor. *OncoImmunology*, 5(2):e1062969, 2016.

[172] J. Schreiner, D.S. Thommen, P. Herzig, M. Bacac, C. Klein, A. Roller, A. Belousov, V. Levitsky, S. Savic, W. Moersig, et al. Expression of inhibitory receptors on intratumoral T cells modulates the activity of a T cell-bispecific antibody targeting folate receptor. *Oncoimmunology*, 5(2):e1062969, 2016.

[173] G. Schuler and R.M. Steinman. Murine epidermal langerhans cells mature into potent immunostimulatory dendritic cells in vitro. *Journal of Experimental Medicine*, 161(3):526–546, 1985.

[174] R. Serre, S. Benzekry, L. Padovani, C. Meille, N. André, J. Ciccolini, F. Barlesi, X. Muracciole, and D. Barbolosi. Mathematical modeling of cancer immunotherapy and its synergy with radiotherapy. *Cancer research*, 76(17):4931–4940, 2016.

[175] P. Shankar, M. Russo, B. Harnisch, M. Patterson, P. Skolnik, and J. Lieberman. Impaired function of circulating HIV-specific CD8+ T cells in chronic human immunodeficiency virus infection. *Blood*, 96(9):3094–3101, 2000.

[176] V. Shankaran, H. Ikeda, A.T. Bruce, J.M. White, P.E. Swanson, L.J. Old, and R.D. Schreiber. IFNγ and lymphocytes prevent primary tumour development and shape tumour immunogenicity. *Nature*, 410(6832):1107–1111, 2001.

[177] S.P. Shariatpanahi, S.P. Shariatpanahi, K. Madjidzadeh, M. Hassan, and M. Abedi-Valugerdi. Mathematical modeling of tumor-induced immunosuppression by myeloid-derived suppressor cells: implications for therapeutic targeting strategies. *Journal of theoretical biology*, 2018.

[178] P. Sharma and J.P. Allison. Immune checkpoint targeting in cancer therapy: toward combination strategies with curative potential. *Cell*, 161(2):205–214, 2015.

[179] M.S. Sosa, P. Bragado, and J.A. Aguirre-Ghiso. Mechanisms of disseminated cancer cell dormancy: an awakening field. *Nature Reviews Cancer*, 14(9):611, 2014.

[180] O. Sotolongo-Costa, L.M. Molina, D.R. Pérez, J.C. Antoranz, and M.C. Reyes. Behavior of tumors under nonstationary therapy. *Physica D: Nonlinear Phenomena*, 178(3):242–253, 2003.

[181] R.M. Steinman and Z.A. Cohn. Identification of a novel cell type in peripheral lymphoid organs of mice. *Journal of Experimental Medicine*, 137(5):1142–1162, 1973.

[182] R.M. Steinman and M.D. Witmer. Lymphoid dendritic cells are potent stimulators of the primary mixed leukocyte reaction in mice. *Proceedings of the National Academy of Sciences*, 75(10):5132–5136, 1978.

[183] Z. Szymańska, M. Cytowski, E. Mitchell, C.K. Macnamara, and M.A.J. Chaplain. Computational modelling of cancer development and growth: Modelling at multiple scales and multiscale modelling. *Bulletin of Mathematical Biology*, pages 1–38, 2017.

[184] A. Talkington and R. Durrett. Estimating tumor growth rates in vivo. *Bulletin of Mathematical Biology*, 77(10):1934–1954, 2015.

[185] E. Tartour, H. Pere, B. Maillere, M. Terme, N. Merillon, J. Taieb, F. Sandoval, F. Quintin-Colonna, K. Lacerda, A. Karadimou, et al. Angiogenesis and immunity: a bidirectional link potentially relevant for the monitoring of antiangiogenic therapy and the development of novel therapeutic combination with immunotherapy. *Cancer and Metastasis Reviews*, 30(1):83–95, 2011.

[186] J.M. Taube, R.A. Anders, G.D. Young, H. Xu, R. Sharma, T.L. McMiller, S. Chen, A.P. Klein, D.M. Pardoll, S.L. Topalian, et al. Colocalization of inflammatory response with B7-h1 expression in human melanocytic lesions supports an adaptive resistance mechanism of immune escape. *Science translational medicine*, 4(127):127ra37–127ra37, 2012.

[187] F. Teng, D. Mu, X. Meng, L. Kong, H. Zhu, S. Liu, J. Zhang, and J. Yu. Tumor infiltrating lymphocytes (TILs) before and after neoadjuvant chemoradiotherapy and its clinical utility for rectal cancer. *American journal of cancer research*, 5(6):2064, 2015.

[188] M.W.L. Teng, S.F. Ngiow, A. Ribas, and M.J. Smyth. Classifying cancers based on T-cell infiltration and PD-L1. *Cancer research*, 75(11):2139–2145, 2015.

[189] D.S. Thommen, J. Schreiner, P. Müller, P. Herzig, A. Roller, A. Belousov, P. Umana, P. Pisa, C. Klein, M. Bacac, et al. Progression of lung cancer is associated with increased dysfunction of T cells defined by coexpression of multiple inhibitory receptors. *Cancer Immunology Research*, 3(12):1344–1355, 2015.

[190] R. Toes, F. Ossendorp, R. Offringa, and C. Melief. CD4 T cells and their role in antitumor immune responses. *The Journal of Experimental Medicine*, 189(5):753–756, 1999.

[191] S.L. Topalian, C.G. Drake, and D.M. Pardoll. Immune checkpoint blockade: a common denominator approach to cancer therapy. *Cancer cell*, 27(4):450–461, 2015.

[192] S.L. Topalian, F.S. Hodi, J.R. Brahmer, S.N. Gettinger, D.C. Smith, D.F. McDermott, J.D. Powderly, R.D. Carvajal, J.A. Sosman, M.B. Atkins, et al. Safety, activity, and immune correlates of anti–PD-1 antibody in cancer. *New England Journal of Medicine*, 366(26):2443–2454, 2012.

[193] L.A. Torre, F. Bray, R.L. Siegel, J. Ferlay, J. Lortet-Tieulent, and A. Jemal. Global cancer statistics, 2012. *CA: a cancer journal for clinicians*, 65(2):87–108, 2015.

[194] G. Trinchieri. Biology of natural killer cells. In *Advances in immunology*, volume 47, pages 187–376. Elsevier, 1989.

[195] T. Tsujikawa, S. Kumar, R.N. Borkar, V. Azimi, G. Thibault, Y.H. Chang, A. Balter, R. Kawashima, G. Choe, D. Sauer, et al. Quantitative multiplex immunohistochemistry reveals myeloid-inflamed tumor-immune complexity associated with poor prognosis. *Cell reports*, 19(1):203–217, 2017.

[196] M.E. Turnis, L.P. Andrews, and D.A. Vignali. Inhibitory receptors as targets for cancer immunotherapy. *European journal of immunology*, 2015.

[197] H. Vodopick, E.M. Rupp, L. Edwards, F.A. Goswitz, and J.J. Beauchamp. Spontaneous cyclic leukocytosis and thrombocytosis in chronic granulocytic leukemia. *New England Journal of Medicine*, 286(6):284–290, 1972.

[198] B. Vogelstein and K.W. Kinzler. Cancer genes and the pathways they control. *Nature medicine*, 10(8):789–799, 2004.

[199] E.J. Wherry. T cell exhaustion. *Nature immunology*, 12(6):492–499, 2011.

[200] E.J. Wherry, S.J. Ha, S.M. Kaech, W.N. Haining, S. Sarkar, V. Kalia, S. Subramaniam, J.N. Blattman, D.L. Barber, and R. Ahmed. Molecular signature of CD8+ T cell exhaustion during chronic viral infection. *Immunity*, 27(4):670–684, 2007.

[201] E.J. Wherry and M. Kurachi. Molecular and cellular insights into T cell exhaustion. *Nature Reviews Immunology*, 15(8):486–499, 2015.

[202] K. Wilkie and P. Hahnfeldt. Mathematical models of immune-induced cancer dormancy and the emergence of immune evasion. *Interface Focus*, 3(4):20130010, 2013.

[203] S.R. Woo, M.E. Turnis, M.V. Goldberg, J. Bankoti, M. Selby, C.J. Nirschl, M.L. Bettini, D.M. Gravano, P. Vogel, C.L. Liu, et al. Immune inhibitory molecules LAG-3 and PD-1 synergistically regulate T-cell function to promote tumoral immune escape. *Cancer research*, 72(4):917–927, 2012.

[204] A.E. Wright and S.R. Douglas. An experimental investigation of the role of the blood fluids in connection with phagocytosis. *Proceedings of the Royal Society of London*, pages 357–370, 1903.

[205] A. Yates and R. Callard. Cell death and the maintenance of immunological memory. *Discrete and Continuous Dynamical Systems: Series B*, 1(1):43–59, 2001.

[206] A.J. Zajac, J.N. Blattman, K. Murali-Krishna, D.J.D. Sourdive, M. Suresh, J.D. Altman, and R. Ahmed. Viral immune evasion due to persistence of activated T cells without effector function. *Journal of Experimental Medicine*, 188(12):2205–2213, 1998.

[207] M. Zanetti. Tapping CD4 T cells for cancer immunotherapy: the choice of personalized genomics. *The Journal of Immunology*, 194(5):2049–2056, 2015.

[208] H.M. Zarour. Reversing T-cell dysfunction and exhaustion in cancer. *Clinical cancer research: an official journal of the American Association for Cancer Research*, 22(8):1856, 2016.

[209] Q. Zhang and D.A. Vignali. Co-stimulatory and co-inhibitory pathways in autoimmunity. *Immunity*, 44(5):1034–1051, 2016.

[210] W. Zou, J.D. Wolchok, and L. Chen. PD-L1 (B7-H1) and PD-1 pathway blockade for cancer therapy: Mechanisms, response biomarkers, and combinations. *Science translational medicine*, 8(328):328rv4–328rv4, 2016.